

**RELATIVISTIC EFFECTS IN ATOMS AND
IN URANIUM COMPOUNDS**

VRIJE UNIVERSITEIT

**RELATIVISTIC EFFECTS IN ATOMS AND
IN URANIUM COMPOUNDS**

ACADEMISCH PROEFSCHRIFT

ter verkrijging van de graad van doctor aan
de Vrije Universiteit te Amsterdam,
op gezag van de rector magnificus
dr. C. Datema,
hoogleraar aan de faculteit der letteren,
in het openbaar te verdedigen
ten overstaan van de promotiecommissie
van de faculteit der scheikunde
op donderdag 20 februari 1992 te 15.30 uur
in het hoofdgebouw van de universiteit, De Boelelaan 1105

door

Engelbertus Maria van Wezenbeek

geboren te Noordoostpolder

FEBODRUK Enschede

1992

Promotor: prof.dr. E.J. Baerends

Copromotor: prof.dr. J.G. Snijders

Referent: prof.dr. P. Pyykkö

voor mijn vader† en moeder
voor Saskia

Contents

Summary	9
Chapter 1 General Introduction	13
Chapter 2 The Origin of Relativistic Effects of Atomic Orbitals	45
<i>W.H.E. Schwarz, E.M. van Wezenbeek, E.J. Baerends and J.G. Snijders, J. Phys. B 22 (1989) 1515</i>	
Chapter 3 The Relativistic Bond Lengthening of UO_2^{2+} and UO_2	63
<i>E.M. van Wezenbeek, E.J. Baerends and J.G. Snijders, Theor. Chim. Acta 81 (1991) 139</i>	
Chapter 4a An explanation for the short U-O bond length in UO_2^{2+}	83
<i>in E.M. van Wezenbeek, E.J. Baerends, J.G. Snijders and R.L. DeKock, to be submitted to J. Phys. Chem.</i>	
Chapter 4b A qualitative study of the relativistic effects on the bond between HfCl_3 , ThCl_3 and H	101
<i>E.M. van Wezenbeek, T. Ziegler and E.J. Baerends, to be submitted</i>	

Chapter 4c	The Central Bond in the three CN• Dimers NC-CN, CN-CN and CN-NC: Electron Pair Bonding and Pauli Repulsion Effects.	123
-------------------	---	-----

F.M. Bickelhaupt, N.N. Nibbering, E.M. van Wezenbeek and E.J. Baerends, Submitted to J. Phys. Chem.

Chapter 5	Spectroscopy of Uranyl Compounds	149
------------------	----------------------------------	-----

in E.M. van Wezenbeek, E.J. Baerends, J.G. Snijders and R.L. DeKock, to be submitted to J. Phys. Chem.

Chapter 6	Organoactinide Chemistry: The ground electronic structure of UCp ₃ and interaction with the ligands CO, NO and H	167
------------------	---	-----

E.M. van Wezenbeek, R.L. DeKock and E.J. Baerends, to be submitted

Samenvatting		199
---------------------	--	-----

Nawoord		203
----------------	--	-----

Curriculum Vitae		204
-------------------------	--	-----

Summary

Relativistic effects are important in the study of molecules containing heavy atoms, because in those systems the electrons move very fast near the nucleus. Before investigating relativity in molecules one must understand the relativistic effects on atomic orbitals. Therefore this thesis starts with a chapter on atomic relativistic effects, after a general introduction about relativity and the method of calculation in Chapter 1. The other work concerns molecular calculations, where relativistic effects on bonding, bond-lengths and spectroscopy of molecules containing heavy elements are studied. Also bonds are investigated in a relativistic scheme, without explicit reference to changes due to relativity. Some of the molecules that were studied are built up of open shell fragments. The method that was developed to analyze the bond energies also in these systems, is described extensively in Chapter 1. Using this method we are now able to study the formation of electron pair bonds, which is a very important process in Chemistry. Chapter 4b consists of applications of the electron pair bond method.

For atoms the situation concerning relativistic effects on orbitals is clear: $s_{1/2}$ and $p_{1/2}$ are stabilized and contract, d and f are destabilized and expand, while the behaviour of $p_{3/2}$ orbitals is intermediate. The investigation in Chapter 2 does therefore not concentrate on this, but on the question of the (spatial) origin of the relativistic effects on AOs. The incentive for this work was the result that relativistic corrections on valence AO properties of many-electron atoms depend on the total nuclear charge, instead of the effective charge as was expected. The explanation for this surprising dependence can be found by dividing the integral in the expectation value of an AO property into spatial shells, starting from the nucleus. These shells correspond to the usual K, L, M etc. notation of energy levels. It appears that the direct relativistic first order mass-velocity, Darwin and spin-orbit corrections build up entirely in the neighbourhood of the nucleus, and therefore feel the total nuclear charge. The indirect relativistic effect was investigated too. Usually this is associated with destabilization, due to contraction of inner orbitals. The present work shows some new interesting viewpoints. One should realize that while relativistically contracted s and p orbitals cause indirect destabilization, expanding d and f orbitals can cause indirect stabilization. This is especially important in the case of a filled d or f shell just below a penetrating orbital (s or p). Reasoning along this line it is now understood why the relativistic effects are so large in the central columns of the periodic table, especially the large relativistic effects on Au and its compounds.

The remaining part of this thesis concerns relativistic calculations on molecules, including the investigation of the changes due to relativity on bond length, bonding and

Summary

spectroscopy. The uranyl molecule UO_2^{2+} makes up a substantial part of these investigations. It has a number of special characteristics, that are all related to the special character of the semi-core U 6p orbital. This orbital has both core and valence character. It is spatially even more extended than the valence U 5f, which results in large overlaps in uranyl with its short U-O bond length (see Chapter 4a for an explanation for this). Also in UCp_3L (Chapter 6) the U 6p plays a role, although less important than in uranyl, as the distances between the atoms are larger there.

Relativistic calculations show a bond length expansion for uranyl, in contrast to the usually found contraction for molecules. In Chapter 3 we show that this expansion is not related to the atomic relativistic destabilization of the U 5f orbitals, which is important for the bond in uranyl. The U 6p orbital is the cause of the expansion. The valence character of U 6p causes large overlaps and consequently large interaction with O, in which the short U-O distance also plays a role. The strong interaction with O 2p makes the antibonding U 6p-O 2p combination end up high in the virtual spectrum, above U 5f. The interaction between U 5f and O 2p (in the antibonding U 6p-O 2p) leads to a HOMO with much 5f character. The strong participation of U 6p to the bond in uranyl leads to a depopulation, there is only 1.5 electron left in U 6p: a '6p hole' is present. This hole increases with shorter U-O distance, leading to an increasing loss of stabilizing mass-velocity correction. This effect is important due to the large mass-velocity correction from the core character of U 6p. This effect is clearly expanding. More directly the core character contributes to the expansion also through the off-diagonal mass-velocity element with U 5p.

The lowest virtual orbitals in uranyl are the non-bonding U 5f and 5f orbitals. From the previous it follows that the excitation spectrum is determined by excitation from the mainly 5f HOMO to f, f. In Chapter 5 we give an assignment of the excitation spectrum of $\text{Cs}_2\text{UO}_2\text{Cl}_4$, for which $\text{UO}_2\text{F}_4^{2-}$ was used as model. Due to the F ligand field the f is above f. Using a spin-orbit model our assignment of the spectrum is: $\epsilon_u < \epsilon_u$, $\epsilon_u < \epsilon_u$. This differs from the $\epsilon_u(2x) < \epsilon_u(2x)$ found in the literature. However the differences are only in the second and third origins, and our calculations show extensive mixing between the diagonal spin-orbit split f_{5/2} and f_{5/2} orbitals, which result in these origins. The assignment can therefore not be done to individual ϵ_u or ϵ_u orbitals. Also in Chapter 5 we present results of calculations on the Xray PES spectrum of uranyl. Like the strong interaction with O 2p, the U 6p interaction with O 2s is very large, with bonding and antibonding orbitals split by 14 eV. In experiments the peaks were assigned to individual atomic orbitals. We show that this is not correct: the strong U 6p-O 2s interaction precludes this sort of assignment. The U 6p-O 2s interaction can best be viewed as the result of an interaction where first the spin-orbit splitting acts.

The final study on uranyl in Chapter 4a concerns the short U-O bond length, that is much shorter than for secondary ligands. In this work uranyl was built up from open shell fragments $U^{3+}(5f^3 5f^2)$ and $O_2(2s_u^2 2p_u 2p_g^4 2p_u^2)$. For performing an energy analysis from such open shell fragments a method was developed, which is described in Chapter 1. Using this method one can study the formation of pair bonds. The first application was the investigation of uranyl as given above, with $5f_u - O 2p_u$ and $5f_g - O 2p_u$ pair bonds. The short distance U-O distance in uranyl is surprising, because much repulsion is expected from the spatially extended U 6p orbital. Indeed the U 6p orbital leads to large repulsive effects. The dominant contribution to the steric interaction in uranyl comes from the closed shell U $6p_u - O 2s_u$ Pauli repulsion. The U $6p_u - O 2p_u$ steric effect is surprisingly small, the explanation for which is the cancelling of Pauli repulsion and electrostatic effects. For the same reason the U $5f_u - O 2p_u$ steric interaction is small. Our results show that looking at the Pauli repulsion alone as is done frequently, is not enough, electrostatic effects also play a role. We found that the U $5f_u - O 2p_u$ interaction is responsible for the short U-O distance. Both the U $5f_u - O 2p_u$ and the U $5f_g - O 2p_u$ interactions are important, the former because there is no steric repulsion between U $5f_u$ and O $2p_u$, and the latter because the steric interaction of U $5f_g$ and O $2p_u$ is small. The U 6d orbital has a not unimportant contribution to the bond, but its distance behaviour is flat, and therefore does not play a role in determining the short U-O distance.

Two other applications of the open shell method are described in Chapters 4b and 4c. Chapter 4b contains an investigation of the effect of relativity on the bond between H and on the one hand the transition metal fragment $HfCl_3$ and on the other hand the actinide fragment $ThCl_3$. We found that the non-relativistic and relativistic bond characteristics are similar in $HfCl_3H$, with a larger 5d than 6s contribution. Contrary to this, in $ThCl_3H$ the bonds are completely different, non-relativistically the 6d and 5f contributions are equal, while relativistically the 5f contribution is almost negligible due to the relativistic destabilization of the 5f. This investigation shows that for transition metals the relativistic effects are not large and first order perturbation theory is sufficient, while for actinides quasi-relativistic calculations are necessary.

Chapter 4c presents an investigation of the relative stability of the three CN^* isomers $NCCN$ (**1**), $CNCN$ (**2**) and $CNNC$ (**3**). It is known that the bond weakens in the series **1-3**, while at the same time the central bond distance decreases. An elaborate energy analysis, using the open shell method developed in Chapter 1, shows that not only the pair bond between the singly occupied CN 5 orbitals plays a role, but also the doubly occupied CN 4 orbitals (N lone pairs) are important. The 5 is localized on C, and if only the pair bond were present, the observed stability could be explained directly from this. The situation is complicated however by the presence of the 4 orbitals. Firstly, the

Summary

in-phase $4 + 4'$ and $5 + 5'$ combinations have a repulsive second order interaction, working against the pair bond. This effect is largest in NCCN, because there the $5 / 5'$ overlap is largest and the $4 / 4'$ overlap smallest, bringing the in-phase combinations close together. Secondly, there is a donor/acceptor interaction between the out-phase $4 - 4'$ and $5 - 5'$ combinations, leading to relaxation, which lowers the energy. Due to the overlaps this interaction is largest in CNNC, which is finally responsible for the shorter central bond distance from **1** to **3**. In this investigation also a comparison is made with the results/interpretation of other workers. We show that our Orbital Correlation Diagrams (OCDs) lead to a better understanding of the complex interactions within the CN dimers. An important aspect in making those OCDs is the fact that one should realise that the CN 4 and 5 orbitals are not completely localized on N and C respectively, but both have considerable amplitude at the other nucleus as well.

The final investigation in Chapter 6 of this thesis concerns Organoactinide Chemistry. This field has become increasingly important since the beginning of the 80s. All calculations in this chapter were done quasi-relativistically, as this is necessary for a proper description of actinides. The first part of our investigation deals with the determination of the ground electronic structure of 'planar' UCp_3 . We found that it can best be described as $5f^3 (f^1 f^1 f^1)$. The bond between the fragments Cp_3^{3-} and U^{3+} in UCp_3 has a ionic/covalent ratio of 2:1. In the second part we investigated the interaction of pyramidal UCp_3 and the ligands H, OH, CO and NO. The calculated UCp_3 -L bond energies are -4.37 , -1.93 and -3.83eV for $L = \text{H}, \text{CO}$ and NO with respect to the planar ground state. The interaction in UCp_3L can be divided into a L to U donation in A_1 symmetry, and a back-donation from U to L in E symmetry. In all cases the U $6d$ orbital dominates the donation, while U $5f$ is the most important orbital for the back-donation. The donation to CO is larger than to NO, for which the smaller electronegativity of C and the resulting stronger localization on C and the higher energy of the CO 5 compared to the NO 5 . The back-donation in E symmetry consists of the U $5f$ -L 2 interaction, and is larger for UCp_3CO than for UCp_3NO . However the total bond energy for UCp_3NO is larger because the bonding U $5f$ -L 2 combination is fully occupied. The larger bond energy for UCp_3NO than for UCp_3CO justifies continued investigations to its existence. Finally, there is a small 'U $6p$ hole' in the considered systems, again showing the large spatial extension of this orbital.

Chapter 1

General Introduction

1. Overview

An accurate description of systems containing heavy atoms can only be obtained when additional effort is made compared to solving the usual Schrödinger equation. Because the electrons move very fast near the nuclei of heavy atoms, the effects of the theory of special relativity must be taken into account. The large increase in computational power since the beginning of the 70s made it possible to include relativistic effects and accurately determine the properties of heavy atoms and molecules. Especially in the last decade there has been an enormous increase in the size of the systems that can be investigated. At this moment it is even possible to routinely perform relativistic calculations on large organoactinide complexes such as UCp_3CO and $\text{U}(\text{COT})_2$ [1,2].

In the first part of this chapter (Section 2-4) the theoretical basis for our relativistic method will be treated. We start with the Dirac equation and use the Foldy-Wouthuysen (FW) transformation to reduce it to a two-component formalism, and also the many electron energy expression is subjected to a FW transformation. Also the frozen core and Slater local exchange approximations are discussed.

The method we used in this thesis is known as the Amsterdam Density Functional (DF) program package [3,4] and is dealt with in the second part of this chapter. With this method we are able to perform accurate relativistic calculations in a rather cheap way. An important aspect is the possibility to study the bond energy decomposition for the formation of molecules out of fragments. We describe some aspects of DF theory and the Non-Relativistic (NR) method in Section 5, and in Section 6 the bond energy decomposition scheme is described. Section 7 deals with First Order (FO) perturbation theory for inclusion of relativistic effects. Presently we are using the Quasi-Relativistic (QR) method, which is derived in Section 8. Special attention is given to the theoretical foundation of the QR method. Finally in Section 9 the most important relativistic effects on atoms will be given, and the effects on the bond length of molecules. The two alternative ways to view the bond length contraction that is usually found are discussed.

Part I: Relativity

2. The one-electron Dirac equation

The wave equation for a relativistic electron in an one-electron atom is the so-called Dirac equation [5]. It is a four component equation which is given by* :

$$H_d \psi = E \psi \quad \text{with } H_d = c \boldsymbol{\alpha} \cdot \mathbf{p} + \beta c^2 + V \quad (2.1)$$

where α (x,y,z-components) and β are the 4-4 Dirac matrices, \mathbf{p} is the momentum operator and V is the nuclear potential. In Dirac theory the particles can have positive and negative energies and the energy-spectrum contains the bound states in between a positive and a negative energy continuum. In this thesis we only consider the positive states for the electrons. In that case the upper two components of the wavefunction are much larger than the lower two components (these are largest for negative energy states), and therefore the components are denoted as the large (ψ_L) and small (ψ_S) components.

In non-relativistic one-electron atomic theory the orbital angular momentum operators L^2 and L_z are constants of the motion, and the eigenfunctions of the hamiltonian are labelled by the quantum numbers l and m . The atomic Dirac hamiltonian commutes only with the total angular momentum $\mathbf{j}=\mathbf{l}+\mathbf{s}$, where \mathbf{s} is the electron spin operator. The Dirac equation describes spin-1/2 particles, which can be explicitly shown by reduction to a non-relativistic plus relativistic corrections formalism as described in Section 3.

For an electron moving in a potential V the equations for the upper (L) and lower (S) two components read, after subtracting the electron rest energy mc^2 [5]:

$$\begin{aligned} V \psi_L + c \boldsymbol{\sigma} \cdot \mathbf{p} \psi_S &= (E - mc^2) \psi_L \\ c \boldsymbol{\sigma} \cdot \mathbf{p} \psi_L + (V - 2c^2) \psi_S &= (E - mc^2) \psi_S \end{aligned} \quad (2.2)$$

where $\boldsymbol{\sigma}$ denotes the usual Pauli spin matrices, with $\boldsymbol{\sigma} = 2\mathbf{s}$. Eq. (2.2) shows that the upper and lower components are coupled by the operator $\boldsymbol{\sigma} \cdot \mathbf{p}$. The second equation can be written into the form:

$$\psi_S = \frac{\boldsymbol{\sigma} \cdot \mathbf{p}}{E + 2c^2 - V} \psi_L \quad (2.3)$$

This equation clearly shows that ψ_S is much smaller than ψ_L for positive energy states.

* In this thesis atomic units (a.u.) will be used: $e = m_e = \hbar = 4\pi\epsilon_0 = 1$. The fine-structure constant $\alpha = e^2/4\pi\epsilon_0\hbar c = 1/c$ in a.u. ($1/137$).

3. Foldy-Wouthuysen transformation of the one-electron Dirac equation

In this thesis a relativistic method is used, where the hamiltonian is obtained from a Foldy-Wouthuysen (FW) [6] transformation of the Dirac equation, which reduces the coupling between the upper and lower components of the four component wavefunction. The transformation leads to the presence of additional terms compared to the non-relativistic calculational scheme, which can be evaluated in the same way as the non-relativistic terms. Only for a free electron the FW transformation can be given in closed form, resulting in the hamiltonian $H = \sqrt{p^2c^2 + m^2c^4}$. For the general case where the potential is non-zero, we can only decouple the large and small components up to a given order by a series of FW transformations. In this thesis we use the FW transformation with the largest terms coupling L and S being reduced to order α^5 .

The result of the FW transformation applied to the one-electron atomic Dirac hamiltonian leads to the following hamiltonian for the large components, where the coupling is reduced to order α^5 [5]):

$$H_{FW} = -\frac{1}{2} p^2(1) + V_N(1) - \frac{\alpha^2}{8} p^4(1) + \frac{\alpha^2}{8} p^2 V_N(1) + \frac{\alpha^2}{4} \sigma(1) \cdot (\nabla V_N(1) \times \mathbf{p}(1)) \quad (3.1)$$

The first two terms are the usual non-relativistic kinetic energy and nuclear attraction, while the other terms are relativistic corrections. These are discussed below:

$-\frac{\alpha^2}{8} \nabla^4(1)$: the mass-velocity (MV) correction due to the relativistic mass increase. One might think that this term is only important for deep core electrons, as these move very fast. However, also valence electrons, especially s and p ones, penetrate into the core region, leading to proportionally large mass-velocity corrections for them as well. The mass-velocity correction is definite negative, and therefore leads to stabilization of orbitals. Several studies in recent years [7] showed that especially for large Z elements the use of the mass-velocity (MV) operator is not a correct procedure, as $|p|$ becomes of the order of c . However, we use the frozen core approximation in our calculations, and because the valence electrons move much slower than the speed of light, the MV-operator does not pose any problems.

$\frac{\alpha^2}{8} \nabla^2 V_N(1)$: Darwin (D) correction, which results from the fact that a relativistic electron has imposed on an average movement a highly oscillatory motion called the Zitterbewegung, of which the interaction with the nuclear potential leads to the Darwin correction. For a one-electron atom with only a nuclear potential the Darwin term leads to a delta-function centred on the nucleus, and is thus present only for s orbitals [5].

$\frac{\alpha^2}{4} \sigma(1) \cdot (\nabla V_N(1) \times \mathbf{p}(1))$: spin-orbit (SO) interaction, resulting from the coupling of the spin-magnetic moment of the electron with the magnetic field due to its own orbital

motion in the electric field due to the nucleus. For a Coulomb field it can be written as $\langle r \rangle \mathbf{I} \cdot \mathbf{s}$ with $\langle r \rangle = \frac{2}{3} Z/r^3$ [8]. For all components of a set of AOs with quantum number l the expectation values $\langle r \rangle$ are identical, and are denoted $\langle r \rangle_l$. The hamiltonian commutes only with the total angular momentum $\mathbf{j}=\mathbf{l}+\mathbf{s}$.

As we can write $\mathbf{I} \cdot \mathbf{s} = \frac{1}{2} (j^2 - l^2 - s^2)$, for orbital momentum l the values of j are $l+1/2$ at energy $l/2$, and $l-1/2$ at energy $-(l+1)/2$.

The symmetry groups of molecules with inclusion of the spin-orbit operator are the so called double groups, as twice as many operators are needed to describe the group properties. An extensive discussion of double groups is given by Snijders [9].

Contrary to the spin-orbit operator which may split and/or couple non-relativistic representations, the MV and D operators do not split the spin-orbit components of a set of MOs. Therefore these are termed scalar relativistic corrections. For example, if we have in linear symmetry degenerate p_x and p_y orbitals, the effect of the scalar relativistic operators are identical for them. The MV, D and SO corrections are called direct effects, in contrast to the indirect effects, which are due to the relativistic density changes due to the direct effects. These indirect effects are only present for many-electron systems and will be dealt with in Section 7 and 9.

4. The many-electron hamiltonian

For the many-electron case we start from the hamiltonian consisting of one-electron Dirac hamiltonians and the Coulomb operator [10]:

$$H = \sum_i h_d(i) + \sum_{i<j} \frac{1}{r_{ij}} \quad (4.1)$$

Consider a one-determinantal wavefunction. The Dirac-Fock (DF) energy expression is given by [11]:

$$E_{DF} = \sum_{1,1'} h_d(1) \rho_1(1,1') dX_1 + \frac{1}{2} \sum_{1,2} g(1,2) \rho_2(12,12) dX_1 dX_2 \quad (4.2)$$

with $g(1,2)=1/r_{12}$ and the one- and two-particle density matrices ρ_1 and ρ_2 are expressed in terms of the (four-component) Dirac orbitals, as in Hartree-Fock (HF) theory:

$$\rho_1(1,1') = \rho_1(r_1 s_1, r_1' s_1') = \sum_{i=1}^N d_i(r_1 s_1) d_i^*(r_1' s_1') \quad (4.3A)$$

$$\rho_2(12,12) = \rho_2(1) \rho_2(2) - \rho_1(1,2) \rho_1(2,1) \quad (4.3B)$$

The diagonal element $\rho_1(1,1)$ is denoted as $\rho_1(1)$ in this work. From Eq. (4.3.B), the first

part of the two-electron integral in Eq. (4.2) leads to the Coulomb energy, and the second part to the exchange energy. In the following we will use for the two-electron part of the energy densities that are integrated over the spinor indices (1..4) of the Dirac orbitals d_i , e.g. $\rho(1) = \sum_i d_i(r_1 s_1) d_i^*(r_1 s_1)$. In Density Functional theory the Coulomb/exchange integrals then only involve space coordinates r , but the density will still be denoted $\rho(1)$.

The ideal way to solve the 4-component Dirac-Fock equation is a fully numeric manner (finite difference), but this method is limited to small systems like H_2 and HeH^+ [12]. To study large systems containing heavy atoms such as actinides, approximations have to be made. A number of methods that are presently available for the study of relativistic effects have been reviewed recently by Pepper and Bursten [13]: Local Density Functional applications in the First Order Perturbation Theory and Quasi-Relativistic methods in the Amsterdam DF package [3,4,14 and this thesis] and in the Quasi-Relativistic Multiple Scattering method [15], the Relativistic Extended Hückel [16], Dirac-Fock One Centre Expansion [17], Effective Core Potential methods [18] and the so called algebraic or basis set expansion methods, with a LCAO expansion of the four component wavefunction [19,20].

In this thesis we use the Amsterdam DF program package, where the relativistic method is based on the Foldy-Wouthuysen transformation (as in Section 3) of the DF energy expression Eq. (4.2). Before discussing this, we introduce two further approximations. Firstly, we use the frozen core approximation, i.e. only the valence orbitals are optimized in the calculations, because these are responsible for chemical bonding. The total density $\rho(1,1')$ is split into core (ρ_c) and valence (ρ_v) parts:

$$\rho(1,1') = \rho_c(1,1') + \rho_v(1,1') \quad (4.4)$$

Secondly, we use a local density approximation of the exchange energy. The simplest approximation was given by Slater [21], with the exchange energy and potential given by:

$$E_X[\rho] = \frac{3}{4} \int \rho(1) V_X(\rho(1)) dr_1 \quad \text{with} \quad V_X(\rho(1)) = -3 \epsilon_x \left[\frac{3}{8} \rho(1) \right]^{\frac{1}{3}} \quad (4.5)$$

A more elaborate discussion of Density Functional (DF) theory is given in Section 5. The justification for the use of the Slater form also in the relativistic case was given by Ellis [22]. Together with using frozen cores, the local approximation leads to the Dirac-Slater (DS) energy expression:

$$E_{DS} = \int \rho_d(1) \rho_c(1,1') dX_1 + \int \rho_d(1) \rho_v(1,1') dX_1 + \frac{1}{2} \int \rho(1) V_C(\rho(1)) dr_1 + \frac{3}{4} \int \rho(1) V_X(\rho(1)) dr_1 \quad (4.6)$$

where the Coulomb potential $V_C(\mathbf{r})$ is given by: $\int \rho(\mathbf{r}_2)/r_{12} d\mathbf{r}_2$. The first term of Eq. (4.6) is the constant core part, which will be neglected from now on. Note that the Coulomb and exchange parts of Eq. (4.6) contain the total (core plus valence) density.

We now discuss the Foldy-Wouthuysen transformation of the valence density in E_{DS} to arrive at a two-component theory where the coupling between the upper and lower components of the Dirac spinors is absent to order β^5 (Section 3). The FW transformation is represented by a one-electron operator U_{FW} and relates the Dirac spinors d_i to the FW orbitals d_i^{FW} : $d_i^{FW} = U_{FW} d_i$. The density made up by the FW orbitals is denoted ρ^{FW} . For the one-electron part of Eq. (4.6) we can write:

$$\int \rho^{FW}(\mathbf{r}) d\mathbf{r} = \int \rho^{FW}(\mathbf{r}) d\mathbf{r} = \int \sum_{i=1}^N d_i^\dagger h_d d_i = \int \sum_{i=1}^N d_i^\dagger U_{FW}^{-1} U_{FW} h_d U_{FW}^{-1} U_{FW} d_i = \int \sum_{i=1}^N d_i^\dagger U_{FW} h_d U_{FW}^{-1} d_i = \int \rho^{FW}(\mathbf{r}) d\mathbf{r} \quad (4.7)$$

The transformed operator $U_{FW} h_d U_{FW}^{-1}$ is equal to the one-particle operator H_{FW} of Eq. (3.1), consisting of a non-relativistic part and relativistic corrections:

$$U_{FW} h_d U_{FW}^{-1} = h^0 + h^1 \text{ with } h^0 = -\frac{1}{2} \nabla^2(1) + V_N(1) \quad (4.8)$$

and $h^1 = -\frac{\nabla^2}{8} \nabla^2(1) + \frac{\nabla^2}{8} \nabla^2 V_N(1) + \frac{\nabla^2}{4} \boldsymbol{\sigma}(1) \cdot (\nabla V_N(1) \times \mathbf{p}(1))$

Note that here in the Darwin and spin-orbit operator only the nuclear potential occurs. This changes when the FW transformation is applied to the Coulomb/exchange part of the DS energy expression. The procedure we follow was described by Boerrigter [23]. The density can be written as:

$$\rho = \rho_c + \rho_v = \rho_c + \rho^{FW} + \rho' \text{ with } \rho' = \rho_v - \rho^{FW} \text{ being of order } \beta^2 \quad (4.9)$$

For the Coulomb part we find:

$$\frac{1}{2} \int (\rho_c + \rho_v) V_C(\mathbf{r}) d\mathbf{r} = \frac{1}{2} \int (\rho_c + \rho^{FW} + \rho') V_C(\mathbf{r}) d\mathbf{r} = \frac{1}{2} \int (\rho_c + \rho^{FW}) V_C(\mathbf{r}) d\mathbf{r} + \int \rho' V_C(\mathbf{r}) d\mathbf{r} \quad (4.10)$$

where terms of higher order than β^2 have been neglected, as these are of higher than β^2 order. The second term is rewritten by expressing $\rho_v - \rho^{FW}$ in terms of orbitals, giving:

$$\int \rho' V_C(\mathbf{r}) d\mathbf{r} = \int \sum_{i=1}^N d_i^\dagger V_C(\mathbf{r}) d_i - \int \sum_{i=1}^N d_i^{FW\dagger} V_C(\mathbf{r}) d_i^{FW} \quad (4.11)$$

The operator V_C in Eq. (4.11) is a one-electron operator, for which we can use the same procedure as for the Dirac operator h_d in Eq. (4.7). The first part of Eq. (4.11) then gives:

$$\sum_{i=1}^N d_i U_{FW}^{-1} |U_{FW} V_C(\psi_c + \psi_{FW}) U_{FW}^{-1} |U_{FW} d_i = \sum_{i=1}^N \langle i | U_{FW} V_C(\psi_c + \psi_{FW}) U_{FW}^{-1} | i \rangle \quad (4.12)$$

Because V_C is a one-electron operator, the transformed operator $U_{FW} V_C(\psi_c + \psi_{FW}) U_{FW}^{-1}$ is derived as if $V_C(\psi_c + \psi_{FW})$ were a fixed local potential. The result is [5]:

$$V_C(\psi_c + \psi_{FW}) + \frac{2}{8} \nabla^2 (V_C(\psi_c + \psi_{FW})) + \frac{2}{4} [\boldsymbol{\sigma} \cdot (\nabla (V_C(\psi_c + \psi_{FW}))) \times \mathbf{p}] \quad (4.13)$$

When we fill in this expression in Eq. (4.12) and the result of that in Eq. 4.11), the first term cancels the second term of Eq. (4.11), and this equation is equal to:

$$\int \langle i | \left[\frac{2}{8} \nabla^2 (V_C(\psi_c + \psi_{FW})) + \frac{2}{4} [\boldsymbol{\sigma} \cdot (\nabla (V_C(\psi_c + \psi_{FW}))) \times \mathbf{p}] \right] | i \rangle dr_1 \quad (4.14)$$

The terms are Darwin-like and spin-orbit corrections, with electronic potentials.

For the exchange part of E_{DS} we use a Taylor expansion around $\psi_c + \psi_{FW}$ up to the first power of ψ' :

$$V_X(\psi_c + \psi_{FW} + \psi') = V_X(\psi_c + \psi_{FW}) - 3 \epsilon_{ex} \left(\frac{3}{8}\right)^{\frac{1}{3}} \frac{1}{3} \psi' (\psi_c + \psi_{FW})^{-\frac{2}{3}} \quad (4.15)$$

Substituting Eq. (4.15) into the Exchange part of Eq. (4.6) gives:

$$\begin{aligned} \frac{3}{4} \int (\psi_c + \psi_{FW} + \psi') V_X(\psi_c + \psi_{FW} + \psi') dr_1 &= \frac{3}{4} \int (\psi_c + \psi_{FW}) V_X(\psi_c + \psi_{FW}) dr_1 + \\ \frac{3}{4} \int (\psi_c + \psi_{FW}) (-\epsilon_{ex}) \left(\frac{3}{8}\right)^{\frac{1}{3}} \frac{1}{3} \psi' (\psi_c + \psi_{FW})^{-\frac{2}{3}} dr_1 &+ \frac{3}{4} \int \psi' V_X(\psi_c + \psi_{FW}) dr_1 \end{aligned} \quad (4.16)$$

Adding the two terms on the second line gives:

$$\psi' V_X(\psi_c + \psi_{FW}) dr_1 \quad (4.17)$$

This term is treated in the same way as the Coulomb term in Eqs (4.11)-(4.13), and leads to Darwin and spin-orbit terms from the electronic exchange potential.

The final result of the FW transformation of the DS energy expression is then:

$$E_{DS}^{FW} = \int [h^0(1) + h^1(1)] \langle 1 | U_{FW} (1,1') | 1 \rangle dr_1 + \frac{1}{2} \int \rho_t(1) V_C(\psi_c) dr_1 + \frac{3}{4} \int \rho_t(1) V_X(\psi_c) dr_1 \quad (4.18)$$

where for the Coulomb and exchange energies the total density $\rho_t = \rho_c + \rho_{FW}$ is to be used.

In expression (4.18) h^0 is the non-relativistic one-electron hamiltonian as given in Eq. (4.8). The relativistic operator h^1 differs from Eq. (4.8), as now electronic potentials occur in the Darwin and spin-orbit terms:

$$h^1(1) = h_{MV} + h_D + h_{SO} \quad \text{with } h_D = \frac{2}{8} \nabla^2 (V_N(1) + V_C(\mathbf{r}) + V_X(\mathbf{r})) \quad (4.19)$$

$$h_{MV} = -\frac{2}{8} \nabla^4(1) \quad h_{SO} = \frac{2}{4} \boldsymbol{\sigma}(1) \cdot (\nabla (V_N(1) + V_C(\mathbf{r}) + V_X(\mathbf{r}))) \times \mathbf{p}(1)$$

Ziegler et al. [24] showed that the total electronic (core plus valence) potential may be neglected in the Darwin term, while for the spin-orbit term the valence part can be neglected. We will use this finding, and from now on the Darwin and spin-orbit operators are given by:

$$h_D = \frac{2}{8} \nabla^2 V_N(1) \quad \text{and } h_{SO} = \frac{2}{4} \boldsymbol{\sigma}(1) \cdot (\nabla (V_N(1) + V_C(\mathbf{r}) + V_X(\mathbf{r}))) \times \mathbf{p}(1) \quad (4.20)$$

In Sections 7 and 8 we will discuss two methods to obtain the orbitals Ψ^{FW} . These methods are implemented in the Amsterdam DF program package. First we give in the next two sections a brief description of this package.

Part II The Density Functional program package

5. Density functional theory and the non-relativistic program

The basis for Density Functional (DF) theory is the Kohn-Sham [25] theorem, stating that the ground state energy of a many-electron system is a functional of the electron density $n(\mathbf{r})$. The total non-relativistic energy of a system can then be written as:

$$E[n] = -\frac{1}{2} \int \int \frac{n(\mathbf{r}_1) n(\mathbf{r}_1')}{|\mathbf{r}_1 - \mathbf{r}_1'|} d\mathbf{r}_1 d\mathbf{r}_1' + \int n(\mathbf{r}) V_N(\mathbf{r}) d\mathbf{r} + \frac{1}{2} \int \int n(\mathbf{r}_1) V_C(\mathbf{r}_1, \mathbf{r}_2) d\mathbf{r}_1 d\mathbf{r}_2 + E_{XC}[n] \quad (5.1)$$

The first term on the second line represents the classical Coulomb energy, and $E_{XC}[n]$ is the exchange-correlation energy, of which the exact dependence on the density is not known. Neglecting correlation for the moment, the exchange energy $E_X[n]$ is written as:

$$E_X[n] = - \int \int \frac{n(\mathbf{r}_1) n(\mathbf{r}_2)}{r_{12}} d\mathbf{r}_1 d\mathbf{r}_2 \quad (5.2)$$

In this expression $\rho_x(1,2)$ is the exchange-hole around electron 1. It is defined as the difference between the conditional probability $\rho_2(12,12)/\rho(1)$ of finding an electron at X_2 when there is an electron at X_1 , and the unconditional probability $\rho(2)$. For example, when both electrons have \uparrow spin [26]:

$$\rho_x(1,2) = \frac{\rho_2(12,12)}{\rho(1)} - \rho(2) \quad (5.3)$$

with a similar formula for \downarrow -spin electrons. The integral $E_X[\rho]$ describes the correlation of electrons of the same spin. It arises as a result of the Pauli principle: electrons with the same spin try to avoid each other. Around an electron there is a Fermi-hole, because there can not be two electrons with equal spin at the same position. Note that there is no correlation between electrons of opposite spin, this is introduced by CI (HF case) or correlation functionals in DF theory. Thus $\rho_x(12,12)$ and $\rho_x(12,12)$ are zero in this approximation.

From the property that $\rho_2(12,12)$ integrated over electron 2 gives $(n-1)\rho(1)$, and $\rho(1)$ integrates to n electrons, it is shown that the Fermi-hole contains exactly one electron:

$$\int \rho_x(1,2) dr_2 = -1 \quad (5.4)$$

For DF theory to be of any use, the exchange-correlation part has to be approximated. The simplest way to do this is provided by the Slater statistical exchange approximation [21]. This was introduced as a local approximation to the non-local exchange part of the Fock operator in HF theory, leading to an exchange potential depending only on the one-electron density ρ , for which the uniform-electron-gas model was used. Using this approximation the advantage of DF theory can be seen in Eq. (5.1): There is no need to compute the numerous two-electron integrals for the exchange part: only the density is needed. This makes it an easy to use scheme for routine calculations on even large and heavy systems. The expressions for the exchange energy and exchange potential are:

$$E_X[\rho] = \frac{3}{4} \int \rho(1) V_X(\rho) dr_1 \quad \text{with} \quad V_X(\rho) = \frac{E_X}{\rho} = -3 \text{ex} \left(\frac{3}{8}\right)^{\frac{1}{3}} \rho^{-\frac{1}{3}} \quad (5.5)$$

For the more general case of unrestricted densities $\rho(\mathbf{r})$ we have [27]:

$$E_X^{\text{un}}[\rho] = \frac{3}{4} \int \rho(\mathbf{r}) V_X(\rho) dX_1 \quad \text{with} \quad V_X(\rho) = -3 \text{ex} \left(\frac{3}{4}\right)^{\frac{1}{3}} \rho^{-\frac{1}{3}} \quad (5.7)$$

The Slater exchange approximation leads to the Statistical energy expression:

$$E = -\frac{1}{2} \int \rho^2(1,1') dX_1 + \int \rho(1) V_N(1) dr_1 + \frac{1}{2} \int \frac{\rho(1)\rho(2)}{r_{12}} dr_1 dr_2 + \frac{3}{4} \int \rho(\mathbf{r}) V_X(\rho) dX_1 \quad (5.6)$$

The corresponding Hartree-Fock-Slater (HFS) one-electron equations are obtained when the statistical energy is made stable with respect to changes in the density ρ :

$$(\mathbf{h}^0(1) + V_C(1) + V_X(1)) \psi_i(1) = \epsilon_i \psi_i(1) \quad (5.8)$$

In the Amsterdam DF program package [3,4] the one-electron equations are solved by using a LCAO basis set approximation for the orbitals ψ_i , and the integrals are calculated using numerical techniques. For the evaluation of the Coulomb integrals a fitting procedure is used, to circumvent the calculation of expensive three centre integrals. The density is expressed in a set of fitfunctions f_i centred on the nuclei of the system:

$$\rho(\mathbf{r}) = \sum_i a_i f_i(\mathbf{r}) \quad \text{and} \quad V_C(\mathbf{r}_k) = \sum_i a_i \int \frac{f_i(\mathbf{r})}{|\mathbf{r} - \mathbf{r}_k|} d\mathbf{r} \quad (5.9)$$

where \mathbf{r}_k is an integration point. Note that the Coulomb potentials of the fitfunctions have to be calculated only once, all variation due to the SCF procedure is in the coefficients a_i . Now at most only two-centre Coulomb integrals have to be calculated.

The reason why the HFS method works so well is not completely understood yet, although considerable progress has been made. Tschinke and Ziegler [28] concluded that the form of the Fermi-hole function leads to the rather good performance of the HFS method. It was shown that the Fermi-hole function has its centre always on the nucleus where the reference electron is located. While this behaviour is incorrect in atomic valence tails, it has in molecular systems the effect of a better description of the dissociation of covalent bonds compared to the HF case, where the Fermi-hole extends over both nuclei. It is the explicit ρ -dependence of the exchange potential that leads to the good performance of HFS and LSD in general. The Fermi hole is in line with the combined Coulomb and Fermi holes of a Proper Dissociation function, and in this sense the HFS method contains correlation.

The way to improve HF is to add other configurations in CI, and provided the configuration space is large enough, one will eventually get to the exact (experimental) values of properties. However, in doing this the one-electron picture is lost. In DF theory this does not happen, more accurate calculations can be done by adding corrections to the exchange and correlation potentials, while keeping the one-electron picture. In recent years a large number of suggestions were made for improving the exchange-only schemes. These methods are called Local Spin Density (LSD) and all use the exchange energy and potential of Eq. (57), and differ only in the treatment of correlation, for which usually a homogeneous electron gas parametrization formula is used, e.g. Gunnarson and Lundqvist [29], Vosko-Wilk-Nusair [30]. The exchange and correlation were improved by non-local gradient corrections, due to Becke [31] for the exchange and Perdew [32]

for correlation. Stoll et al. [33] formulated a correction to remove the same-spin correlation, as the fact that this correlation was much smaller in finite systems than in the homogeneous electron gas, caused large correlation errors. Recently the Becke and Perdew potentials were included in the one-electron equations [34]. The results showed small non-local effects on bond distances, vibrational frequencies and bond energies.

LSD results for molecular properties such as bond energies, equilibrium geometries are found to be in good agreement with experiment [35], usually better than for HF theory [36], especially the behaviour for weak bonds.

6. Bond Energy analysis

An important feature of the DF program package is the way the bond energy is evaluated for the process of combining fragments into an overall system. A discussion of this method will be given here for the cases of closed and open shell fragments. The energy analysis for open shell fragments as presented here makes it possible to study the formation of pair bonds in chemistry. In Chapter 4c we will study these pair bonds in the $(\text{CN})_2$ dimers NCCN, CNCN and CNNC.

The bond energy evaluation consists of a decomposition of the bond energy in a steric part and a relaxation part, similar to the procedure suggested by Morokuma [37]. For a more elaborate discussion of the bond energy evaluation we refer to [38] and for aspects of the steric energy discussion to [39,40].

We consider the process where two fragments A and B, being atoms or molecules, combine to form an overall molecular system AB. The bond energy is defined as the energy difference between the fragments and the overall molecule AB:

$$E = E(\text{AB}) - E(\text{A}) - E(\text{B}) \quad (6.1)$$

In principle E could be evaluated by subtracting the total energies of molecule and fragments. However all these energies are large, of the order of 10^2 to 10^5 a.u., while the bond energy is usually a few tenths of an a.u. Thus an accuracy of integration of 8-10 digits must be achieved for a reasonable bond energy. This is impossible, and therefore we calculate the bond energy using the same integration grid for the molecule and fragments, subtracting in each integration point the energy terms of A and B from AB.

As already mentioned above, the method we use consists of two steps. First the steric interaction energy E^0 is calculated, which is defined as the energy difference between separate non-interacting fragments and the composite system described by the

determinantal wavefunction ψ^0 , the anti-symmetrized product of the (overlapping) fragment orbitals:

$$\psi^0 = \left| (\text{closed shells})_A (\text{closed shells})_B \psi_A \psi_B \right| \quad (6.2)$$

$$E^0 = E^0(AB) - E(A) - E(B) = \int \psi^0 |H_{AB}| \psi^0 - \int \psi_A |H_A| \psi_A - \int \psi_B |H_B| \psi_B$$

The orbitals ψ_A and ψ_B are the highest occupied valence orbitals, responsible for the bonding between the fragments. In the closed shell case these are doubly occupied, while for the pair bonding between open shell fragments they have opposite spin. In that case ψ^0 is given by:

$$\psi^0 = \left| (\text{closed shells})_A (\text{closed shells})_B \psi_A(1) \psi_B(2) \right| \quad (6.3)$$

In the steric interaction step there is no relaxation of the fragment orbitals, by which we mean that mixing of occupied and virtual orbitals is not allowed. E^0 includes the classical electrostatic energy $E_{\text{el.stat}}$ between the (unmodified) interpenetrating charge distributions of the fragments:

$$E_{\text{el.stat}} = \frac{Z_A Z_B}{R} + \frac{\int \rho_A(1) \rho_B(2)}{|r_1 - r_2|} dr_1 dr_2 + \int \rho_A(1) V_N^B dr_1 + \int \rho_B(1) V_N^A dr_1 \quad (6.4)$$

The interaction between two systems is usually repulsive at distances shorter than the equilibrium bond length R_e . One could have the idea that the classical electrostatic energy is responsible for that, but this is not the case [39]. In Eq. (6.4) the first two terms are the repulsive nucleus-nucleus and electron-electron interactions, while the last two terms are attractive interactions between the densities on one nucleus with the other nucleus. Because the interaction between penetrating charge clouds is smaller than for point charges [39], the second term decreases when A and B start to overlap, making $E_{\text{el.stat}}$ attractive. Only at very short distances the nuclear repulsion starts to dominate. Therefore the repulsive interaction found for distances shorter than R_e is caused by different effects.

We first look at the density ρ^0 belonging to ψ^0 . Suppose the fragments A and B are one-electron systems with orbitals ψ_A and ψ_B describing the densities, and suppose they have equal spins. Expanding ρ^0 gives:

$$\rho^0(1) = 2 \int |\psi^0(1,2)|^2 dX_2 = \frac{1}{1-S^2} (|\psi_A(1)|^2 + |\psi_B(1)|^2 - 2S \psi_A(1) \psi_B(1)) \quad (6.5)$$

where S is the overlap of the orbitals ψ_A and ψ_B . This shows that due to the overlap of the fragments, the density associated with ψ^0 is not just the sum of the densities of A and B,

but charge flows away from the overlap region to the nuclei. This is a consequence of the Pauli principle: electrons of the same spin are not allowed to be at the same position in space. For discussing the energy changes due to the charge flow away from the overlap region, we need the energy of Ψ^0 , which is given by:

$$E^0 = \langle \Psi^0 | T + V | \Psi^0 \rangle = \langle \Psi^0 | T | \Psi^0 \rangle + \langle \Psi^0 | V | \Psi^0 \rangle = E_{\text{kin}}^0 + E_{\text{Coul}}^0 \quad (6.6)$$

$$\text{with } T = \frac{1}{2} \sum_i \nabla_i^2 \text{ and } V = \sum_i \frac{Z_A}{|r_i - r_A|} + \sum_i \frac{Z_B}{|r_i - r_B|} + \frac{Z_A Z_B}{R} + \sum_{i < j} \frac{1}{|r_i - r_j|}$$

$$\text{and } E^0 = E_{\text{kin}}^0 + E_{\text{Coul}}^0 \text{ with } E_{\text{Coul}}^0 = E_{\text{el.stat}} + E_{\text{Coul}}^{\text{Pauli}} \quad (6.7)$$

The term E_{Coul}^0 contains the electrostatic term Eq. (6.2), because the fragments are at their molecular position. The effect of the anti-symmetry requirement for the Coulomb energy is denoted as $E_{\text{Coul}}^{\text{Pauli}}$. Van den Hoek et al. showed that E_{Coul}^0 is attractive [40]: as we noted, in Ψ^0 electrons move from the bonding region to the nuclear region with favourable potential. Together with the attractive $E_{\text{el.stat}}$ the term E_{Coul}^0 is attractive. The repulsion found in E^0 is thus caused by the term E_{kin}^0 . This has been rationalized as follows in [39,40]: The flow of charge away from the bonding region leads to an increase in density gradient norm, which means a larger kinetic energy.

This rise in kinetic energy dominates not only the short distance behaviour of the steric interaction, but makes the steric interaction repulsive for all distances. As we saw this is ultimately a result of the Pauli principle in Ψ^0 . Therefore we denote the effect of anti-symmetrizing, the sum of $E_{\text{Coul}}^{\text{Pauli}}$ and E_{kin}^0 as the Pauli, or overlap, or exchange repulsion E_{Pauli} , giving for E^0 :

$$E^0 = E_{\text{el.stat}} + E_{\text{Pauli}} \quad (6.8)$$

The steric interaction is also called the steric repulsion, which is familiar when closed shells as bond orbitals overlap [41]. But steric repulsion also arises when valence orbitals of one fragment overlap with deeper lying sub-valence closed shells on the other fragment.

In principle the fragment orbitals are overlapping (i.e. non-orthogonal), and thus in calculating the energy the usual Slater-Condon rules can not be used. However, the energy of a Slater determinant is unchanged if a linear transformation is done of the orbitals. Therefore, if we transform to orthogonal orbitals, we can use the usual Slater-Condon rules for the energy-evaluation for Ψ^0 . This is the procedure we follow for the calculation of E^0 . The density is then simply the sum of the orbital densities and is identical to that from Eq. (6.5).

For the open shell case, we must realise that ψ_A is orthogonal on ψ_B on account of the spin-orthogonality, so there is only a Pauli repulsion from the orthogonality requirement of ψ_A on the closed shells of fragment B, and ψ_B on the closed shells of A, more precisely only the same spin orbitals in the closed shells.

The second step in the bond energy analysis is the relaxation of ψ^0 to the final SCF wavefunction ψ_{SCF} , yielding the orbital interaction energy E_{oi} . For the closed shell fragments case E_{oi} consists of the admixing of the virtual orbitals, including the charge transfer (between different atoms) and polarization (on the same atoms) interactions. In Fig. 1 the various steps of the bond energy analysis are indicated. The destabilizing E^0 and attractive orbital interaction are given at the left for closed shell fragments.

In the open shell fragments case, E_{oi} would in addition to the charge transfer and polarization energies, also contain the energy lowering connected to the formation of the electron pair bond. It is therefore useful to consider separately, as a second step in the energy analysis, the pair bond formation. We consider as the pair bond wavefunction:

$$\psi_{pb}^0 = \left| (\text{closed shells})_A (\text{closed shells})_B (\psi_A + \psi_B)^2 \right| \quad (6.9)$$

The only difference with ψ^0 is that now the electrons from ψ_A and ψ_B have been allowed to pair up in the bonding ψ_{A+B} molecular orbital (assuming equal mixings here). The energy contribution of the electron pair bond is defined as $E_{pb} = E_{pb}^0 - E^0$ (see Fig. 1). An alternative definition of the pair bond energy would of course correspond to the valence bond wavefunction in which ψ^0 (cf. Eq. (6.3)) is combined with the determinant in which the spins are exchanged: $|\psi_A(1)\psi_B(2)|$. The VB wavefunction does give a somewhat lower energy in the case of H_2 , but it is well known [26] that the interpretation of the bonding is not really different in the VB and MO cases: the energy lowering upon bond formation in either the VB or the MO description is caused by the resonance integral (resp. hopping integral, interaction matrix element) $\psi_A |h^{eff}| \psi_B$.

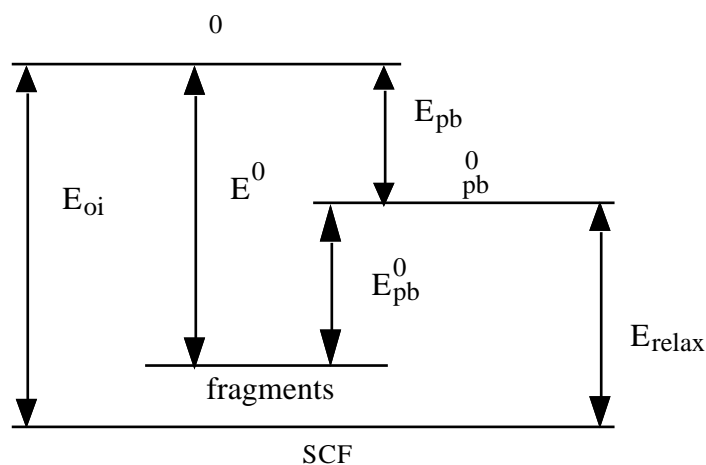


Figure 1. Diagram of the relation between the various energy changes used in the bond energy analysis.

We use the MO wavefunction for the electron pair bond in this work. Note that Ψ_{pb}^0 still contains, apart from the electrostatic interaction energy, the Pauli repulsion between the closed shells, now including the $(A+B)^2$ shell.

The wavefunction Ψ_{pb}^0 not only contains the 'pure' pair bond formation energy but also a repulsive effect between $A+B$ and the occupied closed shells on the fragments. This can be illustrated by the case of NCCN, which will be discussed extensively in Chapter 4c. We only consider σ symmetry here, where the bond orbitals are the 5 singly occupied orbitals of the CN fragments, and the closed shells are the 4 orbitals. In Fig. 2 the various steps of the bond energy analysis are indicated.

The steric energy accompanying the formation of Ψ^0 consists mainly of the 4-electron two-orbital destabilizing interaction between the CN 4s, leading to a stabilized bonding and destabilized antibonding orbital, where the antibonding orbital is more destabilized than the bonding one is stabilized. The 5 orbitals are somewhat destabilized due to the orthogonality requirement on the closed shells.

The second step consists of the formation of Ψ_{pb}^0 , containing the doubly occupied bonding orbital 5_A+5_B , which yields the energy lowering E_{pb} . Conceptually we may consider the change from Ψ^0 to Ψ_{pb}^0 to occur via the formation of the strongly stabilized 5_A+5_B orbital (cf. the gray levels in Fig. 2), which is subsequently destabilized by a

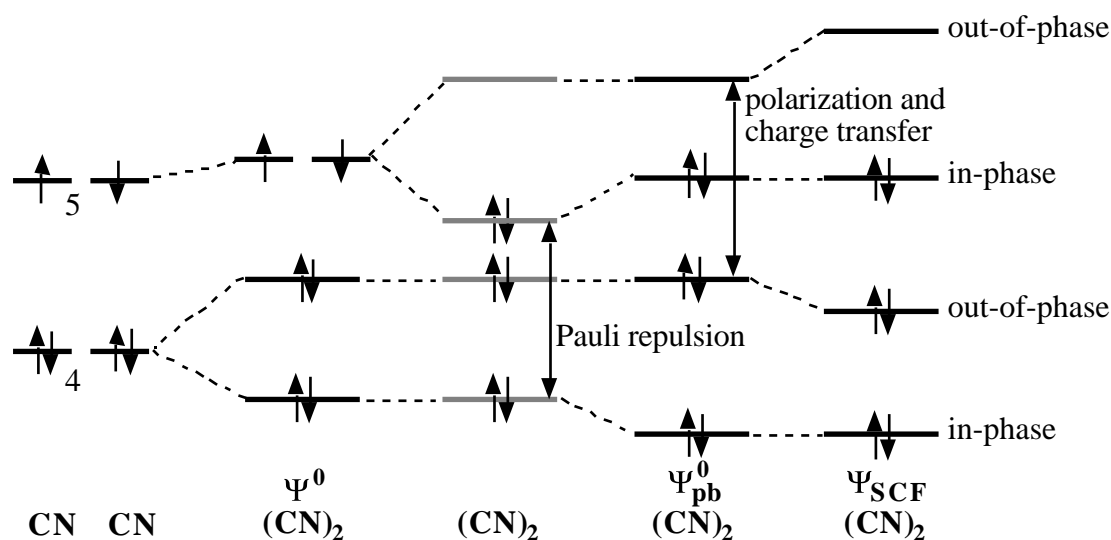


Figure 2. Orbital interaction diagram for σ -symmetry, representing the interaction between the CN 4σ and 5σ fragment orbitals. The first step, formation of Ψ^0 , corresponds to the steric interaction (ΔE^0). The next step, drawn in gray, corresponds to the formation of the 'pure' pair-bond, i.e. the fictitious situation of forming $5\sigma+5\sigma'$ without the Pauli repulsion with the $4\sigma+4\sigma'$ (and $3\sigma+3\sigma'$ etc.) in-phase combinations. Going from Ψ^0 to Ψ_{pb}^0 represents the formation of the pair bond (ΔE_{pb}) including this Pauli repulsion. In the final step, the wavefunction Ψ_{pb}^0 is allowed to relax to the SCF solution Ψ_{SCF} by the admixture of virtual orbitals, yielding ΔE_{relax} .

4-electron repulsive interaction with the occupied 4_{A+4_B} orbital. Although one cannot associate unambiguously a wavefunction with the situation depicted in gray in Fig. 2, it will nevertheless be useful to keep in mind that the total E_{pb} contains also the above mentioned repulsive effect.

In the third step, the virtual orbitals are allowed to mix in, leading to E_{SCF} . This step includes the charge transfer and polarization contributions, that relax the steric repulsion. The energy change is denoted as E_{relax} . In Fig. 1 this step is illustrated. In the case of NCCN (Fig. 2) discussed above, the relaxation consists of the mixing of the virtual orbital 5_{A-5_B} with 4_{A-4_B} . From this it is clear that it is not possible to separate effects such as charge transfer, polarization and relieve of Pauli repulsion. The Pauli repulsion that exhibits itself in the formation of the occupied antibonding combination 4_{A-4_B} is relieved by admixture of 5_{A-5_B} , which similarly leads to occupation of 5 and electron depletion from 4. But electron transfer from 4 to 5 on one fragment may also be termed polarization. We therefore consider these interactions collectively as 'relaxation energy' or (including the electron pair bond) as 'orbital interaction energy'.

We now discuss the calculation of the orbital interaction energy (The same procedure holds for the relaxation energy of open shell fragments). It may be written as:

$$E_{oi} = \int_{E(0)}^{E(SCF)} dE \quad (6.10)$$

If all terms in the energy expression were linearly dependent on the density, this integral could be written in terms of the density and density matrices, and a symmetry decomposition would be straightforward. However the exchange part is non-linear, depending on the 4/3 power of the density, and thus an approximation is needed.

Ziegler [42] developed a method for a symmetry decomposition of E_{oi} , which uses a Taylor expansion of the energy expression around the density halfway between 0 and SCF , the so called Transition State density $TS = 1/2 (0 + SCF)$. In that way the exchange terms are made linear. We will present a different approximation. The integral in Eq. (6.9) can be written in terms of the corresponding P-matrices as:

$$\int_{P^0}^{P^{SCF}} \left(\frac{\partial E}{\partial P_\mu} \right) dP_\mu \quad (6.11)$$

The path from P^0 to P^{SCF} is linearly parametrized using a parameter t which runs from 0 (P^0) to 1 (P^{SCF}). Only the t dependent term survives:

$$P_\mu(t) = P_\mu^0 + (P_\mu^{SCF} - P_\mu^0) t = P_\mu^0 + t (P_\mu^{SCF} - P_\mu^0)$$

and
$$E_{oi} = \int_{P^0}^{P^{SCF}} \left(P_\mu^0 + t (P_\mu^{SCF} - P_\mu^0) \right) \left(\frac{\partial E}{\partial P_\mu} \right) dt \quad (6.12)$$

This expression can be rewritten by expressing the density in terms of P-matrix of the basis functions as $\rho = \sum_{\mu} P_{\mu} \chi_{\mu}$. By differentiating the statistical exchange expression Eq. (5.6) with respect to P_{μ} we just get the Fock-matrix element F_{μ} (see Eq. (5.8)):

$$\frac{\partial E}{\partial P_{\mu}} = F_{\mu} = \int \chi_{\mu} |h^0 + V_C(\rho) + V_X(\rho)| \chi_{\mu} \text{ and } E_{oi} = \int_0^1 P_{\mu} F_{\mu}(t) dt \quad (6.13)$$

The integrals over h^0 and V_C are simple, because the terms are linear in ρ we get matrix elements depending on the Transition state density. The exchange part is calculated using a Simpson integration with two intervals. The final result is:

$$E_{oi} = \int_{\mu} P_{\mu} F_{\mu}^{TS}$$

with: $F_{TS}^{\mu} = \int \chi_{\mu} |h^0 + V_C(\rho^{TS}) + \frac{1}{6} V_X(\rho^0) + \frac{2}{3} V_X(\rho^{TS}) + \frac{1}{6} V_X(\rho^{SCF})| \chi_{\mu}$ (6.14)

If the basis functions are symmetry adapted, the orbital interaction can thus be symmetry decomposed. This is a very important feature of the present method, it enables e.g. the division of the interaction into bonding and backbonding contributions in Carbonyl complexes [43]. In this thesis the symmetry decomposition will be used frequently.

Finally we discuss how the steric terms are calculated. The electrostatic term $E_{el.stat}$ is calculated by analytical and numerical methods [38]. The Pauli repulsion E_{Pauli} is calculated in two steps, where one describes the energy change going from separated fragments to superimposed fragments (the fragments placed at their overall position without anti-symmetrizing), and the other represents the energy change from superimposed fragments to E^0 . For the latter step we use a method analogous to the calculation of E_{oi} , and for the first step only the change in exchange energy has to be calculated, since the other terms are part of $E_{el.stat}$:

$$E_{Pauli} = E_{Pauli}^{TS} + E_{exch} \text{ with } E_{exch} = \frac{3}{4} \int (\rho_{A+B})^{\frac{4}{3}} dX_1 - \frac{3}{4} \int (\rho_A)^{\frac{4}{3}} dX_1 \quad (6.14)$$

From this expression it is immediately clear that for E_{Pauli} it is not possible to make a symmetry decomposition, and therefore the same holds for E^0 .

7. First Order Perturbation Theory

In this section the method of First Order Perturbation Theory (FOPT) [4,24] to include relativity is described. The FW transformed DS energy expression is given in Eq. (4.18). The orbitals χ_i^{FW} are written as $\chi_i^0 + \chi_i^1$, with χ_i^0 being the non-relativistic orbital, and χ_i^1

the relativistic correction of order α^2 . The orbital energy is written as: $\epsilon_i^{FW} = \epsilon_i^0 + \epsilon_i^1$, and by expanding the orbitals the first order density $\rho_i^1(1)$ can be found:

$$FW(1,1') = \rho_i^0(1,1') + \rho_i^1(1,1') \quad (7.1)$$

$$\text{with } \rho_i^0(1,1') = \sum_i \rho_i^{*0}(1) \rho_i^0(1') \text{ and } \rho_i^1(1,1') = \sum_i (\rho_i^{*1}(1) \rho_i^0(1') + \rho_i^{*0}(1) \rho_i^1(1'))$$

Note that ρ_i^0 and ρ_i^1 denote valence densities (frozen core approximation). The total density (core plus valence) that occurs in the Coulomb/exchange potentials is written as:

$$\rho_t = \rho_c^0 + \rho_c^1 + \rho_v^0 + \rho_v^1 \quad (7.2)$$

where ρ_c denotes the difference between a DS core density and the non-relativistic core density. The exchange potential is expanded in terms of the first order density $\rho_c^1 + \rho_v^1$ by using a Taylor expansion around the non-relativistic density $\rho_c^0 + \rho_v^0$. The first order electronic potential is denoted by $V_{el}(1)$ and is given by:

$$V_{el}(1) = \int \frac{(\rho_c^1 + \rho_v^1)}{r_{12}} dr_2 - \text{ex} \left(\frac{3}{8} \right)^{\frac{1}{3}} (\rho_c^0 + \rho_v^0)^{-\frac{2}{3}} (\rho_c^1 + \rho_v^1) = \int \frac{\rho_c^1}{r_{12}} dr_2 - \text{ex} \left(\frac{3}{8} \right)^{\frac{1}{3}} (\rho_c^0 + \rho_v^0)^{-\frac{2}{3}} \rho_c^1 + \int \frac{\rho_v^1}{r_{12}} dr_2 - \text{ex} \left(\frac{3}{8} \right)^{\frac{1}{3}} (\rho_c^0 + \rho_v^0)^{-\frac{2}{3}} \rho_v^1 \quad (7.3)$$

The first order potentials are split into a constant core part $V_{el}(\rho_c)$ in the second line, and a valence part $V_{el}(\rho_v)$ in the third line.

Application of perturbation theory leads to a zeroth order equation which is just the non-relativistic equation of Eq. (5.8), while the first order equation is:

$$(\epsilon_i^0 - \epsilon_i^1) \rho_i^1 = (\epsilon_i^1 - \epsilon_i^0) \rho_i^0 \quad \text{with} \quad (7.4)$$

$$f^0 = h^0 + V_C(\rho_c^0 + \rho_v^0) + V_X(\rho_c^0 + \rho_v^0) \text{ and } f^1 = h^1 + V_{el}(1) \quad (7.5)$$

The constant core part $V_{el}(\rho_c)$ of $V_{el}(1)$ is treated as a new term in h^1 . The valence part $V_{el}(\rho_v)$ contains ρ_v^1 through ρ_v^1 (see Eq. (7.3)) and therefore Eq. (7.4) has to be solved iteratively. The first order equations are solved by expanding ρ_i^1 in terms of the orbitals ρ_i^0 . The expression for the first order change in orbital energy is:

$$\epsilon_i^1 = \epsilon_i^0 |f^1| \rho_i^0 \quad \text{with } f^1 = h_{MV} + h_D + h_{SO} + V_{el}(\rho_c) + h_{ind} \quad (7.6)$$

$$h_{MV} = -\frac{2}{8} \int \rho_i^2(1) \quad h_D = \frac{2}{8} \int \rho_i^2(V_N(1))$$

$$h_{\text{SO}} = \frac{2}{4} \sigma(1) \cdot ((V_{\text{N}}(1) + V_{\text{C}}(\frac{0}{c}) + V_{\text{X}}(\frac{0}{c})) \times \mathbf{p}(1))$$

$h^{\text{ind}} = V_{\text{el}}(\frac{1}{c})$ and $V_{\text{el}}(\frac{0}{c})$ are given in Eq. (7.3)

The operator f^1 consists of the direct relativistic effects (mass-velocity, Darwin operators and spin-orbit), the contribution from the difference between the DS and non-relativistic core densities $V_{\text{el}}(\frac{0}{c})$ and the indirect effect, due to the density change induced by the direct effect. In Section 9 we will review the main relativistic effects on AOs, and in Chapter 2 we will study their origin in detail.

The first order energy expression is found by expanding Eq. (4.18) with substitution of the densities ρ^{FW} (Eq. (7.1)) in the one-electron terms and ρ_{t} (Eq. (7.2)) in the Coulomb/exchange terms:

$$\begin{aligned} E_{\text{DS}}^{\text{FW}} = & (h^0 + h^1) (\rho^0(1,1') + \rho^1(1,1')) dX_1 + \\ & \frac{1}{2} \int \int (\rho_{\text{c}}^+ \frac{0}{c} + \rho_{\text{c}}^0 + \rho_{\text{c}}^1) V_{\text{C}}(\rho_{\text{c}}^+ \frac{0}{c} + \rho_{\text{c}}^0 + \rho_{\text{c}}^1) dr_1 + \\ & \frac{3}{4} \int \int (\rho_{\text{c}}^+ \frac{0}{c} + \rho_{\text{c}}^0 + \rho_{\text{c}}^1) V_{\text{X}}(\rho_{\text{c}}^+ \frac{0}{c} + \rho_{\text{c}}^0 + \rho_{\text{c}}^1) dr_1 \end{aligned} \quad (7.7)$$

To expand the exchange potential we use a Taylor expansion in terms of the first order density $\rho_{\text{c}}^+ \frac{1}{c}$ around the non-relativistic density $\rho_{\text{c}}^0 + \rho_{\text{c}}^0$, as was done in Eq. (7.3). The terms with only zeroth order densities constitute the non-relativistic energy (Eq. (5.6)). The terms linear in the first order densities represent the first order relativistic energy correction E^1 :

$$\begin{aligned} E^1 = & (h^0 + \frac{1}{2} V_{\text{C}}(\rho_{\text{c}}^0 + \rho_{\text{c}}^0) + \frac{3}{4} V_{\text{X}}(\rho_{\text{c}}^0 + \rho_{\text{c}}^0)) \rho^1(1,1') dX_1 + \int \int h^1 \rho^0(1,1') dX_1 + \\ & \int \int \frac{1}{2} (\rho_{\text{c}}^0 + \rho_{\text{c}}^0) V_{\text{C}}(\rho_{\text{c}}^1) dr_1 + \frac{3}{4} (\rho_{\text{c}}^0 + \rho_{\text{c}}^0) (- \epsilon_{\text{ex}}) (\frac{3}{8})^{\frac{1}{3}} \int \int (\rho_{\text{c}}^0 + \rho_{\text{c}}^0)^{\frac{2}{3}} dr_1 + \\ & \frac{1}{2} \int \int \rho_{\text{c}} V_{\text{C}}(\rho_{\text{c}}^0 + \rho_{\text{c}}^0) dr_1 + \frac{1}{2} \int \int (\rho_{\text{c}}^0 + \rho_{\text{c}}^0) V_{\text{C}}(\rho_{\text{c}}^1) dr_1 + \\ & \frac{3}{4} (\rho_{\text{c}}^0 + \rho_{\text{c}}^0) (- \epsilon_{\text{ex}}) (\frac{3}{8})^{\frac{1}{3}} \int \int \rho_{\text{c}} (\rho_{\text{c}}^0 + \rho_{\text{c}}^0)^{\frac{2}{3}} dr_1 + \frac{3}{4} \int \int \rho_{\text{c}}^0 V_{\text{X}}(\rho_{\text{c}}^0 + \rho_{\text{c}}^0) dr_1 \end{aligned} \quad (7.8)$$

The terms in the second line are both linear in ρ^1 , and they can be added to the first terms on the first line to get:

$$\int \int (h^0 + V_{\text{C}}(\rho_{\text{c}}^0 + \rho_{\text{c}}^0) + V_{\text{X}}(\rho_{\text{c}}^0 + \rho_{\text{c}}^0)) \rho^1(1,1') dX_1 \quad (7.9)$$

Expansion of ρ^1 leads to a matrix element where the operator works on ρ_i^0 , and using the fact that ρ_i^0 is a solution of the zeroth order equation, the matrix element $\langle \rho_i^1 | \rho_i^0 \rangle$ is left over. The orbitals ρ_i^0 are normalized, which leads to the relation: $\langle \rho_i^0 | \rho_i^1 \rangle + \langle \rho_i^1 | \rho_i^0 \rangle = 0$. Therefore the integral of Eq. (7.9) vanishes and does not contribute to E^1 . The terms on the third and fourth line can also be added, which finally gives for E^1 :

$$E^1 = \int \rho^1(1,1') dX_1 + \int (\rho_c^0 + \rho^0) V_C(\rho) dr_1 - \int (\rho_c^0 + \rho^0)(-ex) \left(\frac{3}{8}\right)^{\frac{1}{3}} \rho_c(\rho_c^0 + \rho^0)^{\frac{2}{3}} dr_1 \quad (7.10)$$

The first order energy correction clearly does not depend on the relativistic valence density change. The expression differs from previous studies, where only the first term was given [24]. The second and third terms result from the frozen core approximation and should also be included. Note that these terms contain the Coulomb and exchange parts of $V_{el}(\rho)$ respectively. Numerical tests with only the valence non-relativistic density instead of the sum $(\rho_c^0 + \rho^0)$ (for the exchange part the sum in front of the exchange factor), showed a small contribution to the bond energy correction, and more importantly with a flat distance behaviour. We will neglect the contribution from now on.

The first order correction to the bond energy is then [24]:

$$E^1 = \int \rho_{AB}^1 \rho_{AB}^0(1,1') dX_1 - \int \rho_A^1 \rho_A^0(1,1') dX_1 - \int \rho_B^1 \rho_B^0(1,1') dX_1 \quad (7.11)$$

The molecular non-relativistic density $\rho_{AB}^0(1,1')$ is rewritten using the definition of the deformation density $\rho_{AB}^0 = \rho_{AB}^0 - \rho_A^0 - \rho_B^0$, i.e. the density change upon molecule formation. We also make use of the fact that for the mass-velocity operator the integral of $\rho_{AB}^1 \rho_A^0$ is the same as the integral of $\rho_A^1 \rho_A^0$. For the Darwin and spin-orbit operators apart from a term containing ρ_{AB}^0 , off-diagonal terms with the density of fragment A together with the correction due to fragment B (nuclear potential for the Darwin operator and nuclear plus core potential for the spin-orbit operator) result, and also the reversed term arises.

The expression for E^1 then is:

$$E^1 = \int (\rho_{MV} + \rho_D + \rho_{SO}) \rho_{AB}^0(1,1') dX_1 + \frac{2}{8} \int (\rho_D^A + \rho_{SO}^A) \rho_B^0(1,1') dX_1 + \frac{2}{8} \int (\rho_D^B + \rho_{SO}^B) \rho_A^0(1,1') dX_1 \quad (7.12)$$

Where the second line contains the off-diagonal terms, with $\rho_D^A + \rho_{SO}^A$ meaning the fragment A corrections. In the case of closed shell molecules the contributions of the

spin-orbit operators vanish [24]. Also in practice the terms of the second line of Eq. (7.12) may be neglected compared to the first line [24].

8. Quasi-Relativistic method

In Section 7 we described the method of including relativity by means of FO Perturbation Theory. It was found that results for heavy atoms deviated much from fully relativistic DS calculations. In Table 1 the FOPT orbital energies for the typical transition metals Au, and actinide U are compared with DS values. For Au the differences are small (except for Au 6s), but for U the deviations become large.

Another method is to find the orbitals that make the energy expression E_{DS}^{FW} stable with respect to any change in the orbitals ϕ_i^{FW} due to the relativistic corrections in h^1 . Put differently, the relativistic corrections to the valence density due to the first (2) order relativistic operators are calculated variationally up to all orders. Following Bersuker and Budnikov [44] we call this the Quasi-Relativistic (QR) method. Varying the orbitals ϕ_i^{FW} in E_{DS}^{FW} (the valence potentials are absent in the Darwin and spin-orbit operators) leads to a change in density ρ^{FW} , and the energy change ΔE is given by:

$$\begin{aligned}
 \Delta E = & \int [\phi_i^0(1) + \phi_i^1(1)] \phi_i^{FW}(1,1') dX_1 + \\
 & \frac{1}{2} \int \phi_i^{FW}(1) V_C(\rho^{c+ FW}) dr_1 + \frac{1}{2} \int (\rho^{c+ FW})(1) V_C(\phi_i^{FW}) dr_1 + \\
 & \frac{3}{4} \int \phi_i^{FW}(1) V_X(\rho^{c+ FW}) dr_1 + \\
 & \frac{3}{4} \int (\rho^{c+ FW})(1) (-\epsilon_x) \left(\frac{3}{8}\right)^{\frac{1}{3}} \phi_i^{FW}(\rho^{c+ FW})^{\frac{2}{3}} dr_1
 \end{aligned} \tag{8.1}$$

where a Taylor expansion of the exchange potential was used. The Coulomb terms in the second line, and the exchange terms in the third and fourth lines can be taken together:

$$\Delta E = \int [\phi_i^0(1) + \phi_i^1(1) + V_C(\rho^{c+ FW}) + V_X(\rho^{c+ FW})] \phi_i^{FW}(1,1') dX_1 \tag{8.2}$$

We denote the orbitals and energies by ϕ_i^{QR} and ϵ_i^{QR} respectively, and the density ρ^{QR} . The one electron equations are then:

$$(\epsilon_i^0 + \epsilon_i^1 + V_C(\rho^{c+ QR}) + V_X(\rho^{c+ QR})) \phi_i^{QR} = \epsilon_i^{QR} \phi_i^{QR} \tag{8.3}$$

In this procedure the indirect relativistic effects are automatically included, whereas in FOPT the operator h^{ind} needs to be included in the one-electron equations. The densities

occurring in the Coulomb and Exchange potentials are total (core plus valence) densities, with the core part taken from atomic fully relativistic DS calculations.

In the literature there is some confusion about the term Quasi-Relativistic, because the spin-orbit operator is not always explicitly included. In our calculations we have both the scalar (MV and D) relativistic corrections, as well as the spin-orbit operator in QR calculations. The QR equations Eq. (8.3) are solved in the basis of the non-relativistic orbitals, and therefore there problems with stability are absent [4a].

A different meaning of the term QR is found in the QR Multiple Scattering method [1,15]. The QR-MS methods are based on the Cowan Griffin procedure [45], where only the scalar relativistic MV and D corrections are included, without explicit use of the spin-orbit operator. Pepper and Bursten [13] recently reviewed the QR-MS methods.

In our view these methods should be termed Scalar Relativistic. In this thesis the SR method is used frequently. It provides a very convenient way to include relativistic corrections. The procedure consists of the solution of Eq. (8.3) without the spin-orbit operator in h^1 . In this method the mass-velocity, Darwin and indirect effects can not be obtained individually. The spin-orbit correction can be obtained afterwards in the basis of the SR orbitals, leading to the same result as QR. An advantage of the SR method is that with this method also the relativistic bond energy can be divided into steric and symmetry decomposed orbital interactions as in Section 6.

The results of the QR calculations on the atoms in Table 1 show that especially for the heavy U the agreement with DS calculation is better than with FOPT. Also for the lighter Au the QR value of the 6s orbital is much better in agreement with the DS values than the FO result. These results were also found by Ziegler et al. [14]: for elements up to $Z=80$ FOPT is adequate (except for Au 6s, see Table 1), while for heavier elements one needs QR calculations for a proper description.

Table 1. Comparison between DS, FOPT and QR orbital energies (in eV).

Orbital	Non-rel	FOPT	QR	DS
Au: 6s _{1/2}	-3.67	-4.74	-5.23	-5.28
5d _{5/2}	-7.47	-5.68	-5.80	-5.70
5d _{3/2}	-7.47	-7.26	-7.27	-7.24
U: 7s _{1/2}	-2.92	-3.36	-3.62	-3.65
5f _{7/2}	-9.30	-1.90	-1.84	-1.98
5f _{5/2}	-9.30	-2.99	-2.53	-2.81
6d _{5/2}	-3.15	-1.40	-1.52	-1.46
6d _{3/2}	-3.15	-1.99	-1.96	-1.93
6p _{3/2}	-21.62	-20.34	-20.29	-20.16
6p _{1/2}	-21.62	-26.46	-27.73	-29.10
6s _{1/2}	-35.33	-43.03	-47.60	-46.80

9. Effects on atoms and bond lengths

Since the beginning of the seventies there have been many relativistic calculations on atoms and molecules. For an extensive discussion of the results of these studies we refer to excellent reviews on this subject [46-54]. In this section we will mention the most important atomic relativistic effects, and give an explanation of the contraction of the bond length that is usually found in molecules.

9.1 Atomic Relativistic effects.

The general picture for the effect of relativity on Atomic Orbitals is: s and $p_{1/2}$ orbitals are stabilized and contract, d and f orbitals are destabilized and expand, while the behaviour of $p_{3/2}$ orbitals is intermediate [55]. The spin-orbit splitting is a very important relativistic effect. It leads to a splitting of non-s orbitals. For s orbitals the mass-velocity correction dominates over the Darwin correction, while for non-s orbitals the Darwin correction is small, even when the electronic contributions are included [56].

For inner core s and p orbitals the contraction is easily explained by the relativistically increased mass [46,47]. For valence orbitals the relativistic effects can be large too [46,47,54], especially for penetrating s and p ones. The large contraction found for valence s and p orbitals can not be explained from the orthogonality constraint on the contracted core orbitals as Balasubramanian and Pitzer [57] claim, but is the result of admixture of the higher orbitals including continuum orbitals [58].

The general opinion about the indirect relativistic effect is that it leads to a destabilization of orbitals, especially d and f orbitals are severely affected. The explanation that is usually given is that the contraction of the inner orbitals causes a more effective screening of the nucleus. However, as we will show in Chapter 2 [56], the character of the indirect effect depends on the spatial properties of the orbitals concerned. A valence orbital that has a contracting or expanding core orbital completely inside, will not experience any indirect effect of this orbital. Not strongly penetrating valence orbitals (e.g. d or f) experience an indirect destabilization from contracting orbitals of similar radial extent. But relativistically expanding d or f orbitals cause an indirect stabilization, if a filled d or f shell is just inside a penetrating s or p orbital. This happens for example in Au, the expansion of the 5d causes an indirect stabilizing effect on the Au 6s. This is responsible for the large relativistic effects for Au.

The relativistic effects can be seen in Table 1, where they are largest for the heavy U: the 7s and 6p orbitals are stabilized, and the d and f orbitals are destabilized. Note that the indirect destabilization of the d and f orbitals leads to a completely different valence level

ordering in the non-relativistic ($5f < 6d < 7s$) and relativistic case ($7s < 6d < 5f$). Also the extremely large spin-orbit splitting of U 6p should be noted.

9.2. Relativistic contraction of bond lengths.

There has been much discussion concerning the relation between relativistic effects on AOs and molecular relativistic effects on the bond length. Usually the bond length contracts upon including relativity. Originally [59] it was assumed that atomic relativistic corrections would go over to molecules, e.g. a contracting 6s AO on Au would lead to and explain the relativistic contraction found for Au₂. However good agreement with experiment was obtained in Refs [15b,24,60,61] using the FO relativistic correction to the energy, which does not depend on relativistic density changes (see Eq. (7.10)). Other workers also used FOPT successfully to obtain relativistic bond length corrections [62,63]. And even in the complex U(COT)₂, where relativistically expanding orbitals as U 6d and U 5f are involved in bonding, a contraction was found [2]. Thus a relation between atomic and molecular contraction is questionable.

Before we go further into this relation, we will explain the contraction in the view of Refs [24,60,61]. In a molecular calculation the valence orbitals must be orthogonal to all core orbitals. Consider a molecule AB, consisting of an atom A with core orbital $\frac{A}{c}$ and valence orbital $\frac{A}{v}$, and an atom B with valence orbital $\frac{B}{v}$. The bonding combination of $\frac{A}{v}$ and the core-orthogonalized $\frac{B}{v}$ is then:

$$\text{bond} = c_A \frac{A}{v} + c_B \left(\frac{B}{v} - a \frac{A}{c} \right) \quad (9.1)$$

where a is the mixing coefficient of $\frac{A}{c}$ to ensure the core-valence orthogonality, determined by the overlap $\frac{A}{c} | \frac{B}{v}$. The non-relativistic density change $\frac{0}{AB}$ upon molecule formation may be split into a core-valence part $\frac{0}{cv}$, containing core-valence and core-core contributions, and a valence part $\frac{0}{v}$. The core-valence orthogonalization effects are included in $\frac{0}{cv}$. Here we only consider the situation where only the bonding combination bond is occupied. Furthermore, only the sub-valence core orbital has sufficient overlap with the valence orbital on the other atom, e.g. the Au 5s AO mixes with H 1s in AuH. When the distance between the atoms becomes shorter, the coefficient a increases due to a stronger overlap of $\frac{B}{v}$ and $\frac{A}{c}$.

It was shown that the net (steric plus orbital interaction) kinetic energy effect of molecule formation was repulsive, i.e. the kinetic energy increases, and for distances shorter than the equilibrium distance R_e increases faster than the potential energy decreases [60]. The main contribution to the repulsive kinetic energy comes from $\frac{0}{cv}$ [24]: the core orbitals (with high kinetic energy) are stronger admixed with shorter distance. This effect is known as kinetic repulsion.

The first order relativistic correction to the bond energy was given in Eq. (7.12), and only the first line was important:

$$E^1 = \int_{1,1'} (\hbar_{MV} + \hbar_D + \hbar_{SO}) \psi_{AB}^0(1,1') dX_1 \quad (9.2)$$

In previous studies closed shell molecules were considered, in which case the contribution of the spin-orbit operator in Eq. (9.2) vanishes [24]. The mass-velocity correction can be viewed as a correction to the non-relativistic kinetic energy T_{NR} , while the Darwin term can be viewed as a correction to the non-relativistic potential V_{NR} [24]. It was found that the mass-velocity correction dominates the first order energy E^1 of Eq. (9.2), and the most important part is the core-valence part from ψ_{cv}^0 [24,60]. For distances shorter than R_e the energy lowering of the mass-velocity correction becomes stronger with shorter distance, which explains the bond length contraction. One says that the mass-velocity correction reduces the kinetic repulsion. This is pictured in Fig. 3.

In the MO picture we have for ψ_{bond} :

$$\begin{aligned} \langle \psi_{bond} | \hbar_{MV} | \psi_{bond} \rangle &= c_A^2 \langle \psi_A^v | \hbar_{MV} | \psi_A^v \rangle + 2 c_A c_B \langle \psi_A^v | \hbar_{MV} | \psi_B^v \rangle + c_B^2 \langle \psi_B^v | \hbar_{MV} | \psi_B^v \rangle \\ &- 2 c_B^2 a \langle \psi_B^c | \hbar_{MV} | \psi_A^c \rangle - 2 c_A c_B a \langle \psi_A^v | \hbar_{MV} | \psi_A^c \rangle + c_B^2 a^2 \langle \psi_A^c | \hbar_{MV} | \psi_A^c \rangle \end{aligned} \quad (9.3)$$

The reduction of the kinetic repulsion arises from the diagonal core orbital contribution to the mass-velocity correction in Eq. (9.3), and the rise in the coefficient a dominates.

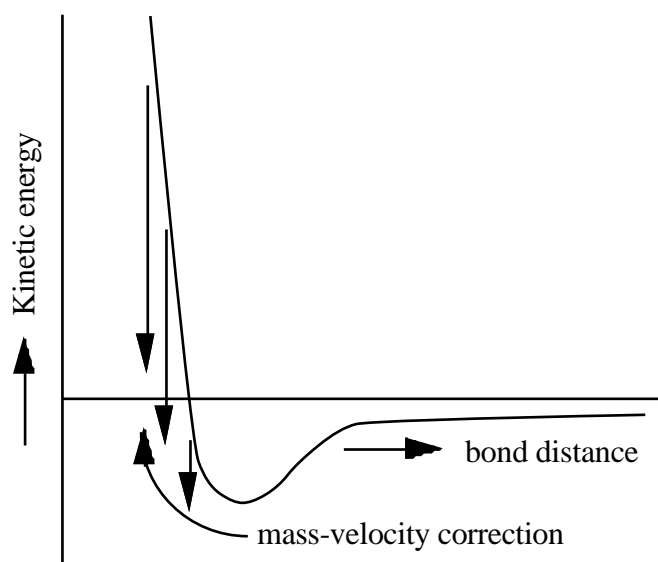


Figure 3. Kinetic repulsion and mass-velocity bond length contraction.

We now put the first order change on the bond length into a form [55], with which we are able to introduce a different view on the bond length behaviour. The relativistic energy of a diatomic molecule near the non-relativistic equilibrium distance R_e is:

$$E(R) = \frac{1}{2} k (R-R_e)^2 + E_1^{\text{rel}}(R) + \dots \quad (9.4)$$

where E_1^{rel} is given by Eq. (9.2). The minimum of the energy determines R_e^{rel} :

$$\frac{d E(R)}{dR} = 0 \quad \text{and} \quad R_e^{\text{rel}} = R_e - \frac{1}{k} \left. \frac{d E_1^{\text{rel}}}{dR} \right|_{R_e} \quad (9.5)$$

which gives for the first order relativistic bond length change:

$$R_{\text{rel}}^1 = R_e^{\text{rel}} - R_e = -\frac{1}{k} \left. \frac{d E_1^{\text{rel}}}{dR} \right|_{R_e} \quad \text{with} \quad \frac{d E_1^{\text{rel}}}{dR} = \frac{d}{dR} \langle \psi^0 | h_{\text{MV}} + h_{\text{D}^+} + h_{\text{SO}} | \psi^0 \rangle \quad (9.6)$$

where ψ^0 denotes the non-relativistic wavefunction. The dominant term in Eq. (9.6) is $\frac{d}{dR} \langle \psi^0 | h_{\text{MV}} | \psi^0 \rangle$: the distance behaviour of the mass-velocity correction, as was shown before (remember we consider closed shell molecules: no spin-orbit effects). The derivative $\frac{d E_1^{\text{rel}}}{dR}$ is usually positive at R_e . The equation can also be written as:

$$\frac{d E_1^{\text{rel}}}{dR} = \langle \psi^0 | \frac{d}{dR} (h_{\text{MV}} + h_{\text{D}^+} + h_{\text{SO}}) | \psi^0 \rangle + \left[\frac{d}{dR} \langle \psi^0 | h_{\text{MV}} + h_{\text{D}^+} + h_{\text{SO}} | \psi^0 \rangle + \text{c.c.} \right] \quad (9.7)$$

This equation consists of two terms, the first term containing the distance behaviour of $h^{\text{rel}} = (h_{\text{MV}} + h_{\text{D}^+} + h_{\text{SO}})$, to which only h_{D^+} and h_{SO} contribute, and the second term describing the effect of the R-dependence of the non-relativistic wavefunction. This term can be written into a different form using FOPT. One could view the energy as depending on two small parameters, i.e. the relativistic parameter λ^2 and $(R-R_e)$. For the distance perturbation the zeroth and first order hamiltonians are the non-relativistic Fock-operator $F^0(R_e)$ and h^{dist} (only the dV/dR contributes, leading to the Hellmann-Feynman force). For the relativistic perturbation the zeroth and first order hamiltonians are the usual non-relativistic Fock-operator F^0 and the first order hamiltonian h^{rel} . Note that for both the perturbations the zeroth order hamiltonians are identical.

The term $[\frac{d}{dR} \langle \psi^0 | \dots | \psi^0 \rangle + \text{c.c.}]$ in Eq. (9.7) has λ^2 in the operator and $(R-R_e)$ in the wavefunction. We will write it into a form where these are interchanged, establishing a relation between R_{rel}^1 and relativistic effects on AOs. This rewriting is an example of Dalgarno's interchange theorem of double perturbation theory [64]. To this end we expand the non-relativistic molecular density ψ^0 in powers of $(R-R_e)$ near R_e [23]:

$$\psi^0(R) = \psi^0(R_e) + (R-R_e) \psi^1 \text{dist} \quad (9.8)$$

where $\psi^1 \text{dist}$ denotes the first order change in the non-relativistic density due to deviation

from R_e , to be evaluated at R_e . We write for ψ_i^{dist} (see Eq. (7.1)):

$$\psi_i^{\text{dist}} = \psi_i^{0*}(R_e) \psi_i^{\text{dist}} + \text{c.c.} \quad (9.9)$$

The second part of Eq. (9.7) can then be written as:

$$2 \operatorname{Re} \frac{d}{dR} \int \psi_i^{\text{rel}} \psi_i^{0*} = \int \psi_i^{\text{rel}} \psi_i^{\text{dist}} dX_1 = \int 2 \operatorname{Re} \psi_i^{0*}(R_e) \psi_i^{\text{rel}} \psi_i^{\text{dist}} \quad (9.10)$$

This equation can be rewritten using the first order equation Eq. (7.4). We have two forms, one with the relativistic perturbation (parameter α^2 , superscript rel), and the other with the distance perturbation (parameter $(R-R_e)$, superscript dist), both with the non-relativistic density at R_e as zeroth order density. In the general case where we have two perturbations, say A and B, we have the following first order equations (cf. Eq. (7.4)):

$$(F^0 - \epsilon_0) \psi_A = (\epsilon_A - h^A - V_{CX}^A) \psi_0 \quad (9.11A)$$

$$(F^0 - \epsilon_0) \psi_B = (\epsilon_B - h^B - V_{CX}^B) \psi_0 \quad (9.11B)$$

where F^0 denotes the zeroth order Fock-operator and h^A and h^B denote the direct first order hamiltonians due to the perturbation A and B respectively, and in the same way ψ_0 is the zeroth order and ϵ_A and ϵ_B are the first order orbital energies. The terms V_{CX}^A and V_{CX}^B denote the first order Coulomb/exchange corrections, which are linear in the first order density (see Eq. (7.3)). The matrix-element in Eq. (9.10) can for the general case be written as $\int \psi_0^\dagger h^A \psi_B$, where one should note that only the direct part h^A of the perturbation A is involved.

We rewrite this matrix-element such that the perturbation B is in the hamiltonian and A in the wavefunction. This can be done by letting h^A work to the left on ψ_0 and using Eq. (9.11A) this gives:

$$\int \psi_0^\dagger h^A \psi_B = \epsilon_A \int \psi_0^\dagger \psi_B - \int \psi_0^\dagger (F^0 - \epsilon_0) \psi_B - \int \psi_0^\dagger V_{CX}^A \psi_B \quad (9.12)$$

The first term from of this equation is zero because ψ_0 and ψ_B are orthogonal, just like in the case of the relativistic perturbation (see text below Eq. (7.9)). Using Eq. (9.11B) we finally obtain:

$$\int \psi_0^\dagger h^A \psi_B = \epsilon_A \int \psi_0^\dagger h^B \psi_0 + \left[\int \psi_0^\dagger V_{CX}^B \psi_0 - \int \psi_0^\dagger V_{CX}^A \psi_B \right] \quad (9.13)$$

Therefore, apart from the first term where the two perturbations are interchanged among operator and wavefunction compared to the original expression for the matrix element, two extra terms arise due to the indirect potential effects. Applying this to the

case of interest with the relativistic and distance perturbations, we find for the matrix-element in Eq. (9.10):

$$\begin{aligned} {}^0_i(\mathbf{R}_e)|h^{\text{rel}}|_i^{\text{dist}} &= {}^{\text{rel}}_i|h^{\text{dist}}|_i^0(\mathbf{R}_e) + \\ &{}^{\text{rel}}_i|V_{\text{CX}}^{\text{dist}}|_i^0(\mathbf{R}_e) - {}^0_i(\mathbf{R}_e)|V_{\text{CX}}^{\text{rel}}|_i^{\text{dist}} \end{aligned} \quad (9.14)$$

To obtain the final expression for the second part of Eq. (9.7), we have to sum over the orbitals in Eq. (9.14). This leads to:

$$\begin{aligned} h^{\text{rel}} \int dX_1 &= h^{\text{dist}} \int dX_1 + \\ \int V_{\text{CX}}^{\text{dist}} dX_1 - \int V_{\text{CX}}^{\text{rel}} dX_1 &= h^{\text{dist}} \int dX_1 \end{aligned} \quad (9.15)$$

where we used the fact that the indirect potential terms are linear in the first order density, and therefore they cancel each other. We finally obtain the alternative expression for the first order bond length change ${}^1_{\text{rel}}\mathbf{R}$ from Eqs (9.6-9.7):

$${}^1_{\text{rel}}\mathbf{R} = -\frac{1}{k} \left(\int \frac{d}{dR} (h_{\text{MV}} + h_{\text{D}} + h_{\text{SO}}) \int dX_1 + h^{\text{dist}} \int dX_1 \right) \quad (9.16)$$

where the integral can also be written as $\int (dV/dR) \int dX_1$. This view was put forward by Schwarz [65,66]: here the second term is interpreted as the change in the Hellmann-Feynman force on the nuclei due to the relativistic density change. Note that the relativistic density includes the indirect effects, while only the direct first order hamiltonian h^{rel} is involved in the alternative expression.

In the second view there seems to be a relation between atomic and molecular relativistic effects. The relativistic density change is written as [66]:

$$= \int_{\text{atoms}}^{\text{rel}} + \int_{\text{rel}}^{\text{mol}} \quad (9.17)$$

Preliminary results [67] showed that explicit calculation of the Hellmann-Feynman force shows a dominating $\int_{\text{rel}}^{\text{mol}}$ term for Au_2 . We already mentioned that in the Actinocenes there was no causal relation between the relativistic bond length change and atomic relativistic effects. Also the diminishing bond contraction effect of including the 5d orbitals in the basis for CsH and BaH^+ was not caused by the relativistic expansion of the 5d, but resulted from a smaller core-valence mixing when the 5d orbitals are present [61]. Thus the connection between atomic and molecular relativistic effects is questionable.

We will show in Chapter 3 that contraction of the bond length is not always found. The uranyl systems UO_2^{2+} and UO_2 show a bond length expansion [55], which is not related to the relativistically expanding U 5f orbital.

References

- 1: B.E. Bursten, L.F. Rhodes and R.J. Strittmatter, *J. Am. Chem. Soc.* **111** (1989) 2758
- 2: P.M. Boerrigter, E.J. Baerends and J.G. Snijders, *Chem. Phys.* **122** (1988) 357
- 3: a) E.J. Baerends, D.E. Ellis and P. Ros, *Chem. Phys.* **2** (1973) 42
 b) E.J. Baerends and P. Ros, *Chem. Phys.* **2** (1973) 51
 c) E.J. Baerends and P. Ros, *Int. J. Quant. Chem.* **S12** (1978) 169
 d) P.M. Boerrigter, G. te Velde and E.J. Baerends, *Int. J. Quant. Chem.* **33** (1988) 87
- 4 a) J.G. Snijders and E.J. Baerends, *Mol. Phys.* **36** (1978) 1789
 b) J.G. Snijders, E.J. Baerends and P. Ros, *Mol. Phys.* **38** (1979) 1909
- 5: R.E. Moss, 'Advanced Molecular Quantum Mechanics', Chapman and Hall, London, 1973
- 6: L.L. Foldy and S.A. Wouthuysen, *Phys. Rev.* **78** (1950) 29
- 7: a) A. Farazdel, W.R. Westgate, A.M. Simas, R.P. Sagar and V.H. Smith Jr, *Int. J. Quant. Chem.* **S19** (1986) 61
 b) R.J. Buenker, P. Chandra and B.A. Hess, *Chem. Phys.* **84** (1984) 1
 c) A.J. Thakkar, *J. Chem. Phys.* **85** (1986) 4509
- 8: a) M. Blume and R.E. Watson, *Proc. Roy. Soc A* **270** (1962) 127, **271** (1963) 565
 b) M. Blume, A.J. Freeman and R.E. Watson, *Phys. Rev A* **134** (1964) 320
- 9: J.G. Snijders, Thesis, Vrije Universiteit Amsterdam, 1979
- 10: J. Sucher, *Int. J. Quant. Chem.* **25** (1984) 3
- 11: A. Szabo and N.S. Ostlund, 'Molecular Quantum Mechanics', McGraw-Hill, 1989
- 12: L. Laaksonen and I.P. Grant, *Chem. Phys. Lett.* **112** (1984) 157
- 13: M. Pepper and B.E. Bursten, *Chem. Rev.* **91** (1991) 719
- 14: T. Ziegler, V. Tschinke, E.J. Baerends, J.G. Snijders and W. Ravenek, *J. of Phys. Chem.* **86** (1989) 3050
- 15: a) J.H. Wood, M. Boring and S.B. Woodruff, *J. Chem. Phys.* **74** (1981) 5225
 b) G. Thornton, N. Edelstein, N. Rösch, R.G. Egdell and R.D. Woodwark, *J. Chem. Phys.* **70** (1979) 5218
 c) D.D. Koelling and B.N. Harmon, *J. Phys. C* **10** (1977) 3107
- 16: a) L.L. Lohr and P. Pyykkö, *Chem. Phys. Lett.* **62** (1979) 333
 b) P. Pyykkö in 'Methods in Computational Chemistry', Vol. 2, 'Relativistic Effects in Atoms and Molecules', ed. S. Wilson, Plenum Press, New York, 1988
- 17: a) J.-P. Desclaux in 'Relativistic Effects in Atoms, Molecules and Solids,' ed G.L. Malli, Plenum Press, 1983
 b) J.G. Snijders and P. Pyykkö, *Chem. Phys. Lett.* **75** (1980) 5
- 18: a) L.R. Kahn, *Int. J. Quant. Chem.* **25** (1984) 149
 b) W.C. Ermler, Y.S. Lee and K.S. Pitzer, *J. Chem. Phys.* **67** (1977) 5861

- c) P.A. Christiansen, W.C. Ermler and K.S. Pitzer, *Ann. Rev. Phys. Chem.* **36** (1985) 407
- d) W.C. Ermler, R.B. Ross and P.A. Christiansen, *Adv. Quant. Chem.* **19** (1988) 139
- 19: a) K.G. Dyall, I.P. Grant and S. Wilson, *J. Phys. B, At. Mol. Phys* **17** (1984) 493
- b) H.M. Quiney, I.P. Grant and S. Wilson, *J. Phys. B* **22** (1989) L15
- d) Y. Ishikawa, R. Baretty and R.C. Binning Jr, *Int. J. Quant. Chem.* **S19** (1986) 285
- e) Y. Ishikawa and H. Sekino, *Chem. Phys. Lett.* **165** (1990) 243
- f) Y. Ishikawa, H. Sekino and R.C. Binning Jr, *Chem. Phys. Lett.* **165** (1990) 243
- h) O. Visser, P.J.C. Aerts, D. Hegarty and W.C. Nieuwpoort, *Chem. Phys. Lett.* **134** (1987) 34
- 20: K.G. Dyall, R.R. Taylor, K. Faegri Jr. and H. Partridge, *J. Chem. Phys.* **95** (1991) 2583
- 21: J.C. Slater, *Phys. Rev.* **81** (1951) 385
- 22: D.E. Ellis, *J. Phys. B* **10** (1977) 1
- 23: P.M. Boerrigter, Thesis, Vrije Universiteit Amsterdam, 1987
- 24: T. Ziegler, J.G. Snijders and E.J. Baerends, *J. Chem. Phys.* **74** (1981) 1271
- 25: W. Kohn and L.J. Sham, *Phys. Rev.* **110** (1965) 1133
- 26: R. WeWeeny, 'Methods of Molecular Quantum Mechanics', Academic Press, London, 1989
- 27: R.G. Parr and W. Yang, 'Density-Functional Theory of Atoms and Molecules', Oxford University Press, 1989
- 28: V. Tschinke and T. Ziegler, *J. Chem. Phys.* **93** (1990) 8051
- 29: O. Gunnarson and B.I. Lundqvist, *Phys. Rev. B* **13** (1976) 4274
- 30: S.H. Vosko, L. Wilk and M. Nusair, *Can. J. Phys* **58** (1980) 1200
- 31: A.D. Becke, *Phys. Rev. A* **38** (1988) 3098
- 32: J.P. Perdew, *Phys. Rev. B* **33** (1986) 8822, **B 34** (1986) 7406 (erratum)
- 33: H. Stoll, E. Golka and H. Preus, *Theor. Chim. Acta* **55** (1980) 29
- 34: L. Fan and T. Ziegler, *J. Chem. Phys.* **94** (1991) 6057
- 35: T. Ziegler, *Chem. Rev.* **91** (1991) 651
- 36: L. Versluis and T. Ziegler, *J. Chem. Phys.* **88** (1988) 322
- 37: a) K. Morokuma, *J. Chem. Phys.* **55** (1971) 1236
- b) K. Kitaura and K. Morokuma, *Int. J. Quant. Chem.* **10** (1976) 325
- 38: E.J. Baerends, 'Bond Energy Evaluation', internal report, 1988
- 39: E.J. Baerends, to be published in 'Cluster Models for Surface and Bulk Phenomena', eds. G. Pacchioni and P.S. Bagus, Plenum Press
- 40: P.J. van den Hoek, A.W. Kleyn and E.J. Baerends, *Comments. At. Mol. Phys.* **23** (1989) 93

- 41: T.A. Albright, J.K. Burdett and M.-H. Whangbo, 'Orbital Interactions in Chemistry', Wiley Interscience, 1985
- 42: T. Ziegler and A. Rauk, *Theor. Chim. Acta* **46** (1977) 1
- 43: E.J. Baerends and A. Rozendaal, in 'The Challenge of Transition Metals and Coordination Chemistry', ed. A. Veillard, Reidel Publishing Company, 1986
- 44: I.B. Bersuker, S.S. Budnikov and B.A. Leizerov, *Int. J. Quant. Chem.* **6** (1972) 849
- 45: R.D. Cowan and D.C. Griffin, *J. Opt. Soc. Am.* **66** (1976) 1010
- 46: P. Pyykkö, *Adv. in Quant. Chem.* **11** (1978) 353
- 47: P. Pyykkö, *Chem Rev.* **88** (1988) 563
- 48: G.L. Malli, 'Relativistic Effects in Atoms, Molecules and Solids', Plenum Press, 1983
- 49: P. Pyykkö and J.-P. Desclaux, *Acc. of Chem. Research* **12** (1979) 276
- 50: P. Pyykkö, *Lecture Notes in Chemistry*, 'Relativistic Theory of Atoms and Molecules', Springer-Verlag, 1986
- 51: S. Wilson, 'Methods in Computational Chemistry', Vol. 2, 'Relativistic Effects in Atoms and Molecules', Plenum Press, 1988
- 52: W.H.E. Schwarz, in 'Theoretical Models of Chemical Bonding', Vol 2, 'The Concept of the Chemical Bond', ed. Z.B. Maksic, Springer Verlag Berlin, 1990, 593
- 53: K. Balasubramanian, *J. Phys. Chem.* **93** (1984) 6585
- 54: K.S. Pitzer, *Acc. of Chem. Research* **12** (1979) 271
- 55: E.M. van Wezenbeek, E.J. Baerends and J.G. Snijders, *Theor. Chim. Acta* **81** (1991) 139
- 56: W.H.E. Schwarz, E.M. van Wezenbeek, E.J. Baerends and J.G. Snijders, *J. Phys. B* **22** (1989) 1515
- 57: K. Balasubramanian and K.S. Pitzer, *Adv. Chem. Phys.* **67** (1987) 287
- 58: E.J. Baerends, W.H.E. Schwarz, P. Schwerdtfeger and J.G. Snijders, *J. Phys. B* **23** (1990) 3225
- 59: a) J.-P. Desclaux and P. Pyykkö, *Chem Phys. Lett.* **29** (1974) 534, **39** (1976) 300
b) P. Pyykkö and J.-P. Desclaux, *Chem Phys. Lett.* **42** (1976) 534, **50** (1977) 300
c) P. Pyykkö and J.-P. Desclaux, *Acc. Chem. Res.* **12** (1979) 276
- 60: T. Ziegler, J.G. Snijders and E.J. Baerends, in 'The Challenge of d and f Electrons', Eds R. Salahub and M.C. Zerner, American Chemical Society, Washington, 1989
- 61: P. Pyykkö, J.G. Snijders and E.J. Baerends, *Chem. Phys. Lett.* **83** (1981) 432
- 62: P.A. Christiansen and W.C. Ermler, *Mol. Phys.* **55** (1985) 1109
- 63: J. Katriel, D. Feller and E.R. Davidson, *Int. J. Quant. Chem.* **26** (1984) 489
- 64: J.O. Hirschfelder, W.B. Brown and S.T. Epstein, *Adv. Quant. Chem.* **1** (1964) 255
- 65: W.H.E. Schwarz, S.Y. Chu and F. Mark, *Mol. Phys.* **50** (1983) 603
- 66: W.H.E. Schwarz, *Phys. Scripta* **36** (1987) 453
- 67: E.M. van Wezenbeek, P.J. Nederkoorn and E.J. Baerends, in preparation

Chapter 2

The Origin of Relativistic Effects of Atomic Orbitals

Abstract

$\epsilon(R) = \int_0^R (\hat{\epsilon} - \epsilon) r^2 dr$ curves are presented for different contributions $\hat{\epsilon}$ to the energy of atomic orbitals. While all radial shells contribute about equally to the non-relativistic kinetic and potential orbital energies, there is almost perfect cancellation of these energies in the inner shells and the total energy of an orbital is nearly solely determined by its outermost shell. In contrast to this, the first-order relativistic mass-velocity, Darwin and spin-orbit energies originate from the innermost shells only, while all radial shells contribute to the so-called indirect relativistic orbital energy correction. The indirect effect is important also for s AOs except for the central columns of the periodic system, where the indirect destabilization is compensated by indirect stabilization. This explains the 'gold maximum' of relativistic corrections. The results of this work offer a rationalization of the finding that the relative relativistic corrections $\sim (Z/c)^2$ are independent of electronic shielding or principal quantum number, while the non-relativistic orbital energies are $\sim (Z_{\text{eff}}/n)^2$. Conclusions on valence-only methods are also drawn.

1. Introduction

For hydrogen like atoms the relative relativistic correction a_{μ} of property a of atomic orbital μ :

$$a_{\mu} = \frac{a_{\mu}^{\text{rel}} - a_{\mu}^0}{a_{\mu}^0} = \frac{a_{\mu}^{\text{rel}}}{a_{\mu}^{\text{rel}}} = O(Z/c)^2 \quad (1.1)$$

is usually of order $(Z/c)^2$ (e.g. for μ and r^n_{μ}), where Z is the nuclear charge. Using atomic units ($\hbar = m_e = 1$) the velocity of light is $c = 1/137$. The upper index 0 indicates non-relativistic values.

For a many-electron atom one may express the orbital energies as:

$$\epsilon_{\mu} = -0.5 \left(\frac{Z_{\mu}^{\text{eff}}}{n_{\mu}} \right)^2 \quad (1.2)$$

where n_{μ} is the main quantum number and Z_{μ}^{eff} is the effective nuclear charge felt by an electron in orbital μ . Since valence orbital energies are of the order of -0.5 a.u. and do not vary much over the periodic table, Z_{μ}^{eff} varies not more than between, say, 2 and 10. If one assumes naively that the relative relativistic correction behaves as $(Z^{\text{eff}}/c)^2$, then only a slight increase of about one order of magnitude is to be expected for the relativistic corrections to valence electron properties of heavy atoms. Surprisingly however, actual relativistic calculations showed that for inner core as well as outer valence orbitals of a given symmetry type l, j :

$$a_{\mu} = c_{lj}^a (Z/c)^2 \quad (1.3)$$

where Z is the *unshielded* nuclear charge [1]. The relative relativistic corrections are thus several orders of magnitude larger for the heaviest atoms than naively expected on the basis of the hydrogenic model. In several cases c_{lj}^a is even somewhat larger for valence orbitals than for core orbitals, for instance for s AOs of group 10 and group 11 elements (the so-called gold maximum), as found by Desclaux [1] and Pyykkö [2,3].

In general, first-order perturbation theory is very useful to estimate and explain relativistic corrections, at least at the qualitative level. The relativistic correction of the orbital energy ϵ_{μ} is given to first order by:

$$\epsilon_{\mu}^1 = \langle \mu | h^1 | \mu \rangle \quad (1.4)$$

where the relativistic first-order one-electron Hamiltonian h^1 is given by [2]:

$$h^1 = h^{\text{dir}} + h^{\text{ind}}, \quad h^{\text{dir}} = h_{\text{MV}} + h_{\text{D}} + h_{\text{SO}} \quad (1.5)$$

The direct perturbation h^{dir} consists of the mass-velocity correction h_{MV} , the Darwin potential h_{D} and the spin-orbit coupling h_{SO} , and h^{ind} is the so-called 'indirect' relativistic first-order change of the Hartree-Fock potential, due to the relativistic first-order change of the occupied AOs.

Originally it had been assumed that direct relativistic effects are important only for 'fast' electrons in inner core shells of heavy atoms. The above mentioned finding of large relativistic effects for the valence shells of heavy atoms has then often been rationalized as being due to large indirect effects caused by the inner core shells (see the references cited by Rose et al. [4]). Rose et al. [4] have shown, however, on the basis of a limited number of numerical investigations, that the direct relativistic stabilization is still large for the outer valence AOs of s and p type, and that the indirect effect is destabilizing and dominant for d and f AOs.

Since the inner tails of valence orbitals become very small, one may get the impression that the relativistic operator does not develop its effect in the innermost core region for these AOs. This presumption seems to be corroborated by the fact that relativistic pseudopotential approaches (Hafner and Schwarz [5] and Lee [6]), where one excludes the valence orbitals from the inner core region by a repulsive potential, reproduce the relativistic corrections with reasonable accuracy.

The relativistic changes of valence s and p AO properties have been interpreted (see e.g. Balasubramanian and Pitzer [7]) as originating from the orthogonality requirement on the relativistically modified orbitals. The repulsive potential in pseudopotential approaches accounts for the orthogonality constraint between the outer core orbitals and the valence AOs. Therefore it seemed plausible that the 'direct' energetic stabilization and spatial contraction of s and p valence AOs is a consequence of the orthogonality of the valence AOs on the relativistic (outer) core orbitals. There are findings, however, that should have cast some doubt on this view. Snijders and Baerends [8], Snijders et al. [9] and Ziegler et al. [10], for instance, obtain reasonable relativistic corrections in first-order valence-only calculations, where the valence orbitals are still orthogonalized on non-relativistic core orbitals. This result parallels a corresponding one by Rose et al. [4].

At this state of affairs it is desirable to clarify the mechanism of relativistic valence orbital modifications and to find out which spatial regions are most important for the action of the relativistic Hamiltonian h^1 . Thereby we will deepen the understanding of the physical mechanism of relativistic effects in atoms and molecules. Furthermore we will derive some guidelines which are important for the design of valence-only approaches for heavy-atom systems.

In Section 2 we will investigate the spatial origin of expectation values of various relativistic and non-relativistic *energy* contributions. Of course, due to Heisenberg's uncertainty principle, local contributions to momentum dependent energy terms (non-relativistic kinetic energy, mass-velocity corrections, Darwin and spin-orbit potentials) are

not defined in a strict quantum mechanical framework. For instance, the local behaviour of the integrand of a definite expectation value may be altered by applying the turn-over rule to the hermitean operators. Nevertheless, local energy contributions make sense in the semiclassical approach. Furthermore, in actual quantum mechanical calculations one has to choose a specific integral representation. It is then important to know its dominant spatial domain, both for designing a numerically stable algorithm, as well as for developing interpretational schemes for the physical rationalization and explanation of the computational results.

Our results and conclusions, as mentioned in the abstract, are worked out and summarized in Section 3.

2. The spatial origin of relativistic and non-relativistic atomic orbital energy contributions

In this Section we will present and analyse $a_{\mu}(R)$ versus R curves,

$$a_{\mu}(R) = \int_0^R \left(\int_{\mu}^* (r) \hat{a}_{\mu}(r) dr \right) r^2 dr \quad (2.1)$$

where μ is an atomic valence orbital or two-component spinor and \hat{a} is a term in the atomic non-relativistic Schrödinger HFS (H^0) or quasirelativistic Schrödinger-Pauli HFS Hamiltonian (H^{SPS}). The numerical HFS (Hartree-Fock-Slater) techniques developed in this laboratory (Baerends et al. [11], Boerrigter et al. [12]) have been applied. The conventional representation of the Pauli one-electron operator h^{dir} is given in Eqs. (2.2a - 2.4a).

$$h_{\text{MV}} = - \frac{p^4}{8c^2} \quad (2.2a)$$

$$h_{\text{D}} = \frac{V_{\text{tot}}^2}{8c^2} = \frac{\rho_{\text{tot}}}{2c^2} \quad (2.3a)$$

$$h_{\text{SO}} = \frac{(\mathbf{V}_{\text{tot}} \times \mathbf{p}) \cdot \mathbf{s}}{2c^2} \quad (2.4a)$$

where V_{tot} and ρ_{tot} is the sum of the nuclear and electronic contributions to the HFS potential and charge density. These expressions are obtained for example by applying the Foldy-Wouthuysen transformation U^{FW} to the Dirac-Slater Hamiltonian H^{DS} . Both h_{MV} and h_{D} lead to local singular $\sim 1/r$ terms at the nuclear point. Therefore they are neither very well suited for stable numerical algorithms nor for simple interpretations. For instance the Darwin potential is related to the 'Zitterbewegung' which causes a smearing of the charge in the Pauli representation of the order of the Compton wave length, $\lambda_c =$

$h/2 mc$. Therefore the expectation value $\langle h_D \rangle$ could be better rationalized if the integrand would contain some smeared out Coulomb potential instead of a local δ -term.

Instead of applying the Foldy-Wouthuysen transformation to the Hamiltonian, one could also apply it to the wave function (χ^P is the relativistic atomic spinor in the Schrödinger-Pauli representation):

$$\langle \chi^P | H^{SPS} | \chi^P \rangle = \langle \chi^P | U^{\dagger} F W^{\dagger} D S U F W^{\dagger} | \chi^P \rangle = \langle U F W^{\dagger} \chi^P | D S | U F W^{\dagger} \chi^P \rangle \quad (2.5)$$

The various terms arising in the evaluation of the rhs may be identified with the mass-velocity, Darwin and spin-orbit terms of H^{SPS} in the lhs (cf. Snijders and Pyykkö [13]), as may also be derived directly by partial integration (Snijders and Baerends [8], Snijders et al. [9]):

$$\langle \chi^P | h_{MV} | \chi^P \rangle = - \frac{p^2 \langle \chi^P | p^2 | \chi^P \rangle}{8c^2} \quad (2.2b)$$

$$\langle \chi^P | h_D | \chi^P \rangle = \frac{\langle \chi^P | \nabla^2 | \chi^P \rangle - \langle \chi^P | \nabla^2 | \chi^P \rangle}{4c^2} \quad (2.3b)$$

$$\langle \chi^P | h_{SO} | \chi^P \rangle = \frac{i \times \langle \chi^P | \nabla | \chi^P \rangle}{4c^2} \quad (2.4b)$$

In Eqs. (2.2c-2.4d) we have explicitly written out the lhs and rhs of Eqs. (2.2b-2.4b) for the 1s and $2p_{1/2}$ states of hydrogenic atoms with nuclear charge Z . In the middle of Eqs. (2.2c-2.4d) the unique common numerical value of the lhs and rhs integrals is given. Note that the spin-orbit terms is zero for the 1s state.

$$\begin{aligned} 1s \quad \frac{1}{8c^2} \int dr \quad {}_{1s}(r) \left(-8 \frac{Z}{r} + \frac{4Z^3}{r} - Z^4 \right) &= - \frac{5Z^4}{8c^2} \\ &= \frac{1}{8c^2} \int dr \quad {}_{1s}(r) \left(-\frac{4Z^2}{r^2} + \frac{4Z^3}{r} - Z^4 \right) \quad (2.2c) \end{aligned}$$

$$\frac{1}{8c^2} \int dr \quad {}_{1s}(r) \left(-4 \frac{Z}{r} \right) = \frac{4Z^4}{8c^2} = \frac{1}{8c^2} \int dr \quad {}_{1s}(r) \left(\frac{4Z^2}{r^2} - \frac{4Z^3}{r} \right) \quad (2.3c)$$

$$\begin{aligned} 2p_{1/2} \quad \frac{1}{8c^2} \int dr \quad {}_{2p}(r) \left(-\frac{4Z}{r^3} - \frac{2Z^2}{r^2} + \frac{Z^3}{r} - \frac{Z^4}{16} \right) &= - \frac{7Z^4}{384c^2} \\ &= \frac{1}{8c^2} \int dr \quad {}_{2p}(r) \left(-\frac{4Z^2}{r^2} + \frac{Z^3}{r} - \frac{Z^4}{16} \right) \quad (2.2d) \end{aligned}$$

$$\frac{1}{8c^2} \int dr \quad {}_{2p}(r) \left(4 \frac{Z}{r} \right) = 0 = \frac{1}{8c^2} \int dr \quad {}_{2p}(r) \left(-\frac{4Z}{r^3} + \frac{6Z^2}{r^2} - \frac{Z^3}{r} \right) \quad (2.3d)$$

$$\frac{1}{8c^2} \int dr \quad {}_{2p}(r) \left(-\frac{4Z}{r^3} \right) = - \frac{Z^4}{48c^2} = \frac{1}{8c^2} \int dr \quad {}_{2p}(r) \left(-\frac{12Z}{r^3} + \frac{4Z^2}{r^2} \right) \quad (2.4d)$$

where $\rho(r)$ is the non-relativistic radial density.

Concerning the mass-velocity and Darwin corrections, Eqs. (2.2, 2.3), the right hand sides contain less local and less singular integrands, for instance, inverse powers of r instead of $1/r$. The dominant contributions to the integral now come from a sphere with radius of order $1/Z$ around the nucleus. The strong cancellation of the mass-velocity and Darwin contributions in the immediate vicinity of the nucleus becomes especially apparent on the rhs of Eqs. (2.2c, 2.3c). A characteristic of the mass-velocity, Darwin and spin-orbit integrands on the rhs is their *oscillatory behaviour*.

We have determined a series of $a_\mu(R)$ curves for different atomic orbitals of a series of heavy atoms using the rhs expression of Eqs. (2.2b-2.4b). A representative selection is presented in Figs. 1-4.

2.1 Non-relativistic energies

All non-relativistic potential (V), kinetic (T) and total orbital energy (E) curves are similar to those of the U 7s AO in Fig. 1a/b, or of the U 5f AO in Fig. 2d. The staircase like structure in Fig. 1a reflects the nodal structure of the 7s orbital: near its nodes the orbital density is very small, resulting in nearly stationary energy curves. All the orbitals of an atom have their radial nodes at nearly coinciding places. The common orbital node structure causes the overall atomic spatial shell structure. In the following we will denote these *spatial* shells by the letters K, L, M, ... which are usually used to specify the energetic levels. In this sense a 3s-valence AO 'consists' of a K-, L- and M-shell; a 3p-valence AO consists of a L- and a M-shell, etc.

Our first observation is (see Figs. 1a, 2d) that each shell i contributes a similar amount V_i , T_i to the potential and to the kinetic orbital energy (i.e. comparable height of all steps). On the other hand, about 90% of the *total* orbital energy is due to the outermost shell, the penultimate shell contributing still several %. Because of:

$$E_\mu(R) = \int_0^R \left(\frac{1}{2} \mu^*(r) H^{SPS} \mu(r) \right) r^2 dr = E_\mu \int_0^R \mu^2(r) 4 r^2 dr = E_\mu P_\mu(r) \quad (2.6)$$

the total orbital energy curve $E(R)$ is proportional to the integrated orbital density curve $P(R)$ (see Fig. 1b), the factor being the orbital energy E_μ . We have found that the density contribution of each innermore shell to the total orbital charge decreases by a factor of about 6 to 10. V -curves are shown too, in Figs. 1a, 1b and 2d. Because the density contribution of the inner tail of an orbital is so small, the corresponding contribution to the total orbital energy is also very small and nearly complete cancellation of potential and kinetic energy (which are individually not small) must happen in the core. This is also implied by the Schrödinger equation, since for valence orbitals the orbital energy E is small in comparison to the potential V in the core region:

$$\frac{T}{V} + 1 = \frac{H}{V} = \frac{E}{V} \quad 0 \text{ inside the core} \quad (2.7)$$

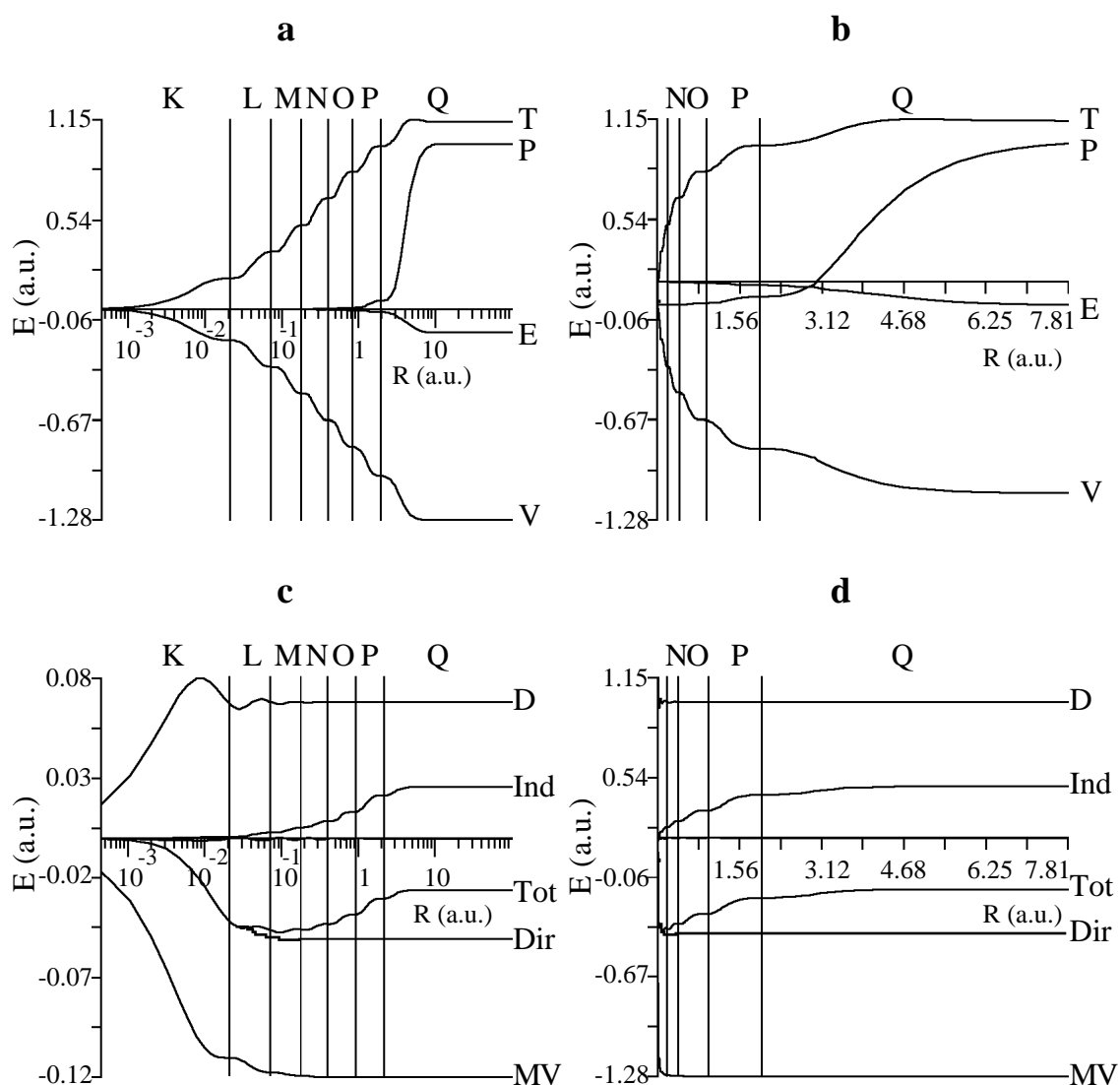


Figure 1. Radially integrated contributions to the orbital energy (see Equation 2.1) of the 7s-AO of U. a) and c): logarithmic R-scale; b) and d): linear R-scale. D, Darwin energy; Dir, direct relativistic energy (sum of Darwin and mass-velocity corrections); E, non-relativistic energy; Ind, indirect relativistic energy; P, integrated orbital density; T, non-relativistic kinetic energy; Tot, sum of direct and indirect relativistic contributions (without spin-orbit term); V, potential energy (nuclear, electronic Coulomb and exchange contributions); MV, mass-velocity correction.

The plot with linear R-scale in Fig. 1b nicely demonstrates that the kinetic and potential energies are 'generated' in the core domain, while the valence region is 'responsible' for the total energy. An interesting quantity is the virial ratio γ , defined as $\gamma = -V/T$. For hydrogenic states $\gamma = 2$. For the individual contributions of spatial shells i of heavy atoms

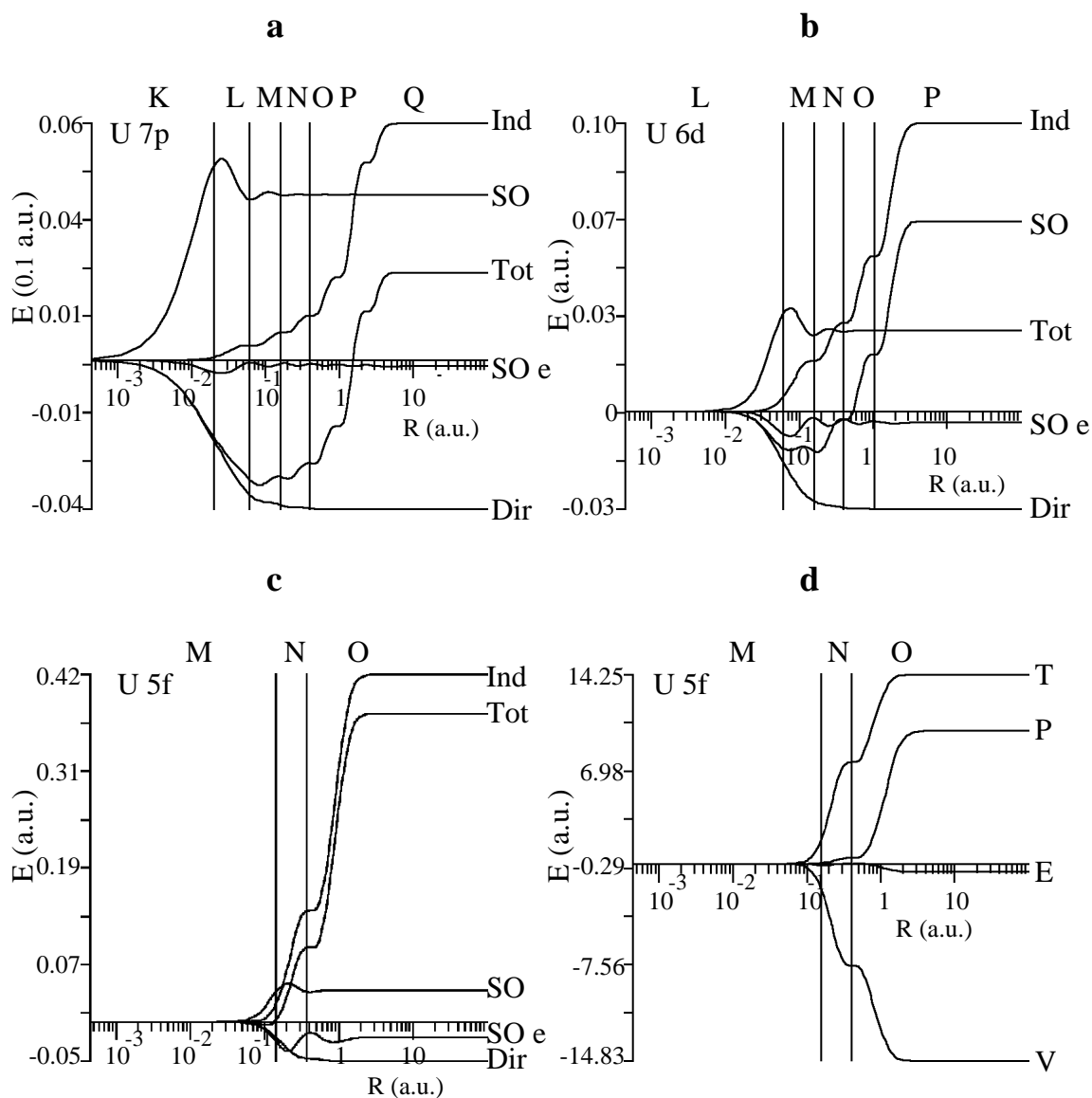


Figure 2. Radially integrated contributions to the orbital energies of the 7p-, 6d- and 5f- AOs of U over a logarithmic R-scale. Details: see Fig.1. SO, spin-orbit splitting; SO e, electronic contribution to the spin-orbit splitting.

we have $T_i - V_i = \text{const}$, where const is the average common step height of the T and V curves. The virial ratio of valence orbitals of heavy atoms is therefore:

$$= -\frac{V}{T} = -\frac{V_i}{T_i} = 1 \quad (2.8)$$

For the heavier elements, we obtained [1.0, 1.2].

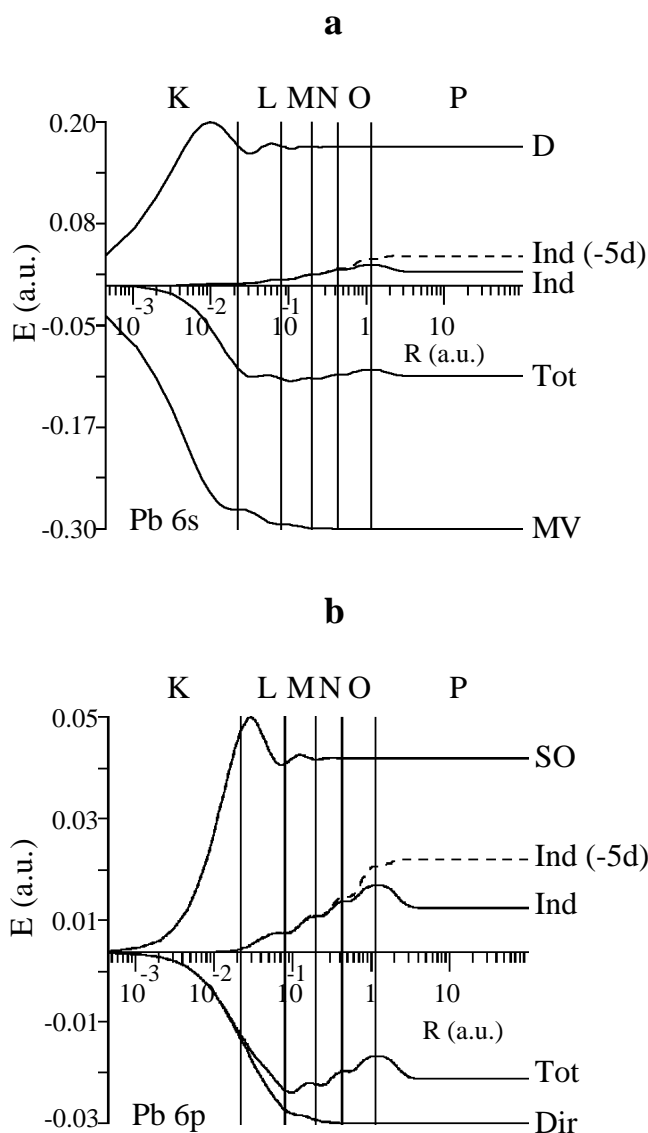


Figure 3. Radially integrated contributions to the orbital energies of the 6s and 6p AOs of Pb. Details: see Fig. 1 SO, spin-orbit splitting, Ind(-5d) = indirect relativistic energy without the contribution from the 5d¹⁰ shell.

2.2 Darwin energies

Contributions to the Darwin energy (D) from the *electronic* potential are negligible in comparison to the Darwin energies from the *nuclear* potential and to the other relativistic energy corrections; they are not plotted explicitly in the Figures. From expression (2.3a) it then follows that only the nuclear Darwin effect of s orbitals plays a role. In representation (2.3b, c) the dominant energy contribution stems from the inner half of the

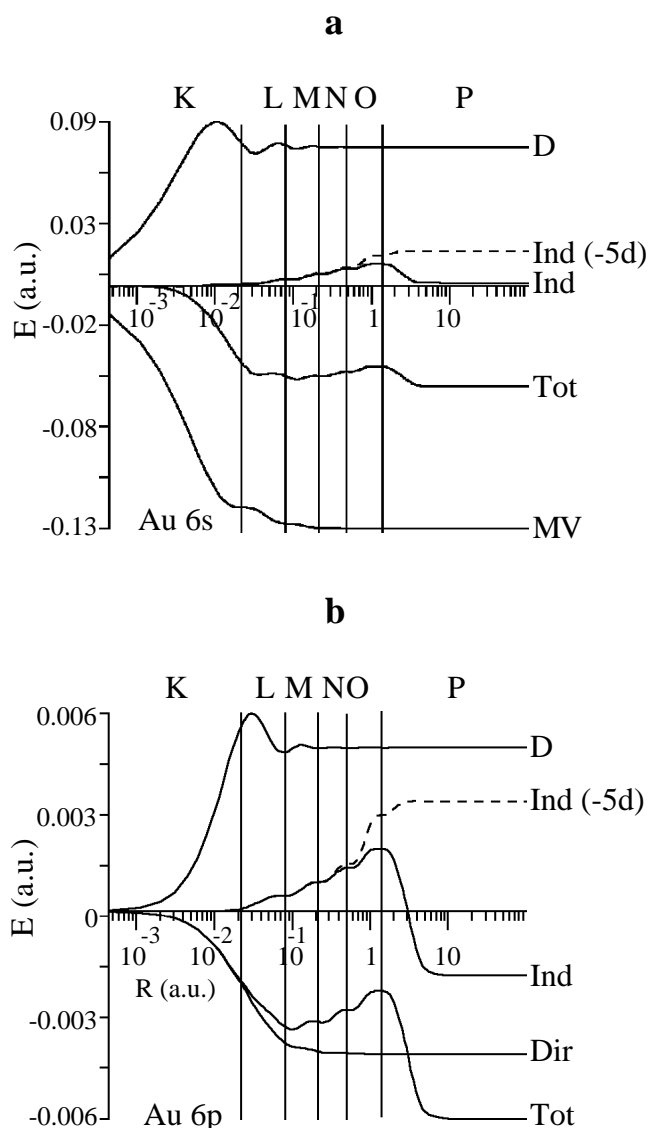


Figure 4. Radially integrated contributions to the orbital energies of the 6s- and 6p-AOs of Au. Details: see Fig. 1. SO, spin-orbit splitting, Ind(-5d) = indirect relativistic energy without the contribution from the $5d^{10}$ shell.

K-shell, while the integrand already levels off in an *oscillatory* manner in the outer part of the K- and in the L-shells (see Figs. 1c, 3a, 4a). Corresponding oscillations of the nuclear Darwin curves for $l > 0$ orbitals are not shown in the Figures, since they add up to zero. The decrease of the Darwin curves in the outer part of the K-shell is *not* due to electronic shielding, which is more than an order of magnitude weaker. The linear R-scale plot (Fig. 1d, compare with Fig. 1c) convincingly demonstrates that the Darwin effect is completely due to the immediate vicinity of the nucleus even when using representation (2.3b).

2.3 Mass-velocity corrections

Mass-velocity energies (MV) are shown in Figs. 1-4 for a series of cases. For the $l > 0$ orbitals only the sum of mass-velocity and Darwin energies, i.e. the direct relativistic effects (DIR), are shown which differ only insignificantly from the MV-contribution, since for $l > 0$ the Darwin energy is small. The dominant contributions come from the innermost shell of an orbital, and from the shell *inside* the innermost shell (i.e. from the M and N shells for f orbitals, see DIR in Fig. 2c; from the L and M shells for d orbitals, see Fig. 2b; from the K and L shells for p orbitals, see Figs. 2a, 3b, 4b; from the K shell, especially from the inner half, for s-orbitals, see Figs. 1c, 3a, 4a). A few % also originate in the second innermost shell. For s orbitals the significant nuclear Darwin effect cancels the mass-velocity effect in the vicinity of the nucleus so that the dominant contribution to the direct effect DIR stems from the *outer* half of the K shell (see Fig. 1c). Despite this cancellation, more than 80% of the direct effect of valence s AOs originate in their K shell tail, which contains only $1.5 \cdot 10^{-4}$ of the orbital density in the case of U 7s.

2.4 Spin-orbit splitting

The spin-orbit splitting (SO) of $l > 0$ orbitals shows a behaviour analogous to the Darwin energy of s orbitals: In both cases the dominant contribution stems from the *inner* tail of the innermost core shell of the valence AO. $l > 0$ -valence AOs penetrate into the shell *inside* their 'own' innermost shell. That is, the contributions come from the K shell for p AOs (see Figs. 2a, 3b and 4b), from the L shell for d AOs (see Fig. 2b) and from the M shell for f AOs (see Fig. 2c). The decrease in the innermost shell itself (i.e. L shell for p AOs, etc.) is mainly due to the oscillatory behaviour of the nuclear spin-orbit integrand (see rhs of Eq. 2.4d). The paradox that the $\mathbf{l} \cdot \mathbf{s}$ coupling decreases with increasing l is explained by the orbital densities in the vicinity of the nucleus decreasing with increasing l .

That part of the core electron density, which is outside the innermost region just discussed, where the nuclear spin-orbit coupling originates, will not shield it. This means that the electronic shielding of the spin-orbit splitting of p AOs is mainly due to the K-shell and consequently is small. Similarly, only the K and L shell density of about 10e will shield the spin-orbit splitting of d AOs. Since the 'relative shielding parameter', i.e. $10/Z$ for d AOs, decreases for increasing Z , the relative contribution of the two-electron terms to the spin-orbit splitting (SO(el)) decreases, too, e.g. from about 30% in the first transition row to about 10% in the actinide row. That is, the percentage of shielding is the larger, the larger the l value and the smaller the Z value.

2.5 Indirect relativistic effect

The relativistic change of the inner AO causes a change of electronic shielding of the nuclear attraction. This results in a change of the potential energy of the orbitals which is called the indirect relativistic effect on the orbital energy. While all three direct effects (MV, D, SO) originate in the immediate vicinity of the nucleus, in particular the outer core shells contribute to the indirect effect (see the Figures).

The indirect effect is generally identified with energetic *destabilization* due to relativistically contracted inner core orbitals. However, two things should be realized. First, the indirect effect of a core orbital on a specific valence orbital depends on their spatial characteristics (relative positions of the maxima, degree of core penetration by the valence AO). If a core orbital is completely inside the valence orbital, relativistic contraction or expansion of this core orbital will not alter the shielding. Note for instance in Figs. 2b, c the lack of indirect contributions from the innermost K or K and L shells to the d and f AO energies, respectively. In general the same shells which contribute to the non-relativistic potential energy, also contribute to the relativistic indirect orbital energy (K, L, .. shells for s AOs; L, M, .. shells for p AOs, etc.). The contributions of the various core shells however differ considerably. In particular core shells near the main maximum of the valence orbital are important. For p AOs the direct and indirect effects are of comparable magnitude, while for the non-penetrating d and in particular f AOs the indirect effects are significantly larger than the direct energy corrections. This reflects the details of the atomic shell structure. For a relatively contracted though not deeply penetrating nd AO (compared to (n+1)s, p) the semi-core ns, np AOs of similar radial extent but much lower energy exert a strong indirect effect. For instance the U 6s, 6p AOs cause a large indirect destabilization of the U 6d AO in the P shell (see Fig. 2b). The U 5f AO, although energetically well above the 6p, is radially even slightly less extended than the 6s, 6p. The relativistic contraction of the 6s, 6p shell therefore contributes strongly to the indirect destabilization of U 5f. Together with the effect of its 'own' spatial O (n=5) shell (Fig. 2c) this makes the indirect destabilization the by far dominating relativistic effect for the f AO. The 6s, 6p shell is well inside the 7s and 7p, which as a result exhibit clear but relatively small indirect destabilizations as compared to 6d and 5f indirect destabilizations (see Figs. 1c, 2a, 2b and 2c).

Secondly it should be realized that, whereas relativistically contracted s and p orbitals cause *indirect destabilization*, as is generally accepted, relativistically expanded d and f orbitals cause an *indirect stabilization*. (see Figs. 3 and 4). This indirect stabilization will be especially important, if a filled d or f shell is just inside a penetrating valence orbital. Consequently, we may distinguish the following situations. First, s and p valence orbitals at and above filled s and p shells will undergo an indirect destabilization, which counteracts the direct effect (which is always stabilizing). This will happen for the main

group elements at the beginning and end of a row of the periodic system. On the other hand, a largely filled relativistically expanded d or f shell just below the s, p valence shell (as occurs for elements from the central columns of the periodic system) will reduce (see Pb, Fig. 3), compensate (Au 6s, Fig. 4a) or even overcompensate (Au 6p, Fig. 4) the above-mentioned indirect destabilization. Consequently, elements of groups 10-12 are special because of their especially large relative relativistic stabilization of the s, p valence AOs, the direct stabilization being not reduced (Au 6s) or even strengthened (Au 6p) by the indirect effect. Going to the right in the periodic system, the 5d shell becomes more core-like and its indirect stabilizing effect diminishes. The s, p valence AOs of higher group elements therefore undergo, as has already been noted, a net indirect destabilization which is however small in comparison to the direct stabilization (see Fig. 3). To the left, for lower group elements, the d (and f) shells become partially unoccupied and their indirect stabilizing effect cannot compete with the indirect destabilization by the underlying filled s, p shell.

3. Discussion

3.1 Non-relativistic valence energies

The basic assumption of valence-only methods is that the energy of the energetically highest shells depends only on the outer spatial regions of the atoms. This is indeed fulfilled to an astonishingly high degree of accuracy. In semi-empirical and pseudopotential approaches, the combination of Hamiltonian and basis set must be tailored so that either there are no core contributions at all to T and V, or that the core-contributions to T and V just cancel, as was already presumed in early pseudopotential work (Philips and Kleinmann [14] and Abarenkov and Heine [15]). The main action of the core (and that must be simulated in semi-empirical and pseudopotential approaches) is to fix the correct phase of the wave function at the outer core boundary.

3.2 Mass-velocity, Darwin and spin-orbit energy corrections

The first-order relativistic correction energy can be calculated either in the commonly used Schrödinger-Pauli or in the standard Dirac representation. In the former case, the Schrödinger-Pauli two-component wave functions are used in combination with the Schrödinger-Pauli operator, that is the Foldy-Wouthuysen transformed Dirac operator. This operator contains the highly singular mass-velocity, spin-orbit and Darwin terms.

In the alternative representation the relativistic first-order energy is given by the standard Dirac operator and a 'first-order Dirac' wave function which is obtained by

Foldy-Wouthuysen back transformation of the Schrödinger-Pauli one. The corresponding energy expressions can be obtained from the conventional Pauli ones by partial integration, corresponding to the use of the turn-over rule for hermitean operators, and they have been used for many years by Snijders et al. [8,9]. These expressions were also used by Herman and Skillman [16] and are equivalent to Rutkowski's first-order expressions [17].

Although the integrands in this second case are less local, their largest contributions, even for valence orbitals, come from the neighbourhood of the nucleus. This can be rationalized as follows: h_{MV} matrix elements for ns-STOs vary approximately as $1/n^2$, where n is the orbital exponent. Typically, the $1/n^2$ values decrease by a factor of about 2 from one shell to the next, so that $h_{MV} \sim 2^{-4n}/n^2$. The contribution of an STO to the orbital expectation value is weighed by its squared linear-combination coefficient c_n^2 . Typically, the coefficients c increase by a factor of 2.5 to 3 from one shell to the next. Consequently, the contribution of shell n to the mass-velocity energy is expected to be of order $2.75^{2n} 2^{-4n} n^{-2} \sim 2^{-n} n^{-2}$ which decreases rapidly for increasing n .

The Darwin energy, of course, originates from the immediate vicinity of the nucleus. Although there is considerable cancellation of the relativistic kinetic and potential energy corrections (h_{MV} , and h_D , resp.), this cancellation is not as complete as that of the non-relativistic kinetic and potential energies in the whole core region. This becomes evident upon inserting the Schrödinger equation in the form $\nabla^2 \psi = 2(V-E_\mu)\psi$ into Eqs. (2.2b) and (2.3b) (Snijders and Baerends [8], Snijders et al. [9]):

$$\begin{aligned} \langle \psi_\mu | h_D | \psi_\mu \rangle &= \left[\langle \psi_\mu | \nabla^2 | \psi_\mu \rangle - E_\mu \langle \psi_\mu | \psi_\mu \rangle + \frac{1}{2} \langle \psi_\mu | \nabla^4 | \psi_\mu \rangle \right] / 2c^2 \\ \langle \psi_\mu | h_{MV} | \psi_\mu \rangle &= \left[- \langle \psi_\mu | \nabla^2 | \psi_\mu \rangle + 2E_\mu \langle \psi_\mu | \psi_\mu \rangle - \frac{1}{2} \langle \psi_\mu | \nabla^4 | \psi_\mu \rangle \right] / 2c^2 \end{aligned} \quad (4.1)$$

The nucleus-nearest contributions $\sim \nabla^2$ cancel, but terms $\sim \nabla^4$ remain:

$$\langle \psi_\mu | h_{MV} + h_D | \psi_\mu \rangle = - \frac{\langle \psi_\mu | \nabla^4 | \psi_\mu \rangle}{4c^2} \quad (4.2)$$

So, while $(T + V)$ of valence orbitals originates in the spatial valence shell, $(h_{MV} + h_D)$ of an AO originates from its innermost core wiggle.

The latter also holds for h_{SO} . Therefore, h_{SO} becomes less important for *increasing* l value. While the angular $\int \mathbf{l} \cdot \mathbf{s}$ integral increases, the radial $1/r \, dV/dr$ spin-orbit coupling factor decreases drastically, because AOs with large l value do not strongly penetrate into the deep core. In addition, only the core shells inside an AO's innermost spatial shell contribute to shielding of the nuclear spin-orbit coupling. The shielding is thus most important for the highest l orbital of given n -value and decreases relatively for increasing nuclear charge.

3.3 Indirect relativistic effects

The region between the innermost and outermost shells is important for the indirect effect. Relativistically contracted s and p core orbitals will, as is well known, increase their non-relativistic Coulomb repulsion on the valence electrons. For nonpenetrating d and f valence orbitals the *innermost core* orbitals already shield the nucleus effectively (see the shielding of the spin-orbit coupling above) and their relativistic contraction has little effect on these valence AOs. The d and f AOs are, however, also rather contracted and therefore experience a strong indirect *destabilization* (and expansion) from the relativistic contraction of the *outer s,p core* orbitals which have a similar spatial extent. As the s and p valence orbitals have their main maximum well outside the core, the effect of the outer core on them is not as strong, but due to their penetration into the inner core they experience weak destabilizing effects also from the innermost shells. Furthermore, it should be realized that relativistically expanded d and f orbitals will *stabilize* the valence orbitals, especially the penetrating s and p ones. So, while d and especially the f orbitals are in general significantly destabilized, it depends on the occupation of the inner s, p, d and f orbitals whether the indirect destabilization predominates for s and p valence AOs or whether it is compensated or even overcompensated by indirect stabilization. The nearly complete cancellation of indirect stabilization and destabilization found for the s valence AO of group 11 elements (Rose et al. [4]) should not be generalized to s valence AOs of all other atoms (Pyykkö [2]).

The direct relativistic effects increase smoothly along a periodic row for each valence orbital. The same does not hold for the indirect effect. Since d and f shells become populated in the middle of a row, i.e. *in the middle of the periodic system, there will occur a maximum of indirect stabilization of the valence s, p orbitals* at the end of the f-d series. There is in fact *a relativistic enhancement of the well-known lanthanide and transition-metal contractions* due to incomplete screening of the nucleus by filled f^{14} and d^{10} shells. This may be called the relativistic lanthanide (or transition-metal) effect. It explains the so-called 'gold maximum', i.e. the specially large relativistic corrections in group 10-12 compounds (Pyykkö [3]). The stability of the 6s AO in the central columns of the periodic system has three origins: the (non-relativistic) transition-metal and lanthanide contractions (also operative in Cu, Zn and Ag, Cd), the direct relativistic stabilization, and the indirect relativistic transition-metal and lanthanide contractions.

3.4 Relativistically corrected valence-only approaches

An accurate treatment of relativistic effects in valence-only approaches seems rather demanding, since the relativistic corrections even for valence orbitals originate in the outer and innermost core regions. h^{dir} lowers the valence orbital energy by 'pulling at the very tip of its inner core-tail' (see Pyykkö and Desclaux [18]).

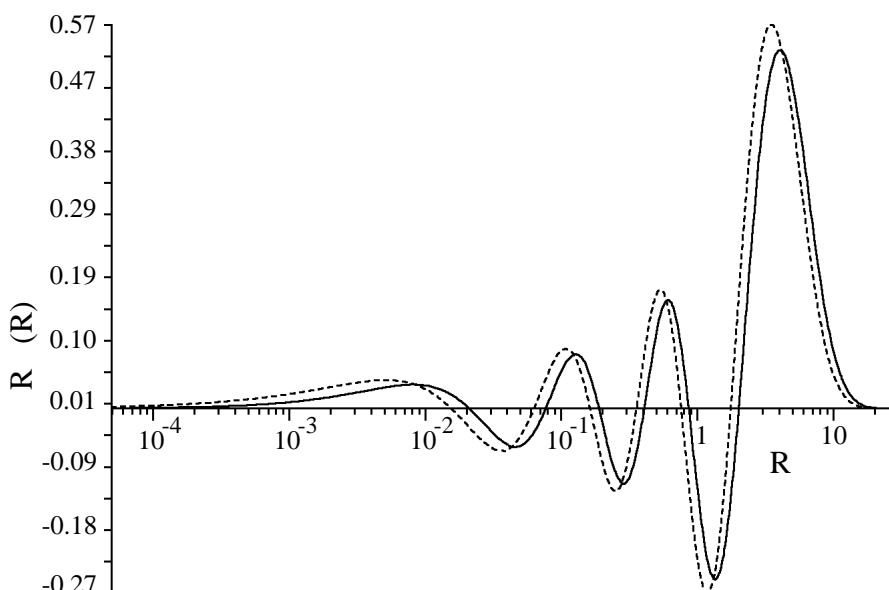


Figure 5. Radial non-relativistic and relativistic (large component) wavefunctions, multiplied by R , for $U7s$ AO. Full curve, non-relativistic; broken curve, relativistic.

In addition the slope of the relativistic wave function near the nucleus is significantly changed (Kutzelnigg [19]). Both the Dirac function as well as the Foldy-Wouthuysen transformed function behave for $r \rightarrow 0$ as r with $\gamma = \{(j+1/2)^2 - Z^2\} - 1$, where γ is smaller than the non-relativistic value l . The corresponding change of phase causes a shift of the inner nodes of the valence orbital which propagates to the outer core edge (see Fig. 5). In semi-classical terms, the relativistic change of phase at the core edge has two contributions. The one,

$$R_{\text{core}} \propto \int_{r_{\text{core}}}^r p_{\text{rel}} dr \quad \text{with}$$

$$p_{\text{rel}} = \left[2(E^{\text{rel}} - V^{\text{rel}}) + \left(\frac{E^{\text{rel}} - V^{\text{rel}}}{c} \right)^2 - \frac{l(l+1)}{r^2} \right]^{1/2} - \left[2(E^0 - V^0) - \frac{l(l+1)}{r^2} \right]^{1/2}$$

stems from the whole core region and is due to the relativistically modified energy and momentum. The other contribution results from a Maslov index relativistically modified at the Coulomb singularity, $r = 0$.

If the valence orbitals of the non-relativistic valence only approach have the usual core wiggles, as for instance in frozen core approaches (Snijders and Baerends [8], Snijders et al. [9]), then the relativistic counterpart should allow for three things:

- i) Correct phase and node shifts of the valence orbital in the core region. For instance, the basis should be chosen so that not only the outer tail of the relativistic valence orbital is correctly reproduced, but also the inner wiggles.
- ii) Correct direct correction to the Hamiltonian. We note that the first-order Pauli operator, or its equivalents, are not capable of reproducing higher order effects and are variationally unbounded. However, if one uses the Pauli operator together with a rigid core basis, one can prevent variational collapse and will exclude higher order corrections, except those ones which are related to valence shell relaxation connected to first-order relativistic energy changes. Variationally stable higher order Hamiltonian corrections have recently been proposed by Chang et al. [20], Hess [21] and Schwarz and Kissel-Phillip [22]. Some other proposals are not accurate enough (e.g. Baretty and Garcia [23]) or even variationally unstable (e.g. Miller [24]).
- iii) Correct indirect correction to the Hamiltonian (i.e. a relativistically corrected core potential). While this effect is automatically accounted for in all-electron calculations, both for the wave function and the total energy, the indirect effect of the relativistic contraction of the core must be considered explicitly in frozen core approaches.

In semi-empirical and effective core potential approaches, the valence orbitals have no (or at most a single) inner core wiggle, and practically no density at the nucleus. In this case the effective Hamiltonian (in combination with the basis) has to simulate the effects of energy shift *and* of phase shift in the outer core region. For instance, in pseudopotential approaches the repulsive core potential has to be modified so that both the orbital energy *and* spatial orbital properties are reproduced. This is done, e.g in the relativistic effective core approach of the Pitzer group (Durand and Barthelat [25], Lee et al. [26], Christiansen [27], Bachelet and Schlüter [28]).

References

- 1: J-P. Desclaux, *At. Data Nucl. Data Tables* **12** (1973) 311
- 2: P. Pyykkö, *Adv. Quantum Chem.* **11** (1978) 353
- 3: P. Pyykkö, *Chem. Rev.* **88** (1988) 563
- 4: S.J. Rose, I.P. Grant and N.C. Pyper, *J. Phys. B* **11** (1978) 1171

- 5: a) P. Hafner and W.H.E. Schwarz, *J. Phys. B* **11** (1978) 217
b) P. Hafner and W.H.E. Schwarz, *J. Phys. B* **11** (1978) 2975
- 6: Y.S. Lee, *Diss. Abstr. Int. B* **39** (1978) 772
- 7: K. Balasubramanian and K.S. Pitzer, *Adv. Chem. Phys.* **67** (1987) 287
- 8: J.G. Snijders and E.J. Baerends, *Mol. Phys.* **36** (1978) 1789
- 9: J.G. Snijders, E.J. Baerends and P. Ros, *Mol. Phys.* **38** (1979) 1909
- 10: T. Ziegler, J.G. Snijders and E.J. Baerends, *J. Chem. Phys.* **74** (1981) 1271
- 11: E.J. Baerends, D.E. Ellis and P. Ros, *Chem. Phys.* **2** (1973) 41
- 12: P.M. Boerrigter, G. te Velde and E.J. Baerends, *Int. J. Quant. Chem.* **33** (1987) 87
- 13: J.G. Snijders and P. Pyykkö, *Chem. Phys. Lett.* **75** (1980) 5
- 14: a) J.C. Phillips and L. Kleinmann, *Phys. Rev.* **116** (1959) 287
b) J.C. Phillips and L. Kleinmann, *Phys. Rev.* **116** (1959) 880
- 15: I.V. Abarenkov and V. Heine, *Phil. Mag.* **12** (1965) 529
- 16: F. Herman and S. Skillman, 'Atomic Structure Calculations', Prentice-Hall, Englewood Cliffs, N.J. 1963
- 17: a) A.W. Rutkowski, *J. Phys. B* **19** (1986) 149
b) A.W. Rutkowski, *J. Phys. B* **19** (1986) 3431
- 18: P. Pyykkö and J-P. Desclaux, *Acc. Chem. Res.* **12** (1979) 276
- 19: a) W. Kutzelnigg, *Z. Phys. D* **11** (1989) 15
b) W. Kutzelnigg, *Proc. Girona Workshop on Quantum Chemistry, 'Basic Aspect and Current trends'*, Elsevier, Amsterdam, 1989
- 20: Ch. Chang, M. Pelissier and P. Durand, *Phys. Scripta* **34** (1986) 394
- 21: B. Hess 1987, *Phys. Scripta* **36** (1987) 412
- 22: W.H.E. Schwarz and M. Kissel-Phillip, *Phys. Rev. A* **38** (1988) 6027
- 23: R. Baretty and C. Garcia, *Int. J. Quant. Chem.* **S22** (1988) 425
- 24: L.D. Miller, *J. Phys. B* **20** (1987) 4309
- 25: P. Durand and J.C. Barthelat, *Theor. Chim. Acta* **38** (1975) 283
- 26: Y.S. Lee, W.C. Ermler and K. Pitzer, *J. Chem. Phys.* **67** (1977) 5861
- 27: Ph. Christiansen, Y.S. Lee and K.S. Pitzer, *J. Chem. Phys.* **71** (1979) 4445
- 28: G.B. Bachelet and M. Schlüter, *Phys Rev. B* **25** (1982) 2103

Chapter 3

The Relativistic Bond Lengthening of UO_2^{2+} and UO_2

Abstract

Relativistic calculations on UO_2 [1] have shown that relativity leads to substantial bond *lengthening* in this compound, in contrast to the bond contraction found almost exclusively for other compounds. The bond lengthening is *not* caused by the relativistic expansion of the $5f$ valence AO of U, which is the primary bond forming orbital on U in UO_2 . The origin of the bond lengthening can be traced back to the semi-core resp. subvalence character of the U $6p$ AO. The valence character of $6p$ shows up in an increasing depopulation of the $6p$ upon bond shortening, and hence loss of mass-velocity stabilization. The core character of $6p$ shows up in large off-diagonal mass-velocity matrix elements $\langle 5p | h_{\text{MV}} | 6p \rangle$ which are shown to have an overall bond lengthening effect. The larger expansion in UO_2 than in UO_2^{2+} is due to destabilization of U levels in UO_2 , caused by repulsion of the two additional $5f$ electrons.

The present analysis corroborates the picture of relativistic bond length effects as was given in Ref. [2].

1. Introduction

Since the beginning of the seventies there has been an increasing number of calculations including relativistic effects on atoms and molecules. For atoms the situation concerning the relativistic changes is clear: s and $p_{1/2}$ orbitals are stabilized and contract, d and f orbitals are destabilized and expand, while the behaviour of $p_{3/2}$ orbitals is intermediate [3-6]. In molecules the relativistic *contraction* of the bond length that is usually found, has initially been related to the contraction of the valence AOs involved in the bond (predominantly s and p) [4-7]. This explanation of relativistic bond length contraction in terms of AO contraction was questioned by Ziegler et al. [2], who obtained and interpreted the bond length contraction using a first-order perturbation theoretical treatment of the relativistic effects [8,9] within a density functional (Hartree-Fock-Slater) approach [10,11]. To first-order, relativistic changes of the wavefunction do not enter the total energy, and therefore it was not necessary to invoke AO contraction in this type of explanation of the bond length contraction. Other studies, using different computational approaches, corroborated these results [12-14].

The essence of the picture of relativistic bond contraction of Ref. [2] is as follows (compare also [16]). Let us write for the bond energy of a diatomic system with non-relativistic harmonic force constant k and equilibrium bond length R_e :

$$E(R) = (1/2) k (R - R_e)^2 + E_1^{\text{rel}} + \dots \quad (1)$$

This yields for the first-order relativistic bond length change:

$${}^1_{\text{rel}}R = R_e^{\text{rel}} - R_e^{\text{nonrel}} = -\frac{1}{k} \left[\frac{d E_1^{\text{rel}}}{dR} \right]_{R_e^{\text{nonrel}}} \quad (2)$$

where one alternative expression [16] is:

$$\begin{aligned} \frac{dE_1^{\text{rel}}}{dR} &= \frac{d}{dR} \langle \text{nonrel} | h_{\text{MV}} + h_{\text{D}} + h_{\text{SO}} | \text{nonrel} \rangle \\ &= \langle \text{nonrel} | \frac{d}{dR} (h_{\text{MV}} + h_{\text{D}} + h_{\text{SO}}) | \text{nonrel} \rangle \\ &+ \frac{d}{dR} \langle \text{nonrel} | h_{\text{MV}} + h_{\text{D}} + h_{\text{SO}} | \text{nonrel} \rangle + \text{c.c.} \end{aligned} \quad (3)$$

It turns out that in general the most important term in dE_1^{rel}/dR is $d/dR \langle \text{nonrel} | h_{\text{MV}} | \text{nonrel} \rangle$. It has been argued in Ref. [2] that this derivative is usually positive. Upon bond shortening the major contribution to the inner repulsive wall of the E versus R curve comes from kinetic energy increase due to the increasing Pauli repulsion of occupied valence orbitals on one atom with subvalence core orbitals on the other atom.

The (negative) mass-velocity correction also increases, i.e. becomes more negative at shorter R , hence the positive $d E_{\text{rel}}^1/dR$ (cf. [2] and Section 3 below).

It has been pointed out by Schwarz et al. [15-17] that one can, considering bond length change and relativity as two perturbations and using the interchange theorem of double perturbation theory [18], obtain an equally valid first-order formulation of the relativistic bond length change in which the relativistic change of the wavefunction (in particular of the electron density) *does* enter. In this alternative formulation, the last line of Eq. (3) is to be replaced by:

$${}^1_{\text{rel}}R = \dots - \frac{1}{k} \left(\frac{dV_{\text{ne}}}{dR} \right) {}^1_{\text{rel}}\rho \, dr \quad (4)$$

Here the bond length change is related to the electrostatic Hellmann-Feynman force exerted by the relativistic change of the molecular electron density, ${}^1_{\text{rel}}\rho$, upon the nuclei. It is not yet completely clear if this formulation proves the traditional association of relativistic bond shortening with relativistic AO contraction correct. It is possible to split ${}^1_{\text{rel}}\rho$ into two parts, the sum of the atomic relativistic density changes and the change in the deformation density:

$${}^1_{\text{rel}}\rho = \sum_{\text{at}} {}^1_{\text{rel}}\rho_{\text{at}} + {}^1_{\text{rel}}\rho_{\text{def}} \quad (5)$$

It is not clear beforehand which one of the two parts yields the dominant contribution to the Hellmann-Feynman force. Most attention has been given to the atomic part and it has been concluded [15,16] that this term is contracting resp. expanding if the valence AOs contract resp. expand. A direct relation would thus exist between AO contraction and bond length contraction, just as in the traditional view, if the atomic contribution is dominant. That would not be the case if the deformation density contribution were dominant. We will elsewhere discuss the explicit evaluation of these contributions to the Hellmann-Feynman force. Here we note that it is interesting to study systems for which relativistically *expanding* AOs make a major contribution to the bond. In the traditional view the bond should expand, whereas according to Ref. [2] contraction would still occur. Almost all of the systems studied to date have valence s and p AOs, which contract. These systems exhibit relativistic bond contraction, except for the somewhat special cases of Tl_2 [19a] and TlH^+ [19b], where spin-orbit coupling dominates. The early actinides, however, have expanding valence $5f$ and $6d$ AOs. An investigation of the electronic structure of the actinocenes $Ac(COT)_2$ [20] showed important $6d$ and $5f$ contributions to the bonding. In spite of the valence AO expansion, the relativistic effect on the bond length was contraction. Recently, however, calculations on UO_2 [1], where f orbitals are important for the bonding, showed the first - in addition to the above-mentioned Tl compounds - well-documented relativistic bond length expansion.

These last two results appear to be contradictory, which prompted us to carry out a detailed investigation into the relativistic effects on the bond length of UO_2^{2+} and UO_2 . Non-relativistic and relativistic calculations are reported on UO_2^{2+} and UO_2 . We have calculated the non-relativistic bond energy and the relativistic correction to it for a number of distances in order to understand the relativistic expansion of the molecules. The bond length expansion can be explained by rather intricate features of the electronic structure of the title molecules, without reference to the expansion of the U $5f$ AO.

The paper is organized as follows. In Section 2 we briefly discuss the computational method used and give a discussion of the electronic structure features of UO_2^{2+} and UO_2 that are relevant for the analysis of the relativistic bond lengthening. This analysis is given in Section 3. Section 4 contains the conclusions.

2. The electronic structure of UO_2^{2+} and UO_2

Electronic structure calculations have been carried out using the simplest density-functional approach, X or Hartree-Fock-Slater (HFS). The HFS computational method used [10,11] is characterized by the use of a density fitting procedure to obtain an accurate Coulomb potential, by accurate numerical integration of the effective one-electron hamiltonian matrix elements [21], and by the possibility to freeze core orbitals. The ($1s-5s$), ($2p-5p$), ($3d-5d$), and $4f$ orbitals on U and the $1s$ orbital on O have been frozen. The valence basis was double- for the U $6s$, $6p$ and $7s$, triple- for $5f$ and $6d$ and double- for the O $2s$ and $2p$. A single $7p$ on U and $3d$ on O were added as polarization functions.

There have been many studies on the uranyl ion UO_2^{2+} [1,22-31], important issues being the linearity of the O-U-O system and the character of the HOMO. In both cases the U $6p$ orbital plays a crucial role, as pointed out a.o. by Tatsumi and Hoffmann [24] and by Jørgensen [22,25]. One would expect the bonding interactions to be primarily the and interactions of O $2p$ with U valence $5f$ and $6d$. This expectation is borne out by the analysis of the non-relativistic orbital compositions (Table 1), cf. also the Mulliken AO populations of (for UO_2^{2+}) $(2p)^{4.0}$ $(5f)^{3.3}$ $(6d)^{0.9}$. The picture is however complicated by the strong interaction of O $2s$ and $2p$ with the filled U $6p$ shell. The U $6p$ orbital cannot be considered a core orbital, since it has a fairly high energy (comparable to O $2s$) and is spatially even more extended than the valence $5f$ orbital. The interaction with the O orbitals squeezes ~ 0.5 electron out of the U $6p$. The details of the various interactions, leading to the level scheme and orbital compositions given in Table 1, are as follows.

Considering first UO_2^{2+} (Table 1a) we observe that the 1_g (mostly U $6s$) and 2_g (mostly O $2s$) orbitals show mixing of U $6s$ with O $2s$: a four electron destabilizing interaction. In σ_u symmetry the interaction of $6p_\sigma$ and $5f_{z^3}$ ($=5f_\sigma$) with O $2p_\sigma$ is of particular interest. It has already been stressed that the interaction between U $6p_\sigma$ and O

Table 1a. Non-relativistic population analysis for orbitals of UO_2^{2+} for U-O distance of 3.25 a.u.

Orbital	Orbital character	Eigen-value (eV)	Atomic composition (%)								
			U 5f	U 6s	U 6p	U 6d	U 7s	U 7p	O 2s	O 2p	
<i>unoccupied orbitals</i>											
4	u	2p-6p anti-b.	-11.47	29	21			1	2	46	
3	u	5f-2p anti-b.	-18.30	55	1					43	
1	u	5f	-21.47	100							
1	u	5f	-22.01	100							
<i>occupied orbitals</i>											
3	u	5f (-2p bond.)	-22.85	71	11				1	17	
3	g	O 2p (-6d bond.)	-23.04		3		15	2	7	74	
1	g	O 2p (-6d bond.)	-23.83				15			85	
2	u	5f-2p -bond.	-23.89	46	3					50	
2	u	6p-2s a.b., -2p b	-29.17	-1	35			-3	51	18	
1	u	6p	-34.27		95					4	
2	g	2s (-6s anti-b.)	-36.20		16		3	-3	85	-1	
1	u	2s-6p bond.)	-43.12	2	31			-2	56	11	
1	g	6s (-2s bond.)	-49.49		79				14	6	
<i>gross populations</i>				3.3	2.0	5.5	0.9	0.0	-0.1	2.2	4.0

Table 1b. Non-relativistic population analysis for orbitals of UO_2 for U-O distance of 3.25 a.u.

Orbital	Orbital character	Eigen-value (eV)	Atomic composition (%)								
			U 5f	U 6s	U 6p	U 6d	U 7s	U 7p	O 2s	O 2p	
<i>unoccupied orbitals</i>											
4	u	7p	3.04	1	1			98	-5	-1	
3	u	5f-2p anti-b.	-0.41	67	1			11		20	
<i>singly occupied orbitals</i>											
1	u	5f	-1.40	100							
1	u	5f	-1.81	100							
<i>occupied orbitals</i>											
3	u	5f (-2p bond.)	-4.93	63	20			3		15	
2	u	5f-2p -bond.	-6.95	26	8			-1		67	
3	g	O 2p (-6d bond.)	-7.29		4		15	5	3	72	
1	g	O 2p (-6d bond.)	-7.93				16		1	84	
2	u	5f (-2p bond.)	-13.15	-1	30			-1	44	28	
1	u	6p	-34.27		91					7	
2	g	2s (-6s anti-b.)	-36.20		20		3	-2	80	-1	
1	u	2s-6p bond.)	-43.12	2	28			-2	60	10	
1	g	6s (-2s bond.)	-49.49		72				20	7	
<i>gross populations</i>				4.3	2.0	5.5	1.0	0.0	0.1	2.0	4.5

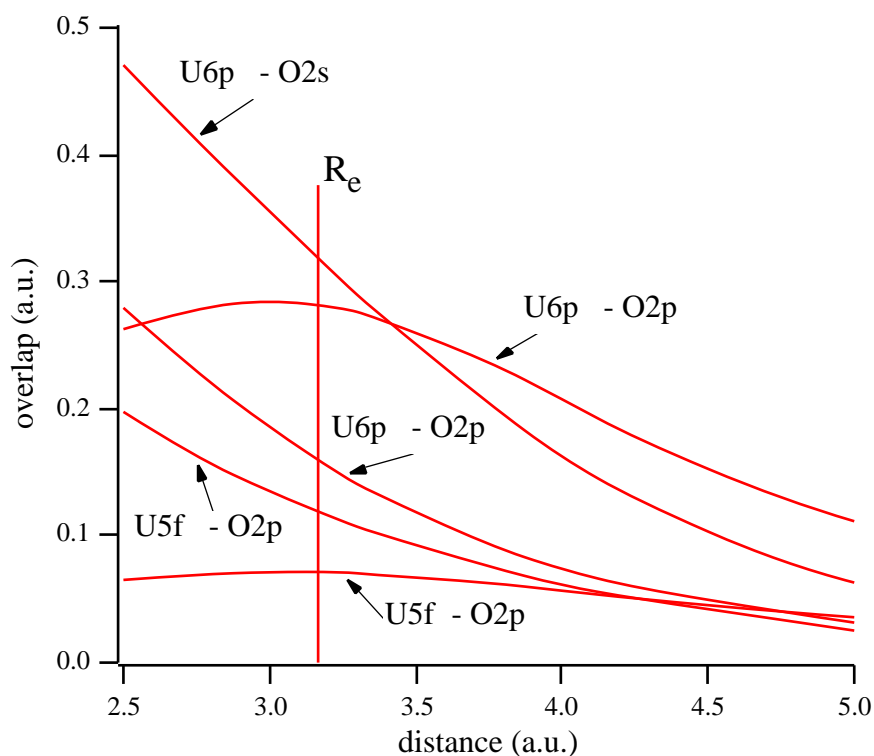


Figure 1. Overlaps between various U and O atomic orbitals as function of the U-O distance.

$2p_{\sigma}$ is very strong [24]. It is interesting in this connection to compare the overlaps between the relevant orbitals, which are given in Fig. 1 as a function of the U-O distance. Fig. 1 shows that the overlap of O $2p_{\sigma}$ with U $6p_{\sigma}$ is very much larger than with U $5f_{\sigma}$. Since the U-O equilibrium distance is rather short (~ 3.25 a.u.), a large splitting between the bonding and antibonding U $6p_{\sigma}$ /O $2p_{\sigma}$ combinations results. The antibonding combination is in fact high up in the virtual spectrum, above the $5f$ orbitals (it becomes the 4_{u}). The (smaller) interaction of O $2p_{\sigma}$ with the $5f_{\sigma}$ causes the 4_{u} to push the $5f_{\sigma}$ orbital down from the $5f$ manifold (to be identified with the position of the 100% $5f$ orbitals 1_{u} , 1_{u}). The resulting 3_{u} , which has 60-70% $5f_{\sigma}$ character, becomes the HOMO. The bonding U $6p_{\sigma}$ /O $2p_{\sigma}$ combination is stabilized and interacts strongly, in a four electron repulsive interaction, with the σ_{u} combination of O $2s$ (cf. Fig. 1): the resulting 1 and 2_{u} orbitals are split by ca. 14 eV. The 2_{u} , which would, on account of its U $6p_{\sigma}$ /O $2p_{\sigma}$ bonding character, be expected to be below the almost noninteracting $6p_{\pi_{\text{u}}}$ (the 1_{u} MO), is in fact pushed considerably above 1_{u} by O $2s$. The whole level pattern of 1_{u} - 4_{u} orbitals and their composition is given in Fig. 2. For future reference pictures of the orbitals are given with the phase with which the U $5p$ core orbital is admixed explicitly indicated. As for the other orbitals, the $2_{\text{u}}/3_{\text{u}}$ pair is clearly the pair

of bonding/antibonding $5f\pi_u/O\ 2p\pi_u$ orbitals. This suggests that the major contribution to the U-O bond comes from the bonding between U $5f$ and O $2p$. The *gerade* combinations of O $2p_\pi$ and O $2p_\sigma$ (1_g and 3_g) reveal some stabilizing contribution from U $6d$ admixture.

We wish to draw attention to a few special features of the electronic structure that will prove important in the analysis of the relativistic bond lengthening. In Table 2 the gross populations (2a) and net populations (2b) of relevant AOs are given for a number of U-O distances. The presence of U $6p_\sigma$ character in the virtual spectrum (cf. 4_u in Table 1a) implies that the U $6p_\sigma$ gross population drops below 2.0: *there is a U 6p 'hole'*. This hole has been noted by Pyykkö and Lohr [27] and has been related by Pyykkö to NQR data [32]. In our calculations the hole is clearly visible in the gross populations and *increases at shorter distances*. At R_e the gross population of U $6p_\sigma$ is 1.53, so there is (with this definition in terms of Mulliken gross population) a hole of 0.47 electron. (Pyykkö and Lohr found a hole of 0.16 electron in their Extended Hückel calculation.). The Table with net populations (2b) shows that the net population differs significantly from the gross population. This is a simple consequence of the large overlaps mentioned before, which cause considerable (negative) contributions to the gross population to come from overlap populations. The table with net populations also shows that in a number of cases these populations are (much) larger than 2.0 (notably O $2s\sigma_u$ and U $6s$). Such high net populations again arise from large overlaps: the coefficients in the antibonding orbitals

Table 2a. Gross populations for some AOs of U and O in UO_2^{2+} at various U-O distances.

Distance	u symmetry				u symmetry			g symmetry	
	U $6p$	U $5f$	O $2s_u$	O $2p_u$	U $6p_x$	U $5f_x$	O $2p_{ux}$	U $6s$	O $2s_g$
2.50	0.95	1.51	2.45	1.19	1.86	0.97	1.17	1.78	2.09
3.00	1.36	1.51	2.27	1.04	1.94	0.92	1.12	1.93	2.11
3.50	1.69	1.41	2.14	0.87	1.98	0.94	1.06	1.96	2.12
4.00	1.87	1.25	2.07	0.86	1.99	1.03	0.96	1.98	2.09
4.50	1.94	1.09	2.04	0.94	1.99	1.17	0.82	1.99	2.05

Table 2b. Net populations for some AOs of U and O in UO_2^{2+} at various U-O distances.

Distance	u symmetry				u symmetry			g symmetry	
	U $6p$	U $5f$	O $2s_u$	O $2p_u$	U $6p_x$	U $5f_x$	O $2p_{ux}$	U $6s$	O $2s_g$
2.50	1.93	1.31	3.83	0.98	1.98	0.71	1.12	2.49	2.62
3.00	1.84	1.37	3.04	0.84	1.98	0.74	1.02	2.30	2.44
3.50	1.92	1.32	2.52	0.73	1.99	0.82	0.95	2.20	2.33
4.00	1.87	1.18	2.25	0.76	1.99	0.95	0.87	2.09	2.22
4.50	2.00	1.04	2.13	0.87	1.99	1.11	0.76	2.09	2.13

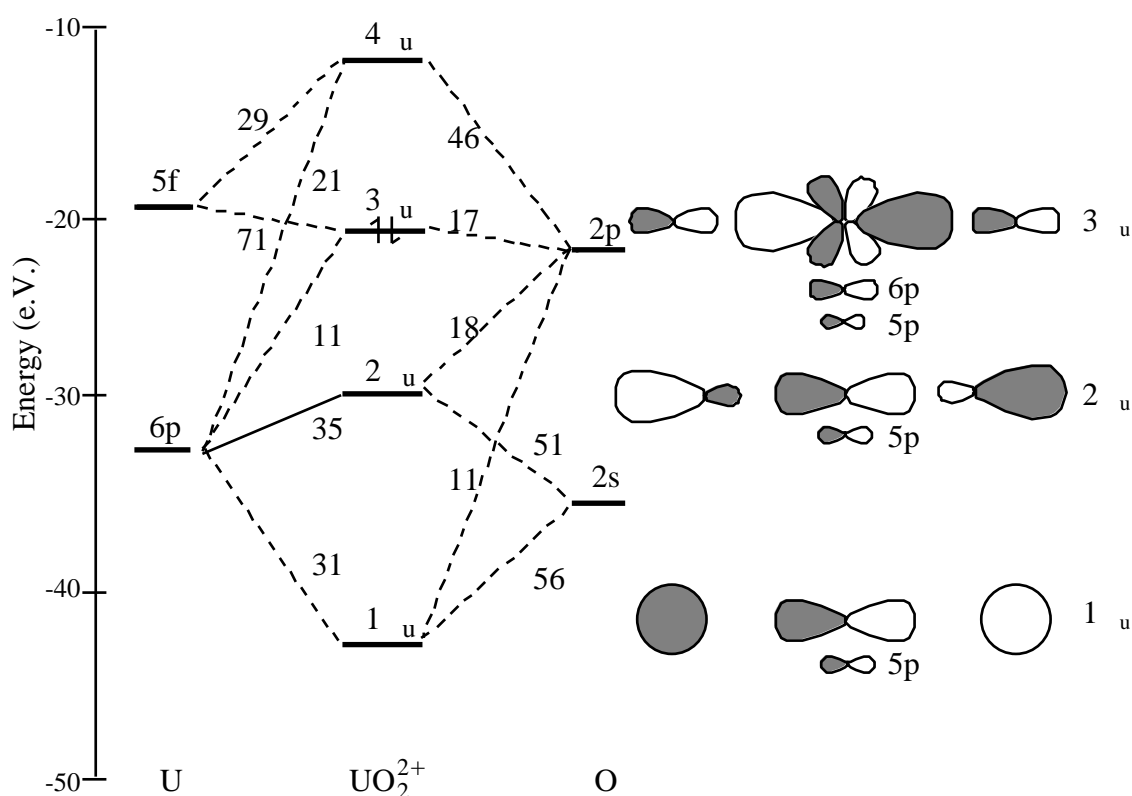


Figure 2. Interaction diagram for the σ_u levels. The percentage contribution of an AO to an MO (based on Mulliken gross populations) is given alongside the corresponding interaction line.

become large due to the normalization factor $1/(2-2S)$ in the symmetrical case; note the larger amplitudes drawn in Fig. 2 for 2_u versus 1_u). The negative overlap population in the antibonding orbital is (much) larger than the positive overlap population in the bonding orbital, the total net population is accordingly larger than 2.0 with a relatively large contribution from the antibonding orbital. These effects are pronounced here due to the short U-O distance c.q. large overlaps and will prove to play a key role in the relativistic bond lengthening.

The overlaps in symmetry σ_u are much smaller (cf. Fig. 1). Therefore the hole effect, which is also present in σ_u symmetry, is much smaller: at R_e the hole is only 0.07 e.

Next we will briefly discuss UO_2 , which has, compared with UO_2^{2+} , two extra electrons in the empty 1_u , 1_u orbitals above 3_u . (The configuration $(1_u)^1(1_u)^1$ is most stable, which relativistically corresponds to $(3e_{3/2u})^1(1e_{3/2u})^1$, see Ref. [1].) Of course going from a 2+ to a neutral species first of all shifts all levels upwards. The second effect is the relatively strong upward shift of the 5f levels, due to the large 5f-5f repulsion of the tight 5f orbital (note the additional electrons are in pure 5f orbitals). As a consequence the gap between the 1_u , 1_u levels and the 3_u widens considerably (see Table 1b). In the $2_u/3_u$ pair the lower bonding orbital is no longer a fifty/fifty mixture

of O $2p$ and U $5f$, but has more pronounced O $2p$ character. It is not even stabilized below the O $2p$ $3g$ and $1g$, as it was in UO_2^{2+} . The U $5f$ -O $2p$ π bond is therefore probably weaker. Since the repulsive effects in the lower levels between the occupied U $6s$, $6p$ and O $2s$ do not seem to be much different from UO_2^{2+} , the bond length may be expected to be longer, as indeed it is (cf. Table 3). In the upper part of the spectrum the U $7p$ is now below the antibonding U $5f_{\sigma}$ /O $2p\sigma_u$ combination and has become the $4u$. The $6p$ holes are 0.43 e for $6p_{\sigma}$ and 0.02 e for $6p_{\pi}$ at R_e . This is slightly smaller than for UO_2^{2+} , but in UO_2 the hole increases faster on going to shorter U-O distance.

Up to this point only non-relativistic calculations have been considered. The relativistic corrections to the levels have been discussed extensively elsewhere [31] and are not given here. We do give, however, a Table with atomic relativistic corrections (Table 4) which will be needed in the next section. Note the large mass-velocity terms for U $6p$ and U $5p$.

Table 3. Calculated non-relativistic and relativistic bond-distances (in bohr) and force constant (in $mdyn/\text{\AA}$) for UO_2^{2+} and UO_2 .

	UO_2^{2+}	UO_2
R_e non-relativistic	3.163	3.326
R_e relativistic	3.191	3.464
R_e relativistic (quasi-)	3.213	3.466
Expansion (1st order) in %	0.89	4.15
k (non-relativistic)	19.3	13.1

Table 4. Relativistic corrections for orbitals of U atom. Energies are given in eV. Δ_{MV} : mass-velocity; Δ_D : Darwin; Δ_{SO} : spin-orbit; Δ_{POT} : potential correction due to relativistic density change.

orbital	E_{NREL}	MV	D	SO	POT	E_{REL}	spinor
5s	-240.10	-164.20	93.14	-27.32	21.46	-317.00	$s_{1/2}$
5p	-190.97	-33.51	-0.20	-38.58	20.61	-242.66	$p_{1/2}$
		-33.51	-0.20	12.21	20.61	-191.86	$p_{3/2}$
6s	-35.29	-32.43	18.35	-4.01	5.05	-47.81	$s_{1/2}$
6p	-21.65	-5.54	-0.03	-5.72	4.71	-28.23	$p_{1/2}$
		-5.54	-0.03	2.02	4.71	-20.49	$p_{3/2}$
6d	-3.13	-0.68	-0.01	-0.38	2.18	-2.03	$d_{3/2}$
		-0.68	-0.01	0.08	2.18	-1.52	$d_{5/2}$
5f	-8.88	-1.13	-0.03	-1.04	8.44	-2.63	$f_{5/2}$
		-1.13	-0.03	-0.36	8.44	-1.95	$f_{7/2}$

Off-diagonal element $\langle 5p | h_{MV} | 6p \rangle = 13.63$ eV

The U $6p$ is already sufficiently core-like to have a large mass-velocity correction, but of course the U $5p$ has a much larger mass-velocity correction still, and even the off-diagonal term, $5p |h_{MV}| 6p$, is quite large. It is a special feature of the U atom that it has, apart from the true $5s$, $5p$ core shell, also the $6s$, $6p$ shell which has both core-like features (large MV terms) and valence character (high energy, large radius).

3. Relativistic bond lengthening in UO_2^{2+} and UO_2

Calculations on UO_2^{2+} and UO_2 were done for a number of U-O distances, both non-relativistically and including first-order relativistic corrections. As noted before [1], second order relativistic effects are large and quasi-relativistic calculations of the type described in Ref [33], which include certain types of higher order corrections, are to be preferred for elements as heavy and relativistic as U. Such quasi-relativistic calculations have been performed on UO_2^{2+} and UO_2 and yield results for the bond lengthening that differ little from those obtained in first-order, as can be seen in Table 3. For purposes of analysis we may therefore focus on the first-order calculations. Non-relativistic bond-energy curves, and those including the first-order relativistic corrections are given in Fig. 3. The equilibrium distances of UO_2^{2+} and UO_2 are given in Table 3. The relativistic curves are destabilized and show equilibrium bond lengths larger than the non-relativistic ones. The expansion of UO_2 (4%) is much larger than the expansion of UO_2^{2+} (1%). The expansion of UO_2 of 0.14 a.u. is close to the value found by Allen et al. [1]. Our equilibrium bond length is smaller.

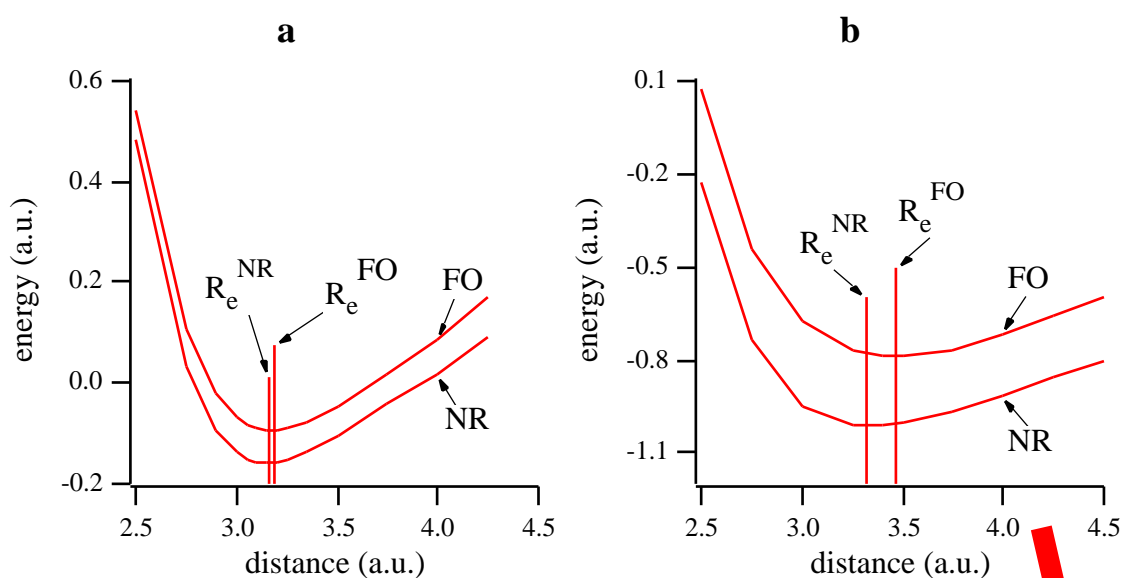


Figure 3. Energy versus R for UO_2^{2+} (a) and UO_2 (b).

Since the only difference with the calculations in Ref. [1] is a larger basis set, in particular the addition of polarization functions on the oxygens, the present shorter bond lengths provide another example of the well-known bond shortening effect of these polarization functions (cf. [34] for CO). Note that the weaker bonding in UO_2 anticipated in the previous section shows up in the more shallow bond energy curve of Fig. 3. To some extent this explains the difference in expansion between UO_2^{2+} and UO_2 (smaller k in Eq. 2).

Before discussing the uranyl case, we first briefly review the explanation of the relativistic contraction given in previous studies on e.g. AuH, AuCl, Au₂ [2]. Suppose we have a heavy atom A (with core) and a light atom B (no core, for simplicity), the bonding being between the valence orbitals $\begin{smallmatrix} v \\ A \end{smallmatrix}$ and $\begin{smallmatrix} v \\ B \end{smallmatrix}$. Due to core-valence orthogonality, the core orbitals of A mix into the valence orbital of B. For properties such as T and h_{MV} , only the admixing of the subvalence core orbital of A, $\begin{smallmatrix} c \\ A \end{smallmatrix}$, is important (see below). The molecular orbitals are then given by:

$$\text{bond} = c_A \begin{smallmatrix} v \\ A \end{smallmatrix} + c_B \left(\begin{smallmatrix} v \\ B \end{smallmatrix} - a \begin{smallmatrix} c \\ A \end{smallmatrix} \right) \quad \text{anti-bond} = c_A^* \begin{smallmatrix} v \\ A \end{smallmatrix} - c_B^* \left(\begin{smallmatrix} v \\ B \end{smallmatrix} - a \begin{smallmatrix} c \\ A \end{smallmatrix} \right) \quad (6)$$

where a is the coefficient with which the core-orbital $\begin{smallmatrix} c \\ A \end{smallmatrix}$ has to mix into $\begin{smallmatrix} v \\ B \end{smallmatrix}$ to ensure orthogonality on the core of A ($a \sim \begin{smallmatrix} v \\ B \end{smallmatrix} | \begin{smallmatrix} c \\ A \end{smallmatrix}$). The superscript * denotes the antibonding orbital. In general the coefficients of the antibonding orbital are larger than those of the bonding one: $|c^*| > |c|$, e.g. for a homonuclear molecule: $1/(2-2S) > 1/(2+2S)$, with S the overlap of the atomic orbitals.

In the systems studied to date, typically only the bonding combination bond was occupied. If the bond length is shortened, $\begin{smallmatrix} c \\ A \end{smallmatrix}$ is more strongly admixed, because the overlap of $\begin{smallmatrix} c \\ A \end{smallmatrix}$ with $\begin{smallmatrix} v \\ B \end{smallmatrix}$ increases. This leads non-relativistically to a rise in kinetic energy (kinetic repulsion).

The mass-velocity effect:

$$|h_{MV}| = -\frac{|p^4|}{8m^2c^2} = -\frac{T^2}{8m^2c^2} \quad (7)$$

is negative definite and increases when T increases (classically the MV term is $-T^2/2c^2$). In the MO picture this effect arises from the diagonal core orbital contribution to the mass-velocity correction for the bonding MO:

$$\begin{aligned} \text{bond} |h_{MV}| \text{bond} &= c_A^2 \begin{smallmatrix} v \\ A \end{smallmatrix} |h_{MV}| \begin{smallmatrix} v \\ A \end{smallmatrix} + 2 c_A c_B \begin{smallmatrix} v \\ A \end{smallmatrix} |h_{MV}| \begin{smallmatrix} v \\ B \end{smallmatrix} + c_B^2 \begin{smallmatrix} v \\ B \end{smallmatrix} |h_{MV}| \begin{smallmatrix} v \\ B \end{smallmatrix} \\ &- 2 c_B^2 a \begin{smallmatrix} v \\ B \end{smallmatrix} |h_{MV}| \begin{smallmatrix} c \\ A \end{smallmatrix} - 2 c_A c_B a \begin{smallmatrix} v \\ A \end{smallmatrix} |h_{MV}| \begin{smallmatrix} c \\ A \end{smallmatrix} + c_B^2 a^2 \begin{smallmatrix} c \\ A \end{smallmatrix} |h_{MV}| \begin{smallmatrix} c \\ A \end{smallmatrix} \end{aligned} \quad (8)$$

Usually the matrix elements on the first line are negligible, and the diagonal core contribution (the last term on the second line) is very much larger than any other term. The coefficient a in this term increases on shortening the A-B distance since the overlap of $\overset{v}{B}$ with $\overset{c}{A}$ increases, whereas the coefficient c_B changes much more slowly. Therefore the diagonal core contribution causes the mass-velocity correction to become increasingly more negative: it relaxes the kinetic repulsion. The ensuing bond contraction can be quite large: AuH: 0.23 and Au₂: 0.46 Å [2].

We have singled out the diagonal core term with $\overset{c}{A}$ being *the upper core orbital* as the most important term for both kinetic repulsion (for which Eq. (8) applies with h_{MV} replaced with T) and its mass-velocity reduction. More deep-lying core orbitals will have (much) larger T and h_{MV} matrix elements, but are in general so tight that the overlap with $\overset{v}{B}$ becomes very small and therefore the a^2 factor reduces the corresponding $c_B^2 a^2 \overset{c}{A} |h_{MV}| \overset{c}{A}$ term to insignificance. Numerical evidence will be provided below.

In order to understand the relativistic effect in uranyl, the above analysis has to be extended. If we associate U $6p$ with the valence orbital $\overset{v}{A}$, it should be realized that this orbital has some core character in the sense that its diagonal MV matrix element is not negligible, and neither is the off-diagonal matrix element with the true core orbital (U $5p$). Moreover, U $6p$ is sufficiently deep-lying that also *antibonding* orbitals involving U $6p$ are occupied. The combination of these factors leads to bond lengthening MV effects in the following way. First, the diagonal term $c_A^2 \overset{v}{A} |h_{MV}| \overset{v}{A}$ (first term on the first line in Eq. (8)) yields negative contributions in all occupied orbitals. If the sum of these contributions becomes less negative when $R(U-O)$ decreases, this term has a bond lengthening effect. Shortening the U-O distance does indeed decrease the total negative contribution since less U $6p$ character remains in the occupied orbitals. This is clear from the increasing $6p$ hole noted before (note that the net population directly reflects this term with h_{MV} replaced with the unit operator). In the second place, the contribution of the off-diagonal term $-2 c_A c_B a \overset{v}{A} |h_{MV}| \overset{c}{A}$ has to be taken into account. The recent results of Schwarz et al. [35] enable us to establish the sign of this contribution. It has been shown in Ref. [35] that the mass-velocity matrix elements originate from the innermost core wiggle of the AOs in the matrix element, i.e. the $2p$ wiggle for a matrix element between $6p$ and $5p$. If we take the phases of the $6p$ and $5p$ orbitals such that the outer lobes are positive in the positive z direction - as is assumed when we take c_A and c_B and a all positive in Eq. (6) - the inner $2p$ wiggles of the two orbitals have opposite phase, and the matrix element will be positive instead of negative. The overall minus sign of this term in a bonding orbital makes it negative again. Since the off-diagonal term scales with a , i.e. increases upon shortening $R(U-O)$, it contributes to the contraction.

However, for an *antibonding* orbital the off-diagonal term will be $+ 2 c_A^* c_B^* a \overset{v}{A} |h_{MV}| \overset{c}{A}$, which is positive. This off-diagonal contribution in an antibonding orbital is therefore expanding and is rather important for two reasons.

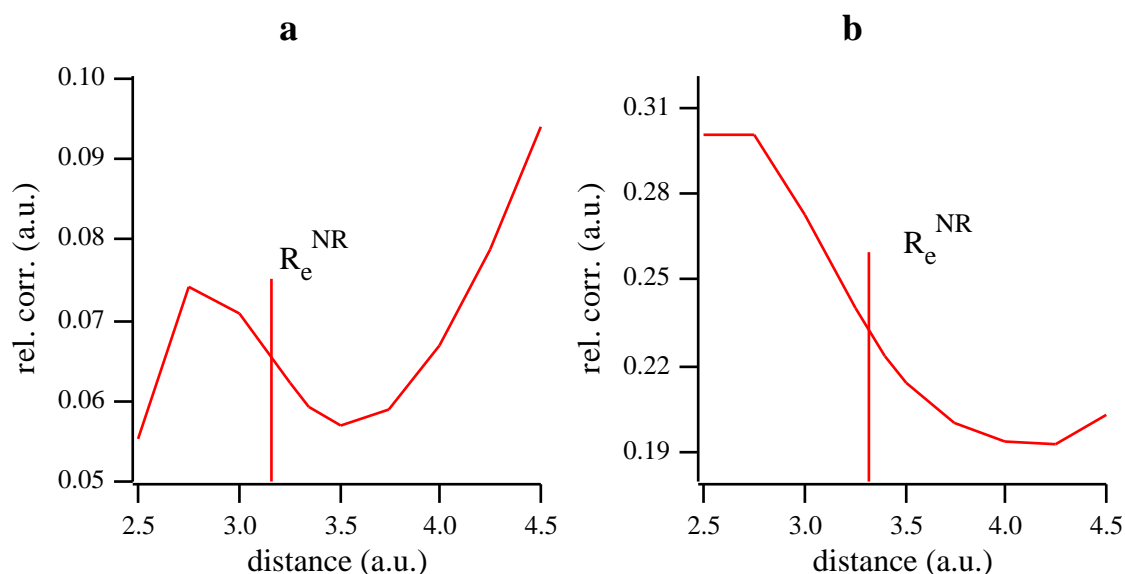


Figure 4. The total first-order relativistic energy correction for UO_2^{2+} (a) and UO_2 (b).

First, its derivative w.r.t. R scales as da/dR , not as the smaller $2a da/dR$ (the behaviour of the diagonal core contribution). Second, the coefficients (c_A^* , c_B^*) are larger than in the bonding orbital, particularly when the overlaps are large.

The overall result when bond and anti-bond are both occupied, depends on the relative importance of the individual mass-velocity elements. Expanding contributions have however been identified and will, if they dominate, lead to relativistic bond lengthening.

We now examine the uranyl case. The calculated first-order corrections (sum of MV and Darwin) to the bond energy are given in Fig. 4a, b. For UO_2^{2+} we see in Fig. 4a the normal decrease with decreasing $R(\text{U-O})$ in the beginning and at the end of the curve. But in the range 3.5-2.7 bohr the curve rises, and this region is the most important one, because it includes the non-relativistic R_e . The derivative $d E_{\text{rel}}^1/dR$ is obviously negative at R_e , causing relativistic expansion of the molecules. The curve for UO_2 in Fig 4b shows this anomalous behaviour more strongly (the derivative $d E_{\text{rel}}^1/dR$ is more negative) and over a larger distance range. The relatively large expansion in UO_2 is therefore caused by both a smaller k and a larger $d E_{\text{rel}}^1/dR$.

The relativistic correction has been split into contributions from different symmetries by simply summing the first-order corrections over the occupied orbitals of a given symmetry. The result is given in Fig. 5. The two symmetries that are responsible for the negative slope of E_{rel}^1 around R_e are u and u . Symmetry g shows the 'normal' contracting behaviour, whereas g also exhibits some anomalous behaviour, but only at shorter distances than are relevant here.

a

b

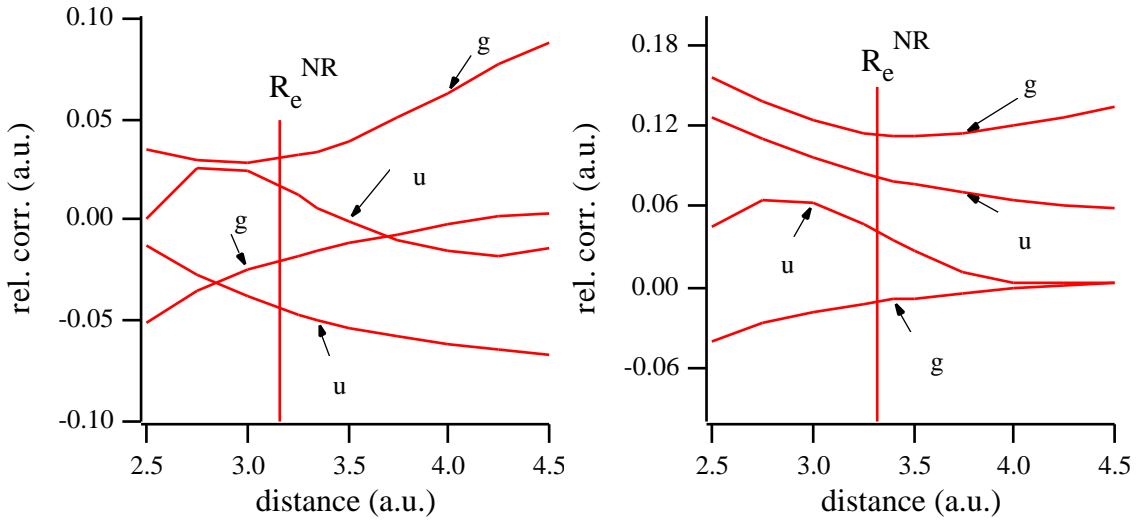


Figure 5. Contributions in various symmetries to the first-order relativistic energy correction for UO_2^{2+} (a) and UO_2 (b).

The *ungerade* symmetries are therefore singled out for closer scrutiny. It turns out that in these symmetries the mass-velocity effect is dominating, as before [2]. From now on only mass-velocity results are given.

In Table 5a the contributions per u orbital to $-\frac{1}{k} d E_{rel}^1/dR$ are given for the various terms specified in Eq. (8). The diagonal valence contribution $c_A^2 \langle h_{MV} \rangle_A$ corresponds to the term $6p|6p$. This term is positive (expanding) in 1_u and 2_u , which corresponds to loss of $6p$ character in these orbitals when the bond length is shortened. This $6p$ character is regained partly in 3_u , but not completely as some $6p$ character builds up in the virtual spectrum, notably the 4_u . There is a net expanding contribution from the $6p|6p$ terms, corresponding to the increasing $6p$ hole at shorter distances. The diagonal core contributions $5p|5p$ have the normal contracting behaviour. They are however not much larger than the $6p|6p$ contributions, although the mass-velocity matrix element (Table 4) itself is very large (we return to this point below). Still, they cancel much of the $6p|6p$ contribution. For that reason the off-diagonal $5p|6p$ terms are important. They behave as predicted, contracting in the bonding orbital 1_u , where $6p$ and $5p$ have opposite phase, and expanding in the upper two orbitals where they are equal in phase (cf. Fig. 2). The net contribution is therefore expanding.

For neutral UO_2 the $6p$ hole formation is relatively more important, which fits in with the destabilization of the U AOs because of the two additional $5f$ electrons.

Table 5a. The most important mass-velocity contributions to the approximate bond length change $-\frac{1}{k} d\Delta E_{rel}^1/dR$ for symmetry σ_{ir}

The derivative has been approximated by a finite difference at $R = 3.5$ and 3.0 bohr.

Orbital	MV-element	UO_2^{2+}	UO_2
1 _u	6p 6p	0.0368	0.0581
	5p 5p	-0.0376	-0.0626
	5p 6p	-0.0735	-0.1005
2 _u	6p 6p	0.1189	0.2126
	5p 5p	-0.0079	-0.0002
	5p 6p	0.0361	-0.0031
3 _u	6p 6p	-0.0815	-0.0955
	5p 5p	-0.0090	-0.0200
	5p 6p	0.0589	0.1040
sum	6p 6p	0.0742	0.1752
	5p 5p	-0.0545	-0.0828
	5p 6p	0.0214	0.0004
		+-----+	
total		0.0412	0.0928
total MV _u		0.0413	0.0869

In the u symmetry (Table 5b) the picture is analogous, the loss of $6p$ character now being the most important effect. Again the $6p$ hole is more important in UO_2 than in UO_2^{2+} . The off-diagonal $5p|6p$ contributions in 1_u and 2_u have the signs expected from bonding resp. antibonding orbitals with O $2p$, but play a much more modest role than in u since they almost cancel each other. In fact, it is slightly artificial to consider 1_u and 2_u from the point of view of bonding resp. antibonding U $6p$ -O $2p$ character. These orbitals mix very little in 1_u and 2_u. It is therefore more natural and illuminating to consider the 2_u orbital as the f - p bond which it primarily is (1_u is nearly pure U $6p$ with very little O $2p$ admixed; see Table 1). So 2_u is just like bond in Eqs (6-8), with f and p being ψ_A^v and ψ_B^v respectively. The $6p$ in this orbital is then simply the highest core orbital ψ_A^c in this MO. The term $6p|6p$ now represents the diagonal core contribution $c_B^2 a^2 \langle \psi_A^c | h_{MV} | \psi_A^c \rangle$ of Eq. (8). It is strongly contracting, in agreement with the contracting role we attribute to the core orbital in a simple bonding orbital. Note that this contraction occurs irrespective of the nature of the valence AO, whether contracting

Table 5b. The most important mass-velocity contributions to the approximate bond length change $-\frac{1}{k} d\Delta E_{rel}^I/dR$ for symmetry π_u .

off-diagonal contribution between the two core AOs will have opposite sign to the diagonal contributions and may be larger than the diagonal deep core contribution if the off-diagonal MV matrix element is significant. This is clearly demonstrated by the $5p|6p$ contribution in 2_{u} . Note that the present orthogonality argument for the sign of the $5p|6p$ contribution in 2_{u} does not contradict the previous one based on antibonding U $6p$ -O $2p$ character: the U $6p$ has opposite phase to the O $2p_{\text{u}}$ combination (and therefore the same phase as U $5p$ in this MO) whether considered as antibonding valence orbital to O $2p\pi_{\text{u}}$ or as mixing into O $2p\pi_{\text{u}}$ for orthogonality reasons. The importance of the upper core orbital that we have pointed out here is of course not contradicted by the fact that the MV matrix elements build up almost completely [35] in the inner core wiggle ($2p$ in this case) of the upper core AO. This *does not mean* that the actual innermost core AOs such as $1s$ or $2p$ have any special importance for the relativistic effects on the bond length.

4. Summary

The origin of the unusual relativistic expansion of the bond length in UO_2^{2+} and UO_2 has been traced to the special shell structure of the U atom. The presence of the semi-core $6p$ shell in U is the most important single electronic structure feature that leads to the bond lengthening. The $6p$ shows some core character in that it has large MV matrix elements, both diagonal and off-diagonal (with $5p$). The U $6p$ is not true core in the sense that it is fairly extended, even more so than the valence $5f$, and is not at very deep energy. The short bonds set up by the $5f$ cause the $6p$ to overlap strongly with the O orbitals and it is sufficiently high in energy that some $6p$ character can appear in the virtual spectrum: there is a $6p$ hole. Bond shortening increases the $6p$ hole, leading to a loss of mass-velocity stabilization. This is the most important cause for a negative slope of E_{rel}^1 .

The second contribution comes from off-diagonal $5p|h_{\text{MV}}|6p$ matrix elements, which lead to bond expansion if $6p$ and $5p$ occur in an MO with the same phase. The $5p$ will always have opposite phase to the dominant O AOs because of the core orthogonality condition. There are also occupied orbitals in which the $6p$ has opposite phase to the O AOs, i.e. is antibonding to them, since the $6p$ is sufficiently deep in energy that both bonding and antibonding orbitals are occupied. This situation holds for the 2_{u} and 3_{u} . In 2_{u} the $6p$ is not the main valence AO on U, but the $5f$ is. The antibonding phase of $6p$ in this orbital with respect to O $2p_{\text{u}}$ combination, which it shares with the $5p$, may be looked upon either as a 'core' orthogonality effect, or as antibonding counterpart to the slight in phase mixing between $6p$ and O $2p$ in 1_{u} .

In our first-order relativistic perturbation approach, relativistic bond length changes are not connected with relativistic changes of the valence AOs. Bonding by a relativistically

expanded $5f$ AO, such as in orbital $2\sigma_u$ here and in the actinocenes [20], leads to contraction by the MV reduction of the kinetic energy repulsion coming from the core orthogonality condition (the Pauli repulsion), just as in the case of bonding by relativistically contracting s valence AOs [2]. In uranyl, however, the main MV effects do not come from the $f-p$ bond (orbital $2\sigma_u$) but from other orbitals in which the U $6p$ with its special characteristics plays a major, bond expanding, role. The present analysis of the 'anomalous' bond lengthening in uranyl thus corroborates the picture of relativistic effects on bond lengths given in Ref. [2].

References

- 1: G.C. Allen, E.J. Baerends, P. Vernooijs, J.M. Dyke, A.M. Ellis, M. Fehrer and A. Morris, *J. Chem. Phys.* **89** (1988) 5363
- 2: a) T. Ziegler, J.G. Snijders and E.J. Baerends, *Chem. Phys. Lett* **75** (1980) 1
b) T. Ziegler, J.G. Snijders and E.J. Baerends, *Chem. Phys.* **74** (1981) 1271
- 3: J-P. Desclaux, *At. Data and Nuc. Data Tables* **12** (1973) 311
- 4: a) J-P. Desclaux and P. Pyykkö, *Chem. Phys. Lett* **29** (1974) 534
b) J-P. Desclaux and P. Pyykkö, *Chem. Phys. Lett* **39** (1976) 300
- 5: a) P. Pyykkö and J-P. Desclaux, *Chem. Phys. Lett* **42** (1976) 545
b) P. Pyykkö and J-P. Desclaux, *Chem. Phys. Lett* **50** (1977) 503
- 6: P. Pyykkö and J-P. Desclaux, *Acc. of Chem. Research* **12** (1979) 276
- 7: P. Pyykkö, *Chem. Rev.* **88** (1988) 563
- 8: J.G. Snijders, E.J. Baerends, *Mol. Phys.* **36** (1978) 1789
- 9: J.G. Snijders, E.J. Baerends and P. Ros, *Mol. Phys.* **38** (1979) 1909
- 10: a) E.J. Baerends, D.E. Ellis and P. Ros, *Chem. Phys.* **2** (1973) 42
b) E.J. Baerends and P. Ros, *Chem. Phys.* **2** (1973) 51
- 11: E.J. Baerends and P. Ros, *Int. J. Quant. Chem.* **S12** (1978) 169
- 12: J.G. Snijders, P. Pyykkö, *Chem. Phys. Lett* **75** (1980) 5
- 13: P.A. Christiansen and W. C. Ermler, *Mol. Phys.* **55** (1985) 1109
- 14: J. Katriel, D. Feller and E.R. Davidson, *Int. J. Quant. Chem.* **26** (1984) 489
- 15: W.H.E. Schwarz, S.Y. Chu and F. Mark, *Mol. Phys.* **50** (1983) 603
- 16: W.H.E. Schwarz, *Phys. Scripta* **36** (1987) 403
- 17: A. Rutkowski, W.H.E. Schwarz, *Theor. Chim. Acta* **76** (1990) 391
- 18: J.O. Hirschfelder, W.B. Brown and S.T. Epstein, *Adv. Quant. Chem.* **1** (1964) 255
- 19: a) P.A. Christiansen, K.S. Pitzer, *J. Chem. Phys.* **74** (1981) 1162
b) P. Schwerdtfeger, *Phys. Scripta* **36** (1987) 453
- 20: P.M. Boerrigter, E.J. Baerends and J.G. Snijders, *Chem. Phys.* **122** (1988) 357

- 21: P.M. Boerrigter, G. te Velde and E.J. Baerends, *Int. J. Quant. Chem.* **33** (1988) 87
- 22: C.K. Jørgensen and R. Reisfeld, *Structure and Bonding* **50** (1982) 121
- 23: a) R.G. Denning, T.R. Snellgrove and D.R. Woodwark, *Mol. Phys* **32** (1976) 419
b) R.G. Denning, T.R. Snellgrove and D.R. Woodwark, *Mol. Phys* **37** (1979) 1089
- 24: K. Tatsumi and R. Hoffmann, *Inorg. Chem.* **19** (1980) 2656
- 25: C.K. Jørgensen, *Chem. Phys. Lett.* **89** (1982) 455
- 26: P. Pyykkö and L. Laaksonen, *J. Phys. Chem.* **88** (1984) 4892
- 27: P. Pyykkö and L. Lohr, *Inorg. Chem.* **20** (1981) 1950
- 28: S. Larsson and P. Pyykkö, *Chem. Phys.* **101** (1986) 355
- 29: J.H. Wood, M. Boring and S.B. Woodruff, *J. Chem. Phys.* **74** (1981) 5225
- 30: P.F. Walch and D.E. Ellis, *J. Chem. Phys.* **65** (1976) 2387
- 31: R.L. DeKock, E.J. Baerends, P.M. Boerrigter and J.G. Snijders, *Chem. Phys. Lett.* **105** (1984) 308
- 32: P. Pyykkö, *Inorg. Chim. Acta* **139** (1987) 243
- 33: T. Ziegler, V. Tschinke, E.J. Baerends, J.G. Snijders and W. Ravenek, *J. Phys. Chem.* **93** (1989) 3050
- 34: E.J. Baerends, P. Vernooijs, A. Rozendaal, P.M. Boerrigter, M. Krijn, D. Feil and D. Sundholm, *J. Mol. Struct. (THEOCHEM)* **133** (1985) 147
- 35: W.H.E. Schwarz, E.M. van Wezenbeek, E.J. Baerends and J.G. Snijders, *J. Phys. B* **22**(1989) 1515

Chapter 4a

An explanation for the short U-O bond length in UO_2^{2+}

Abstract

Scalar-Relativistic calculations on the uranyl ion UO_2^{2+} show that the main reason for the very short U-O bond length in this compound is the $U\ 5f\text{-}O\ 2p$ interaction. Especially the closed shell $U\ 6p\text{-}O\ 2s_{\text{u}}$ Pauli repulsion is large, and it mainly provides the repulsion present in uranyl. Concerning the $U\ 6p\text{-}O\ 2p_{\text{u}}$ and $U\ 5f\text{-}O\ 2s_{\text{u}}$ steric effects, the Pauli repulsions are cancelled by electrostatic effects, resulting in a small steric contribution. The small $U\ 5f\text{-}O\ 2s_{\text{u}}$ steric effect makes that we find an important bonding contribution from the $U\ 5f$ orbital with $O\ 2p_{\text{u}}$. The $U\ 6d\text{-}O\ 2p$ interaction is not unimportant, but is not sensitive to variation in the U-O distance.

In the bond energy analysis uranyl was built up from open shell fragments, for which the recently developed method described in Chapter 1 was used.

1. Introduction

The linear uranyl ion UO_2^{2+} has attracted attention for a long time. Already in 1833 the luminescence was noted, which later indirectly led to the discovery of radioactivity [1]. A remarkable feature of the UO_2^{2+} geometry is the very short U-O distance, typically 1.7 to 1.8 Å, which is much shorter than for secondary ligands [2].

Up to now a large number of experimental and theoretical studies have been done on uranyl, which can roughly be divided into three categories: electronic structure calculations on the bonding characteristics [1..13], both at the non-relativistic and relativistic level, studies on excitation spectra containing the UO_2^{2+} moiety [5,6,14..16], and X-ray PES studies [9..11,13,17]. Recently, Pepper and Bursten reviewed the issues concerning uranyl [18]. The present work deals with the bonding characteristics of the UO_2^{2+} ion, while its spectroscopy is investigated in Chapter 5. It appeared that the bonding in uranyl was best described when open shell fragments were used. The method we used is the Amsterdam Density Functional (DF) program package [19..21]. This method and the extensions implemented for dealing with open shell fragments are described in Section 2.

The electronic structure of UO_2^{2+} has been much discussed recently. Experimental and theoretical studies have shown that it is linear and the HOMO is of σ_u symmetry [1..12,14]. In the explanation for both these effects the U 6p orbital plays a role. This orbital is spatially quite extended, e.g. more extended than the valence U 5f [12]. This leads to very large overlaps and interaction between U 6p and the σ_u combinations of O 2s and O 2p. The antibonding U 6p-O 2p combination ends up high in the virtual spectrum, above U 5f. Interaction with U 5f then leads to an orbital which has predominantly 5f character and is the HOMO. The large interaction with O 2s creates a large gap between the $1\sigma_u$ (bonding U 6p - O 2s σ_u) and $2\sigma_u$ (antibonding U 6p - O 2s σ_u). Due to the strong participation of U 6p to the bonding in uranyl, 0.5 electron is squeezed out of it [12]. This 6p hole has also been noted by Pyykkö and Lohr [7] and was recently shown by van Wezenbeek et al. [12] to be important for the explanation of the relativistic expansion of UO_2^{2+} and UO_2 . The U 6p orbital has valence character, resulting in large interaction with O and a 6p hole, and also core character, leading to large diagonal and off-diagonal (with U 5p) mass-velocity elements. The expansion is caused by expanding contributions from both mass-velocity elements.

The question of the short U-O bond length has not been addressed so often. It is very surprising that the bond length is so short in the first place, because the U 6p orbital is spatially large and thus should lead to huge repulsion at short U-O distances. Therefore another interaction must be present which overcomes this repulsion. Larsson and Pyykkö and Pyykkö et al. [8], using Relativistic Extended Hückel calculations, qualitatively explain the short U-O bond length by the fact that the HOMO $3\sigma_u$ is mainly U 5f, which

relieves the U 6p-O 2p antibonding character. In Section 3 we will discuss the results of our investigation to the short U-O bond-length, from which also conclusions about the relative 5f and 6d contributions to the bonding are drawn. Veal et al. [17c] concluded from Xray spectra (XPS) that the 5f involvement to the U-O bond in uranyl compounds was small. On the other hand, Cox [13] showed on the basis of MO calculations and XPS that the 5f participation was considerable. From our investigation to the short U-O bond length we will show to agree with Cox [13]. Also we will comment on a recent investigation of Denning and Morrison [15] on the absorption spectrum of the excited state of $\text{Cs}_2\text{UO}_2\text{Cl}_4$, in which they concluded that the 6d orbitals are more important to the bonding in uranyl than the 5f orbitals.

2. Method

The calculations have been carried out using the Amsterdam DF program package [19..21], characterized by the use of a density fitting procedure to obtain an accurate Coulomb potential, by accurate numerical integration of the effective one-electron hamiltonian matrix elements and by the possibility to freeze core orbitals. The LSD exchange potential was used, together with the Vosko-Wilk-Nusair [22] parametrization for correlation, with a correction of Stoll [23]. The calculations were done using the Scalar-Relativistic (SR) option, where the scalar first order (FO) mass-velocity ($- \frac{1}{8} \beta^4$), Darwin ($\frac{1}{8} \nabla^2(V_N)$) and indirect potential (due to relativistic density changes in the inner core shells) relativistic operators are added from the start to the non-relativistic operators. Problems with the mass-velocity operator are circumvented by solving the one-electron equations in the same space as the non-relativistic equations. Compared to FO perturbation theory, in the QR method also higher order corrections due to the first order operators are taken into account [24]. For a more extensive discussion of the SR method we refer to Chapter 1. The SR method has proven to be better than FO perturbation theory (as in [25..27]), especially for elements heavier than third row transition metals [6,24]. An important characteristic of the SR method is the possibility to make a decomposition of the bond energy into steric energy and symmetry decomposed interaction energy terms. We did not study the influence of the spin-orbit splitting, because uranyl is a closed shell molecule, in which case the spin-orbit interaction does not have influence on the energy [27].

The ($1s-5s$), ($2p-5p$), ($3d-5d$), and $4f$ orbitals on U and the $1s$ orbital on O have been frozen. The valence basis was double- for the U $6s$, $6p$ and $7s$, triple- for $5f$ and $6d$ and double- for the O $2s$ and $2p$. A single $7p$ on U and $3d$ on O were added as polarization functions.

The method for analyzing bonding energies is an extension of the decomposition scheme of Morokuma [28] for closed shell systems. The bond energy E is calculated in two steps: First the steric repulsion E^0 is calculated, which is defined as the energy difference between the separate fragments and the overall system described by the determinantal wavefunction ψ^0 , the anti-symmetrized product of the overlapping fragment orbitals:

$$\psi^0 = \left| \begin{array}{cc} \phi_A^1 & \phi_B^1 \\ \vdots & \vdots \\ \phi_A^n & \phi_B^n \end{array} \right| \quad (1)$$

$$E^0 = \langle \psi^0 | H_{AB} | \psi^0 \rangle - \langle \phi_A | H_A | \phi_A \rangle - \langle \phi_B | H_B | \phi_B \rangle \quad (2)$$

In Eq. (1) ϕ_J^i denotes an occupied orbital of fragment J. The steric energy may be divided in two contributions, a) $E_{\text{el.stat}}$, the electrostatic interaction between the unmodified fragments and b) E_{Pauli} , the Pauli, exchange, or overlap repulsion:

$$E^0 = E_{\text{el.stat}} + E_{\text{Pauli}} \quad (3)$$

The Pauli repulsion E_{Pauli} dominates over $E_{\text{el.stat}}$, making E^0 positive (repulsive). The most important contribution to the Pauli repulsion comes from the rise in kinetic energy compared to the separate fragments [29]. This repulsive effect is largest for a two orbital four electron interaction and prevents e.g. the formation of He_2 . Seen in an orbital picture, the antibonding combination of two orbitals is always destabilized more than the bonding combination is stabilized.

When two closed shells interact, one generally lets the wavefunction ψ^0 relax to the SCF solution ψ^{SCF} , which is accompanied by the orbital interaction energy E_{oi} , containing the charge transfer and polarization energies. The bond energy is thus given by:

$$E = E^0 + E_{\text{oi}} \quad (4)$$

If the basis functions are symmetry adapted, the orbital interaction energy can accordingly be symmetry decomposed [30]. Denoting the orbital interaction belonging to symmetry μ as E_{μ} , and the density matrices for the initial wavefunction (ψ^0) and final wavefunction (ψ^{SCF}) by P^i and P^f , the formula for the interaction energy is:

$$E_{\text{oi}} = \sum_{\mu} E_{\mu} = \sum_{\mu} \langle F_{\mu}^{\text{TS}} | P_{\mu}^{\text{TS}} \rangle \quad (5)$$

where F^{TS} is the transition state Fock matrix: $F^{\text{TS}} = F[(P^i + P^f)/2]$, $P = P^f - P^i$ and the summation runs over the symmetry adapted basis functions of the irreducible representations μ .

The uranyl ion UO_2^{2+} can be viewed as originating from two open shell fragments, as will be shown in Section 3. In this case we use a recently developed method for calculations from open shell fragments [31]. We define:

$$^0 = \left| (\text{closed shells})_A (\text{closed shells})_B \begin{smallmatrix} \circ \\ \text{A} \end{smallmatrix} (1) \begin{smallmatrix} \circ \\ \text{B} \end{smallmatrix} (2) \right| \quad (6)$$

with $\begin{smallmatrix} \circ \\ \text{A} \end{smallmatrix}$ and $\begin{smallmatrix} \circ \\ \text{B} \end{smallmatrix}$ denoting the open shells on A and B respectively, with opposite spins. The orbital interaction step in this case consists besides the relaxation and charge transfer, of the pair bond energy, i.e. the energy gained by pairing the open shell electrons in the bonding combination of the orbitals. In this work we do not view the pair bonding as a separate step, as was done by Bickelhaupt et al. [31] in a study on the relative stability of the three CN^* dimers.

3. An explanation for the short U-O distance in UO_2^{2+}

As already mentioned in the introduction, the U-O distance in UO_2^{2+} is very short compared to distances of U to secondary ligands [2]. In view of the large overlaps of U 6p and O [12] this seems strange. We therefore investigated the bonding in UO_2^{2+} to get more insight into this apparent paradox. As an introduction we give in Fig. 1 a level scheme for the highest occupied and lowest virtual orbitals of UO_2^{2+} for an U-O distance of 3.25 a.u. in Scalar-Relativistic (SR) and non-relativistic (NR) calculations. The distance chosen is close to the SR equilibrium distance of 3.24 a.u. (see later).

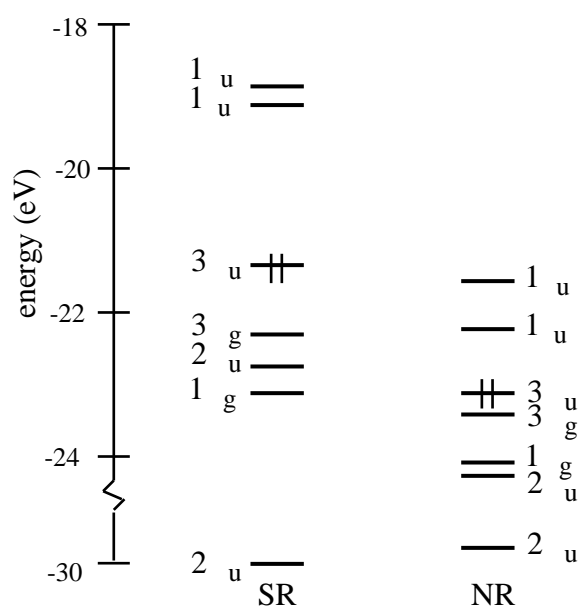


Figure 1. SR and NR level schemes of UO_2^{2+} for U-O distance of 3.25 a.u.

Concentrating first on the levels of SR UO_2^{2+} , note the σ_u HOMO and the virtual level ordering $f < p$. In Table 1 the result of a Mulliken population analysis is given. The large interaction between U 6p and O orbitals in σ_u symmetry was mentioned before in the introduction and has been stressed in [12]. The resulting levels $1_{\sigma_u} \dots 4_{\sigma_u}$ are given in Fig. 2. The cause of the large interaction is large overlaps between U and O, a selection of which is plotted in Fig. 3. The overlap between U 6p and O 2p is much larger than that between U 5f and O 2p. The U 6p-O 2s overlap is almost as large, leading to a huge splitting between 1_{σ_u} and 2_{σ_u} (see Chapter 5). Orbital 3_{σ_u} is the HOMO, with much 5f character, as explained before in the introduction. Also 4_{σ_u} contains some 6p character: the 6p hole which was already mentioned is found here. The interaction in π_u symmetry is of interest too: The U 6p-O 2p π_u interaction is smaller than the corresponding U 6p-O 2p σ_u interaction in σ_u symmetry, due to a smaller overlap. Together with a reasonably large U 6p-O 2p energy difference, this leads to an orbital 1_{π_u} which is almost a pure U 6p orbital. The orbitals 2_{π_u} and 3_{π_u} are the bonding and antibonding U 5f-O 2p π_u combinations, respectively. The considerable overlap between U 5f and O 2p and their small energy difference leads to a heavy mixing: the bonding combination is a 35%-65% mixture. Note that although near R_e the U 5f-O 2p overlap is nearly equal to the U 6p-O 2p overlap, the U 5f-O 2p mixing is much larger by the smaller energy difference.

Table 1. Scalar-Relativistic population analysis for orbitals of UO_2^{2+} for U-O distance of 3.25 bohr.

Orbital	Orbital character	Eigen-value (eV)	Atomic composition (%)							
			U 5f	U 6s	U 6p	U 6d	U 7s	U 7p	O 2s	O 2p
<i>unoccupied orbitals</i>										
4_{σ_u}	2p-6p anti-b.	-10.67	32		8			10	2	45
3_{σ_u}	5f-2p anti-b.	-15.84	66					2		31
1_{π_u}	5f	-18.62	100							
1_{σ_u}	5f	-19.07	100							
<i>occupied orbitals</i>										
3_{σ_u}	5f (-2p bond.)	-21.47	57		7				3	42
3_{σ_g}	O 2p (-6d bond.)	-22.33		1		13	1		9	76
2_{π_u}	5f-2p π -bond.	-22.69	35		1					64
1_{σ_g}	O 2p (-6d bond.)	-23.08				19				80
2_{π_u}	6p-2s ab., -2p b.	-30.05	4		28			-3	61	7
2_{σ_g}	2s (-6s anti-b.)	-36.78		2		4	-3		94	2
1_{π_u}	6p	-38.52			97					2
1_{σ_u}	2s-6p bond.	-44.25			42			-3	46	13
1_{σ_g}	6s (-2s bond.)	-64.57		88					4	6
<i>gross populations</i>			2.6	1.8	5.5	1.1	0.0	-0.1	2.2	4.3

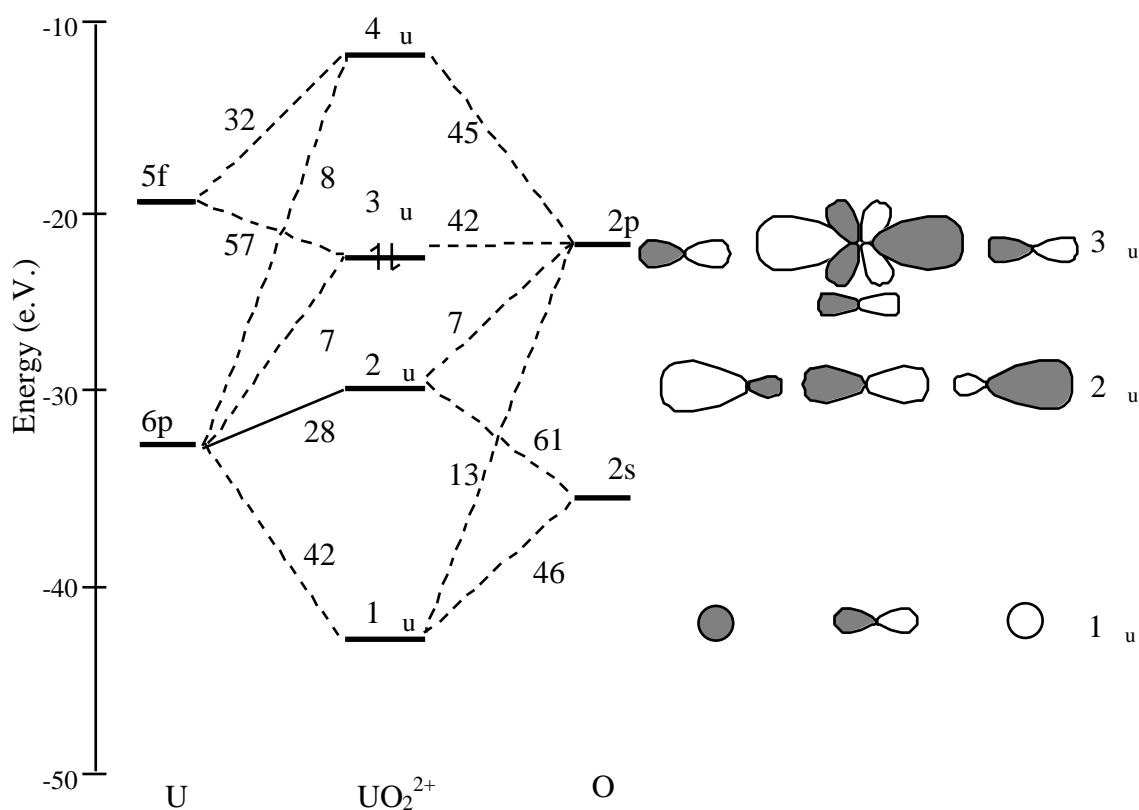


Figure 2. Level scheme for σ_u in UO_2^{2+} for U-O distance of 3.25 bohr.

It is interesting to note that the overlap between U 5f and O 2p is larger than that between U 5f - O 2p, while on the contrary for U 6p the overlap in σ_u is larger. This can be explained by looking at the directional properties of U 5f and U 6p. The U 5f orbital is more directed towards O, while U 6p is perpendicular to the U-O axis. In the gerade symmetries there is also interaction, in σ_g between U 6s, U 6d and O 2s and O 2p, while in π_g only between U 6d and O 2p. The origin for the considerable interaction of U 6d is large overlaps with O 2s and 2p, from Fig. 3b these are even larger than those with U 6p, not unexpected, as the U 6s and 6d orbitals have the same main quantum number as U 6p. Note also that the U 6d overlaps are relatively insensitive to the U-O distance. Also interesting from Table 1 is that the mixing in ungerade symmetries is larger than for gerade symmetries, which is a result of the fact that the atomic U 5f is closer to O 2p than U 6d. In a previous study on the relativistic expansion of uranyl [12], the non-relativistic situation was the starting point. In Table 2 the NR Mulliken analysis for uranyl with U-O distance 3.25 a.u. is given, and the highest levels are included in Fig. 1.

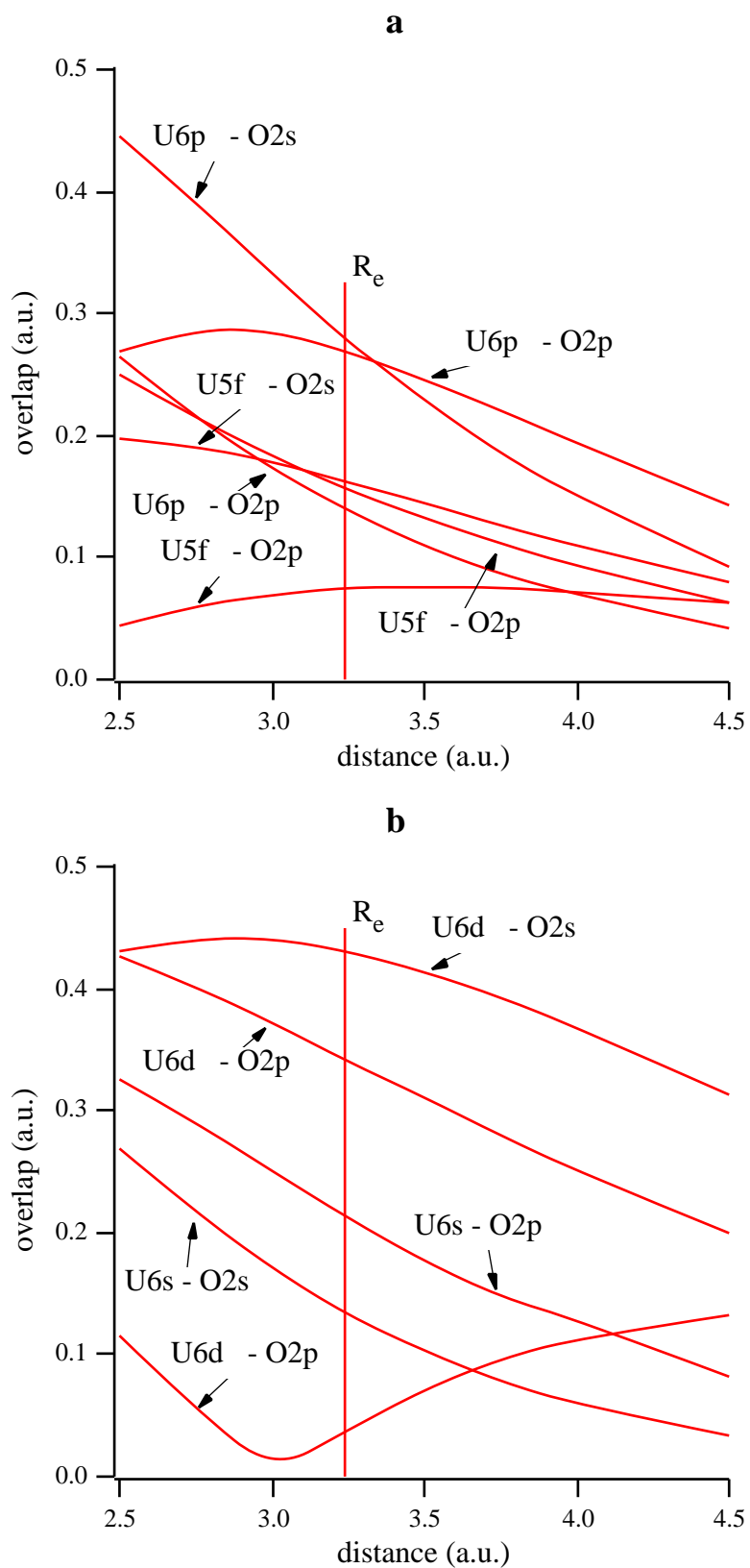


Figure 3. Overlaps between orbitals of U and O in symmetries σ_u and π_u (a) and in σ_g and π_g (b).

Table 2. Non-relativistic population analysis for orbitals of UO_2^{2+} for U-O distance of 3.25 bohr.

Orbital	Orbital character	Eigen-value (eV)	Atomic composition (%)								
			U 5f	U 6s	U 6p	U 6d	U 7s	U 7p	O 2s	O 2p	
<i>unoccupied orbitals</i>											
4 _u	2p-6p anti-b.	-11.61	29		21					2	46
3 _u	5f-2p anti-b.	-18.46	56		1						43
1 _u	5f	-21.69	100								
1 _u	5f	-22.26	100								
<i>occupied orbitals</i>											
3 _u	5f (-2p bond.)	-23.08	70		11					1	18
3 _g	O 2p (-6d bond.)	-23.28		3		15	2			7	74
1 _g	O 2p (-6d bond.)	-24.10				15					84
2 _u	5f-2p -bond.	-24.12	46		3						51
2 _u	6p-2s a.b., -2p b	-29.38	-1		35			-3		52	17
1 _u	6p	-34.61			95						4
2 _g	2s (-6s anti-b.)	-36.40		16		3	-3			85	-1
1 _u	2s-6p bond.	-43.35	2		32			-2		55	12
1 _g	6s (-2s bond.)	-49.79		79						14	6
<i>gross populations</i>			3.2	2.0	5.5	0.9	0.0	-0.1		2.1	4.0

Comparing the NR and SR results, the well known relativistic effects on atomic orbitals can be seen [12], i.e. stabilization of s and p orbitals, and destabilization of d and f orbitals. The low 1,2_u and 1_g orbitals contain much U 6p and 6s character and are consequently stabilized. Also the character of those AOs is more found in lower orbitals in the SR calculation. The destabilization of U 5f is seen in the non-bonding f, f orbitals and the higher energy and the smaller 5f content in the SR HOMO 3_u. Apparently the gap of the destabilized U 5f orbital and the O 2p_u combination, pushed up by U 6p, is smaller in the relativistic case, leading to more mixing, and therefore less U 5f character. Also note that the 3_u has a gap of 1.13 eV with the 3_g below, while the corresponding non-relativistic 3_u and 3_g were separated by only 0.19 eV (Table 2). The reason is the larger 5f than 6d contribution in _u resp. _g and consequently larger (indirect) relativistic destabilization of the 3_u. Also the U 5f orbital itself has a larger relativistic destabilization.

Next we arrive at the investigation of the short U-O bond length. For the analysis to be given, first it must be determined from which fragments uranyl can best be seen to originate. To this end Mulliken gross orbital populations (SR) are given at the bottom of Table 1. From those and the populations per orbital it follows that the formation of UO_2^{2+}

can be seen as the reaction of (excited) O_2^- ($2s_g^2 2s_u^2 2p_u^2 2p_g^2 2p_g^4 2p_u^1$) with O-O distance as in uranyl and U^{3+} ($6s^2 6p^2 6p^4 5f^2 5f^1 6d^0 7s^0$). Both fragments are open shell systems in u and u . The interaction in these symmetries is then viewed as a pair bond, i.e. between $U 5f_u$ and $O 2p_u$ in u and between $U 5f_{-2}$ and $O 2p_{-2}$ in u . We used the recently developed method for calculating bond energies from open shell fragments [31], which was described in Section 2. The bond energy for the formation of UO_2^{2+} was calculated with respect to spherical, spin restricted neutral atoms. In this process first the fragments U^{3+} and O_2^- were prepared, which is accompanied by the energy change E_{excit} . The term E_{excit} is added to E^0 and E_{oi} to obtain the total bond energy E . It has no influence on the equilibrium U-O bond length in uranyl, because for all U-O distances the same U^{3+} fragment is used, and the oxygen atoms are well separated in the fragment O_2^- . For all U-O distances the value of E_{excit} is 30 eV. In the final step the fragments U^{3+} and O_2^- are allowed to interact, leading to the SCF solution. The bond energy curve for UO_2^{2+} is given in Fig. 4a. The equilibrium U-O distance R_e is 3.24 a.u. = 1.71 Å. This agrees nicely with the experimental value of 1.77 Å for the U-O distance in $Cs_2UO_2Cl_4$ reported recently by Denning and Morrison [14]. It is also close to the value 3.21 a.u. found in the previous study on uranyl [12] where the Slater X exchange potential [32] was used.

Before discussing the bond energy decomposition we will describe the most important repulsions between the fragments. Especially the closed shell repulsions are important, as was mentioned in Section 2. In the gerade symmetries we have in g the repulsion between $U 6s$ and the $O 2s_g$ and $2p_g$ combinations, and in g there is no repulsion, as there are no occupied U orbitals. The ungerade symmetries are more complicated. In u we have the (from their large overlap, see Fig. 3a) strong closed shell repulsion of $U 6p_u$ and $O 2s_u$. Also the $U 5f_{-1} - O 2s_u$ and $U 6p_{-1} - O 2p_u$ repulsions are present, both of which are expected to be strong too, as their overlap in Fig. 2a is large. Of course there is no repulsion (opposite spins) between $U 5f_u$ and $O 2p_u$. Finally in u symmetry we only have the $U 6p_{-1} - O 2p_u$ repulsion, which is much smaller than its u analogue due to a smaller overlap (Fig. 3a).

The decomposition of the bonding energy into E^0 and E_{oi} is given in Fig. 4b. In Table 3 the energy terms are given for an U-O distance of 3.25 a.u. The second until fourth column will be discussed later. The excitation energy is quite large, about 30 eV, for which the U to U^{3+} ionization is responsible. We see from Fig. 4b that E^0 is repulsive as usual, with a dominant Pauli repulsion E_{Pauli} . This has already been mentioned in the introduction. On the other hand the orbital interaction curve is attractive for all U-O distances and accounts for the bonding. At short distances the steric repulsion dominates, which is responsible for the building up of the repulsive wall.

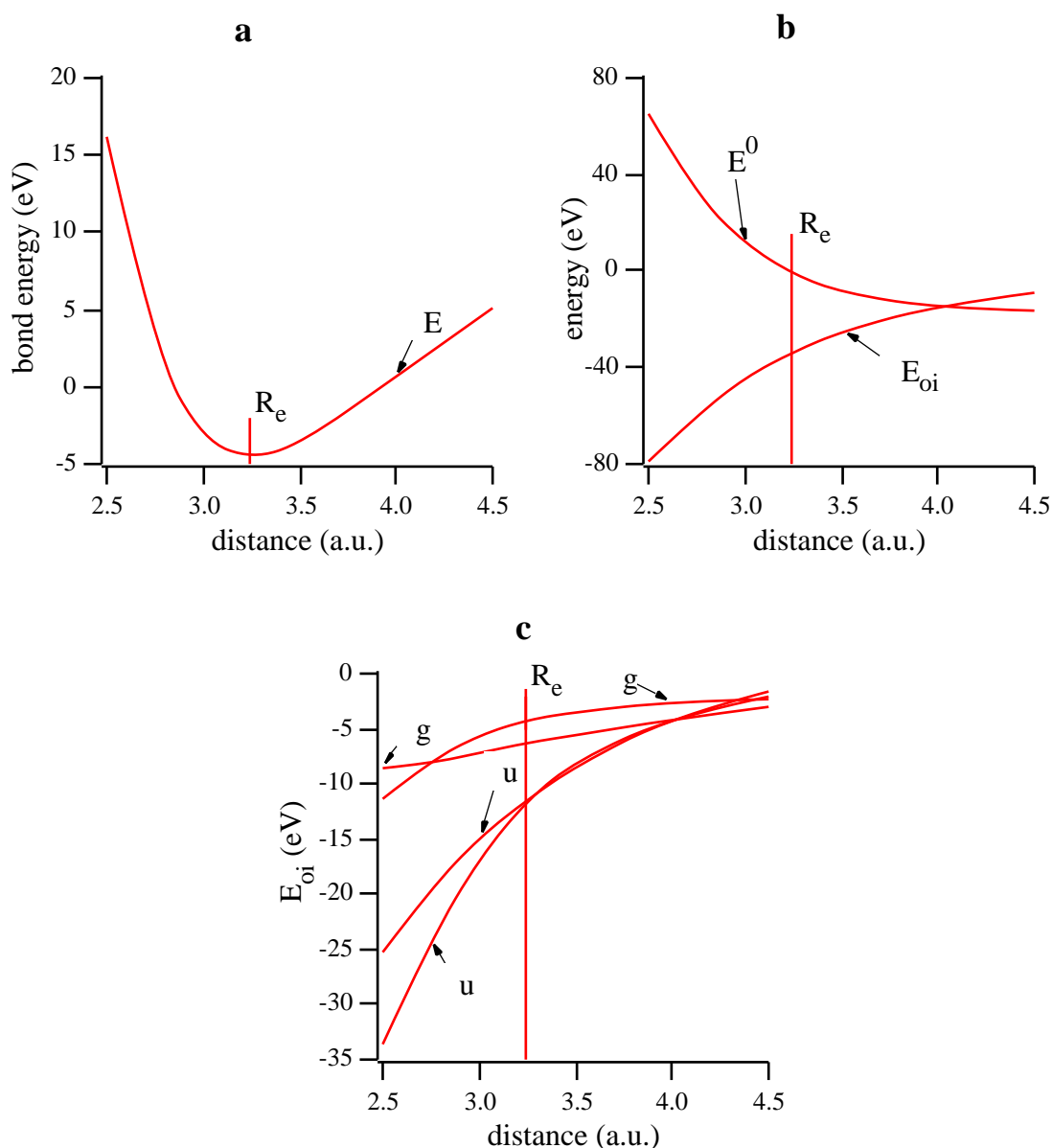


Figure 4. Bond energy decomposition for UO_2^{2+} from open shell fragments (see text). a) Total bond energy ΔE . b) Bond energy split into ΔE^0 and ΔE_{oi} . c) ΔE_{oi} split up into symmetry contributions.

The symmetry decomposition of the orbital interaction is given in Fig. 4c and Table 3 and shows that the interaction energies in the ungerade symmetries u and u are larger than those in gerade symmetries. We can understand this, because in the gerade symmetries we have the interaction between U 6d and O, and we already showed in Table 1 that the mixings in these symmetries were smaller than in the ungerade symmetries. Furthermore the g and g curves are relatively insensitive to the U-O distance, which does not follow from the overlap curves (Fig. 3b). So there is U 6d-O bonding, but

because it is not sensitive to distance variation, it does not play a role in determining the short U-O distance. In contrast to the gerade symmetries, the σ_u and π_u interaction energies both are large. As in those symmetries the bonding between U 5f and O takes place, the question is whether this proves that the 5f σ and 5f π orbitals are responsible for the short U-O distance. First we concentrate on σ_u symmetry. The destabilized U 6p σ -O 2p σ_u level is close to U 5f σ , and their interaction is consequently large and leads to the HOMO 3 σ_u . The U 5f σ -O 2p σ_u interaction relieves a lot of the U 6p σ -O 2p σ_u repulsion. Larsson and Pyykkö and Pyykkö et al. stated [8] that this relief of antibonding U 6p σ -O 2p character might be the reason for the short U-O bond length.

The situation is more complicated however. One must realize that in σ_u considerable Pauli repulsion is still present. The occupied U 6p σ orbital interacts with the O 2s σ_u combination and the partially filled O 2p σ_u . Also the 5f σ electron has repulsion with O 2s σ_u . The formation of the pair bond between U 5f σ and O 2p σ_u certainly reduces the effect of the repulsion, but the question is whether it relieves it completely, or the repulsion still dominates. Another complication may be the fact that also the electrostatic contributions from the orbitals may be important. For example, occupation of O 2p σ_u leads to repulsion with U 6p σ , but also has an attractive effect on $E_{\text{el.stat}}$. It therefore appears that looking only at the interaction energy is not enough in this case, we also need the values of the steric contributions from U 5f and 6p with O 2s and 2p in symmetry σ_u .

But before doing so, the different situation in π_u symmetry must be noted. We already showed that the interaction between U 6p π and O 2p π is much smaller than its σ_u analogue, 1 π_u is nearly pure U 6p. From this fact it is deduced that the repulsion between

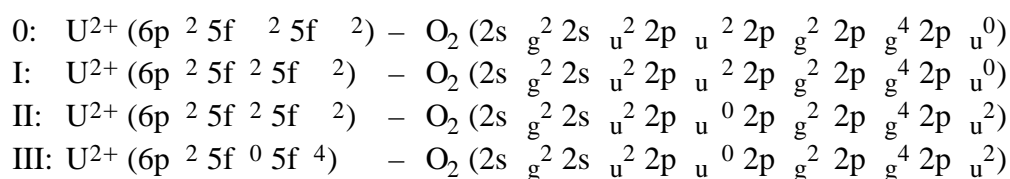
Table 3. Bond energy analysis for UO_2^{2+} from fragments at U-O bond length 3.25 a.u.

Energy term	$U^{3+} - O_2^-$	Comb. 0	Comb. I	Comb. II	Comb. III
E_{excit}	30.24	15.03	18.61	20.29	19.41
$E_{\text{el. stat}}$	-46.38	-14.70	-27.18	-33.22	-24.53
E_{Pauli}	44.73	31.62	42.01	60.76	42.57
E^0	-1.65	16.9	14.8	27.54	18.04
<i>Orbital interaction energies:</i>					
E^g	-4.26		-3.26		
E^g	-6.37		-4.45		
E^g	-11.29		-16.85		
E^u	-11.30		-13.44		
E_{oi}	-33.23		-38.01		
E	-4.63		-4.57		

U 6p and O 2p_u is small. Also the O 2p_u combination is only half filled in the O₂⁻ fragment, giving smaller than maximal repulsion. In _u symmetry the U 5f -O 2p_u interaction is then expected to dominate over the repulsion.

Next we describe the determination of the steric interactions between U and O orbitals in _u symmetry. It is not possible to make a symmetry decomposition for E⁰ as was mentioned in Chapter 1 Section 6. The only way we can get an estimate of the orbital contributions is by performing calculations from a number of fragments, differing in the occupation of specific _u orbitals. From the differences in E_{Pauli} and E_{el.stat} values we will then be able to deduce approximate values for the U 5f -O and U 6p -O contributions to the steric repulsion.

We did calculations on uranyl from fragments U²⁺ and O₂. Different fragments were chosen compared to the one we discussed up to now, because it allows us to isolate the relevant Pauli repulsions. The following combinations of fragments were compared:



In all combinations we have the closed shell repulsions in _g (U 6s- O 2s_g) and _u (U 6p - O 2s_u), where the U 6p - O 2s_u repulsion is the most important one, as these orbitals are closest in energy and have the largest overlap (see Fig. 3). In combination 0 this U 6p - O 2s_u closed shell repulsion is the only repulsion, and the steric energy is thus mainly a measure of the U 6p - O 2s_u repulsion in _u. The orbital interaction has to go against this repulsion in all considered configurations. In addition to the closed shell repulsion, in combination I the 5f -2s_u, in combination II the 6p -2p_u, 5f -2s_u and 5f -2p_u, and in combination III the 6p -2p_u repulsions are present. Note also that compared to 0 and I, in II and III there is no U 6p -O 2p_u repulsion. We already have shown that this repulsion is very small and therefore we neglect it, together with electrostatic contributions from it. Furthermore, in combination 0 we have two electrons in U 5f, which are transferred to other orbitals in the combinations I-III. We assume that these very contracted 5f electrons have very small electrostatic interaction. Our steric energy analysis is based on the neglect of the above mentioned 5f electrostatic and U 6p -O 2p_u steric energies, and is therefore approximate.

From Table 3 combination 0 we see that the closed shell repulsion, which is dominated by the U 6p - O 2s_u repulsion, is equal to 16.9 eV. This repulsion is also present in the other cases, and is seen to be dominant there also, i.e. the other steric

effects are all smaller than the closed shell repulsion. Note the much smaller E_{excit} compared to the $U^{3+}-O_2^-$ fragments case, because now only 2 electrons are ionized from U. The E_{Pauli} values from our approximate analysis differ considerably, and knowing which repulsions are present in u symmetry, we will be able to get an estimate of their magnitude. Adding the electrostatic effects then results in the overall steric energy contributions of U-O orbital combinations. The symmetry decomposition of the orbital interaction is only given for I, because the fragments for 0, II and III are not representative for the final situation in uranyl.

From the difference between the Pauli repulsions of combinations I and 0 we deduce that the $5f-2s_u$ Pauli repulsion is equal to 10.4 eV. However also the change in electrostatic energy $E_{\text{el.stat}}$ must be taken into account. Neglecting the U 5f electrostatic energy, we see that putting two electrons in U 5f leads to an increase in electrostatic energy which is larger than the increase in Pauli repulsion. The total steric effect of the $5f-2s_u$ interaction is -2.1 eV. In the same way the $6p-2p_u$ Pauli repulsion is calculated as 11.0 eV from the difference in Pauli repulsions of combinations III and 0. However, occupation of O $2p_u$ in III also has a large attractive electrostatic effect. The overall $6p-2p_u$ steric effect is still repulsive, but only by 1.1 eV. Finally, subtracting the E^0 value of III from II we find that the sum of the steric effects of $5f-2s_u$ and $5f-2p_u$ is equal to 9.5 eV. The $5f-2s_u$ effect being -2.1 eV, the $5f-2p_u$ steric effect is thus 11.6 eV. This is the only interaction which is very repulsive so far, but it is not important for the formation of uranyl from U^{3+} and O_2^- , as U 5f and O $2p_u$ have opposite spins in the fragments.

Now we come to the discussion of the short bond length in uranyl, built from the fragments U^{3+} and O_2^- . First the value of the steric repulsion is determined from the values of the steric interactions between U 5f, U 6p and O 2s, 2p as determined above. The Pauli repulsion part of E^0 can be compared directly to the previous cases, as the orbitals change little. Adding the closed shell Pauli repulsion of combination 0 (31.6 eV) and half of the U 6p-O $2p_u$ and U 5f-O $2s_u$ Pauli repulsions which together amount to 10.7 eV ($1/2(11.0+10.4)$), we arrive at 42.3 eV, which is close to the E_{Pauli} value of 44.7 eV for uranyl from U^{3+} and O_2^- . Therefore the values for the steric effects determined above approximately hold also in the present case.

First we discuss the closed shell repulsion, dominated by the U 6p-O $2s_u$ repulsion. From the results of Table 1 it follows that we may view the U 6p-O $2p_u$ interaction as largely independent from the U 6p-O $2s_u$ interaction, because there is hardly any O 2s character above the mainly bonding and antibonding O 2s-U 6p orbitals 1_u and 2_u , and the O 2p character is found mainly above 1_u and 2_u . From this it follows that the large U 6p-O $2s_u$ interaction, leading to a huge splitting between 1_u and 2_u of 15.8 eV, determines the closed shell repulsion. The closed shell repulsion is an effect in u

symmetry, which is separated from the interactions between U 5f, 6p and O 2p. It is only important in providing the repulsive wall in the bond energy curve.

For a discussion of the relative importance of steric and orbital interaction contributions we therefore confine ourselves to the U 5f, 6p and O 2p orbitals. As to the steric interaction, half of the U 6p -O 2p_u and U 5f -O 2s_u effects are present, which amounts to -0.5 eV (1/2 (-2.1+1.1)). Looking only at the Pauli repulsion would have resulted in a value of 10.7 eV (1/2 (11+10.4)). From Table 3 the orbital interaction amounts to -11.3 eV, which is much larger than the combined steric effects of the U 5f, 6p and O 2p. As the orbital interaction is mainly made up of the pair bond between U 5f and O 2p_u (Table 1), we must conclude that the U 5f -O 2p_u pair bond is dominant in the U 5f, 6p and O 2p orbital manifold in σ_u . Although the orbital interaction is larger than the steric effect in σ_u , still the Pauli repulsion between U 6p and O 2p_u is important in that it destabilizes the O 2p_u combination, which then afterwards can have a very favourable interaction with U 5f. However the large increase in electrostatic energy which is also present when occupied U 6p and O 2p_u orbitals interact in a repulsive way, reduces the pure Pauli repulsion to a large extent. It appears that in uranyl the simple one-electron picture of only Pauli repulsion is too simplified, the large electrostatic effects must be considered too.

For σ_u symmetry we showed that the U 6p -O 2p_u repulsion may be neglected, and the orbital interaction energy consists only of the U 5f -O 2p_u pair bond. The interaction energy is identical to the σ_u interaction energy, -11.3 eV. Thus although the situation in σ_u is different than in σ_g , with no closed shell repulsion from O 2s and a negligible repulsion of U 6p -O 2p_u, the net energies (steric plus orbital interaction) are similar. A strong U 5f -O 2p_u bond is found, analogous to the U 5f -O 2p_u bond.

The final picture that emerges for the explanation of the short U-O bond length in uranyl is then as follows. The U 5f orbital plays a decisive role, both in σ_u and σ_g symmetries, where the main interactions are between U 5f, 6p and O 2p. The dominant contribution to the overall interaction is provided by the U 5f -O 2p_u and U 5f -O 2p_g pair bonds, both are approximately -11 eV (Table 3). This is very surprising when looking at the much larger (approx. a factor of two) f -2p_u overlap in Fig. 3a, and the fact that there are two σ bonds. Although the f -2p_u overlap is smaller than the f -2p_g overlap, the interactions are equal by the better interaction of f with the O 2p_u orbital which was destabilized by U 6p. Such an effect is not present in σ_u symmetry. The U 6p orbital does not interact with O 2p and stays nearly pure, a direct consequence of the overlap. That the U 5f interacts so strongly with O 2p compared to U 6p is caused by a smaller energy difference between U 5f and O 2p, as their overlaps are nearly identical (Fig. 3a).

Working against the U 5f-O interaction are the steric effects. As we showed before, in σ_u we have below O 2p σ_u the completely filled O 2s σ_u combination, having a large closed shell repulsion with U 6p σ_u . This effect is however separate from the interactions in the U 5f, 6p and O 2p manifold. It provides the repulsive wall the U 5f interactions have to go against. The steric interactions between the orbitals that in the second step of orbital interaction provide the relaxation energy, are very small both in σ_u and σ_g . For σ_u symmetry this was expected, but in σ_g the steric interaction appeared to be very complicated. Looking only at the Pauli repulsion is not enough, as also electrostatic effects are important. The net effect is then a small repulsive effect from the U 6p σ_u -O 2p σ_u interaction, while in the 5f σ_g -2s σ_u interaction a small attractive effect results from a dominant electrostatic effect. The overall σ_u steric effect was slightly attractive.

Adding the steric and orbital interaction energies, the conclusion from the above results must be that the U 5f σ_g -O 2p σ_u and U 5f σ_g -O 2p σ_u pair bond interactions are responsible for the short U-O distance in uranyl. The closed shell repulsion between U 6p σ_u -O 2s σ_u appears in the same symmetry as the f σ_u pair bond, but is not related to it. It merely provides the repulsive wall in the uranyl bond energy curve. Near R_e it is of the same order of magnitude as the 5f-O 2p interactions, and therefore a short U-O distance is needed to have an effective interaction. The U 6d σ_g -O 2p σ_g bond in σ_g is not small, but not relevant to the shortness of the U-O distance due to the fact that its interaction curve (Fig. 4c) is so flat.

Finally we will comment on the question of the relative importance of the 5f and 6d orbitals to the bonding in uranyl. From our results presented above we find a more important 5f than 6d contribution, in agreement with Cox [13]. The short bond length in uranyl is caused by the 5f-O 2p bond, and furthermore our Mulliken analysis in Table 1a shows more mixing in σ_u , σ_u orbitals than in the σ_g and σ_g orbitals. We showed that the U 6d σ_g interaction is important because it has a net attractive effect, although much smaller than the 5f σ_g interaction. However, the 5f interaction is larger and becomes stronger at shorter U-O distance, while for the 6d σ_g interaction there is almost no distance behaviour. Recently, Denning and Morrison [15] studied the excited state absorption spectrum of Cs₂UO₂Cl₄. They conclude from the fact that excitation from the 3 σ_g leads to a larger expansion of the U-O bond length than excitation from the 3 σ_u that the U 6d orbitals are more important in the bonding in uranyl than the 5f orbitals. Our results do not corroborate this conclusion, and also do not agree with those of Veal et al. [17c], who found no 5f participation to the bond in uranyl.

4. Conclusion

We showed that the short U-O bond-length in uranyl is mainly caused by the strong U 5f -O 2p_u and U 5f -O 2p_u interactions. In symmetry _u there is a large closed shell U 6p_u and O 2s_u repulsion, which is separated from the main interacting orbitals U 5f, 6p and O 2p. The steric effects from U 6p_u -O 2p_u and U 5f -O 2s_u are small, because the repulsive Pauli repulsions are cancelled by electrostatic effects. The contribution from U 6d_u to the bond in uranyl is also attractive, but smaller than the U 5f interactions and not important for the short U-O bond length, because it has a flat distance behaviour.

The role of the U 6p orbital in the present work is that a short U-O length is needed to overcome the large U 6p-O 2s repulsion. The U 6p orbital is very extended (larger than the valence U 5f) and the consequently large interaction with O leads to its presence in virtual orbitals: the 6p hole. This together with large mass-velocity elements from its core character explains the relativistic expansion of uranyl [12]. This expansion however is only present because the U-O distance is so short. Thus we arrive at the result of the present study, i.e. our investigation of why the U-O distance is so short.

The strong interaction of U 6p and O also has the consequence of the HOMO being of _u symmetry and having much 5f character. This determines the excitation spectrum as measured by Denning et al. [14,15], which is therefore indirectly influenced by U 6p. Finally, also the U 6p and O 2s interaction is very large, and this fact is important for an understanding of the ionization spectrum measured by Veal and Lam [17]. We will give a detailed description and explanation of the ionization and excitation spectra in Chapter 5.

References.

- 1: C.K. Jørgensen and R. Reisfeld, Chem. Phys. Lett. **35** (1975) 441
- 2: C.K. Jørgensen and R. Reisfeld, Structure and Bonding **50** (1982) 121
- 3: C.K. Jørgensen, Chem. Phys. Lett. **89** (1982) 455
- 4: K. Tatsumi and R. Hoffmann, Inorg. Chem. **19** (1980) 2656
- 5: R.L. DeKock, E.J. Baerends, P.M. Boerrigter and J.G. Snijders, Chem. Phys. Lett. **105** (1984) 308
- 6: P.M. Boerrigter, Thesis, Vrije Universiteit Amsterdam, 1987
- 7: P. Pyykkö and L. Lohr, Inorg. Chem. **20** (1981) 1950
- 8: a) S. Larsson and P. Pyykkö, Chem. Phys. **101** (1986) 355
b) P. Pyykkö, L.J. Laaksonen and K. Tatsumi, Inorg. Chem. **28** (1989) 1801
- 9: P.F. Walch and D.E. Ellis, J. Chem. Phys. **65** (1976) 2387

- 10: J.H. Wood, M. Boring and S.B. Woodruff, *J. Chem. Phys.* **74** (1981) 5225
- 11: C.Y. Yang, K.H. Johnson and J.A. Horsley, *J. Chem. Phys.* **68** (1978) 1001
- 12: E.M. van Wezenbeek, E.J. Baerends and J.G. Snijders, *Theor. Chim. Acta* **81** (1991) 139
- 13: L.E. Cox, *J. of Electr. Spectr. and Related Phenom.* **26** (1982) 167
- 14: a) R.G. Denning, T.R. Snellgrove and D.R. Woodwark, *Mol. Phys.* **32** (1976) 419
b) R.G. Denning, T.R. Snellgrove and D.R. Woodwark, *Mol. Phys.* **37** (1979) 1089
- 15: R.G. Denning and I.D. Morrison, *Chem. Phys. Lett.* **180** (1991) 101
- 16: T.J. Barker, R.G. Denning and J.R.G. Thorne, *Inorg. Chem.* **26** (1987) 1721
- 17: a) B.W. Veal and D.J. Lam, *Phys. Rev. B* **10** (1974) 4902
b) B.W. Veal, D.J. Lam, W.T. Carnall and H.R. Hoekstra, *Phys. Rev. B* **12** (1975) 5651
c) B.W. Veal, D.J. Lam, W.T. Carnall and H.R. Hoekstra, in 'Plutonium and Other Actinides', Eds H. Blank and R. Linder, North-Holland, Amsterdam, 390
- 18: M. Pepper and B.E. Bursten *Chem. Rev.* **91** (1991) 719
- 19: a) E.J. Baerends, D.E. Ellis and P. Ros, *Chem. Phys.* **2** (1973) 42
b) E.J. Baerends and P. Ros, *Chem. Phys.* **2** (1973) 51
c) E.J. Baerends and P. Ros, *Int. J. Quant. Chem.* **S12** (1978) 169
- 20: a) J.G. Snijders and E.J. Baerends, *Mol. Phys.* **36** (1978) 1789
b) J.G. Snijders, E.J. Baerends and P. Ros, *Mol. Phys.* **38** (1979) 1909
- 21: P.M. Boerrigter, G. te Velde and E.J. Baerends, *Int. J. Quant. Chem.* **33** (1988) 87
- 22: S.H. Vosko, L. Wilk and M. Nusair, *Can. J. Phys.* **58** (1980) 1200
- 23: H. Stoll, E. Golka and H. Preus, *Theor. Chim. Acta* **55** (1980) 29
- 24: T. Ziegler, V. Tschinke, E.J. Baerends, J.G. Snijders and W. Ravenek, *J. Phys. Chem* **93** (1989) 3050
- 25: J.G. Snijders and E.J. Baerends, *Mol. Phys.* **36** (1978) 1789
- 26: J.G. Snijders, E.J. Baerends and P. Ros, *Mol. Phys.* **38** (1979) 1909
- 27: T. Ziegler, J.G. Snijders and E.J. Baerends. *Chem. Phys.* **74** (1981) 1271
- 28: K. Morokuma, *J. Chem. Phys.* **55** (1971) 1236
- 29: P.J. van den Hoek, A.W. Kleyn and E.J. Baerends, *Comments At. Mol. Phys.* **23** (1989) 93
- 30: T. Ziegler and A. Rauk, *Theor. Chim. Acta* **46** (1977) 1
- 31 F.M. Bickelhaupt, N. Nibbering, E.M. van Wezenbeek and E.J. Baerends, submitted to *J. Phys. Chem.*
- 32: J.C. Slater, *Phys. Rev.* **81** (1951) 385

Chapter 4b

A qualitative study of the relativistic effects on the bond between HfCl_3 , ThCl_3 and H

Abstract

The relativistic effects on the bonds between H and MCl_3 (M=Hf,Th) were investigated by comparing Non-Relativistic (NR), Scalar-Relativistic (SR) and First Order Relativistic Perturbation Theory (FOPT) calculations on the title systems.

The bonding between the transition metal fragment HfCl_3 and H is qualitatively the same in Non-Relativistic and Scalar-Relativistic schemes: the 5d contribution to the bond is larger than the 6s contribution. In the SR calculation the 6s is stabilized and therefore relatively more 6s character is present. In line with the small relativistic effects, FOPT in this system is sufficient for a proper description of the bonding to H.

In the heavier actinide system ThCl_3H there are large differences between the NR and SR schemes. Non-relativistically there is a dominant 5f and 6d bonding to H, but in the Scalar-Relativistic calculation mainly the Th 6d is important. The 7s orbital hardly contributes to the bond with H. Also in ThCl_3H ultimately the relativistic atomic (Th) effects are responsible for the effects of relativity on the molecule: The relativistic destabilization of Th 5f reduces its contributions to the bonding, while the stabilization of the 7s increases the importance of this orbital, though still small compared to the Th 6d. The large relativistic effects also show up in the large difference between E_{SR} and E_{FO} , or put differently First Order Perturbation theory is not adequate for a description of the bond in ThCl_3H .

1. Introduction

In the last decade calculations including relativistic effects on molecules have become almost routine. Out of the large number of methods available, we mention the First-Order Perturbation Theory (FOPT) and the Quasi-Relativistic (QR) methods in the Amsterdam Density Functional (DF) program package [1..5 and Chapter 1], the basis set expansion method to solve the Dirac Hamiltonian [6] and Relativistic Effective Core-Potentials [7].

It has been shown that for systems containing elements up to Au and Hg ($Z = 80$) FOPT is adequate [3,5]. In this method there is no contribution of the relativistic change of the density to the first order relativistic energy change.

However, for actinides FOPT is not sufficient, as was demonstrated recently [5]. Relativistic corrections significantly change the relative energies of the 7s, 6d and 5f AOs and have important effects on the dissociation energies of the molecules MCl_3H and MCl_3CH_3 , with $M = Th, U$. In order to get agreement with experiment in these systems, Quasi-Relativistic (QR) calculations are needed. In actinides relativity leads to changes in the bonding scheme, i.e. a different participation of the atomic orbitals in the molecular orbitals compared to the non-relativistic case.

The aim of the present study is a qualitative analysis of the relativistic changes in the bonding characteristics with H of a typical transition metal fragment $HfCl_3$ compared to an actinide system $ThCl_3$, as ThL_3 is a common fragment in organoactinide chemistry [8]. In Section 2 the geometrical data is given for the compounds considered, and also the method we used in the calculations is described. In the relativistic calculations we used the Scalar Relativistic method that was described in Chapter 1. Section 3 contains a discussion of the atomic energy levels of Hf and Th, while in Section 4 the fragments $HfCl_3$ and $ThCl_3$ are treated. In Section 5 the importance of relativity for the compounds $HfCl_3H$ and $ThCl_3H$ is assessed from the calculated NR, SR and first order relativistic bond energies, and the bond between the MCl_3 fragments and H is treated in Section 6 (Hf) and 7 (Th). As the fragments in this process have a singly occupied Frontier Orbital (FO), we used the method for calculating open shell bond energies described in Chapter 1. Section 8 contains our conclusions.

2. Geometrical parameters and method

The geometrical data are given in Table 1a and were taken from previous calculations [9] for $HfCl_3H$, while for $ThCl_3H$ we optimized the geometry. The molecules considered have symmetry C_{3v} , for which the irreducible representations of the atomic orbitals are given in Table 1b. We are only interested in the A_1 symmetry, where the interaction with H takes place. The Cl 3s and 3p orbitals lead to A_1 , A_2 and E combinations. In A_1 symmetry we have the 3s,3p and 3p bonding combinations. Only the 3p combinations

Table 1a. Geometric data for $HfCl_3H$ and $ThCl_3H^a$.

Parameter	HfCl ₃ H	ThCl ₃ H
M - Cl (Å)	2.35	2.58
angle Cl - M - z-axis (°)	109	109
M - H (Å)	1.80	2.09

^a: optimized SR geometry.

Table 1b. Irreducible representations of orbitals in symmetry C_{3v} .

Representation	Cl ₃ -combination	Metal orbitals
A ₁	3s, 3p and 3p	s, p _z (p) d _(z) ² (d) f _z ³ (f), f _{x(x²-3y²)} (f)
A ₂	3p	f _{y(3x²-y²)} (f)
E	3s, 3p and 3p (twice)	p _x ,p _y (p) d _{xz} ,d _{yz} (d) d _{x²-y²} ,d _{xy} (d) f _{xyz} , f _z (f)

are involved in the bond with the metal, the 3s lies too deep in energy. Note that in A₁ symmetry we have the metal orbitals s, p , d , f and one f (f_{x(x²-3y²)}).

The calculations reported in this work have been done with the Amsterdam DF program system [1..5]. The LSD exchange potential was used [10], together with the Vosko-Wilk-Nusair [11] parametrization for correlation, omitting the correlation between electrons of equal spin, as suggested by Stoll [12]. For the bonding between the open shell fragments MCl₃ and H we used a recently developed method for the analysis of the bond energy for open shell systems [13]. This method was described in Chapter 1, to which we refer for additional information. The bond energy is divided into two steps [14]: first the steric repulsion E^0 is calculated, consisting of the electrostatic interaction $E_{el.stat}$ between the fragments, and the Pauli, exchange, or overlap repulsion E_{Pauli} :

$$E^0 = E_{el.stat} + E_{Pauli} \quad (1)$$

This steric energy corresponds to the energy difference between the separate fragments and the overall system described by the determinantal wavefunction Ψ^0 , which is the antisymmetrized product of the overlapping fragment orbitals. For the reaction of MCl₃ and H, with the singly occupied FO on MCl₃ and H 1s, Ψ^0 reads:

$$\Psi^0 = |(\text{core shells})_{MCl_3} \text{FO}_{MCl_3} (1) \text{H } 1s (2)| \quad (2)$$

In this case there is only Pauli repulsion between H1s and the closed shells on MCl₃ (only

for spin of course), but there is no Pauli repulsion between FO and H1s on account of their spin-orthogonality. The Pauli repulsion is large when occupied orbitals overlap, which corresponds to the simple picture of a more destabilized antibonding combination than a stabilized bonding one [15].

The second step in the bond energy analysis consists of the relaxation of Ψ^0 to the final SCF wavefunction Ψ_{SCF} , accompanied by the orbital interaction E_{oi} . For closed shell fragments, this step consists of the charge transfer and polarization energies, but for open shell fragments also the effect of the pair bond formation is included. In the present study we do not separately study the pair bond, contrary to a recent study on the CN dimers [16 and Chapter 4c]. If the basis functions are symmetry (σ) adapted, the orbital interaction can be decomposed accordingly [17]: $E_{\text{oi}} = E_{\text{oi}}^{\sigma}$.

Relativity was taken into account using the Scalar Relativistic method, i.e. the scalar relativistic mass-velocity (h_{MV}) and Darwin (h_{D}) corrections are added to the non-relativistic one-electron equations. For a more detailed discussion of the SR method we refer to the general introduction in Chapter 1. Here we note that it is a special form of the Quasi-Relativistic method, viz. the spin-orbit operator is omitted. In the SR method the higher order corrections of the first order operators are taken into account, in contrast to FOPT where only the first order relativistic density change is included.

Calculating both the SR bond energy and the first order relativistic bond energy change, we are able to assess the importance of relativistic density changes to the energy, and the validity of FOPT. The First Order relativistic correction to the bond energy only depends on the non-relativistic density change $\rho^0(1,1')$ (see Chapter 1 and in [3]):

$$E^1 = \int \rho^0(1,1') [h_{\text{MV}} + h_{\text{D}}] dX_1 \quad \text{with } h_{\text{MV}} = -\frac{2}{8} \frac{4}{1}, h_{\text{D}} = \frac{2}{8} \frac{2}{1} V_{\text{N}} \quad (3)$$

The higher order relativistic energy correction E^{high} is obtained from:

$$E^{\text{high}} = E^{\text{SR}} - E^{\text{NR}} - E^1 \quad (4)$$

3. The influence of relativity on the Atomic Orbitals of Hf and Th

The NR and SR atomic energy levels of Hf and Th are given in Figs 1 and 3 (Section 4). The familiar atomic relativistic effects are found, stabilization of s orbitals, and destabilization of d and f orbitals [17,18]. The assumed valence orbital occupation in both cases is s^2d^2 . Also the energy levels of MCl_3 and MCl_3H are indicated in these figures.

For Hf, the valence level ordering is 6s below 5d, with an energy difference of 0.6 eV in the NR case, but in the SR calculation the energy difference increased to 2.6 eV, as a result of the stabilization of 0.9 eV for Hf 6s and the destabilization of 1.1 eV for Hf 5d.

For the heavier Th the situation is completely different: the order is $5f < 6d < 7s$ in the NR case, while in the SR scheme it is $7s < 5f < 6d$. The main reason for this change is the large indirect destabilization of 6.45 eV for Th 5f, while Th 6d also has a considerable destabilization of 1.37 eV. With the 3.2 eV stabilization of Th 7s, the order of 7s and 6d is reversed, and 5f ends up between them. Therefore the most remarkable difference between the NR and SR schemes is the relative ordering of s and d levels

4. Calculations on HfCl₃ and ThCl₃

For a proper understanding of the interaction in between MCl₃ and H in MCl₃H we first discuss the MCl₃ fragments. As both the MCl₃ and MCl₃H compounds have C_{3v} symmetry, we distinguish the orbitals of the MCl₃ fragments by a superscript f (for fragment). Furthermore, since the interaction with H takes place in A₁ symmetry, only the 6s and 5d orbitals on Hf, and the 7s, 6d and 5f orbitals in Th are involved. We denote the d orbitals by d.

Overlaps between normalized Cl₃-combinations and H with atomic orbitals of Hf and Th are given in Table 2. The phases of the metal orbitals were chosen such that the s orbital was positive, and for the d and f orbitals the lobes pointing towards H were positive. The Clp combination has the positive lobes directed towards the metal. For our investigation it is important to note that the d-Clp overlaps are negative, and much smaller than the d-Clp ones. This is a consequence of the nodal character of the d orbital. The Clp orbital overlaps mainly with the central lobe of the d, but this is partly cancelled by overlap with the outside lobe. As expected the overlaps of the s orbitals with the p combinations are zero. The effects of relativity on the overlaps are rather small. The SR d-p overlaps are larger than in the NR scheme, as a consequence of the relativistic d expansion. However, also for the s overlaps the SR ones are larger, contrary to what is expected from a relativistically contracted s orbital.

The explanation for this anomaly might be that the Cl atoms are very close to the metal

Table 2. Overlaps (in a.u.) in A₁ symmetry of some metal atomic orbitals with normalized Clp combinations.

Overlaps	Hf		Th		
	6s	5d	7s	6d	5f
Clp -NR	0.37	-0.10	0.24	-0.12	0.04
Clp -SR	0.42	-0.10	0.32	-0.11	0.05
Clp -NR	0.00	0.18	0.00	0.19	0.02
Clp -SR	0.00	0.21	0.00	0.22	0.03
H-NR	0.48	0.31	0.40	0.35	0.07
H-SR	0.48	0.34	0.42	0.38	0.10

so that contraction of the s orbital may lead to a larger overlap, while for the radially less extended d orbital the Cls are more towards the outside of the orbital.

As to the overlap with H, the s overlaps are larger than the d ones, which are in turn much larger than the 5f ones (Th), in accordance with the radial extent of the orbitals. Nevertheless the relativistic contraction of the Th 7s leads to a larger SR overlap.

In Tables 3,4 the population analyses and main bonding characteristics for some A_1 orbitals of $HfCl_3$ and $ThCl_3$ are given. Also the occupation numbers for the highest orbitals are included, as well as the gross Mulliken AO populations. The orbitals up to $5a_1^f$ are ligand based orbitals, with some metal character admixed in a bonding fashion. The highest valence orbitals are mainly metal in character, slightly antibonding metal-Cl. The bonding characteristics were determined by looking at the coefficients of the orbitals involved in the MOs. The Mulliken population analysis may be misleading, as is shown by the example of the $7a_1^f$ orbital in SR $HfCl_3$, where the 6s coefficient is largest, while the Mulliken population of the 5d dominates. Also the Cl coefficients are much larger than is apparent from their Mulliken populations, which would suggest almost no interaction took place. The bond between M and the Cls is thus mainly ionic of character, but still there is appreciable M-Cl mixing. As the valence orbitals are involved in the interaction with H, special attention will be given in this section to their metal participation and bonding characteristics. In Figs 1,3 the interactions in the MCl_3 and MCl_3H compounds are given, using drawn and dotted lines for the main and smaller interactions respectively.

Table 3. Population analysis for some A_1 orbitals of $HfCl_3$.

NR	Orbital	Orbital character	Energy (eV)	%Hf-contribution			%Cl-contribution	
				6s	6p	5d	p	p
	$7a_1^f$	$(s-Clp)-(d-Clp)$	-1.39	44	25	21	5	5
	$6a_1^f$	$(d-Clp)+(s-Clp)$	-3.77	26	6	64	1	3
	$5a_1^f$	Cl (-d bond)	-8.13		2	5	4	89
	$4a_1^f$	Cl (-s,d bond)	-9.14	7		5	84	2
Gross Populations				0.42	0.10	0.84	1.87	1.86

SR	Orbital	Orbital character	Energy (eV)	%Hf-contribution			%Cl-contribution	
				6s	6p	5d	p	p
	$7a_1^f$	$(s-Clp)-(d-Clp)$	-1.53	32	19	35	8	7
	$6a_1^f$	$(d-Clp)+(s-Clp)$	-3.95	39	7	51	1	3
	$5a_1^f$	Cl (-d bond)	-8.19		3	5	1	91
	$4a_1^f$	Cl (-s,d bond)	-9.73	14		3	80	1
Gross Populations				0.73	0.13	0.67	1.64	1.84

Note: coefficients in $7a_1^f$: 6s: 0.73, 5d: 0.70 p :0.16 and p : 0.23.

HfCl₃

As was found in a previous study on MCl₃ [9], the singly occupied frontier orbital (FO) of HfCl₃ in the NR and SR schemes is a mainly metal d orbital 6a₁^f. Actually this orbital is slightly antibonding with respect to the 5d-Cl and 6s-Cl interactions (Table 3). In Fig. 1 we find deep lying orbitals that are mainly Cl with some metal admixed in a bonding fashion, followed by the mostly metal 6a₁^f. In the virtual orbital 7a₁^f we also have antibonding 5d-Cl and 6s-Cl interactions, here with a dominant 6s participation. It will turn out that for a proper understanding of the HfCl₃ to H bonding, the relative phases of the 6s and 5d orbitals in the 6a₁^f and 7a₁^f orbitals are important. We can understand the phases by looking at the bonding characteristics of the 5d and 6s orbitals with Cl. From the overlaps of Table 2 we see that the 6s only overlaps with the Cl p combination, while for the 5d orbital the overlap with the p combination is much larger than that with p .

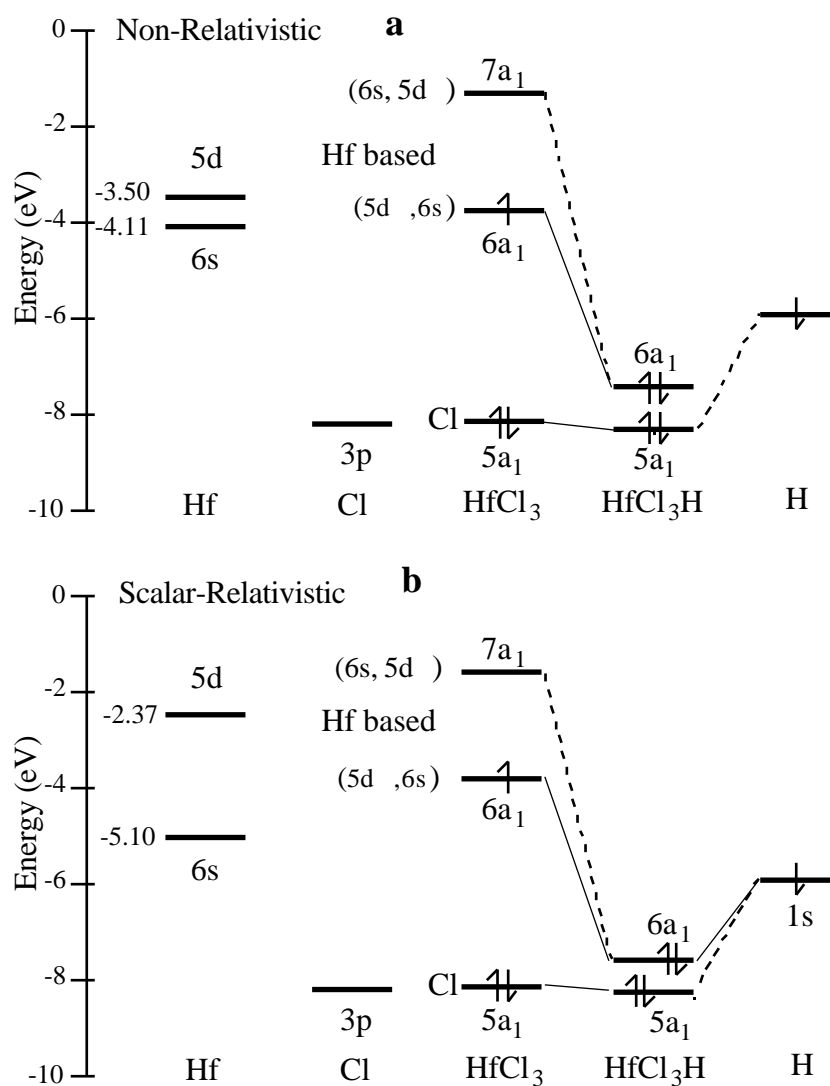


Figure 1. Level scheme for the Hf compounds. a): Non-relativistic. b): Scalar-relativistic.

Therefore, the 6s interacts with the p combination, while the 5d interacts predominantly with the p combination. The bonding combinations are found in the $4a_1^f$ and $5a_1^f$ orbitals, while for the antibonding character in the orbitals $6a_1^f$ and $7a_1^f$ we see in Table 3 that in the $6a_1^f$ more 5d character is found, while in the $7a_1^f$ the 6s character prevails. Therefore the following model is proposed, sketched in Fig. 2.

The interaction of the 6s and 5d orbitals with Cl is divided in two steps. In the first step the main interactions of 6s-Clp and 5d-Clp take place. Here the 6s-p antibonding combination ends up above the antibonding 5d-p combination (from fact that finally in Table 3 the antibonding 5d character is found lower in energy), and deep in energy the bonding combinations are found. The interaction of 6s with Cl is larger than for 5d as can be seen in the $4a_1^f$ orbital. This is expected from a smaller energy difference and larger overlap (Table 2) of 6s and Cl compared to the 5d. The antibonding 6s-Cl character is found at higher energy than the antibonding 5d-Cl character. In the second step there is mixing of the antibonding 6s-p and 5d-p combinations because there is an interaction matrix element between p and 5d (non-zero overlap) and even between 5d and 6s since the effective field is not atomic (note the electric field of the approximately negative Cl⁻).

The antibonding combinations were close in energy, and mix considerably. To determine the phase with which they mix, we need the 5d-p and 5d-6s interaction matrix elements. We calculated both these matrix elements, and found that the 5d-p element was by far the largest of the two, and of positive sign, which is in agreement with the negative 5d-p overlap. With the information given above we understand that for a positive 5d-p interaction the phases of 5d and Clp should be opposite, which means that the interaction between the 6s-p and 5d-p combinations leads to a lowest level where these are coupled with a positive sign [(5d-p) + (6s-p)] having equal 6s and 5d phases, while a highest level results where the 6s and 5d have opposite phases [(6s-p) - (5d-p)]. The $6a_1^f$ is then identified with the lowest level, with equal 6s and 5d phases, while in the $7a_1^f$ the phases are opposite. The orbital characteristics in Table 3 have the same notation as is used in Fig. 2.

The overall effect of the different interactions of Hf 6s and Hf 5d is a larger 5d population in the NR case: 0.42 and 0.84 for 6s and 5d respectively. The reason for this is the larger 5d (64% vs. 26% 6s) participation in the $6a_1^f$ FO (see also Fig. 2).

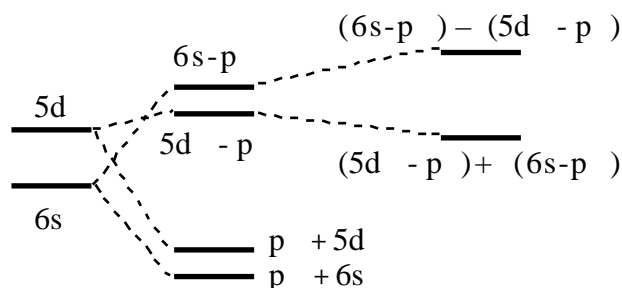


Figure 2. Interaction between 6s and 5d AOs of Hf with Cl combinations.

In the SR scheme we also have more mixing of Hf 6s with Cl than for Hf 5d, but in this case the Gross population of Hf 6s is 0.73, slightly larger than the 0.67 for Hf 5d. This is mainly due to the larger 6s content of the $4a_1^f$ orbital. The same scheme as for the NR case holds in understanding the relative 6s and 5d phases in the $6a_1^f$ and $7a_1^f$.

The larger SR 6s participation compared to the NR case is explained by the relativistic stabilization of Hf 6s leading to a larger interaction with Cl, and a gross population which is larger than for Hf 5d. Because the atomic Hf 6s is lower in energy (closer to Cl), we find more 6s-Cl bonding in the SR $4a_1^f$ compared to the NR $4a_1^f$ orbital. Concerning the orbitals with antibonding 6s-Cl character, the $6a_1^f$ and $7a_1^f$, these are also found at lower energy than in the NR case. The larger Hf 6s-Cl interaction in the SR case would suggest that compared to the NR case these orbitals were destabilized, but apparently this is compensated by the relativistic atomic stabilization of Hf 6s. Note that in the FO $6a_1^f$ also more 6s character is found than in the NR case. This is explained by reference to Fig. 2. In the SR case the antibonding 6s-Clp combination is still higher, but closer to the antibonding 5d-Clp combination, and therefore they mix more heavily in the second step. Hence, although the 6s-Clp combination contains less 6s character, the increased mixing with the 5d-Clp leads to more 6s character in the $6a_1^f$. In the $7a_1^f$ we then find more 5d character than in the NR case. The Hf 5d orbital is relativistically destabilized, and the larger energy difference with Cl leads to less d character in the bonding combination with Cl. In the antibonding combination we find more 5d, and also the increased interaction with the 6s-p combination then leads to more 5d character in the $7a_1^f$. Notwithstanding the atomic 5d destabilization, the FO $6a_1^f$ still contains more Hf 5d (51%) than Hf 6s (39%).

Summarizing, the NR and SR HfCl₃ molecules are very similar, with more 5d than 6s participation. In the SR case the 6s participation is relatively more important due to the atomic stabilization of the Hf 6s and destabilization of Hf 5d.

ThCl₃

Next we discuss ThCl₃ (Table 4 and Fig. 3). Non-relativistically the lowest configuration is .. $(6a_1^f)^1$, but we excite to $(6a_1^f)^0(7a_1^f)^1$, because the $6a_1^f$ (mainly f) does not interact with H (see Section 7). The FO is the mainly f (92%) orbital $7a_1^f$, in line with the atomic level ordering. The 5f orbital is by far the lowest valence orbital, and will be occupied before the 6d and 7s ones in the $8a_1^f$ and $9a_1^f$. Note that there is hardly any 7s (0.09) and only a small amount of 6d (0.16) character present. Concerning the bonding characteristics with Cl, as in HfCl₃ the bonding combinations are found in the $4a_1^f$ and $5a_1^f$. Note that contrary to HfCl₃, in the $4a_1^f$ we have more 6d character, which is in line with the reversed (compared to Hf) atomic level ordering of the 6d below the 7s (Fig. 3). The somewhat larger 7s-Clp than 6d-Clp overlap (Table 2) does not lead to a larger interaction because the 7s is higher in energy than the 6d. In accordance with the larger 6d

Table 4. Population analysis for some A_1 orbitals of ThCl_3 .

NROrbital	Orbital character	Energy (eV)	%Th-contribution				%Cl-contribution	
			7s	6d	5f	5f	p	p
$9a_1$	$(s-\text{Clp})-(d-\text{Clp})$	-0.22	44	28	2	4	3	2
$8a_1^{0.0}$	$(d-\text{Clp})+(s-\text{Clp})$	-2.10	38	57				3
$7a_1^{1.0}$	f -Cl b.	-3.13	3	1	92		1	1
$6a_1^{0.0}$	f	-3.69	4	2	2	88	3	
$5a_1$	Cl	-7.27	1	1	2		61	22
$4a_1$	Cl -(d, f bond)	-7.92	1	6		5	23	71
Gross Populations			0.09	0.16	0.99	0.15	1.74	1.89

SROrbital	Orbital character	Energy (eV)	%Th-contribution				%Cl-contribution	
			7s	6d	5f	5f	p	p
$9a_1$	$(d-\text{Clp})-(s-\text{Clp})$	-0.47	28	22	6	16	6	2
$8a_1$	5f	-2.56		1	66	32		1
$7a_1^{0.0}$	$(d-\text{Clp})-(s-\text{Clp})$	-2.82	1	40	23	34		3
$6a_1^{1.0}$	$(s-\text{Clp})+(d-\text{Clp})$	-3.48	60	24	3	12		2
$5a_1$	Cl (-d bond)	-7.82	1	4	1		6	88
$4a_1$	Cl -(s, d) bond)	-8.81	7	4	1	3	78	4
Gross Populations			0.79	0.41	0.07	0.20	1.69	1.87

interaction we find a larger 6d gross population. In the antibonding metal-Cl levels $8a_1^f$ and $9a_1^f$ we have the antibonding 6d-p combination lower than the antibonding 7s-p one, as in Fig. 2. Hence in this case we find both the bonding and antibonding 6d-p characters lower than the corresponding 7s-p ones. This contrasts the situation in HfCl_3 , where the larger 6s interaction caused the Cl-6s bonding character to be found lower in energy than the bonding Cl-5d character, and the antibonding 6s-Cl character was found at higher energy than the 5d-Cl character. In ThCl_3 this is different, which might be related to a smaller interaction due to the larger M-Cl distance in ThCl_3 (see Table 1a).

For the antibonding metal-Cl interactions we thus find the same ordering as in Fig. 2. In the case of ThCl_3 the 6d-Clp interaction matrix element is positive, and larger than the 6d-7s element. The same interaction as in HfCl_3 between the antibonding M-Cl combinations takes place, and hence in the $8a_1^f$ the 7s and 6d phases are equal, while in the $9a_1^f$ the phases are opposite to each other.

In the SR calculation a completely different picture emerges. The ThCl_3 compounds are very different in the NR and SR schemes, due to the large atomic relativistic effects for the actinide atom Th. The FO is the $6a_1^f$, which is mainly a Th 7s orbital (60%), with smaller contributions from 6d (24%) and 5f (12%) and 5f (3%), apart from some 2%

Cl character. The relativistic destabilization of the Th 5f causes it to be found in the higher MOs $7a_1^f$ and $8a_1^f$. The gross populations show a dominant Th 7s participation (0.79), followed by 6d (0.42) and 5f (0.27), in line with the atomic level ordering. The Th 5f does not participate in the bonding.

The bonding interactions with Cl are again found in the low orbitals, and the 7s orbital dominates. In the antibonding combinations we also have the 7s character lowest (in the FO $6a_1^f$). We find that the 6d-p interaction matrix element is positive, and because the antibonding 7s-p ended up lowest, the FO $6a_1^f$ mainly is the $[(7s-p) + (6d-p)]$ combination containing more 7s than 6d character. For the other levels there is interaction

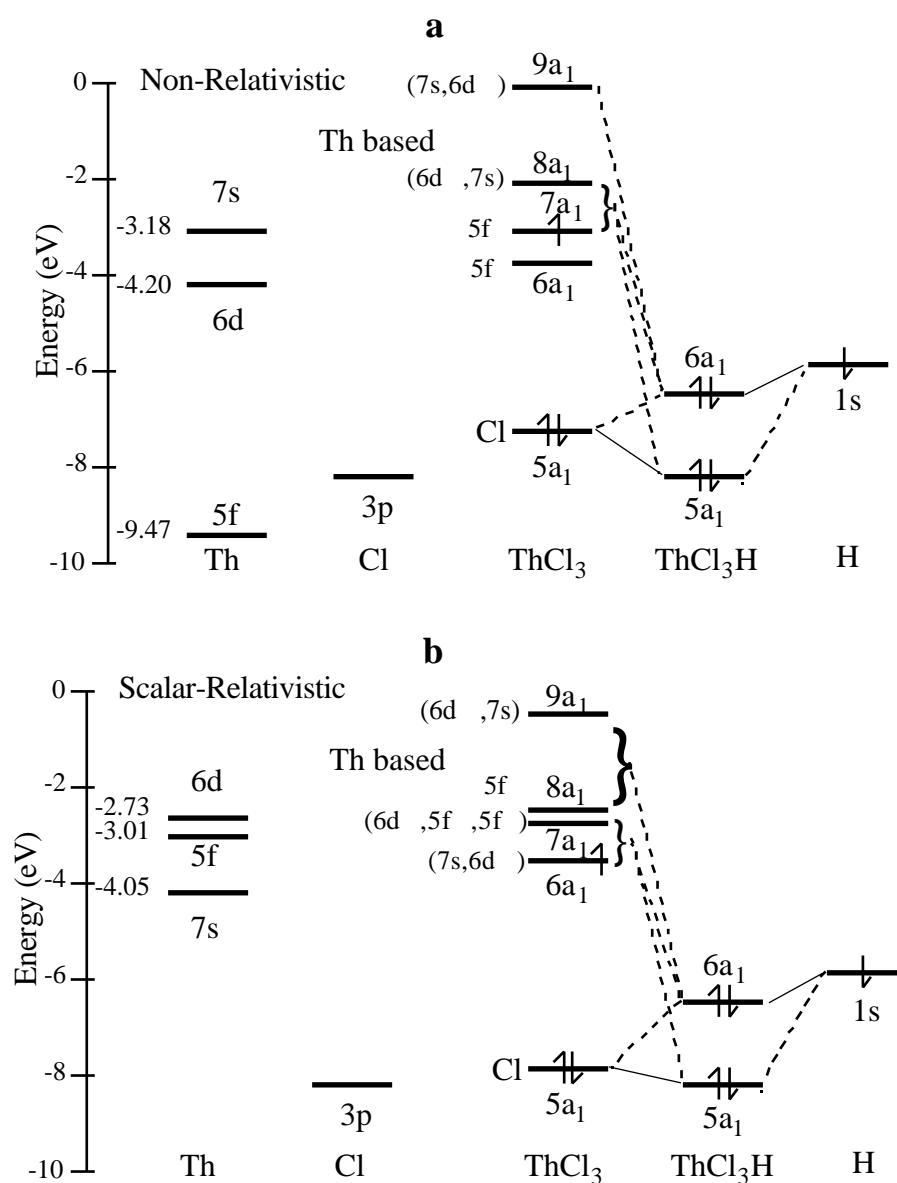


Figure 3. Level scheme for the Th compounds. a): Non-relativistic. b): Scalar-relativistic

with the 5f, which is present in between the 6d and 7s levels in the atom (Fig. 3). The FO is not influenced by this, but the mixing of the antibonding Cl combinations and 5f (by the field of the Cls and interaction matrix elements) is important for the levels 7-9a₁^f. We do not enter in details here, but note that from Table 4 we see that the [(7s-p) – (6d-p)] combination is divided among the 7a₁^f (the coefficient of the 7s is much larger relative to the 6d than the Mulliken populations suggest) and 9a₁^f, while the 8a₁^f is mainly a f orbital. For our investigation the relative 7s and 6d phases in the orbitals are important: in the FO 6a₁^f the 6d and 7s orbitals have equal phases, while in the virtual 7a₁^f and 9a₁^f orbitals their phases are opposite.

Summarizing the results for the MCl₃ compounds, we thus found that HfCl₃ as well as for ThCl₃ the effects of relativity are connected to the atomic relativistic effects. For the subsequent interaction with H we note that in SR ThCl₃ the virtual levels are found closer to the FO 6a₁^f than in SR HfCl₃. Therefore we expect in SR ThCl₃ a stronger participation of these orbitals to the bond with H.

5. Validity of FOPT and comparison with other studies and experiment

The Bond Energies for reactions of ThCl₃ and HfCl₃ with H were calculated in the NR and SR schemes. The first order relativistic energy change E^1 was calculated using expression (3) and E^{high} was obtained from expression (4). All numbers are with respect to spin unrestricted open-shell fragments and are given in Table 5.

For Hf, the SR, NR and first order relativistic Bond energies are almost the same. The first order correction is small, 5.4 kcal/mol, which is a small fraction (7%) of the NR value. Going from FOPT to SR, i.e. including the higher order relativistic density changes, has a stabilizing effect. The small E^{high} for Hf is in accordance with the fact that relativistic effects for this transition metal metal are not very large.

For the heavier Th, the relativistic correction to the bond energy is very large, almost twice as large as the NR value itself. In this case one needs relativity to get the proper bond energy. The FOPT value overshoots the experimental value, and the SR value is in better agreement with experiment. The higher order correction E^{high} is significant here.

Table 5. Bond energies (in kcal/mol) for MCl₃H (M = Hf and Th).

Compound	E ^{NR}	E ^{FO} ^a	E ^{SR}	E ^{high} ^b	Exptl ^c
HfCl ₃ H	76.9	82.3	84.0	1.7	-
ThCl ₃ H	45.4	88.8	83.0	-5.8	80

^a: First-order relativistic bond energy from Eq. (3) ^b: Higher order correction to FOPT bond energy from Eq. (4) ^c: Experimental bond energy from Ref. [5].

The values for Hf calculated here are close to those of a previous study [5], but for Th there are differences, which might be due to the use of a more accurate integration scheme [4]. In the following two sections we study the bonding between MCl_3 and H, and show the different effect of relativity for the Hf and Th compounds.

6. The Cl_3Hf-H bond

The interaction between $HfCl_3$ and H is indicated in Fig. 1, and in Table 6 the Mulliken population analyses and the bonding characteristics of the orbitals are given. Note that the bond with H is mainly a pair bond between the $HfCl_3$ $6a_1^f$ FO and H, resulting in the $6a_1$ HOMO. The $4a_1$ and $5a_1$ are nearly pure $HfCl_3$ fragment orbitals. For NR $HfCl_3H$ the gross Mulliken populations are 0.73 for 5d and 0.22 for 6s, which means a dominant d contribution as in the fragment, although the s character decreased relative to the d character. The same thing happens in the SR calculation, where in contrast to the fragment even a larger 5d (0.65) than 6s (0.50) population is present. The bonding to H only involves $HfCl_3$ orbitals that are mainly metal in character, and by subtracting the gross Mulliken populations for $HfCl_3$ from that of $HfCl_3H$, the effect of bonding to H is obtained. We find in the NR case that bonding to H leads to a $-0.22e$ loss of s character, and a loss of $-0.11e$ d character. In the SR case the decreases in s and d character amount to $-0.23e$ and $-0.02e$ respectively. The H 1s orbital gained charge in the interaction with $HfCl_3$, 0.27e in NR $HfCl_3H$ and 0.22 e in the SR case.

Table 6. Population analysis of highest occupied A_1 orbitals of $HfCl_3H$

NR	Orbital	Orbital char.	Energy (eV)	%Hf-contr.			%HfCl ₃ -contr.				%H-contr.
				6s	6p	5d	4a ₁ ^f	5a ₁ ^f	6a ₁ ^f	7a ₁ ^f	
	6a ₁	5d,6s-H b.	-7.37	5	4	22		6	37	2	59
	5a ₁	5a ₁ ^f -H b.	-8.48	1	2	10		94	6		4
	4a ₁	4a ₁ ^f	-9.39	6		4	98				1
	Gross Populations			0.22	0.12	0.73					1.27
SR	Orbital	Orbital char.	Energy (eV)	%Hf-contr.			%HfCl ₃ -contr.				%H-contr.
				6s	6p	5d	4a ₁ ^f	5a ₁ ^f	6a ₁ ^f	7a ₁ ^f	
	6a ₁	5d,6s-H b.	-7.56	6	6	20		7	38	1	53
	5a ₁	5a ₁ ^f -H b.	-8.45	1	2	11		93	1		4
	4a ₁	4a ₁ ^f	-9.94	16		1	97				2
	Gross Populations			0.50	0.16	0.65					1.22

The orbital mainly responsible for the bond with H is the HfCl_3 FO $6a_1^f$. From the 37% character of the FO $6a_1^f$ in the HfCl_3H $6a_1$ HOMO we expected 10% s character in the NR case [37% times 26% (s character in the $6a_1^f$)], while we find only 5%. Similarly for Hf 5d we expected 24% and find 22%. For the SR case the expected contributions are 15% 6s and 19% 5d, while we find 6% 6s and 20% 5d.

The reduction of 6s character can be explained by the small admixing of the virtual orbital $7a_1^f$. We already noted that the relative phases of the 6s and 5d are equal in the FO $6a_1^f$, and opposite in the virtual $7a_1^f$. Whether admixing of the $7a_1^f$ leads to weakening of 6s and strengthening of 5d contributions depends on the relative phases with which $6a_1^f$ and $7a_1^f$ enter the $6a_1$ HOMO. These phases follow from the strengths of the H 1s-6s and H 1s-5d interactions. If the Hf 6s-H 1s interaction would dominate, we would expect the $6a_1^f$ and $7a_1^f$ to be mixed so as to be both 6s bonding to H, from which it follows that admixing of the $7a_1^f$ (with opposite 5d phase compared to the $6a_1^f$) would lead to an increase in 6s character and a decrease in 5d character. We have seen however that the 6s population decreased by bonding to H, which is opposite to what is to be expected from a dominant 6s interaction. We calculated the Hf 6s-H 1s and Hf 5d-H 1s interaction matrix elements, and found a larger 5d interaction matrix element, in spite of the larger overlap of H 1s with 6s (cf. Table 2). In that case the 5d phase is determined so that the 5d-H interaction is optimally bonding. This means that the 6s phases of $6a_1^f$ and $7a_1^f$ in $6a_1$ are opposite, explaining the decrease in 6s character. Because the $7a_1^f$ admixing is small, and the 6s and 5d phases are equal in $6a_1^f$, the Hf 6s-H 1s interaction is still bonding.

The Mulliken population of the main bonding $6a_1$ orbital is a better measure for the importance of the AOs than the overall gross populations. From this we conclude that the main contribution to the bond between HfCl_3 and H comes from the Hf 5d orbital.

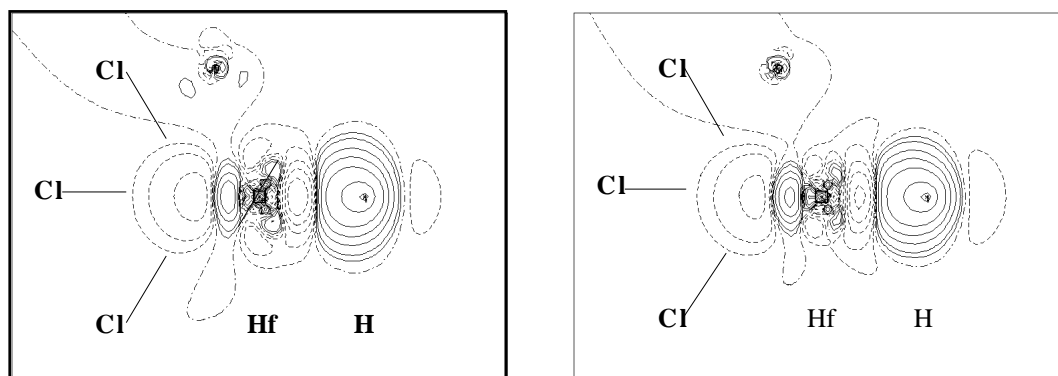


Figure 4. The deformation density $\Delta\rho$ for HfCl_3H from HfCl_3 and H. a): $\Delta\rho^{\text{NR}}$. b): $\Delta\rho^{\text{SR}}$. Densities are plotted in xz -plane. Drawn lines: positive, dashed lines: negative, and dash-dotted lines: zero. Contour values: 0.5, 0.2, 0.1, 0.05, 0.02, 0.01, 0.005, 0.002, 0.001, 0.0, -0.001, -0.002, -0.005, -0.01, -0.02, -0.05, -0.10, -0.20, -0.50.

In the SR calculations the bond to H 1s is similar, with again a decrease in 6s character. The gross population in Table 6 shows there is more 6s character in the SR case, while the 5d character decreased somewhat. This originates from the $4a_1$ orbital. Therefore, like in the HfCl_3 fragment, the differences between the NR and SR schemes show the atomic relativistic effects on Hf, i.e. a lower 6s and higher 5d. A difference that is also connected to the fragment orbitals is the smaller H participation in SR HfCl_3H , because the SR HfCl_3 fragment orbitals were lower in energy and thus closer to H 1s. This leads to a larger interaction in the SR case, and hence a smaller H 1s population.

The effect of bonding to H can be illustrated by a plot of the deformation density ρ_{def} , defined as $\rho_{\text{def}} = \rho_{\text{Cl}_3\text{HfH}} - \rho_{\text{Cl}_3\text{Hf}} - \rho_{\text{H}}$. The deformation densities $\rho_{\text{def}}^{\text{NR}}$ and $\rho_{\text{def}}^{\text{SR}}$ are given in Fig. 4 and clearly show the decrease in 6s and increase H 1s character, while the effect on the 5d is not visible. The deformation densities are very similar: the NR and SR bonds to H are practically equal.

In Table 7 the bond energy analysis is given. The orbital interaction energy E_{A_1} is slightly larger in the SR case, because the FO $6a_1^f$ and H 1s were closer in energy (note the smaller H 1s population) than in the NR case. Moreover the steric 'repulsion' E^0 contributes to the larger SR bond energy as it is more attractive in the SR case. In this effect the FO does not play a role, as we used open shell fragments in the calculation: H 1s and the FO $6a_1^f$ have opposite spin and are thus orthogonal. The smaller E^0 is caused by the lower energy of the HfCl_3 $4a_1^f$, related to the relativistic atomic 6s stabilization, which in turn leads to a somewhat smaller Pauli repulsion with H 1s.

Summarizing the results for HfCl_3H we can say that the bond between HfCl_3 and H in the NR and SR schemes are qualitatively the same, with a dominant Hf 5d contribution.

Table 7. Energy analysis for HfCl_3H and ThCl_3H .

	HfCl ₃ H from HfCl ₃ and H			ThCl ₃ H from ThCl ₃ and H	
	NR	SR		NR	SR
$E_{\text{el.stat}}$	-2.76	-2.79	$E_{\text{el.stat}}$	-1.40	-1.74
E_{Pauli}	2.35	2.20	E_{Pauli}	2.43	1.98
E^0	-0.42	-0.60	E^0	1.03	0.24
E_{A_1}	-3.33	-3.43	E_{A_1}	-3.01	-3.84
E_{A_2}	0.0	0.0	E_{A_2}	0.00	0.00
E_{E_1}	0.01	0.01	E_{E_1}	0.03	0.02
E_{oi}	-3.09	-3.18	E_{oi}	-3.00	-3.83
E	-3.51	-3.77	E	-1.97	-3.60

7. The Cl₃Th-H bond

From the population analysis of Table 8 we see that interaction with H takes place predominantly in the 6a₁ orbital. In the 5a₁ orbital we also have some ThCl₃ 5a₁^f-H bonding, while in the 6a₁ there are many orbitals involved in the bonding to H. Therefore it is not possible to speak (as in HfCl₃H) of a dominant Frontier Orbital to H bond. There is a strong admixing of virtual orbitals to the highest occupied orbitals due to the bonding with H, which leads to large effects on the 7s, 6d and 5f (NR scheme only) populations. This was already expected in Section 4 from the fact that the virtual orbitals are close to the FO in ThCl₃. Also the 5a₁^f is more strongly mixed with H than in HfCl₃H, because in ThCl₃ it is closer in energy to H.

In the NR case we find a decrease in f character from 0.99e in ThCl₃ to 0.42e in ThCl₃H. The 5f (in 6a₁^f) does not interact with H (overlap with H is zero from Table 2). The s character is decreased too (0.09e vs. 0.07e). The d character increases considerably from 0.16e to 0.52e. The d character in the 6a₁ is much larger than expected from only 5a₁^f and 7a₁^f contributions (both with 1% d character in Table 4), due to the admixing of the virtual 8a₁^f and 9a₁^f orbitals. The explanation for this is found in the relative phases of the 7s and 6d orbitals in the 8a₁^f and 9a₁^f orbitals. As explained in Section 4 these were equal in the 8a₁^f, but opposite in the 9a₁^f. The increase in 6d character is explained by a larger Th 6d-H 1s interaction matrix element than for Th 7s-H 1s, while (as for the Hf 6s and Hf 5d in HfCl₃H) the overlaps in Table 2 would suggest the opposite. As the Th 6d-H 1s bonding dominates, the 8a₁^f and 9a₁^f are admixed with equal 6d phases.

Table 8. Population analysis of highest occupied A₁ orbitals of ThCl₃H.

NR	Orbital	Orbital char.	Energy	%Th-contribution				%ThCl ₃					%H
				(eV)	7s	d	f	f	4a ₁ ^f	5a ₁ ^f	7a ₁ ^f	8a ₁ ^f	
	6a ₁	5f, 6d -H b.	-6.27	1	14	15		6	17	20	1	56	
	5a ₁	5a ₁ ^f -H b.	-7.97	1	4	5	1	94	7			4	
	4a ₁	4a ₁ ^f	-8.55	1	7		8	99					
Gross Populations				0.07	0.52	0.42						1.24	

SR	Orbital	Orbital char.	Energy	%Th-contribution				%ThCl ₃					%H
				(eV)	7s	d	f	f	4a ₁ ^f	5a ₁ ^f	6a ₁ ^f	7a ₁ ^f	
	6a ₁	6d, 7s, 5f, -H b.	-6.43	5	18	2		5	19	13	1	2	61
	5a ₁	5a ₁ ^f -H b.	-8.12	1	8	2		95	1				3
	4a ₁	4a ₁ ^f	-8.98	6	3	1	3	99					1
Gross Populations				0.30	0.60	0.10							1.37

This leads to the observed increase in 6d character, and at the same time explains the (small) effect on the 7s population, because the 7s phases are opposite in the $8a_1^f$ and $9a_1^f$. The resulting HOMO $6a_1$, where most of the bonding to H takes place, finally has nearly equal 5f and 6d contributions. The decrease in f character is mainly caused by the fact that the FO $7a_1^f$ (92% f) is present with only 17% in the HOMO. H 1s has an increased population (0.24e) due to the bonding.

The SR calculation also shows extensive mixing of fragment orbitals and H. The effects on the AO populations are a loss of 7s character of -0.49e, and a gain of 0.29e for 6d. The total 5f content stayed nearly equal compared to the fragment. Again these effects are the result of virtual orbital admixing. In the fragment we have the antibonding 7s and 6d interactions with Cl in the $6a_1^f, 7a_1^f$ and $9a_1^f$, where the 7s and 6d phases are equal in the $6a_1^f$ and opposite in the $8, 9a_1^f$ (see Section 4). Like in the previous cases here the 6d-H 1s interaction dominates over the 7s-H 1s, and therefore all three orbitals $6a_1^f, 7a_1^f$ and $9a_1^f$ are admixed with equal 6d phases. This explains the increase in 6d character, and the 7s character decreases due to the contributions from the $8a_1^f$ and $9a_1^f$ to the FO $6a_1^f$. The 7s effect is really dramatic, the admixing of the virtual orbitals leads to almost absence of the 7s in the ThCl_3H HOMO $6a_1$, while it was the most important orbital in the ThCl_3 FO $6a_1^f$. The final situation in this case shows a dominant 6d contribution in the main bonding orbital $6a_1$, and in the gross metal populations. The 7s (0.30) and 5f (0.10) populations have become small compared to 6d (0.60).

The differences between the NR and SR ThCl_3 bonds to H are thus large, in the NR case we have important 5f and 6d contributions, with negligible 7s contribution. But in the SR case we find a dominant 6d participation, with smaller 5f and 7s (much larger than in NR) contributions. This correlates nicely with the effects on the AOs as given in Fig. 3. However, as also found in HfCl_3H , the main effects on the AOs are the same as including relativity in the fragment ThCl_3 . Bonding to H leads to enormous changes in metal participation, but comparing NR and SR ThCl_3H we see the 'normal' atomic effect as in the fragment of more 7s and 6d and less 5f character. Note that this is approximate, a closer look at Tables 4 and 8 shows that in the fragment the increases in 7s and 6d character and the decrease in 5f character due to relativity are much more extreme than in the overall molecule.

Note that H has a larger population (1.37e) than in the NR case (1.24e). We did not analyse this, because the NR and SR schemes are so very different.

Density difference plots for NR and SR are given in Fig. 5. Surprisingly they look very similar, although the number and appearance of the contours is different. The following effects of bonding to H can be seen: the increase in H 1s population, and in the NR case a large loss of f character and (smaller) increase in d character, visible from the depletion along the Th-H axis. In the SR case the loss of 7s character can be seen, and

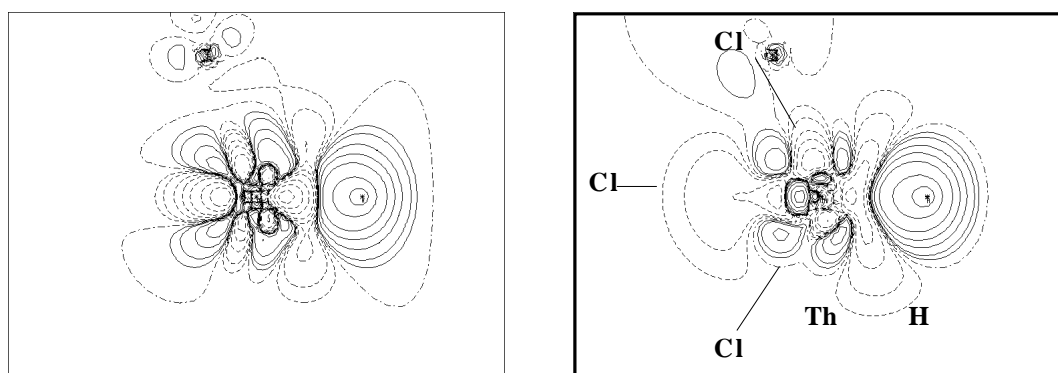


Figure 5. The deformation density $\Delta\rho$ for ThCl_3H from ThCl_3 and H . a): $\Delta\rho^{\text{NR}}$. b): $\Delta\rho^{\text{SR}}$. Densities are plotted in xz -plane. Drawn lines: positive, dashed lines: negative, and dash-dotted lines: zero. Contour values: 0.5, 0.2, 0.1, 0.05, 0.02, 0.01, 0.005, 0.002, 0.001, 0.0, -0.001, -0.002, -0.005, -0.01, -0.02, -0.05, -0.10, -0.20, -0.50.

the other effects, decrease in f character and increase in d character, although from Table 8 very different from the NR scheme, are not very different from the NR plot. As in HfCl_3H the density differences are not a good indication of the bonding to H , the use of orbital populations is to be preferred.

The bonding energy of Table 6 shows that the SR energy is twice as large as the NR energy. The terms in the energy decomposition that are responsible for this are the steric repulsion E^0 and the interaction energy in A_1 symmetry. E^0 is less repulsive in the SR calculation, which is caused by a smaller Pauli repulsion and a more attractive $E_{\text{el.stat}}$. The reason for this is not found in the A_1^f orbitals given in Table 4, as the $6a_1^f$ has opposite spin to H and the others are mostly Cl . However, the smaller repulsion is explained from the position of the $2a_1^f$ and $3a_1^f$ orbitals of ThCl_3 , resulting from the interaction of $\text{Th } 6p$ and $\text{Cl } 3s$. The fully occupied $\text{Th } 6p$ orbital is spatially quite extended, and therefore leads to large Pauli repulsion with $\text{H } 1s$. In the NR calculation the $\text{Th } 6p$ is above $\text{Cl } 3s$, and therefore the $3a_1^f$ contains most of the $6p$ character (antibonding with $\text{Cl } 3s$). The relativistic stabilization of $\text{Th } 6p$ brings it below $\text{Cl } 3s$ and in the SR calculation the $2a_1^f$ contains most of the $6p$ character. This orbital is lower in energy than the NR $3a_1^f$, and thus in the interaction with H , the overlap is smaller and the energy-difference is larger in the SR case, which leads to less Pauli repulsion. The larger SR a_1 interaction is explained from the lower FO and virtual ThCl_3 orbitals, resulting in more interaction with H .

We now come back to the difference between HfCl_3H and ThCl_3H . In ThCl_3H we found much more admixing of virtual orbitals, accompanied by larger effects on the metal participations. This was explained by the lower energies of the virtual orbitals in ThCl_3 .

Another difference is the larger s participation in HfCl₃H in the orbitals where the bond to H takes place. For the NR case this was already true in HfCl₃ vs ThCl₃, and is explained by the presence of the Th 5f orbital. In the SR fragment there was more s character in the FO of ThCl₃, but due to the stronger admixing of virtual ThCl₃ orbitals in ThCl₃H finally there is less s character present in the bond to H than in HfCl₃H. Also note that the main contribution to the SR bond with H comes from the valence d orbital in both MCl₃H systems. From the orbital populations in Tables 6 and 8 it follows that the bonds to H are very similar for HfCl₃H and ThCl₃H, except for NR ThCl₃H.

Concerning the relativistic effects on the bonds with H, we showed that in HfCl₃H these were not very large. Both in NR and SR schemes there was a dominant 5d contribution and a smaller 6s one, in the SR scheme the 6s was relatively more important due to the atomic relativistic stabilization of the 6s and destabilization of the 5d.

In ThCl₃H the situation is more complicated. In the NR scheme the 5f is available for bonding, and the main bonding orbital is a mostly 5f and 6d bond to H, while in the SR calculation the 6d contribution was largest, with smaller contributions from 5f and 7s. The 6d orbital took over the role of the 5f in the SR case, even though it is destabilized relativistically. In this case we have a strong mixing between the highest occupied and lowest virtual orbitals, which reduces the 7s character that was more important than the 6d in SR ThCl₃, and the 6d character was increased. Also, in ThCl₃H the relativistic effects are clear in the bonding to H, and these are much larger for the heavy actinide Th than for the transition metal Hf.

The mixing of occupied and virtual levels we encountered in ThCl₃H and to a smaller extent in HfCl₃H leads to effects on the AO participation that can only be understood from the interplay between the M-Cl and M-H interactions. In Chapter 6 we will encounter such effects also in UCp₃H. We showed in Table 4 that the valence s orbital has larger overlap with H than the d orbital, and also the energy difference with H is smaller. Therefore the larger d than s participation that is found in the calculations can not be explained in terms of AO level ordering. The explanation is that the virtual MCl₃ orbitals are admixed to the frontier orbital. Compared to the frontier orbital, these virtual orbitals have equal d phases, but opposite s phases. The larger d-H 1s than s-H 1s interaction matrix element then determines that the d phases are equal in the participating orbitals, and consequently the s phases are opposite. The overall result of this virtual orbital admixing is a dominant d orbital participation to the bond with H in the MCl₃H compounds.

8. Conclusion

Investigation of the bonding of the transition metal fragment HfCl_3 and H showed that the bond is mainly between the $6a_1^f$ orbital of HfCl_3 and H. The NR and SR calculations are qualitatively the same: the 5d contribution to the bond is larger than the 6s contribution. In the SR calculation the 6s is stabilized and therefore more 6s is present. That the relativistic effects are not very large is also proved by the fact that FOPT in this system is sufficient for a proper description of the bonding energy.

On the other hand, the bonding between the actinide fragment ThCl_3 and H shows very different characteristics in the NR and SR schemes. In the NR calculation we have a mostly 6d and 5f bond, but in the SR calculation the bonding to H comes mainly from the 6d, with smaller contributions from 5f and 7s. The d orbital again contributes more than others, especially in comparison with the 7s, which dominated the SR ThCl_3 fragment. The small 7s contribution is caused by admixing of virtual orbitals, reducing the 7s character. However the 7s participates still more than in the NR case. Therefore also in ThCl_3H the molecular relativistic effects are essentially atomic in nature. In atomic Th these are larger than in Hf, and we find the same for the MCl_3H compounds. Relativity destabilizes the 5f, and makes it from the most prominent orbital in NR the least significant one in SR. That FOPT is not enough in this system, is shown by the fairly large difference between E_{SR} and E_{FO} .

Concluding, the MCl_3H systems containing Hf and Th need different kinds of calculations for a proper description of the bond to H. For Hf FOPT is sufficient and relativistic effects are not large, while for Th one needs Scalar-Relativistic calculations. In ThCl_3H relativity leads to a different bonding scheme in contrast to HfCl_3H , which is ultimately related to the atomic relativistic effects that are much larger in Th.

References

- 1: a) E.J. Baerends, D.E. Ellis and P. Ros, *Chem. Phys.* **2** (1973) 42
 b) E.J. Baerends and P. Ros, *Chem. Phys.* **2** (1973) 51
 c) E.J. Baerends and P. Ros, *Int. J. Quant. Chem.* **S12** (1978) 169
- 2: a) J.G. Snijders and E.J. Baerends, *Mol. Phys.* **36** (1978) 1789
 b) J.G. Snijders, E.J. Baerends and P. Ros, *Mol. Phys.* **38** (1979) 1909
- 3: T. Ziegler, J.G. Snijders and E.J. Baerends, *Chem. Phys.* **74** (1981) 1271
- 4: P.M. Boerrigter, G. te Velde and E.J. Baerends, *Int. J. Quant. Chem.* **33** (1988) 87
- 5: T. Ziegler, E.J. Baerends, J.G. Snijders and W. Ravenek, *J. Chem. Phys.* **93** (1989) 3056

- 6: a) Y. Ishikawa, R.C. Binning and K.M. Sando, *Chem. Phys. Lett.* **101** (1983) 111
b) P.J.C. Aerts and W.C. Nieuwpoort, *Chem. Phys. Lett.* **113** (1985) 165
c) I.P. Grant, *J. Phys. B: At. Mol. Phys.* **19** (1986) 3187
- 7: a) P.A. Christiansen, W.C. Ermler and K. Pitzer, *Ann. Rev. Phys. Chem.* **38** (1985) 407
b) P. Hafner and W.H.E. Schwarz, *J. Phys. B: At. Mol. Phys.* **11** (1978) 217
- 8: a) I.L. Fragalà, E. Ciliberto, R.D. Fischer, G.R. Sienel and P. Zanella, *J. of Organometallic Chem.* **120** (1976) C9
b) I.L. Fragalà, J. Goffart, G. Granozzi and E. Ciliberto, *Inorg. Chem.* **22** (1983) 216.
- 9: T. Ziegler, V. Tschinke, L. Versluis, E.J. Baerends and W. Ravenek, *Polyhedron* **7** (1988) 1625
- 10: R.G. Parr and W. Yang, 'Density-Functional Theory of Atoms and Molecules', Oxford University Press, New York, 1989
- 11: S.H. Vosko, L. Wilk and M. Nusair, *Can. J. Phys.* **58** (1980) 1200
- 12: H. Stoll, and E. Golka and H. Preus, *Theor. Chim. Acta* **29** (1980) 29
- 13: F.M. Bickelhaupt, N.M.M. Nibbering, E.M. van Wezenbeek and E.J. Baerends, submitted to *J. Phys. Chem.*
- 14: a) K. Morokuma, *J. Chem. Phys.* **55** (1971) 1236
b) K. Kitaura and K. Morokuma, *Int. J. Quant. Chem.* **10** (1976) 325
- 15: T.A. Albright, J.K. Burdett and M.H. Whangbo, 'Orbital Interactions in Chemistry', Wiley, New York, 1985
- 16: T. Ziegler and A. Rauk, *Theor. Chim. Acta* **46** (1977) 1
- 17: P. Pyykkö, *Chem. Rev.* **88** (1988) 563
- 18: E.M. van Wezenbeek, E.J. Baerends and J.G. Snijders, *Theor. Chim. Acta* **81** (1991) 139

Chapter 4c

The Central Bond in the three CN• Dimers NC-CN, CN-CN AND CN-NC: Electron Pair Bonding and Pauli Repulsion Effects.

Abstract:

The bond between the CN radicals in the three linear isomers NCCN (**1**), CNCN (**2**) and CNNC (**3**) is investigated. An explanation is given for the fact that while the energy increases in the series **1** - **3**, still the central bond length decreases.

The explanation requires that, apart from the pair bond between the CN 5 MOs, the following effects be taken into account: a) Pauli repulsion ('steric hindrance') between the 4 ('N lone pair') orbitals; b) Pauli repulsion between the 4 and 5 orbitals; c) donor/acceptor interaction between the 4 and 5 orbitals; d) donor/acceptor interaction between the occupied 1 and unoccupied 2*. Each of these contributions is numerically significant. The singly occupied 5 plays, apart from the pair bonding, a dual role, causing Pauli repulsion (with the N lone pair) as an occupied orbital and causing charge transfer interaction in its capacity of unoccupied acceptor orbital. Detailed consideration of the balance between the repulsive and attractive energy components and their *R*-dependence is required to explain *why* the central CN/CN' bond considerably weakens when going from **1** to **3**, and why it still contracts.

Density Functional calculations including gradient corrections to the exchange and electron gas parametrization for the correlation are shown to achieve an accuracy for the systems under consideration which is comparable to conventional high-level ab-initio methods like CEPA and the CCD(+ST) coupled cluster approach.

In this work a recently developed energy decomposition scheme for studying interactions between open-shell systems was used.

1. Introduction

The prototype of an electron pair bond is the H-H bond in H₂. It is *the* textbook example for illustrations of quantumchemical methods and of concepts of bonding, yet it is rather atypical in the sense that in all other systems the electron pair bond has to coexist with and is affected by the presence of other orbitals: core orbitals on the atoms forming the bond and, for larger fragments, occupied bonding and lone pair orbitals as well as virtual orbitals. 'Secondary' effects from these other orbitals may be quite large.

An example of a situation where these secondary effects are very important is the variation of the strength of the bond between two CN• radicals in the three linear C₂N₂ isomers cyanogen (NC-CN;**1**), isocyanogen (CN-CN;**2**) and diisocyanogen (CN-NC;**3**).



While the most stable isomer NCCN [1] is known already for a long time, the much less stable CNCN has first been synthesized in 1988 by Van der Does and Bickelhaupt [2]. Only very recently, it was discovered [3,4] that a small fraction of the CNCN produced was in fact the very unstable CNNC isomer. Many spectroscopic and other experimental investigations on NCCN [5-7], CNCN[8-13] and the radical cations NCCN^{+•} and CNCN^{+•} [14] have been performed.

Early calculations on these systems were done by Haese and Woods [15] and by Sana and Leroy [16] who conceived **1** - **3** explicitly as dimers of the cyanide radical. Since the recent synthesis of CNCN, there have been many theoretical investigations of the C₂N₂ systems **1** - **3** and quantities such as geometries, harmonic vibrational frequencies, relative stabilities and Transition State structures were calculated [17-22]. Recently Scheller et al. [23] studied the last possible linear C₂N₂ isomer CCNN. This experimentally unknown species can be classified as a codimer of the two closed-shell monomers C₂ and N₂. As it is beyond the scope of this investigation, CCNN will not be examined here.

The purpose of the present chapter is an elucidation and comparison of the bonding mechanism between the CN monomers in the dimers **1** - **3**. The calculations are performed using the Amsterdam DF program system [24-29]. To study the bonding between the CN monomers, an energy decomposition scheme is used for analyzing interactions between open-shell systems that is a straightforward extension of standard methods for analyzing interactions between closed-shell systems [30,31]. This method has been described in Chapter 1 (Section 6), and is briefly reviewed in Section 2, where also the accuracy of our method is compared with conventional ab-initio methods.

In Section 3 the bond mechanism in the CN dimers is investigated. Especially, it is investigated why the bond strength decreases going from **1** to **3**, while at the same time the length R₂ of the central CN/CN bond *decreases*, whereas intuitively in this isomeric

series one might expect that a weaker bond corresponds to a *longer* bond length. The following issues will be treated: Can the bond be considered as a simple σ electron pair bond in each of the three cases, or do other effects (charge transfer in the π system, electronic relaxation, *vide infra*) play a significant role? Does π bonding make a contribution? In particular we try to understand *why* N-N coupling is so much weaker than C-C coupling. Section 4 contains a comparison with the recent results of Scheller et al. [18] with respect to the question how strong the interaction is between CN fragments. Finally Section 5 contains our conclusions.

We will show that the differences between the (CN)₂ dimers can only be understood if the different strengths of the electron pair bond between the singly occupied 5σ orbitals *and* the differences in the Pauli repulsions due to the doubly occupied orbitals of the monomers are simultaneously taken into account. The latter effects are not always given due attention in qualitative MO considerations; the bonding in the title systems provides a good example of their importance. A further point of interest is the extent to which the singly occupied 5σ , is able to act as an acceptor orbital. It should be noted that a pair bonding singly occupied orbital such as 5σ is energetically low compared to the more common acceptor orbitals in the virtual spectrum, such as $2\pi^*$.

2. Method

The MOs were expanded in Slater type orbitals (STOs). The basis is of double- ζ quality (two STOs per *nl* shell). A 3d polarization function was added on each atom. Geometries were optimized with the X exchange potential [24] using gradient techniques [32]. As the pure X σ -energies are too strongly bonding, the energy data reported were obtained in the optimum geometry with more sophisticated density-functionals for exchange and correlation, in which a non-local correction according to Becke [33-35] is added to the X exchange, and the correlation is treated in the Vosko-Wilk-Nusair [36] parametrization, with a correction of Stoll et al. [37].

Open shell bond energy calculation

The bonding energy for the combination of the open shell CN fragments is calculated in three steps, as described in Chapter 1 Section 6. First the steric interaction energy E^0 is calculated, next the formation of the 5σ electron pair bond and finally the remaining energy contributions such as electron relaxation in the π framework and the π bonding.

The steric energy E^0 is defined as the energy difference between the separate fragments and the composite system described by the determinantal wavefunction Ψ^0 , the

anti-symmetrized product of the overlapping fragment orbitals of CN_A and CN_B :

$$\psi^0 = \left| (\text{closed shells})_A (\text{closed shells})_B \psi_A(1) \psi_B(2) \right| \quad (1)$$

$$E^0 = \int \psi^0 |H_{AB}| \psi^0 - \int \psi_A |H_A| \psi_A - \int \psi_B |H_B| \psi_B$$

E^0 is divided into $E_{\text{el.stat}}$, the electrostatic interaction between the (unmodified, interpenetrating) charge distributions of the fragments (usually attractive), and the Pauli repulsion E_{Pauli} (also known as exchange-, or overlap repulsion):

$$E^0 = E_{\text{el.stat}} + E_{\text{Pauli}} \quad (2)$$

The steric energy E^0 is positive (repulsive) from a dominating Pauli repulsion, and is also termed steric repulsion. The most important contribution to the Pauli repulsion (cf. vd Hoek et al. [38]) comes from the rise in kinetic energy accompanying the formation of ψ^0 . In the present case, steric repulsion occurs if a lone pair orbital, such as the N lone pair orbital ψ_4 of CN, overlaps with occupied lone pair-, bond- or core orbitals on the other monomer. As for ψ one must realise that ψ is orthogonal to ψ on account of the spin orthogonality, so there is only a Pauli repulsion effect from the orthogonality requirement of the ψ on the opposite closed shells (of course only same-spin orbitals).

The second step of the bond energy analysis contains the energy lowering connected to the formation of the electron pair bond between the CN ψ orbitals. We consider:

$$\psi_{\text{pb}}^0 = \left| (\text{closed shells})_A (\text{closed shells})_B (\psi_A + \psi_B)^2 \right| \quad (3)$$

as the pair-bond wavefunction. The only difference with ψ^0 is that now the electrons in the ψ orbitals have been allowed to pair up in the bonding $\psi_A + \psi_B$ molecular orbital.

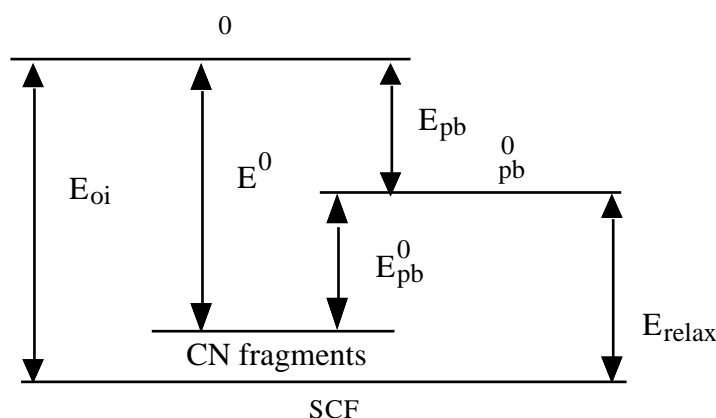


Figure 1. The relation between the various energy changes used in the interaction energy analysis.

The energy of the electron pair bond is defined as $E_{pb} = E_{pb}^0 - E^0$ (see Fig. 1). Note that E_{pb}^0 still contains, apart from the electrostatic interaction energy, the Pauli repulsion between the closed shells, including the $(5_A + 5_B)^2$ shell.

In the third step of the bond energy analysis the wavefunction Ψ_{pb}^0 is allowed to relax to the SCF solution Ψ_{SCF} by the admixture of virtual orbitals, yielding E_{relax} (see Fig. 1). This step contains the polarization and charge transfer contributions, which serve to relieve the steric repulsion. The various steps can be illustrated with the Orbital Correlation Diagram (OCD) of Fig. 2, where only the 4 and 5 orbitals are used. This figure only serves to illustrate the ideas of the various interactions, it does not represent one of the dimers. The OCDs for the three dimers are given in Figs 7a-c. These will be discussed in Section 4, where a comparison with previous results [18] is made.

The steric interaction energy, corresponding to E^0 , consists for a large part of the 4-electron destabilizing interaction between the two occupied 4 orbitals that leads to a stabilized bonding and a destabilized antibonding orbital. The 5 s are somewhat destabilized due to the orthogonality requirement on the closed shells.

The second step consists of the formation of Ψ_{pb}^0 , containing the doubly occupied bonding orbital $5_A + 5_B$, which yields the energy lowering E_{pb} . Conceptually we may consider the change from Ψ^0 to Ψ_{pb}^0 to occur via the formation of the strongly stabilized $5_A + 5_B$ bonding orbital (gray levels in Fig. 2), which is subsequently destabilized by a

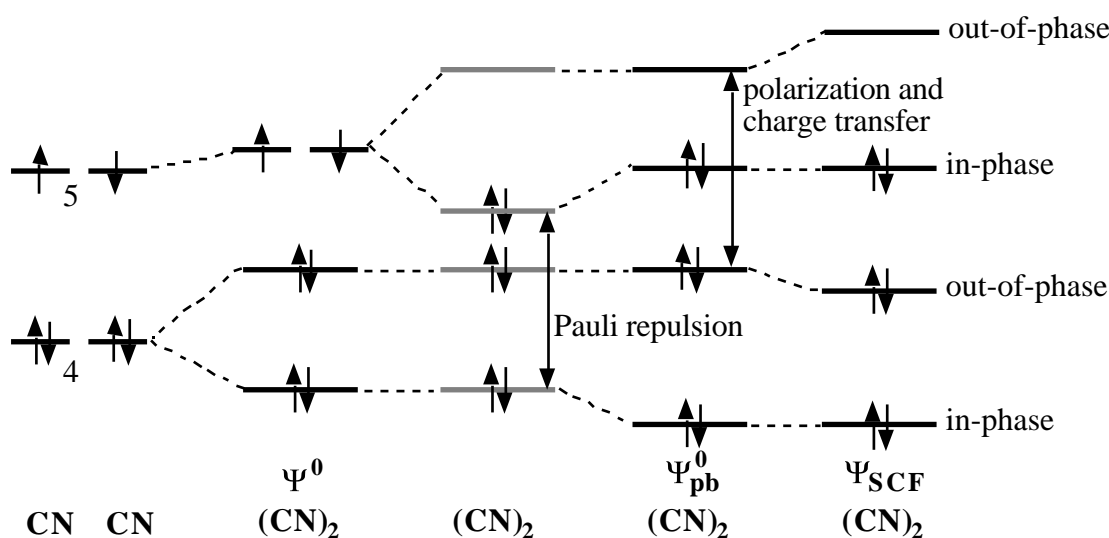


Figure 2. Orbital interaction diagram for σ -symmetry, representing the interaction between the CN 4σ and 5σ fragment orbitals. The first step, formation of Ψ^0 , corresponds to the steric interaction (ΔE^0). The next step, drawn in gray, corresponds to the formation of the 'pure' pair-bond, i.e. the fictitious situation of forming $5\sigma + 5\sigma'$ without the Pauli repulsion with the $4\sigma + 4\sigma'$ (and $3\sigma + 3\sigma'$ etc.) in-phase combinations. Going from Ψ^0 to Ψ_{pb}^0 represents the formation of the pair bond (ΔE_{pb}) including this Pauli repulsion. In the final step, the wavefunction Ψ_{pb}^0 is allowed to relax to the SCF solution Ψ_{SCF} by the admixture of virtual orbitals, yielding ΔE_{relax} .

4-electron repulsive interaction with the occupied 4_A+4_B orbital. Although one cannot associate unambiguously a wavefunction with the situation depicted in gray in Fig. 2, it will nevertheless be useful to keep in mind that the total E_{pb} contains not only the 'pure' pair bond formation energy but also the above mentioned repulsive effect. In the third step the SCF wavefunction Ψ_{SCF} is formed by allowing the virtual orbitals to mix in. In particular the virtual 5_A-5_B orbital will mix with 4_A-4_B . Here the 5 acts effectively as acceptor orbital and relieves the Pauli repulsion of the N lone pairs by stabilizing the antibonding partner in the bonding/antibonding set of 4 derived orbitals.

It is not possible to separate effects such as charge transfer, polarization and relieve of Pauli repulsion. This may be made clear from the example of the $(CN)_2$ system (see Fig. 3). One may envisage some bonding to occur by donative bonding (charge transfer) from the occupied 1_A to the virtual 2_B and vice versa. At the same time, however, the Pauli repulsion that exhibits itself in the formation of the occupied antibonding combination 1_A-1_B is relieved by admixture of 2_A-2_B , which similarly leads to occupation of 2 and electron depletion from 1 . But electron transfer from 1 to 2 on one monomer may also be considered as polarization. We therefore consider these interactions collectively as 'relaxation energy' or (including the electron pair bond) as 'orbital interaction energy', as in the case of closed shell fragments.

It is possible to make a symmetry decomposition for the energy contributions due to the relaxation and orbital interaction energies [42]: $E = \mu \sum_{\mu} F_{\mu}^{TS} P_{\mu}$, where the 'transition state' Fock matrix is defined as $F^{TS} = (F(P^i) + F(P^f))/2$, with P^f the density matrix belonging to Ψ_{SCF} , and P^i belongs to Ψ^0 or Ψ_{pb}^0 .

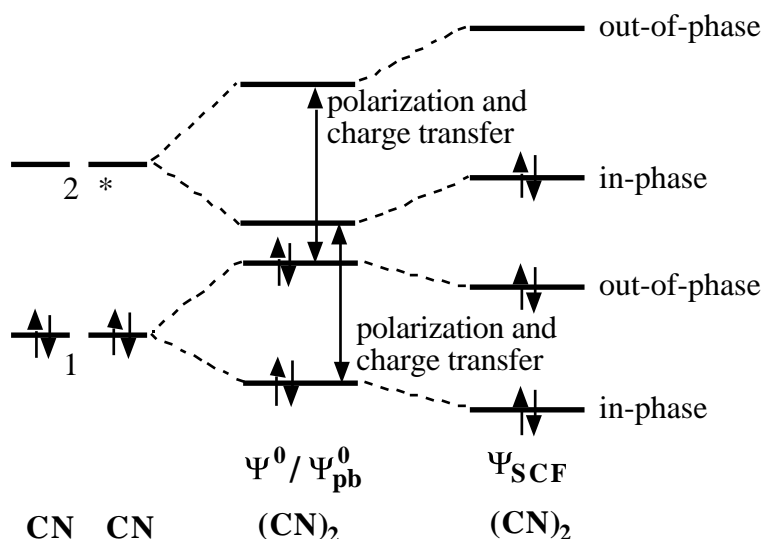


Figure 3. Orbital interaction diagram for π symmetry. Note that the π electronic structures are identical for Ψ^0 and Ψ_{pb}^0 .

Table 1. Comparison of the relative energies (eV) E_{1-2} and E_{1-3} between the isomeric C₂N₂ systems **1** - **3** as calculated by a number of theoretical methods.

Method	E_{1-2}	E_{1-3}
X ^a	0.97	2.86
DFT ^b	1.01	3.06
CEPA ^c	1.05	3.13
CCD+ST ^d	0.96	3.13
CCD ^d	0.88	3.04
MP4SDTQ ^d	1.17	3.32
MP4SDQ ^d	1.08	3.21
MP4DQ ^d	1.09	3.20
MP3 ^d	1.05	3.17
MP2 ^d	1.37	3.65
HF ^d	0.64	2.68

^a: This work; X = exchange-correlation potential [24] ^b: This work; more sophisticated density-functionals (see text) [33-37] ^c: Botschwina and Sebal (basis B: 132 CGTOs) [20], calculations are performed at the equilibrium geometries obtained with the 104 CGTO basis set. ^d: Sunil et al. [22], MP2-optimized geometries.

Although the symmetry decomposition is not rigorous, since changes in e.g. P_{σ} , i.e. the 'field', affect the Fock matrix and therefore E_{σ} , one nevertheless obtains a semi-quantitative assessment of e.g. E_{σ} and E_{relax} contributions to the total bond strength. If this symmetry decomposition is applied to E_{relax} the contribution only contains the rearrangement in the σ system due to admixture of virtual orbitals, if it is applied to E_{oi} the contribution also includes the electron pair bond. As an example of the interdependence of E_{σ} and E_{relax} contributions we note (cf. Table 4 and 5) that E_{oi} , E_{pb} + E_{relax} , (e.g. -10.39 resp. -10.08 eV for NC-CN) and E_{oi} , E_{relax} , (-2.95 resp. -3.31 eV). The reason for this is that the σ -electrons experience a stronger repulsive 'field' in σ_{pb} compared to σ_{σ} .

Accuracy of the applied density functional

In Table 1 we compare our DFT results for the relative energies E_{1-2} and E_{1-3} between the C₂N₂ species with the results obtained by other methods. The DFT results are in nice agreement with the results of a number of high-level coupled cluster approaches. The differences between the E_{1-2} and E_{1-3} values obtained by DFT and for instance CEPA amount to only 0.04 and 0.07 eV, respectively.

Table 2. Comparison of the geometry parameters (pm) of the linear species CN, HCN and HNC as obtained by X α theoretical and experimental methods.

method	CN		HCN		HNC	
	C-N	H-C	C-N	H-N	N-C	
<i>Theoretical</i>						
X ^a	117.3	108.2	115.9	101.9	117.2	
<i>Experimental</i>						
	117.18 ^b	106.5 ^c	115.3 ^c	99.4 ^d	116.9 ^d	

^a: This work, X exchange-potential [24]. ^b: Infrared: Herzberg [43]. ^c: Microwave: Winnewisser et al. [44]. ^d: High-resolution Infrared (HR-IR): Creswell and Robiette [45].

It is interesting to note that the X results achieve considerably better agreement with the coupled cluster and CEPA results than the conventional ab initio HF and MP2 methods. An other interesting quantity to compare is the CN/CN bonding energy E_b . Only for NCCN (**1**) the experimental value is known and amounts to -6.0 eV [46]. The DFT value of -5.55 eV (Table 4) only deviates by $+0.45$ eV. An extensive comparison of theoretical and experimental geometry parameters is presented in Tables 2 and 3. In Table 2 X and experimental values for the geometry parameters of the free CN radical and the

Table 3. Comparison of the geometry parameters (pm) of NCCN and CNCN obtained by a number of theoretical and experimental methods (see scheme 1 for definition of geometry parameters).

method	NCCN		CNCN			Average BL deviation ^a
	R ₁ =R ₃	R ₂	R ₁	R ₂	R ₃	
<i>Theoretical</i>						
X ^b	117.0	135.7	119.0	129.4	117.2	1.9
HF ^c	113.4	139.7	116.4	131.2	113.5	1.4
MP2 ^c	118.5	138.1	119.6	131.8	118.4	2.0
HF ^d	–	–	117.3	130.5	114.6	–
CI ^d	–	–	118.0	132.0	115.7	–
CEPA ^e	115.8	139.5	118.1	132.2	115.8	0.5
CISD ^f	117.7	140.1	119.5	132.9	117.7	1.8
HF ^g	114.5	137.8	117.3	130.5	114.6	1.0
HF ^h	113.4	139.7	116.4	131.2	113.5	1.4
MP2 ^h	118.5	138.1	119.6	131.7	118.4	2.0
<i>Experimental</i>						
HR-IR	115.4 ⁱ	138.9 ⁱ	117.5 ^j	131.4 ^j	116.0 ^j	–

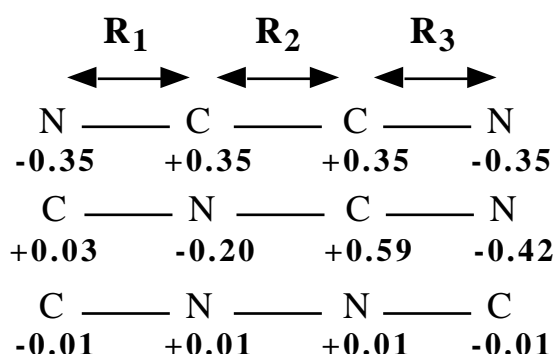
^a: Average Bond Length deviation defined as: $\bar{R} = 1/6 \sum |R_i^{\text{calc.}} - R_i^{\text{exp.}}|$. ^b: This work, X exchange potential [24]. ^c: Sunil et al. [22], 6-31G* basis. ^d: Schöller et al. [18], DZP basis. ^e: Botschwina and Sebald [20]. ^f: de Almeida and Hinchliffe, basis D95 [21]. ^g: Sana and Leroy, basis 6-31G. ^h: Nguyen [19], basis 6-31G*. ⁱ: Maki. [6]. ^j: Stroh and Winnewisser [9].

prototypes of cyanide and isocyanide compounds, HCN and HNC, respectively, are compared. For the cyanide radical the X–CN bond distance deviates by only 0.12 pm from the experimental value. For HCN and HNC the deviations between the X– and experimental bondlengths amount to about 2 pm. In Table 3 the geometry results of a number of theoretical and experimental studies on NCCN (**1**) and CNCN (**2**) are listed (for CNNC no experimental data are available). From the data of Table 3 it follows that the bondlengths obtained by theoretical methods ranging from HF, X^α, MP2 and CISD all have comparable deviations (in the order of 2 to 3 pm) from the experimental values, while the values for CEPA are better than for the other methods. The average bondlength deviation $\bar{R} = 1/6 \sum_i |R_i^{\text{calc.}} - R_i^{\text{exp.}}|$ ranges from 0.5 pm (CEPA) to 2.0 pm (MP2), and our X^α method with \bar{R} an average deviation of 1.9 pm fits in nicely with the considered high-level ab-initio methods.

Considerable experience with the DF approach shows that interaction energies in molecules involving main group elements and metals are described to an accuracy of a few tenths of an eV (5 kcal/mol) [14,32,39-41]. Summarizing, we conclude that the DF method leads to an accuracy comparable to that of conventional high-level methods like CEPA and the CCD(+ST) coupled cluster approach for the systems under consideration.

3. The bonding mechanism in the CN dimers

The results of a detailed analysis of the bonding mechanism and of a number of molecular parameters are presented in Table 4. For all three C₂N₂ isomers, the optimized CN bondlengths R₁ and R₃ (see scheme 1 below) of the CN monomers deviate only slightly from the calculated value of 117.3 pm in the free CN radical (Table 2).



Scheme 1: Definition of geometry parameters, and charges on atoms in the CN dimers.

Table 4. Calculated parameters for NCCN, CNCN and CNNC (see scheme 1 for the definition of geometry parameters). Geometries come from X α calculations. The other quantities are obtained from more sophisticated DFT calculations in the X α geometries.

	NC-CN	CN-CN	CN-NC
<i>Geometry (pm)</i>			
R ₁	117.0	119.0	118.6
R ₂	135.7	129.4	125.2
R ₃	117.0	117.2	118.6
<i>Overlaps <CN CN'></i>			
<4 4 ' >	0.26	0.31	0.39
<5 5 ' >	0.47	0.31	0.21
<4 5 ' >	0.35	0.41	0.28
<5 4 ' >	0.35	0.23	0.28
<1 1 ' >	0.10	0.12	0.15
<2 2 ' >	0.31	0.20	0.15
<1 2 ' >	0.20	0.24	0.15
<2 1 ' >	0.20	0.12	0.15
<i>Populations (el.)^a</i>			
P(4)	1.86	1.50/1.81	1.42
P(5)	1.06	1.53/0.93	1.42
P(1)	1.92	1.83/1.92	1.88
P(2)	0.09	0.10/0.11	0.12
<i>Energies (eV)^b</i>			
E	-10.39	-13.65	-16.74
E	-2.95	-3.96	-4.45
E _{rest}	0.00	0.01	0.01
<hr/>			
E _{oi}	-13.34	-17.60	-21.19
E ⁰	7.78	13.06	18.70
E(C N)	0.01	0.00	0.00
<hr/>			
E	-5.55	-4.54	-2.49
E _{atom}	-20.92	-19.84	-17.81
<i>Dipole moment (D)</i>			
μ	0.00	0.67 ^c	0.00

^a: P() is the gross Mulliken population that the fragment orbital acquires in the dimer. For the asymmetric CN-CN', the populations are denoted as P()/P('). ^a: E⁰ is the steric repulsion that comprises both the four-electron destabilizing interactions between occupied orbitals ('exchange repulsion') and the electrostatic interaction between the electronic and nuclear charge distributions of the fragments. E_{oi} is the orbital interaction. E(C N) is the energy required to stretch the C-N distance from the value in the free diatomic to the value in the dimer. E_{atom} is the energy difference between the C₂N₂ species and the free atoms. ^c: Experimental value: 0.7074(52) D [11].

The maximum deviation amounts to only +1.7 pm in the case of R_1 in CNCN (**2**). In contrast to this, the length R_2 , which couples the two CN monomers, considerably decreases in the series **1** - **3** from 135.7 (**1**) via 129.4 (**2**) to 125.2 pm (**3**). This observation is in line with the interpretation of the C_2N_2 species as being constituted by two internally strongly bound CN fragments which interact to give the overall molecule. Energetic considerations confirm this picture. From the CN/CN bond energy E and the energy difference E_{atom} between the C_2N_2 systems and the free atoms one can estimate the (average) bond energy of a terminal CN bond, which for each of the C_2N_2 species **1** - **3** amounts to some -7.7 eV. This is indeed considerably stronger than the CN/CN bond energies of -5.55 (**1**), -4.54 (**2**) and -2.49 eV (**3**), respectively. Therefore, it seems indeed justified to conceive all three C_2N_2 isomers as CN-dimers. This was also concluded in a recent study by Scheller et al. [18].

In the following subsections the character and importance of the σ and the π bond are discussed. After this the question is addressed *why* the CN radicals preferentially combine via carbon and not via nitrogen, and also an explanation for the decreasing central bond R_2 is given. Finally, a comparison is made between our MO description and the VB picture.

3.1 The σ bond and the importance of pair bonding

We first address the question, to what extent the σ interaction can be considered as a simple electron pair bond in each of the three cases **1** - **3**. From the energy analysis in Table 4 it follows that the steric repulsion E^0 strongly increases from 7.78 eV in NC-CN (**1**) via 13.06 eV in CN-CN (**2**) to 18.70 eV in CN-NC (**3**). At the same time however the orbital interaction energy E_{oi} also increases (becomes more bonding). In all cases **1** - **3** the major contribution (nearly 80%) to the orbital interaction E_{oi} comes from the interaction in the irreducible representation, E , which amounts to -10.39 (NCCN), -13.65 (CNCN) and -16.74 eV (CNNC), respectively. The increase in E_{oi} does diminish, but does not completely cancel the more unfavourable steric repulsion in going from **1** to **3**, so the net effect is a weakening of the CN/CN' bond for N-N coupling compared to C-C coupling.

In order to see whether these trends agree with intuitive expectations, the CN 4σ and 5σ orbitals are inspected in Fig. 4. From the orbital contour plots it follows that the CN 5σ MO, containing the unpaired electron, has a more extended and intense lobe at the C side, although it is by no means limited to the C side. The CN 4σ MO (the 'N lone pair orbital') has a higher amplitude on the nitrogen side, the lobe at the N side however being only slightly less extended than the lobe on the carbon side. Accordingly, going from C-C (**1**) via C-N (**2**) to N-N coupling (**3**), the $4\sigma|4\sigma'$ overlap (Table 4) increases from 0.26 via 0.31 to 0.39, while at the same time the $5\sigma|5\sigma'$ overlap decreases from 0.47

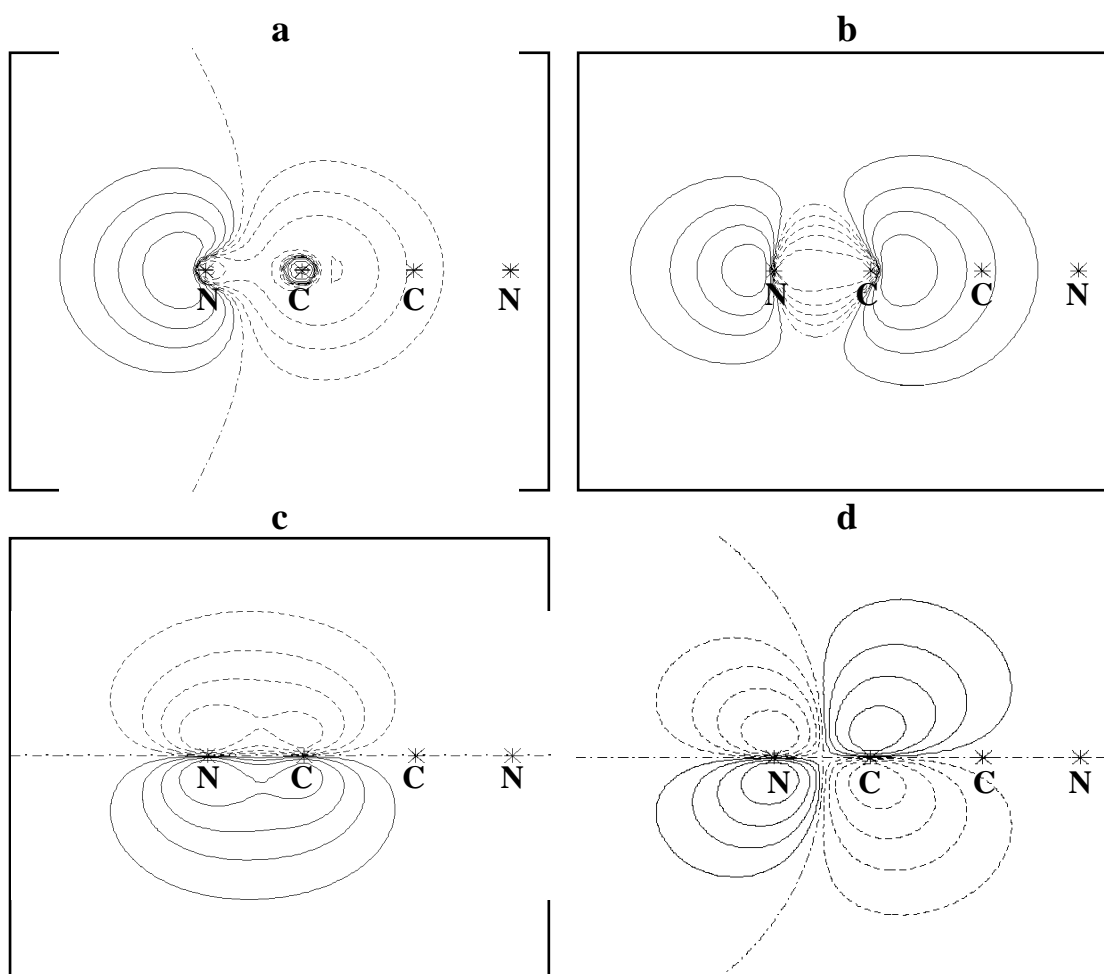


Figure 4. Frontier orbitals of CN in NCCN. a) 4σ . b) 5σ . c) 1π . d) 2π . Note that in each orbital plot the positions of the nuclei of the other CN fragment are indicated.

via 0.31 to 0.21. The behaviour of these overlaps as a function of the central distance R_2 is depicted in Fig. 5. The difference between C-C and N-N coupling is large for the $5 | 5'$ overlaps. These overlaps go through a maximum at 120 pm, approximately the equilibrium distance, because at shorter distances the positive lobe of one 5 extends over the nodal plane of the other 5 . The $4 | 4'$ overlaps are larger for N-N coupling, as expected, although the difference between N-N and C-C coupling is not as extreme as for the $5 | 5'$ overlaps.

Since a large $5 | 5'$ overlap is expected to be favourable for a strong electron pair bond and a large $4 | 4'$ overlap unfavourable because of strong Pauli repulsion, we expect that switching from C-C to N-N coupling is unfavourable on two accounts: the steric repulsion between the N lone pairs should increase and the orbital interaction energy should decrease. This expectation is borne out by the behaviour of E^0 , but E_{oi}

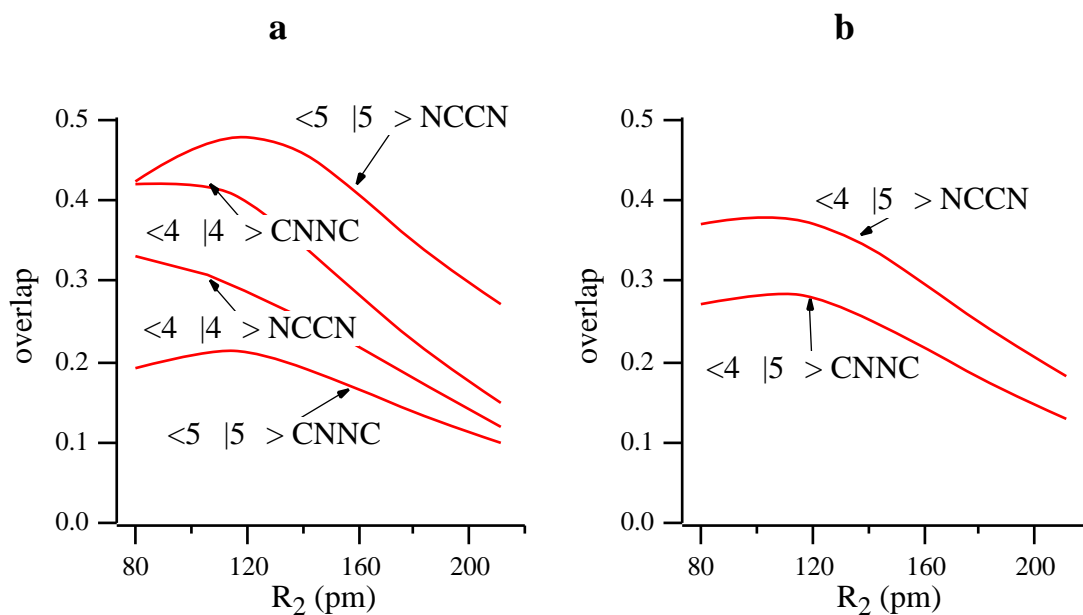


Figure 5. Overlaps (S) in σ symmetry between CN fragment orbitals in NC-CN and CN-NC as a function of the bondlength R_2 between the CN-monomers (see scheme 1 for the definition of geometry parameters. a) cross diagonal overlaps. (b) cross off-diagonal overlaps.

shows the opposite trend. We therefore proceed to a more detailed examination of E_{oi} .

As indicated in the diagram of Fig. 1, E_{oi} consists of two contributions, the pair bond energy E_{pb} , associated with the formation of the pair-bond wavefunction ψ_{pb}^0 from ψ^0 , and the energy E_{relax} , the relaxation of ψ_{pb}^0 to the final wavefunction ψ_{SCF} by the mixing in of virtual orbitals, i.e. both polarization and charge transfer (Fig. 2 and Section 2). For technical reasons this decomposition was done only for the symmetrical isomers NCCN (**1**) and CNNC (**3**). However, the values of the asymmetric isomer CNCN (**2**) are expected to be located in between those of **1** and **3**. In Table 5 the results of the energy analysis are presented. The following points are worth noting. 1) The pair bond energy E_{pb} is not the major component of the orbital interaction energy E_{oi} , as it contributes by only -5.66 and -6.48 eV to the bond in NCCN and CNNC, respectively. 2) E_{pb} is not much larger for C-C coupling (even smaller), in spite of the much larger $5 | 5'$ overlap. 3) An important, in the case of CN-NC even dominating component of the bond is constituted by the relaxation energy, E_{relax} , which amounts to -4.42 (NCCN) and -9.26 eV (CNNC).

We first consider the behaviour of E_{pb} . In Fig. 6c E_{pb} is plotted as a function of R_2 . At large distances E_{pb} is indeed larger for C-C coupling, as expected from the larger $5 | 5'$ overlap. At a distance slightly larger than the equilibrium R_2 s, however, the two curves cross and at shorter distances E_{pb} for C-C coupling actually decreases.

Table 5. Pair bonding energies for NCCN and CNNC.

	NC-CN	CN-NC
<i>Energies (eV)</i>		
E_{relax}	-4.42	-9.26
E_{relax}	-3.31	-5.45
$E_{\text{relax,rest}}$	0.05	0.00
E_{relax}	-7.73	-14.71
$E_{\text{relax,pb}}^{\text{a}}$	-5.66	-6.48
E^0	7.78	18.70
E_{pb}	-5.66	-6.48
$E(\text{C})$	0.01	0.00
E	-5.55	-2.49

^a: E_{pb} is the pair bonding energy calculated from $E_{\text{pb}}^0 - E^0$, as explained in the section on the interaction energy analysis for open-shell fragments. For the meaning of the other terms see text and table.

To explain this behaviour we have to consider the orbital interactions depicted in Fig. 2. In E_{pb} not only the 'pure' electron pair bond but also the interaction between the *in-phase* combinations of the 4 and 5 orbitals has to be taken into account. C-C coupling implies a larger $5|5'$ overlap and therefore, in the imaginary intermediate step indicated in gray in Fig. 2, a more strongly stabilized $5+5'$ orbital and at the same time a smaller $4|4'$ overlap and therefore less stabilized $4+4'$ orbital. These two orbitals would therefore be energetically closer in the case of C-C coupling and at the same time their interaction matrix element would be larger, judging from the larger $4|5'$ overlap in case of C-C coupling (cf. Fig. 5b). The four electron destabilizing interaction between the occupied ($4+4'$) and ($5+5'$), which is embodied in E_{pb}^0 , is therefore larger for C-C coupling and increases with shorter R_2 . For N-N coupling this repulsive effect will not increase since the energetic spacing between ($4+4'$) and ($5+5'$) increases with shorter R_2 (Figs 2 and 5). This explains the loss of the initial advantage, at large distance, of E_{pb} for C-C over N-N coupling when R_2 becomes shorter. [We have tried to estimate 'pure' pair bonding at equilibrium distance by switching off the Pauli repulsion, artificially putting the $4|5'$ overlap to zero. In that case E_{pb} is, just as for large R_2 where the 'secondary' repulsive effects are relatively less important, considerably larger indeed for C-C coupling]. At distances shorter than the equilibrium R_2 , E_{pb} for C-C coupling actually starts to decrease.

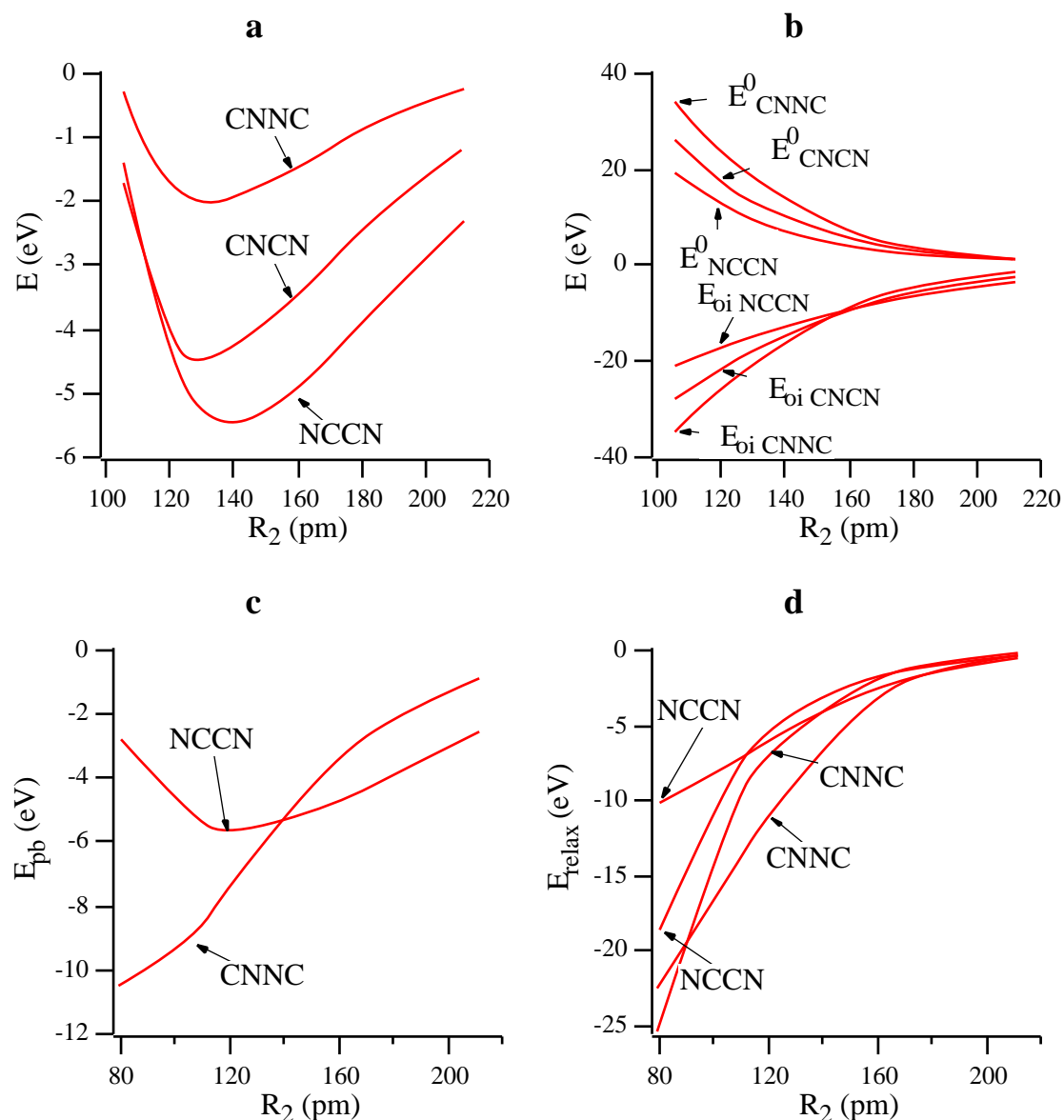


Figure 6. Interaction energies for NC-CN, CN-CN (only in (a) and (b)) and CN-NC as function of the bondlength R_2 between the CN-monomers (see figure 3 for the definition of geometry parameters):. a) the net bonding energy $\Delta E = \Delta E^0 + \Delta E_{oi}$. b) the steric repulsion ΔE^0 and orbital interaction $\Delta E_{oi} = \Delta E_{pb} + \Delta E_{relax,\sigma} + \Delta E_{relax,\pi}$. c) the pair-bond energy ΔE_{pb} . d) the relaxation energies $\Delta E_{relax,\sigma}$ and $\Delta E_{relax,\pi}$.

This behaviour is probably related to the diminishing $5 \mid 5'$ overlap at such short distances (see Fig. 5), but has not been analyzed in detail. The point we wish to emphasize in relation to the foregoing discussion, is that for a full understanding of the pair bonding energy not only the 5 frontier orbital containing the unpaired electron has to be considered but the underlying fully occupied 'N lone pair' orbital as well.

The second point that requires elucidation is the large E_{relax} , particularly for N-N coupling. In CN-NC (**3**) E_{relax} (-9.26 eV) is even more than 40% stronger than E_{pb} (-6.48 eV). The electronic relaxation is ascribed mainly to the interaction of the unoccupied $5 - 5'$ with the occupied $4 - 4'$ orbital, as indicated in Fig. 2. (Note that for E_{relax} the *out-of-phase* combinations of the 4 and 5 orbitals are important). This follows from the gross Mulliken populations that the CN 4 and 5 orbitals acquire in the SCF wavefunction of the CN dimers (Table 4). In line with increasing relaxation effects going from **1** to **3** the population $P(5)$ increases from 1.06 el. in NCCN to 1.42 el. in CNNC, while at the same time $P(4)$ decreases from 1.86 to 1.42 el.. This means that in CNNC nearly half an electron is transferred from CN 4 to CN 5 orbitals, by mixing in of the virtual $5 - 5'$ into the doubly occupied $4 - 4'$ combination. The dimer thus has experienced a considerable rearrangement of the electronic structure in which the CN 5 character of the electron distribution is increased. This fits in with the overlap results of Fig. 5a. In **1** - **3**, the $4/4'$ interaction and thus the destabilization of the $4 - 4'$ out-of-phase combination increases (hence the larger E^0), while the $5/5'$ interaction and thus the destabilization of the $5 - 5'$ out-of-phase combination strongly decreases. Consequently, going from **1** to **3** the MO energy levels corresponding to the doubly occupied $4 - 4'$ and the virtual $5 - 5'$ come closer to each other (see Fig. 2), and their mutual interaction increases in spite of a decrease of the interaction matrix element (Fig. 5b). Therefore CN-NC (**3**) experiences the strongest electronic rearrangement. As the pair-bond energy E_{pb} does not change considerably in the series **1** - **3**, it is the dominating relaxation energy which leads to an increase of the orbital interaction going from **1** to **3**. It is to be noted that N-N coupling, despite the large steric repulsion it experiences from the N lone pairs, is 'saved' by the large relaxation energy which is in fact a relief of the steric repulsion through a stabilization of the antibonding $4 - 4'$ orbital by the close-lying $5 - 5'$. Effectively the 5 orbital is acting here as an acceptor orbital, receiving electrons from the fully occupied N lone pair donor orbital. Such donor/acceptor interaction, which is here symmetry separated from the pair bonding interaction (σ_u resp. σ_g), may occur readily in pair bonding situations since the orbital containing the unpaired electron is usually at much lower energy (i.e. closer to the donor orbitals) than the acceptor orbitals in the virtual orbital spectrum.

3.2 The π bond

In π symmetry the only means of providing a bonding interaction is electronic relaxation (including both polarization and donor-acceptor interaction), from mixing of both the out-of-phase (antibonding) and in-phase (bonding) combinations of the unoccupied CN-2 MOs into those of the occupied CN-1 MOs (see Fig. 3).

Going from **1** - **3**, the E contribution to the total orbital interaction energy E_{oi} increases from -2.95 to -4.45 eV, which is small compared to E (Table 4). If the pair bonding energy E_{pb} is separated from E_{oi} , the contributions E_{relax} to the relaxation energy, -3.31 and -5.45 eV in **1** and **3** respectively (Table 5), are somewhat larger than the E parts of E_{oi} . This has been pointed out in Section 2 already. Furthermore, the E_{relax} are smaller than the E_{relax} . This is in agreement with the fact that the 2 orbital is truly a virtual orbital, i.e. more separated from the occupied orbitals than the singly occupied 5 . Moreover, the overlaps between CN MOs (less than 0.25, Table 4) are smaller than those between CN MOs (larger than 0.25). The origin of the increase of E_{relax} going from **1** to **3** is analogous to that of the increase of E . Inspection of Fig. 4 reveals that the bonding CN 1 MO has a higher amplitude and is somewhat more extended on the nitrogen side of the cyanide radical, whereas the antibonding CN 2 is more intense and substantially more extended on carbon. As a consequence, going from **1** to **3** the $1 | 1'$ overlap increases from 0.10 via 0.12 to 0.15, and the $2 | 2'$ overlap decreases strongly from 0.31 via 0.20 to 0.15. Due to this, in **1** - **3** the $1 / 1'$ interaction and the energy gap between the $1 / 1'$ in-phase and out-of-phase combinations increases, while the $2 / 2'$ interaction and energy gap between the $2 / 2'$ in-phase and out-of-phase combinations decreases. Therefore the MO energy levels of the doubly occupied $1 - 1'$ and the virtual $2 - 2'$ out-of-phase combinations come closer to each other, and their mutual interaction increases. The reverse is true for the in-phase $1 + 1'$ and $2 + 2'$ combinations. The net effect is a moderate increase of E_{relax} in going from **1** - **3**. In line with increasing relaxation effects going from **1** to **3** the population $P(2)$ increases slightly from 0.09 el. in NCCN (**1**) to 0.12 el. in CNNC (**3**), while at the same time $P(1)$ decreases from 1.92 to 1.88 el.. The dimer thus has experienced a rearrangement of the electronic structure in which the CN 2 character of the electron distribution is slightly increased.

3.3 The preference of C-C over N-N coupling

In the following, the question is addressed *why* C-C coupling is preferred over N-C and more so over N-N coupling. An interesting phenomenon in this context is the fact that going from **1** to **3** in the $(CN)_2$ series, the bond energy E decreases whereas the equilibrium length R_e for the central CN/CN-bond R_2 becomes shorter. This is clearly shown by the $E(R)$ curves (R stands for R_2) in Fig. 6a. In order to explain the features mentioned above, we investigate the behaviour of the bonding interactions, i.e. the steric repulsion (Fig. 6b), the pair bond (Fig. 6c) and the E_{relax} relaxation energies (Fig. 6d) as a function of R .

First, the steric repulsion is considered. As discussed previously in Section 3.2, the overlaps $4 | 4'$ and $1 | 1'$ increase going from coupling via carbon to coupling via

nitrogen. It is clear from Fig. 6b that in accordance with this the steric repulsion is largest and also rises most steeply for N-N coupling at all distances. In order for R_e to become shortest for N-N coupling this has to be compensated by larger positive derivatives from the orbital interaction energies. For E_{pb} (Fig. 6c) this is clearly the case due to the minimum that occurs for C-C coupling but not for N-N coupling. This effect has already been discussed: the pair bonding is hampered in the case of C-C coupling by increasing Pauli repulsion effects with shorter R_2 , whereas in case of N-N coupling the 'pure' pair bonding increases *and* the $4/5$ Pauli repulsion diminishes since the increasing $4/4'$ overlap with shorter R_2 leads to stabilization of the doubly occupied $4+4'$ relative to the $5+5'$. The change in the behaviour of E_{pb} going from C-C to N-N coupling thus has the effect of shortening R_2 .

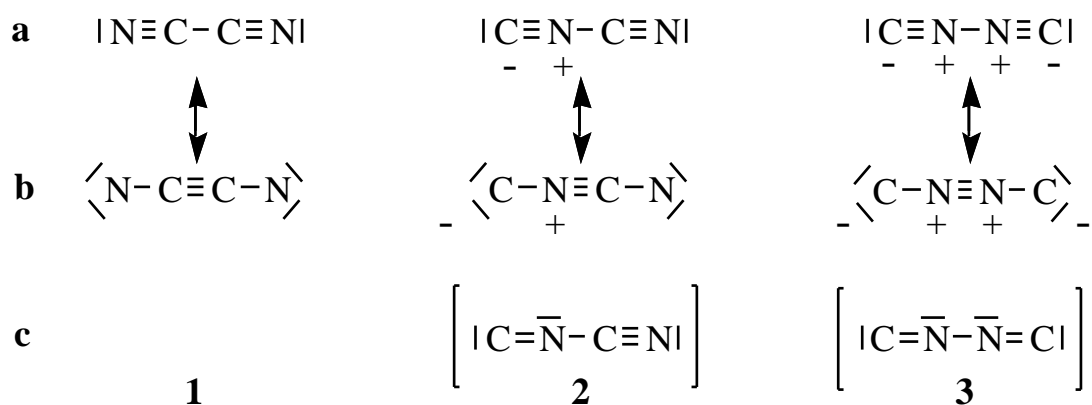
The relaxation energy is seen to have the same effect in Fig. 6d. As discussed previously, the relaxation energy E_{relax} is mainly caused by the mixing of the out-of-phase combinations $4-4'$ with the $5-5'$ ($E_{relax, \sigma}$), and also by the mixing of the out-of-phase and (to a lesser extent) the in-phase combinations $1 \pm 1'$ with the $2 \pm 2'$ ($E_{relax, \pi}$). Fig. 6d shows a steeper gradient of both types of relaxation energy when the distance is shortened. This is the result of increasing $\langle 4|5 \rangle$ and $\langle 1|2 \rangle$ overlaps *and* increasing $4/4'$ and $1/1'$ interactions. The latter, which lead to increasing spacings between the bonding and antibonding combinations of these orbitals and are responsible of course for much of the steric repulsion, lead at the same time to a reduction of the energy gap between the mixing out-of-phase combinations in σ and π symmetry, respectively (Figs 2 and 3). The $5/5'$ and $2/2'$ interactions weaken the relaxation mixing as they enlarge the energy gap between the mixing out-of-phase combinations. Going from **1** to **3** substantially *increases* the $4/4'$ and $1/1'$ interactions and *decreases* the $5/5'$ and $2/2'$ interactions. As a result, the relaxation energy E_{relax} increases considerably and acquires a steeper gradient.

At values of R_2 around 125 pm it is clear that both the pair bonding energy E_{pb} and the relaxation energy E_{relax} , and therefore E_{oi} , have steeper gradients in case of N-N coupling. The absolute values, however, differ less from those for C-C coupling than the repulsive E^0 contribution (Fig. 6b). The absolute value of the total bonding energy E is therefore still smaller in case of N-N bonding, although the steeper gradients of the attractive energy components do contract the bond length.

3.4 VB structures

Although relatively small, E_{relax} is substantial in the sense that it is in the same order of magnitude as the total bonding energy. In CNNC the total bond energy E (-2.49 eV) would not even be bonding without this relaxation ($E_{relax} = -5.45$ eV) which is

more than twice as large. This leads to the conclusion that in classical valence bond (VB) terms the CN/CN-bond R_2 can be conceived to have a considerable double bond character. In fact, in VB terms one should even speak of a partial triple bond as there exist besides the σ bond two equivalent sets of CN- MOs which interact. We therefore propose to represent the electronic structure of **1** - **3** by the resonance diagrams:



Scheme 2: Valence bond structures for the CN dimers.

Based on the dominance of the σ bonding between the CN monomers, it is concluded that the structures **1a** - **3a** represent the major components compared to **1b** - **3b**. The ionic character of the mesomeric structures **2a/b** and **3a/b** for CNCN and CNNC, respectively, is in agreement with the atom charges indicated in scheme 1. While the charges in NCCN with its neutral mesomeric structures **1a/b** are nearly the same as in the free CN radical (CN: $Q(C) = +0.35$ el., $Q(N) = -0.35$ el.), they are clearly different in CNCN. In that part of CNCN where the resonance structures **2a/b** give an ionic contribution, the charges on C and N have been reduced considerably to $+0.03$ el. and -0.20 el., respectively. In CNNC signs have even been inverted to $Q(C) = -0.01$ el. and $Q(N) = +0.01$ el. confirming the picture of the ionic structure **3a/b**. The occurrence of the ionic structures **3a** and **3b** in the case of CNNC compensates for the atomic charges which are built up within the CN monomers due to the electronegativity difference [47] between carbon and nitrogen. This leads to a significantly more balanced charge distribution in CNNC compared to NCCN (scheme 1).

We wish to emphasize that resonance structures as depicted in scheme 2 should be interpreted with caution. The structures **a** do indeed suggest charge distributions for the three isomers which are in qualitative agreement with the results of the calculations, but they do not explain the large quantitative differences that still exist, for instance for the isocyanide nitrogen in **2** resp. **3** and the cyanide carbon in **1** resp. **2** (cf. scheme 1). Furthermore, whereas the triple bonding in structures **b** may be considered to represent the moderate contribution of central π bonds, the neutral resonance structures **2c** and **3c**,

respectively, do not represent the electronic structure of CNCN (**2**) and CNNC (**3**) in an appropriate way. According to their linear symmetry **2** and **3** have π MOs, which always come in two symmetry-equivalent sets. Therefore, the meaning of just one double bond between two constituting atoms and a lone pair on a central nitrogen is not very clear.

4. Comparison with previous studies

To our knowledge, the only other study where the interaction in the $(\text{CN})_2$ isomers is described in terms of MOs of the CN fragments, is a recent investigation by Scheller et al. [18]. For comparison with their results, we present Orbital Correlation Diagrams (OCDs) in Figs 7a-c. In these OCDs the compositions of the $(\text{CN})_2$ orbitals are given in terms of the CN fragment orbitals. Only the π -orbitals are investigated, as these are the most interesting ones. The various steps in which the interaction is divided, are only a schematic way to arrive at the final situation.

In NCCN (Fig. 7a) we first allow pair bonding and repulsion between the 4π orbitals (this corresponds to the grey levels in Fig. 2). As the 5π is localized mostly at C, the 5π interaction is large and the in-phase 5π combination ends up lower than the corresponding 4π one, with a small energy difference. The final situation is obtained by allowing Pauli repulsion between the in-phase combinations and the relaxation, consisting of the mixing of the out-of-phase $4\pi-4\pi'$ and $5\pi-5\pi'$ combinations. In this combined step, the in-phase $5\pi+5\pi'$ combination is stabilized heavily by mixing with $4\pi+4\pi'$, as these orbitals were close in energy and the (cross off-diagonal) overlaps $4\pi|5\pi'$ and $5\pi|4\pi'$ are large (Fig. 5). The $4\pi+4\pi'$ combination is destabilized, with an overall repulsive effect for the in-phase combinations. The $4\pi-4\pi'$ combination is stabilized by mixing with $5\pi-5\pi'$, although not so much as the mixing between the in-phase combinations. The large in-phase mixing results in the observed energy ordering of a mostly in-phase $4\pi+4\pi'$ gerade combination $5\pi_g$ above the mainly $4\pi-4\pi'$ combination $4\pi_u$. From this one could conclude that the interactions in NCCN were small, with the 4π combinations close together between the 5π combinations. This would be a wrong conclusion, because also the 4π has considerable weight on C (see Fig. 4), and thus also the 4π splitting is large. Moreover, the cross off-diagonal overlaps between the fragments are large too. This results in a heavy interaction, with the result as explained above.

For CNNC (Fig. 7b) the OCD shows a large splitting between the 4π combinations, as the CN 4π is localized mostly at N, bringing the out-of-phase $4\pi-4\pi'$ combination closely below its $5\pi-5\pi'$ analogue. Note that the 5π has also considerable weight on N (although less than the 4π), resulting in a considerable splitting too. The subsequent interaction between the out-of-phase combinations stabilizes the $4\pi-4\pi'$ to a large extent, and the resulting orbital also has much $5\pi-5\pi'$ character.

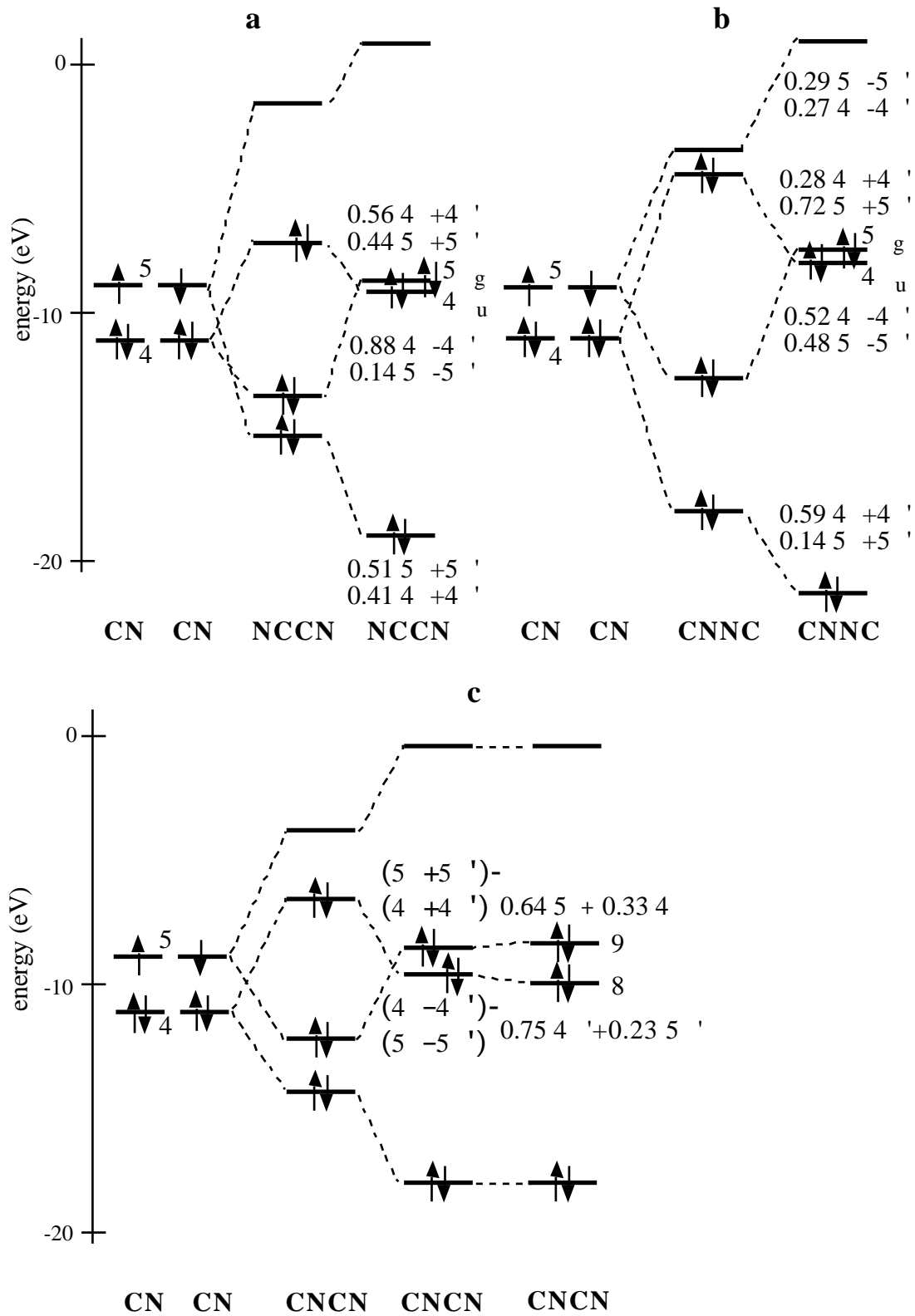


Figure 7. Orbital Correlation Diagram for the (CN)₂ dimers NCCN (a), CNNC (b) and CNCN (c).

The repulsion between the in-phase combinations destabilizes the $5 + 5'$ combination. The final result is a mainly $5 + 5'$ orbital 5_g above a mainly $4 - 4' + 4_u$, in which also much $5 - 5'$ character is present (almost 1:1). Thus, again the small splitting between these orbitals is not caused by a small interaction (between 5 orbitals), but is the result of a complicated interplay of repulsive and relaxation contributions.

Finally we consider CNCN in Fig. 7c. This is a special case, as due to its C_v symmetry, orbitals are allowed to mix which was forbidden in the symmetric NCCN and CNNC. Of special interest is the localization of the middle two levels 8 and 9 as CN $4'$ (right) and 5 (left) respectively. The difference with the other isomers is that after the combined Pauli repulsion/relaxation step we allow mixing between the middle two levels, as these are closest to each other. In this step the $((5 + 5') - (4 + 4'))$ combination interacts in an antibonding fashion with the $((4 - 4') - (5 - 5'))$ combination. It is emphasized that the latter results from the bonding admixture of the $4 - 4'$ and $5 - 5'$, which follows from the phases of the orbitals. When the interactions are assumed to be equal, adding the contributions to the final orbitals then qualitatively explains the localization. In the 8 orbital the main contribution comes from $4'$ (right CN), while in the 9 orbital the 5 (left CN) orbital dominates.

Next we compare our results with those of Scheller et al. [18]. The relative energies of their orbitals are approximately equal to ours, but for all three isomers they conclude that there is only a small interaction between the CN fragments. They describe the central bond between the monomers by the interaction of the orbitals localized at that side of CN, where the coupling takes place. In their view the localization of the 4 and 5 is complete, i.e. the 5 is located entirely at C and the 4 at N. Thus they have going from NCCN via CNCN to CNNC, a $5 - 5$ bond, a $5 - 4$ bond and a $4 - 4$ bond respectively. As the 4 is doubly occupied, there are 0,1 and 2 'surplus' electrons in this series compared to an optimal 2-electron 2-orbital bond. The most interesting orbitals to compare are those in the middle, which we have described above.

For CNCN Scheller et al. [18] conclude there is no interaction between the CN fragments, the 8 orbital is identified as the right CN $4'$, while the 9 orbital is the left CN 5 , which is lowered in energy by a hybridization with the left CN $4'$ accompanying donation of one surplus electron in it. However, as we showed above, the localization arises just because the interaction between the monomers is large, which is ultimately the result of the fact that the localization of the CN $4'$ and 5 is not at one side of the molecule, but both have considerable weight on the other atom too. From the populations in Table 4 it can be seen that the CN $4'$ orbital ends up with a much larger population than the $4'$, and the same is found for the 5 compared to the $5'$ orbital. This localization resulted from a strong interaction between the monomers. For CNNC and NCCN our view of the orbitals in the middle, 5_g and 4_u , is also very different from

that of Scheller et al. [18]. They identify these orbitals as the combinations of the 4σ and 5σ orbitals for NCCN and CNNC respectively, with the strange result that the out-of-phase combinations end up lower than the in-phase combinations. In the case of CNNC both orbitals are severely stabilized resulting from the donation of two surplus electrons from the high-lying $4\sigma - 4\sigma'$ combination. This does not explain the ungerade below gerade 5σ combination however. A very different picture emerges from our calculations. The large splitting of the out-of-phase 4σ combination and subsequent interaction with the $5\sigma - 5\sigma'$ combination, together with a destabilization of the in-phase $5\sigma + 5\sigma'$ combination by the low lying $4\sigma + 4\sigma'$ combination, leads to the observed level ordering. In our calculation all orbitals are mixed considerably, and there is a large donation from the $4\sigma - 4\sigma'$ into the $5\sigma - 5\sigma'$ combination. In our picture the concept of surplus electrons is not needed. Finally in NCCN, Scheller et al.[18] find the 4σ combinations with the wrong ordering, in between the 5σ combinations, again with a small interaction. We showed that although we find qualitatively the same ordering with respect to the main contributing levels, especially the small gap and ordering of the $5\sigma_g$ and $4\sigma_u$ can only be explained by a strong interaction between the CN monomers.

Concluding, we find qualitative agreement with Scheller et al. [18] as to the level ordering, but in our view this level ordering is not the result of a small interaction between the CN monomers, but on the contrary a very large interaction takes place between them. In contrast to Scheller et al. we do not need the concept of surplus electrons, but describe the bonding in terms of well known energy concepts such as Pauli-repulsion, acceptor-donor interactions and pair-bonding. The differences with Scheller et al. are ultimately related to the fact that one can not view the CN 4σ and 5σ orbitals as being localized on N and C respectively as Scheller et al. do, but both orbitals have appreciable character on the other side of CN as well. The orbital plots of Fig. 4 convincingly demonstrate this.

5. Conclusions

We have shown that the picture in which the cyanide radicals in the three CN dimers are mainly coupled by a simple electron pair bond by the singly occupied 5σ frontier orbitals is an incorrect oversimplification of the complex bonding mechanism for the species.

The doubly occupied 4σ ("N lone pair") orbitals also play a key role. In the first place they cause considerable Pauli repulsion, in particular for N-N coupling where the $4\sigma/4\sigma'$ overlap is largest. One would in fact expect C-C coupling to be strongly preferred for two reasons: strongest electron pair bond due to most favourable $5\sigma/5\sigma'$ overlap and least steric hindrance by the N lone pairs. There is, however, a subtle interplay between the 4σ

and 5 orbitals that has the effect of reducing considerably the difference between the various coupling modes of the CN monomers, making the CN-CN isomer also firmly bound and even the CN-NC monomer stable with respect to the monomers. The first effect is the repulsive interaction between the occupied *in-phase* combinations $4 +4'$ and $5 +5'$. For C-C coupling the small $4 /4'$ overlap, and large $5 /5'$ overlap act together to make the spacing between the $4 +4'$ and $5 +5'$ levels 'before interaction' smallest and therefore this repulsive contribution largest. Here the 5 acts as occupied orbital, having Pauli repulsion with other occupied orbitals. The second effect is the donor/acceptor interaction between the 4 and 5 orbitals, showing itself in a stabilizing interaction between the *out-of-phase* combinations $5 -5'$ (unoccupied) and $4 -4'$ (occupied). The same simple overlap argument shows the spacing between these levels 'before interaction' to be smallest for N-N coupling and therefore the stabilization largest in that case. Here the 5 acts as unoccupied acceptor orbital. It should be noted that an orbital containing an unpaired electron is potentially a good acceptor orbital, as it is usually not being separated by a HOMO/LUMO gap from the occupied orbitals. In addition to the bonding effects there is a bonding contribution, which is mainly due to the mixing of the doubly occupied $1 -1'$ with the virtual $2 -2'$ out-of-phase combinations. The bonding reduces the differences between the isomers as it was found to be increasingly important in **1 - 3**. Numerically, none of the effects mentioned so far is negligibly small compared to the other ones.

The steric repulsion by the CN 4 and 1 MOs, with highest amplitudes at the N side, is the most important cause of the overall *weakening* of the CN/CN' bond when going from C-C to N-N coupling. However, due to the behaviour of both E_{pb} and E_{relax} , the E_{oi} versus R_2 curve becomes steeper. Therefore, going from C-C to N-N coupling, the CN/CN' bond length R_2 *contracts* in spite of the *decreasing* bond strength. It is interesting to note, that the most weakly bound species, CNNC, does not only have the shortest bond length but also has experienced the strongest deformation of the electronic structure of the CN monomers.

References

- 1: L.J. Gay-Lussac, Ann. Chim. (Paris) **95** (1815) 175
- 2: T. van der Does and F. Bickelhaupt, Angew. Chem. **100** (1988) 998
- 3: S.J. Goede and F. Bickelhaupt, J. Am. Chem. Soc. **113** (1991) 6104
- 4: F. Stroh, B.P. Winnewisser, M. Winnewisser, H.P. Reisenauer, G. Maier, S.J. Goede and F. Bickelhaupt, Chem. Phys. Lett. **160** (1989) 105
- 5: C.K. Møller and B.P. Stoicheff, Can. J. Phys. **32** (1954) 635
- 6: A.G. Maki, J. Chem. Phys. **43** (1965) 3193

- 7: Y. Morino, K. Kuchitsu, Y. Hori and M. Tanimoto, *Bull. Chem. Soc. Jpn.* **41** (1968) 2349
- 8: O. Grabandt, C.A. de Lange, R. Mooyman, T. van der Does and F. Bickelhaupt, *Chem. Phys. Lett.* **155** (1989) 221
- 9: F. Stroh and M. Winnewisser, *Chem. Phys. Lett.* **155** (1989) 21
- 10: K.M.T. Yamada, M.W. Markus, G. Winnewisser, W. Joentgen, R. Kock, E. Vogel and H.-J. Altenbach, *Chem. Phys. Lett.* **160** (1989) 113
- 11: M.C.L. Gerry, F. Stroh and M. Winnewisser, *J. Molec. Spectrosc.* **140** (1990) 147
- 12: I. Weiss, H. Oberhammer, S.J. Goede, P.J.K.M. Eeken and F. Bickelhaupt, personal communication (1989)
- 13: R. Boese and F. Bickelhaupt, personal communication (1990)
- 14: F.M. Bickelhaupt, R.H. Fokkens, L.J. de Koning, N.M.M. Nibbering, E.J. Baerends, S.J. Goede and F. Bickelhaupt, *Int. J. Mass Spectrom. Ion Processes* **103** (1991) 157
- 15: N.N. Haese and R.C. Woods, *J. Chem. Phys.* **73** (1980) 4521
- 16: M. Sana and G. Leroy, *J. Molec. Struct. (THEOCHEM)* **76** (1981) 259
- 17: L.S. Cederbaum, F. Tarantelli, H.-G. Weikert, M. Scheller and H. Köppel, *Angew. Chem.* **101** (1989) 770
- 18: M.K. Scheller, H.G. Weikert, L.S. Cederbaum and F. Tarantelli, *J. Electr. Spectr.* **51** (1990) 75
- 19: M.T. Nguyen, *Chem. Phys. Lett.* **157** (1989) 430
- 20: P. Botschwina and P. Sebald, *Chem. Phys.* **141** (1990) 311
- 21: W.B. de Almeida and A. Hinchliffe, *J. Molec. Struct. (THEOCHEM)* **206** (1990) 77
- 22: K.K. Sunil, J.H. Yates and K.D. Jordan, *Chem. Phys. Lett.* **171** (1990) 185
- 23: M.K. Scheller, L.S. Cederbaum and F. Tarantelli, *J. Am. Chem. Soc.* **112** (1990) 9484
- 24: J.C. Slater, 'Quantum Theory of Molecules and Solids', Vol. 4, McGraw-Hill, New York, 1974
- 25: R.G. Parr and W. Yang, 'Density-Functional Theory of Atoms and Molecules', Oxford University Press, New York 1989
- 26: E.J. Baerends, D.E. Ellis and P. Ros, *Chem. Phys.* **2** (1973) 41
- 27: P.M. Boerrigter, G. te Velde and E.J. Baerends, *Int. J. Quant. Chem.* **33** (1988) 87
- 28: E.J. Baerends and P. Ros, *Chem. Phys.* **8** (1975) 412
- 29: E.J. Baerends and P. Ros, *Int. J. Quant. Chem.* **S12** (1978) 169
- 30: K. Morokuma, *J. Chem. Phys.* **55** (1971) 1236
- 31: K. Kitaura and K. Morokuma, *Int. J. Quant. Chem.* **10** (1976) 325
- 32: L. Versluis and T. Ziegler, *J. Chem. Phys.* **88** (1988) 322
- 33: A.D. Becke, *Int. J. Quant. Chem.* **23** (1983) 1915

- 34: A.D. Becke, *J. Chem. Phys.* **85** (1986) 7184
- 35: T. Ziegler, V. Tschinke and A. Becke, *Polyhedron* **6** (1987) 685
- 36: S.H. Vosko, L. Wilk and M. Nusair, *Can. J. Phys.* **58** (1980) 1200
- 37: H. Stoll, E. Golka and H. Preus, *Theor. Chim. Acta* **55** (1980) 29
- 38: P.J. van den Hoek, A.W. Kleyn and E.J. Baerends, *Comments At. Mol. Phys.* **23** (1989) 93
- 39: T. Ziegler, V. Tschinke and C. Ursenbach, *J. Am. Chem. Soc.* **109** (1987) 4825
- 40: T. Ziegler, V. Tschinke, L. Versluis and E.J. Baerends, *Polyhedron* **7** (1988) 1625
- 41: L. Fan and T. Ziegler, *J. Chem. Phys.* **92** (1990) 3645
- 42: T. Ziegler and A. Rauk, *Theoret. Chim. Acta* **46** (1977) 1
- 43: G. Herzberg, 'Molecular Spectra and Molecular Structure', Vol. 2, 'Infrared and Raman Spectra of Polyatomic Molecules', Van Nostrand, Princeton 1945
- 44: G. Winnewisser, A.G. Maki and D.R. Johnston, *J. Mol. Spectrosc.* **39** (1971) 149
- 45: R.A. Creswell and A.G. Robiette, *Mol. Phys.* **36** (1978) 869
- 46: G. Herzberg, 'Molecular spectra and molecular structure', Vol. 3, 'Electronic spectra and electronic structure of Polyatomic Molecules', Van Nostrand, New York, 1966
- 47: T.A. Albright, J.K. Burdett and M.H. Whangbo, 'Orbital Interactions in Chemistry', Wiley, New York 1985

Chapter 5

Spectroscopy of uranyl compounds

Abstract

The excitation spectrum of $\text{Cs}_2\text{UO}_2\text{Cl}_4$ was investigated using $\text{UO}_2\text{F}_4^{2-}$ as a model. Based on the dominance of the spin-orbit splitting over the ligand field splitting in the U 5f manifold, we propose the assignment: $\sigma_u\delta_u < \sigma_u\phi_u$, $\sigma_u\delta_u < \sigma_u\phi_u$. This is different from previous studies, but in agreement with experiment, especially the position/splitting of the non-bonding f orbital. In the second part of the present work, it is shown from ionization calculations on UO_2^{2+} that due to the large overlap and consequently *strong interaction between U 6p and O 2s*, the peaks in the X-ray PES spectrum can not be assigned to individual AOs.

This study again points out that many of the special features of uranyl are related to the special character of the *sub-valence U 6p* orbital. We already showed that it provides much of the *repulsion* between U and O, despite of which the U-O bond length is short (Chapter 4a), causes the HOMO to be of σ_u symmetry (Chapter 3 and 4a), determines the excitation spectrum of $\text{Cs}_2\text{UO}_2\text{Cl}_4$, and the strong interaction with O 2s makes an interpretation of the X-ray PES spectrum in terms of pure atomic states impossible (present work). Furthermore it is known from earlier studies to be important in making UO_2^{2+} linear and responsible for the relativistic expansion of UO_2^{2+} and UO_2 (Chapter 3).

1. Introduction

As the last part of our thorough investigation of the linear uranyl ion UO_2^{2+} in this Chapter the spectroscopy of compounds containing the uranyl unit will be discussed.

Besides the large number of investigations to the bonding characteristics in uranyl [1..12], also studies have been done on excitation spectra containing the UO_2^{2+} moiety [5,6,13..15], and X-ray PES studies [9..11,16]. The present work is an extension of these studies, and shows that the unique features of UO_2^{2+} are all related to the very strong U-O interaction, where the U 6p orbital plays an important role. This strong interaction has also been found in the study on the relativistic expansion of uranyl in Chapter 3 (see also [12]), and in the explanation for the short U-O bond length given in Chapter 4a. For all calculations the Amsterdam Density Functional (DF) program package [17..20] was used. A short description of this method is given in Section 2.

The electronic structure of UO_2^{2+} has been discussed extensively in Chapters 3 and 4a. For the present work, it is important that the HOMO is of π_u symmetry [1..14]. The reason for this is the large interaction between U 6p and the π_u combinations of O 2s and 2p. The antibonding U 6p-O 2p combination ends up high into the virtual spectrum, above U 5f. Interaction with U 5f then leads to an orbital which has predominantly 5f character and is the HOMO. The lowest virtual orbitals are the U 5f and 5f. The excitation spectrum originates from excitation out of the HOMO $3\pi_u$ to these virtual levels. The large interaction of U 6p and O 2s leads to a large gap between the $1\pi_u$ and $2\pi_u$ orbitals, which has important consequences for the ionization spectrum.

The optical excitation spectrum of $\text{Cs}_2\text{UO}_2\text{Cl}_4$ has been a subject of considerable debate for over more than a decade. Denning et al. [13,14] gave an assignment of the spectrum: $\pi_u \pi_u^* \pi_u \pi_u < \pi_u \pi_u^* \pi_u \pi_u$ for the excited configurations resulting from the occupation of one electron in the π_u HOMO and one electron in the U 5f or U 5f. DeKock et al [5] found $\pi_u \pi_u < \pi_u \pi_u < \pi_u \pi_u < \pi_u \pi_u$ in calculations on $\text{UO}_2\text{F}_4^{2-}$. This assignment was questioned by Denning et al. [14], especially the position (highest virtual) and B_{2g} , B_{3g} splitting of the non-bonding f orbital. Boerrigter [6] showed that the older calculation of DeKock was wrong due to errors in the numerical integration of the f orbitals: use of a more accurate integration method [19] led to agreement with experiments [6]. In Section 3 we will present the results of calculations on $\text{UO}_2\text{F}_4^{2-}$ as were also done by Boerrigter [6], but we will give a more elaborate assignment.

The X-ray spectrum of a number of hexavalent uranyl compounds has been recorded by Veal et al [16]. They showed that the high energy part of the spectrum of many substances containing the UO_2^{2+} moiety has four peaks and claimed that the highest two ionizations come from the U $6p_{1/2}$ and O 2s orbitals, while the lowest two come from the U $6p_{3/2}$ orbital, which is split by the electrostatic field of the Oxygens. This assignment

assumes that the peaks in the spectrum can be assigned to individual orbitals, especially, pure atomic U $6p_{3/2,3/2}$ and U $6p_{3/2,1/2}$ levels are assigned. A number of theoretical studies already showed that this view is not correct, e.g. Walch and Ellis [9], Wood et al. [10] and Yang et al. [11] all found, using different methods, that there is strong interaction between U $6p$ and O $2s$, and therefore one can not speak anymore of peaks as being due to particular Atomic Orbitals. The results of our ionization calculations of UO_2^{2+} are presented in Section 4. We introduce there a relativistic molecular population analysis based on fully relativistic fragments. Finally in Section 5 our conclusions are given.

2. Method

All calculations have been carried out using the Amsterdam DF program package [17..20], characterized by the use of a density fitting procedure to obtain an accurate Coulomb potential, by accurate numerical integration of the effective one-electron hamiltonian matrix elements and by the possibility to freeze core orbitals. The Slater X exchange potential [21] was used in the excitation calculations on $\text{UO}_2\text{F}_4^{2-}$ (Section 3), while for the ionization calculations the LSD exchange potential in the Vosko-Wilk-Nusair parametrization [22] was used, together with the Stoll correction [23]. All calculations were done Quasi-Relativistically [24], where the effects of the first order (FO) relativistic operators, consisting of the scalar mass-velocity ($-\frac{1}{2}v^2/c^2$), Darwin ($\frac{1}{4}\nabla^2(V_N)$) and indirect potential (due to relativistic first order density changes of the occupied orbitals) operators and the spin-orbit operator are added to the non-relativistic operators. To accomplish this, two methods can be used. In the first, used in the calculations on $\text{UO}_2\text{F}_4^{2-}$, all first order operators are added to the non-relativistic operator, and this is diagonalized in the basis of the Non-Relativistic (NR) orbitals until self-consistency. In the second method, used in the ionization calculations on uranyl described in Section 4, first the scalar relativistic operators are added to the non-relativistic operators in a Scalar Relativistic (SR) calculation, and afterwards the spin-orbit interaction is determined self-consistently in a calculation using the SR orbitals as basis. In the SR method the indirect potential effects (due to relativistic density changes) are taken into account implicitly. For an extensive discussion of the QR and SR methods see Chapter 1.

Compared to FO perturbation theory, in the QR method also higher order corrections due to the first order operators are taken into account. The QR method has proven to be better than FO perturbation theory (as in [20,25]), especially for elements heavier than third row transition metals [6,23].

For the calculation of excitations and ionizations the Slater Transition State method [26] was used.

The $(1s-5s)$, $(2p-5p)$, $(3d-5d)$, and $4f$ orbitals on U and the $1s$ orbital on O have been frozen. The valence basis was double- for the U $6s$, $6p$ and $7s$, triple- for $5f$ and $6d$

Table 1. Scalar-Relativistic population analysis for orbitals of UO_2^{2+} for U-O distance of 3.25 bohr.

Orbital	Orbital character	Eigen-value (eV)	Atomic composition (%)								
			U 5f	U 6s	U 6p	U 6d	U 7s	U 7p	O 2s	O 2p	
<i>unoccupied orbitals</i>											
4	u	2p-6p anti-b.	-10.67	32		8			10	2	45
3	u	5f-2p anti-b.	-15.84	66					2		31
1	u	5f	-18.62	100							
1	u	5f	-19.07	100							
<i>occupied orbitals</i>											
3	u	5f (-2p bond.)	-21.47	57		7				3	42
3	g	O 2p (-6d bond.)	-22.33		1		13	1		9	76
2	u	5f-2p -bond.	-22.69	35		1					64
1	g	O 2p (-6d bond.)	-23.08				19				80
2	u	6p-2s ab., -2p b.	-30.05	4		28			-3	61	7
2	g	2s (-6s anti-b.)	-36.78		2		4	-3		94	2
1	u	6p	-38.52			97					2
1	u	2s-6p bond.	-44.25			42			-3	46	13
1	g	6s (-2s bond.)	-64.57		88					4	6
<i>gross populations</i>				2.6	1.8	5.5	1.1	0.0	-0.1	2.2	4.3

The highest QR levels are 5f orbitals, resulting from the effect of spin-orbit splitting on the 5f_{5/2}, 5f_{7/2} orbitals in the NR or SR schemes.

Before explaining the SO effects in uranyl, a short explanation of the method of Boerrigter et al. [5,6] we use for taking the spin-orbit interaction into account, will be given. It does not matter if the starting point is the NR or SR, since the spin-orbit components of a set of MOs are not split by the scalar relativistic corrections. The spin-orbit operator is written as: $\mathbf{l} \cdot \mathbf{s}$, which can be expanded as $l_z s_z + 1/2 (l_+ s_- + l_- s_+)$. In this expression the first part describes the diagonal SO splitting, and the second part is the off-diagonal SO interaction, containing the shift up and down operators l_{\pm} and s_{\pm} , which couple different non-relativistic (or SR) symmetries. For f orbitals in linear symmetry, the situation is given in Fig. 2a. The non-relativistic symmetries f_0, f_2, f_4 ($l=0,1,2,3$) split due to the diagonal splitting into $E_{\pm 1/2}$, for $l=0$, one going up by $l/2$ and one down by $l/2$. This leads to the levels $1/2, 1/2, 3/2, 3/2, 5/2, 5/2$ and $7/2$. Subsequent off-diagonal interaction in relativistic symmetries between symmetries f_2 and f_4 , e.g. of $5/2$ and $5/2$ then leads to the atomic splitting at the right. In Table 2 the composition of the resulting atomic levels is given. An important aspect of this method of looking at the effects of spin-orbit splitting is that when e.g. due to ligand effects the f level is shifted with respect to the f level, the resulting level pattern can be

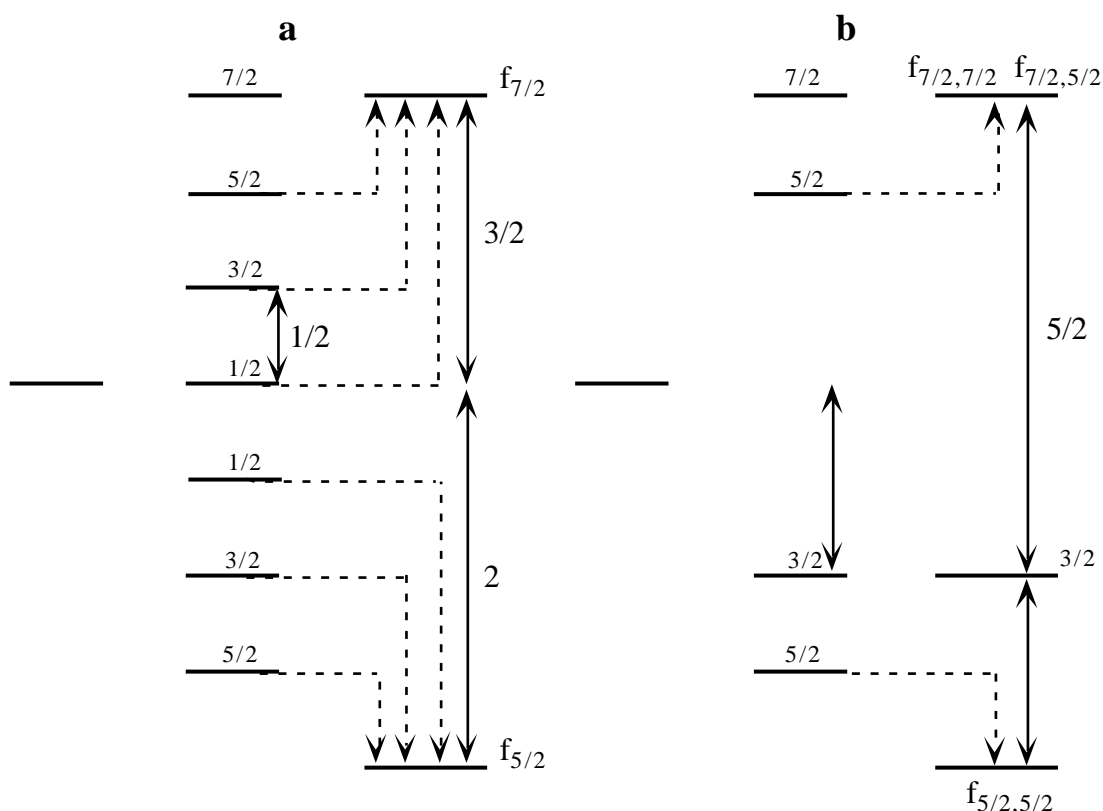


Figure 2. Spin-orbit splitting for f orbitals in linear symmetry. a): all components degenerate. b): degenerate f_{δ} , f_{ϕ} orbitals.

deduced immediately. Applications of this method will be given later in this work.

We now discuss the spin-orbit splitting in uranyl, for which the SR calculation is taken as starting point. The f and f levels are split off by the interaction with O. The atomic U 5f spin-orbit splitting is 0.68 eV ($7/2$) [12], much smaller than the energy-difference (ligand field splitting) of 2.39 eV between the non-bonding f and the HOMO $3_u(f)$.

Table 2. Spin-orbit mixing of atomic p and f orbitals.

	$ m_j $	p	p		$ m_j $	f	f	f	f
$p_{3/2}$	3/2	0	100	$f_{7/2}$	7/2				100
	1/2	66.7	33.3		5/2			85.8	14.2
					3/2		71.4	28.6	
$p_{1/2}$	1/2	33.3	66.7		1/2	57.1	42.9		
				$f_{5/2}$	5/2			14.2	85.8
					3/2		28.6	71.4	
			1/2		42.9	57.1			

The f_{δ} is even lower, while the antibonding orbitals containing f_{δ} , f_{ϕ} ($3_{\delta u}$ and $4_{\phi u}$) are far away high in the virtual spectrum (about 3 eV). If the f_{δ} and f_{ϕ} orbitals were degenerate, we would have the quenched spin-orbit splitting in a f_{δ} , f_{ϕ} manifold as given in Fig. 2b: diagonal spin-orbit interaction then leads to the four levels $f_{5/2}$, $f_{3/2}$, $f_{5/2}$ and $f_{7/2}$, and subsequent off-diagonal spin-orbit interaction between the $f_{5/2}$ and $f_{5/2}$ leads to the pattern at the right, while $f_{3/2}$ and $f_{7/2}$ do not have a partner to interact with and stay at their diagonal levels. Very important is the composition of the $f_{5/2,5/2}$ and $f_{7/2,5/2}$. From Table 2 it is seen that the $f_{5/2,5/2}$ is a mixture of $f_{5/2}$ (14.2%) and $f_{5/2}$ (85.8%), while for the $f_{7/2,5/2}$ this is reversed. Excitation from the HOMO $4_{\phi u}$ then would result in three peaks, each from occupation of one of the levels of Fig. 2b. Yet this picture is already too simple for the bare uranyl ion. From Table 1 we see that the f_{δ} orbital is ~ 0.4 eV (approx. 2λ) higher than the f_{ϕ} orbital, due to the non-spherical molecular potential. Inclusion of diagonal spin-orbit splitting then leads to Fig. 3, where the $f_{5/2}$ and $f_{5/2}$ are separated by $9/2\lambda$, much more than the $5/2\lambda$ in the atom, and $f_{7/2}$ and $f_{3/2}$ are found close together. Diagonalization of the $5/2$ symmetry leads to an off-diagonal energy effect of 0.3λ , less than in the atom ($1/2\lambda$). The lowest orbital is calculated to be 94% $f_{5/2}$ and 6% $f_{5/2}$ while for the highest one this is reversed. Fig. 1 shows that this is exactly what the relativistic calculation gives: $1e_{7/2u}$ ($f_{7/2}$) and $3e_{3/2u}$ ($f_{3/2}$) close together with a gap of 0.1 eV ($1/2\lambda$), in the order predicted, the $1e_{5/2u}$ 0.6 eV (3.1λ) below $f_{3/2}$, being 94% $f_{5/2}$ and 6% $f_{5/2}$, while for $2e_{5/2u}$ (0.40 eV (2.1λ)) above $1e_{7/2u}$ this is reversed. Thus in uranyl due to the non-degeneracy of the f_{δ} , f_{ϕ} orbitals a somewhat different picture emerges than in the atom, where the lowest $f_{5/2,5/2}$ was 85.8% $f_{5/2}$ and 14.2% $f_{5/2}$. This can be understood using the spin-orbit method described above.

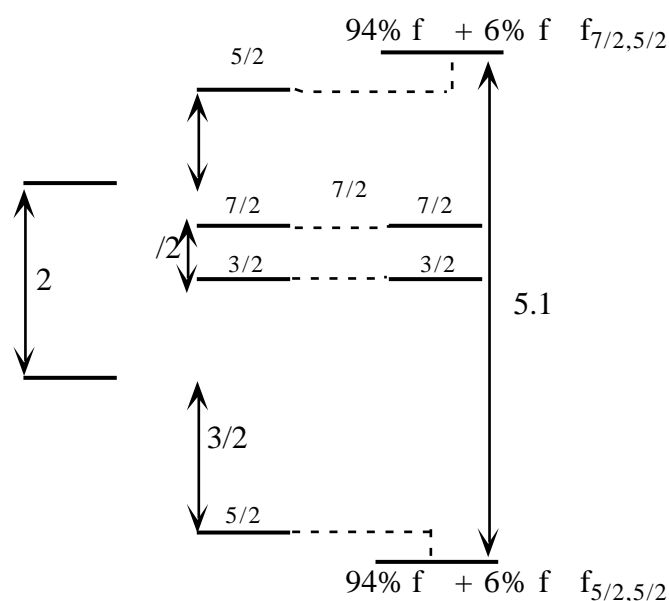


Figure 3. Spin-orbit splitting for f_{δ} , f_{ϕ} orbitals in uranyl.

When four fluorines are put around uranyl in D_{4h} symmetry, the f and f orbitals have different interactions with them. The f orbitals transform as e_{1u} , while the f orbitals split into b_{1u} and b_{2u} . The ligand p orbitals transform as e_{1u} and b_{1u} , but there is no b_{2u} combination, so the f (b_{2u}) is non-bonding, while the f (b_{1u}) and the f (e_{1u}) are destabilized by interaction with the ligands. The non-bonding f is therefore expected to be lowest.

The first assignment of the spectrum was given by Denning et al. [13], and is reproduced in Table 3, together with the correspondence between electronic configurations and multiplet states in the (double) groups D_h and D_{4h} . The u_u and u_u configurations that arise from the excitation of 1 electron from the u HOMO to u and u , split up under the influence of the ligand field and the spin-orbit splitting of the U 5f orbitals. Basically Denning et al. propose a splitting of f and f orbitals where first the ligand field acts upon the f -levels, and afterwards the small spin-orbit splitting takes place. They then assign the first four excitations (g , g , g and g in D_H) to u_u parentage and the others to u_u parentage. An important point of their assignment, which was stressed again later [14], is that the non-bonding f is lowest and that the field splittings of the 3g and 1g of the u_u configuration into B_{1g} and B_{2g} have opposite signs. For the lowest g (3g), the B_{2g} is lowest, but for 1g the reversed order is found.

We did Quasi-Relativistic calculations on $UO_2F_4^{2-}$, the highest orbitals of which are given at the right of Fig. 1. Next to the non-relativistic orbitals their composition is given. We find the 3_u (much 5f) uranyl HOMO mostly in the $3a_{2u}$ (71%) and to a lesser extent in the $4a_{2u}$ (27%), leading to too much fluorine and too little U 5f character in the HOMO $4a_{2u}$. This already was the case in earlier studies [5,6]. It is not consistent with the experimental finding by Denning et al. [14] that the U-Cl vibrational frequency of the ground state and excited states are nearly equal. We tried to mimic the surrounding cation field by placing point charges around $UO_2F_4^{2-}$, but this did not lead to a significant reduction of the F content in the HOMO. Therefore this discrepancy with experiment was not investigated further. The virtual level ordering of the f , f orbitals has been subject to much debate. The f orbitals split into b_{1u} and b_{2u} , with $1b_{2u}$ (at 3.81 eV) being non-bonding, while the $2b_{1u}$ (at 4.02 eV) is antibonding with F 2p. Orbital $6e_{1u}$ (at 4.54 eV) is antibonding f with F 2p. Concerning the position of the non-bonding f orbital, in the present calculation we find the non-bonding f ($1b_{2u}$) lowest, in agreement with Denning. In the older calculations it ended up as highest virtual orbital, which could not be true as Denning et al. [14] remarked. The improvement compared to the older calculation is the result of a more accurate integration scheme [19], as was mentioned in the introduction.

In order to understand the nature of the lowest virtual orbitals it is important to realise that there are important differences compared to the simple picture of degenerate f , f orbitals sketched in Fig. 2b.

Table 3. Spectral assignment for $Cs_2UO_2Cl_4$.

origin	D _h *	D _{4h} *	D _{2h} *	Wavenumber/cm ⁻¹	original [1,2]	present
I	g	E _g	B _{2g}	20095.7	u u	u 3/2u
II			B _{3g}	20097.3		
III	g	B _{2g}	B _{1g}	20406.5		
IV		B _{1g}	A _g	21310		
V	g	E _g	B _{2g}	22021	u u	u u ('f _{5/2,5/2} ')
VI			B _{3g}	22076		
VII	g	B _{1g}	A _g	22410		
VIII		B _{2g}	B _{1g}	22750		
IX	g	E _g	B _{2g}	26197.3	u u	u u ('f _{7/2,5/2} ')
X			B _{3g}	26247.3		
XI	g	A _{2g}	B _{1g}	27719.6		u u ('f _{7/2,7/2} ')
XII		A _{1g}	A _g	27758		
XIII	g	B _{1g}	A _g	29277	u u	u u ('f _{7/2,5/2} ')
XIV		B _{2g}	B _{1g}	29546		

configuration	D _h *	reduction	reduction	D _{4h} *	configuration
u1/2 3/2		g	E _g		e _{1/2u} e _{3/2u}
		g	B _{1g}		
			B _{2g}		
u1/2f _{5/2,5/2}		g	B _{1g}		e _{1/2u} e _{3/2u}
			B _{2g}		
		g	E _g		
u1/2f _{7/2,5/2}		g	B _{1g}		e _{1/2u} e _{3/2u}
			B _{2g}		
		g	E _g		
u1/2f _{7/2,7/2}		g	A _{1g}		e _{1/2u} e _{1/2u}
			A _{2g}		
		g	E _g		

In Fig. 4 a scheme describing the effect of spin-orbit splitting on the f , f levels in $UO_2F_4^{2-}$ is given. We first note that the Ligand Field splitting of f (ca 0.21 eV, energy difference between $2b_{1u}$ and $1b_{2u}$ in Fig. 1) is much smaller than the 0.68 eV spin-orbit splitting of U 5f [12]. So it seems correct to look only at the spin-orbit splitting and neglect the ligand field splitting of the f orbital. The f is ca. 0.50 eV (2.6 μ) higher than f . Diagonal spin-orbit splitting brings the $f_{5/2}$ down by $3/2$, while $f_{5/2}$ comes up by $3/2$, thereby bringing these states of the same symmetry close together. The $f_{5/2}$ seems to

be lowest, but the energy difference with $f_{5/2}$ is very small, and the ligand splitting of the f , which we first neglected, is of the same order. So the only thing we can predict is a much larger off-diagonal interaction and mixing between the $f_{5/2}$ and $f_{5/2}$ than in the atom, where the energy-difference is $5/2$ after diagonal spin-orbit splitting. The result of the relativistic calculation is given in Table 4. A population analysis based on relativistic atomic orbitals is given for the lowest four virtual orbitals $7e_{3/2u}$ up to $10e_{1/2u}$. Also the composition in terms of non-relativistic orbitals is included. The $7e_{3/2u}$ orbital is the non-bonding f orbital, in accordance with Denning et al. [13, 14], and has a ratio of $U 5f_{5/2}$ to $U 5f_{7/2}$ character consistent with a dominating $f_{3/2}$ composition (see Table 2). The orbital $10e_{1/2u}$ is seen to be the $f_{7/2,7/2}$. The $8e_{3/2u}$ and $9e_{3/2u}$ are identified as mostly $f_{5/2,5/2}$ and $f_{7/2,5/2}$, but neither of them is pure, and therefore we denote them ' $f_{5/2,5/2}$ ' and ' $f_{7/2,5/2}$ '. The non-relativistic composition of $8e_{3/2u}$ shows a dominating $f_{5/2}$ contribution, while this is reversed for $9e_{3/2u}$, with a dominant $f_{5/2}$ composition.

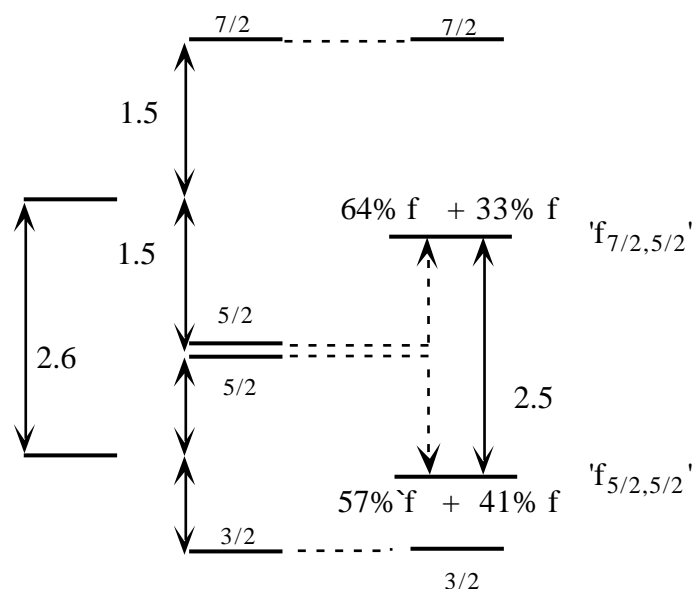


Figure 4. Spin-orbit splitting for f_{δ} , f_{ϕ} orbitals in $UO_2F_4^{2-}$.

Table 4. Population analysis of the f_{δ} , f_{ϕ} manifold in $UO_2F_4^{2-}$.

Orbital	Energy (eV)	% Non-rel comp.			% Atomic composition			Notation
		$1b_{2u}$	$2b_{1u}$	$6e_{1u}$	$f_{5/2}$	$f_{7/2}$	F 2p	
$10e_{1/2u}$	6.16			95	1.4	91.8	4.7	$f_{7/2}$
$9e_{3/2u}$	5.91	25	39	33	5.7	89.7	4.2	' $f_{7/2,5/2}$ '
$8e_{3/2u}$	5.38		41	57	84.3	7.6	7.9	' $f_{5/2,5/2}$ '
$7e_{3/2u}$	5.18	73	17	8	78.6	18.8	1.7	$f_{3/2}$

Table 5. Excitation calculations for $UO_2F_4^{2-}$.

Non-relativistic		Relativistic		Excit. energy/cm ⁻¹
4a _{2u}	1b _{2u}	9e _{1/2u}	7e _{3/2u}	23880
4a _{2u}	2b _{1u}	9e _{1/2u}	8e _{3/2u}	25900
4a _{2u}	6e _{1u}	9e _{1/2u}	9e _{3/2u}	30040
		9e _{1/2u}	10e _{1/2u}	33477

Thus the level ordering of Fig. 4 with respect to the middle two levels is not correct, the $f_{5/2}$ orbital is lowest. This is also shown by the atomic composition of $f_{5/2,5/2}$ and $f_{7/2,5/2}$ in Table 2, although that refers to the atomic case. As expected the spin-orbit mixings of the non-relativistic orbitals are very large, consistent with large off-diagonal spin-orbit interactions as noted above. For example, an atomic $f_{7/2,5/2}$ consists of 85.8% $f_{7/2}$ and 14.2% $f_{5/2}$, but in $9e_{3/2u}$ (which we denote by ' $f_{7/2,5/2}$ ') we find a ratio of 64% $f_{7/2}$ ($2b_{1u}+1b_{2u}$) vs. 33% $f_{5/2}$ ($6e_{1u}$). Also the $8e_{3/2u}$ (' $f_{5/2,5/2}$ ') orbital is more heavily mixed than in the atom, 57% $f_{5/2}$ and 41% $f_{7/2}$. This large mixing was expected above and is important for the assignment of the excitation spectrum, to which we turn now.

The transition state energies we calculated for the excitation of 1 electron from the HOMO $9e_{1/2u}$, the NR $4a_{2u}$, to the four virtual levels are given in Table 5. Our assignment for the spectrum is: $u u < u u$, $u u < u u$, where the $u u$, $u u$ order in the middle is approximate, as we have shown that the $f_{7/2}$ and $f_{5/2}$ orbitals are heavily mixed. The assignment is included in Table 3, and will be clarified below.

The first two states g and g in D_{4h} (origins I-IV) come from the non-bonding $f_{7/2}$ orbital, in accordance with Denning et al. [13,14]. We now also have the correct B_{1g} , B_{2g} splitting in the g state in D_{4h} symmetry. The next two states, g below g (origins V-VIII) result in Denning's view from $f_{5/2}$ parentage, as $f_{5/2}$ parentage should give rise to the g state below g [13]. Denning explains the splitting of the g state into B_{2g} and B_{3g} in D_{2h} symmetry by CI with the $f_{5/2}$ state above. We find in the calculation the $8e_{3/2u}$ as the second virtual orbital, leading to the g and g states. The $8e_{3/2u}$ (' $f_{5/2,5/2}$ ') is a strong mixture of 57% $f_{5/2}$ and 41% $f_{7/2}$, which is much larger than in the atomic $f_{5/2,5/2}$, as was explained before. On the basis of our results we then assign $u u$ parentage to the states g and g (origins V-VIII). The absence of the g state below g can be explained by CI with the g states below and above this g state, or by CI of the g states (origins V,VI and IX,X). The $f_{5/2}$ contribution in $8e_{3/2u}$ explains the B_{1g} below B_{2g} splitting of the g state in D_{4h} , reversed compared to the non-bonding $f_{7/2}$ [13]. In our view the next state g (Origins IX and X) comes from the $9e_{3/2u}$, which is a mixture of dominating 64% $f_{7/2}$ and 33% $f_{5/2}$. The other state belonging to $9e_{3/2u}$ is the g state of origins XIII,XIV, and the g state in between those

two belongs to $7/2$ parentage to be discussed later. Denning assigns the g and g states to g parentage, with a smaller contribution from g . We have the reversed situation, more $5/2$ character (66%) than $5/2$ in $9e_{3/2u}$. The $5/2$ character in it causes the B_{1g}, B_{2g} splitting (origins XIII, XIV) in D_{4h} as in the g state of origins VII, VIII, while the $5/2$ character causes the B_{2g}, B_{3g} splitting in D_{4h} (origins IX, X) as in the g state of origins V, I. Probably the g state is so high from CI with the other g states, as was mentioned before. We must stress that because the interaction between $5/2$ and $5/2$ is so very strong, assignment of the second and third parentages as $u u$ and $u u$ respectively, resulting from excitation out of $8e_{3/2u}$ and $9e_{3/2u}$, is not strict in the sense that the orbitals from which the excitation takes place are strong mixtures of $5/2$ and $5/2$. The fact that the lower orbital contains more $5/2$ character leads to our assignment, which can explain all features of the spectrum. Our assignment and that of Denning are therefore very similar, once the heavy mixing between $5/2$ and $5/2$ has been recognized.

Summarizing, we propose an assignment that is in good agreement with experiment and almost agrees with Denning et al. [13,14]. The only remaining differences are the second and third configurations. We find a mainly $5/2$ configuration below the $5/2$ configuration, but our calculations showed that these are heavily mixed by the spin-orbit splitting. The resulting levels then get much of each others lower symmetry splittings. Due to the strong mixings it is difficult to assess the character of these states, neither of them is pure.

Our transition state excitation energies are in reasonable agreement with experiment. When we take averages of the experimental energies, the values for the four excitation centers are approximately 20500, 22300, 27800 and 28900 cm^{-1} . The last value is calculated assuming the eighth excitation (not measured) to be at 30000 cm^{-1} , so perhaps the center at 28900 cm^{-1} is too low. The third value is from the origins IX, X, XIII and XIV (Table 3). Our values are about 3000 cm^{-1} higher than the experimental values, but the relative orderings are much better.

4. X-ray Spectroscopy of uranyl compounds

In this part we give the results of QR calculations of ionizations from the relativistic orbitals $1e_{1/2u}, 2e_{1/2u}, 3e_{1/2u}, 1e_{3/2u}$ in UO_2^{2+} using the LSD VWN-Stoll parametrization [21,22]. The considered orbitals correspond to the $1_u, 2_u$ and 1_u SR orbitals without spin-orbit splitting (see Table 1). Table 6 contains the results of our calculations as well of previous studies, and also the experimental values of Veal et al. [16] for UO_2CO_3 are given.

We find reasonable agreement with previous studies [9..11]. Especially the agreement with Yang et al. [11] was not expected, because their calculation did not include the indirect relativistic effects (usually destabilizing), especially important for f orbitals [12]. The agreement with experiment concerning the relative values of our ionization energies is excellent. The shift in absolute values of our ionizations is of course due to the CO_3^{2-} Ligand Field.

We will now discuss how the interaction between U 6p and O 2s can best be viewed. To this end a population analysis of the relativistic MOs in terms of the relativistic fragment orbitals is given in Table 7. Also included is the analysis in terms of SR orbitals (i.e. without spin-orbit splitting).

In principle there are two ways of looking at the U 6p-O 2s interaction. Firstly, one can assume that the ligand field dominates over the spin-orbit splitting. In the case of U 5f orbitals in uranyl, the interaction with O effectively removes the $5f_{\text{u}}$ and $5f_{\text{g}}$ from the 5f manifold, resulting in a quenched spin-orbit splitting in the the f_{u} , f_{g} manifold.

The question now is, whether a similar effect exists in the U 6p-O 2s interaction. Is the interaction with O 2s strong enough to decouple the $6p_{\text{u}}$ and $6p_{\text{g}}$ orbitals? Looking at the levels in Table 1 we see that there is a large gap of about 14 eV between 1_{u} , the bonding O 2s-U 6p combination, and 2_{u} , the corresponding antibonding combination.

Table 6. Calculated and experimental ionizations for UO_2^{2+} .

Ionization	Walch [9]	Wood [10]	Yang [11]	Present	Exp. ^a	Exp. ^b
$3e_{1/2u}$	31.56	31.18	33.97	34.18	14	34.92
$1e_{3/2u}$	38.64	34.36	38.13	40.95	19	39.92
$2e_{1/2u}$	43.81	40.26	43.48	44.87	24	44.92
$1e_{1/2u}$	50.89	47.47	50.73	50.92	30	50.92

^a: Experimental, UO_2CO_3 [16]. ^b: shifted highest experimental value from [16] to agree with ionization from orbital $1e_{1/2u}$.

Table 7. Relativistic Population analysis for relevant orbitals of UO_2^{2+} for U-O distance of 3.25 a.u.

QR orbital	Eigen-value (eV)	SR eigen-value (eV)	SR comp. (%)		U Composition (%)					O
			1_{u}	2_{u}	1_{u}	$6p_{1/2}$	$6p_{3/2}$	$2s_{1/2}$	$2p_{1/2}$	
$3e_{1/2u}$	-29.78	-30.05		95	4	3	29	57	5	4
$1e_{3/2u}$	-36.28	-38.52			100		96			3
$2e_{1/2u}$	-40.28	-38.52	29	3	68	25	49	19	4	
$1e_{1/2u}$	-46.07	-44.25	71		28	58	1	31	2	10

In between, 6 eV above 1_{1u} , we find the pure U 6p orbital 1_{1u} . It is tempting to assume that these energy differences are large enough to view this situation as a case of quenched spin-orbit interaction. But the spin-orbit splitting of U 6p is about 7.7 eV (~ 5 eV) [12] (pure X value, but VWN-Stoll value is almost identical, although different from DS value of about 9 eV in Chapter 1), and the orbital energy differences are of this order too. Also note that the $1_{1/2u}$ moves down towards the 1_{1u} due to the diagonal spin-orbit interaction, thereby closing the gap with $1_{1/2u}$ and widening that with $2_{1/2u}$ of the same relativistic symmetry. These three orbitals are coupled by the off-diagonal spin-orbit interaction. The coupling is reduced somewhat because the 1_{1u} orbitals are not pure 6p orbitals. When the interaction between $1_{1/2u}$ and $1_{1/2u}$ were small, the result would be a lowest orbital $1e_{1/2u}$, the 6p character being pure p, with a $6p_{1/2}$ to $6p_{3/2}$ character ratio of 1:2 (Table 2). In Table 7 we see that this is not at all the case, the $1e_{1/2u}$ is pure $6p_{1/2}$ with respect to the U 6p character. And the $2e_{1/2u}$ from $1_{1/2u}$ has a ratio of $6p_{1/2}$ to $6p_{3/2}$ character of 1:2, while from the quenched spin-orbit interaction this should be reversed. Therefore the result of Table 7 shows that there is large interaction between the $1_{1/2u}$ and $1_{1/2u}$ levels. Orbital $2_{1/2u}$ does not mix heavily, only a small amount of 4% 1_{1u} gets mixed in. Nevertheless the final ratio of $6p_{1/2}$ to $6p_{3/2}$ character in this 2_{1u} derived orbital $3e_{1/2u}$ is 9:1, whereas from a pure p orbital this would have been 1:2. So, the small 1_{1u} mixing has large consequences here.

Using the spin-orbit operator as given in Section 3, we can understand the composition of the relativistic orbitals in terms of the scalar-relativistic ones without spin-orbit splitting. We approximate the interaction by neglecting the 2_{1u} orbital, which is separated considerably from the 1_{1u} and 1_{1u} after diagonal spin-orbit splitting. Diagonal spin-orbit splitting lowers 1_{1u} by $\lambda/2$, reducing the gap with 1_{1u} to 3.5 eV. When we diagonalize the off-diagonal spin-orbit splitting in the two level system of 1_{1u} and 1_{1u} , with the same off-diagonal element of $1/2 \lambda$ as in the U atom, the resulting levels are split by 7.9 eV (1.58 λ), and the lowest level is 72% 1_{1u} and 28% 1_{1u} , while the highest level is 78% 1_{1u} and 28% 1_{1u} . Comparing these results with Table 7, the agreement is very good: $1e_{1/2u}$ and $2e_{1/2u}$ are as calculated by the spin-orbit model, and 2_{1u} hardly mixes, which justifies our assumption of neglecting it in the interaction. Note also that the composition of $1e_{1/2u}$ and $2e_{1/2u}$ is almost reversed from that in Table 2, and the quenched off-diagonal spin-orbit picture. Therefore both from the the $p_{1/2,3/2}$ composition as well as from the spin-orbit picture given above, the conclusion must be that we can not view the U 6p-O 2s interaction as an example of quenched spin-orbit interaction.

Therefore we are led to the second way to look at the interaction between U 6p and O 2s. The spin-orbit interaction dominates, splitting the U 6p orbital in $6p_{1/2}$ and $6p_{3/2}$ levels, and subsequent interaction with O $2s_{1/2}$ finds place in a three level system in the $e_{1/2u}$ symmetry, while the $6p_{3/2,3/2}$ stays approximately at the atomic level.

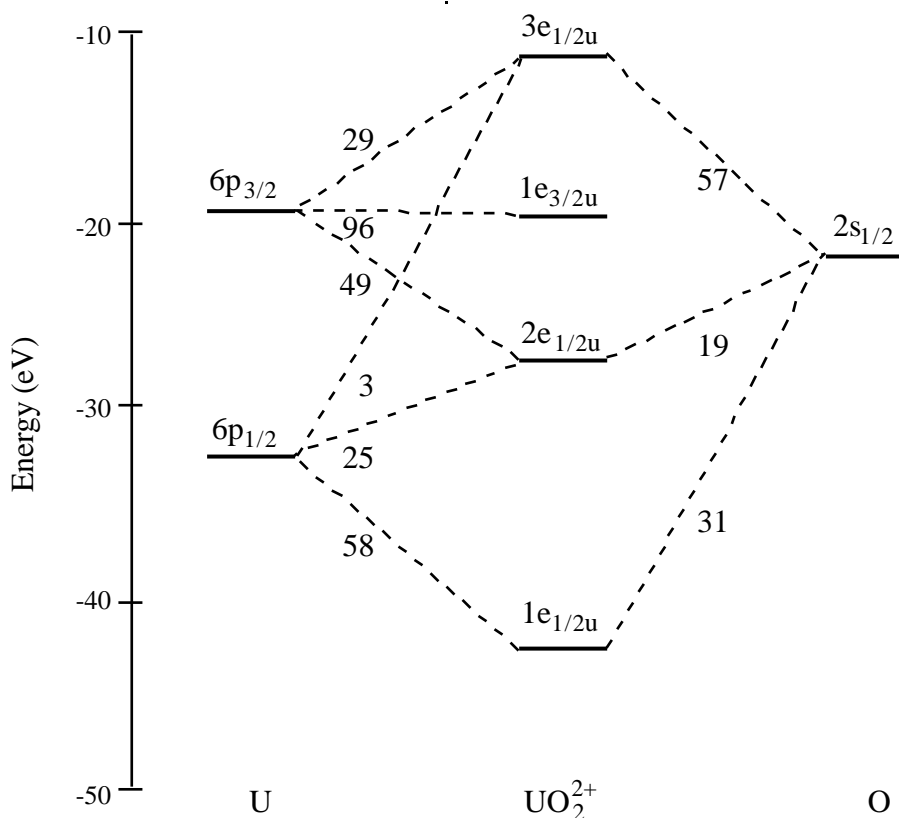


Figure 5. Interaction between U 6p and O 2s in uranyl.

The situation is pictured in Fig. 5. The lowest orbital $1e_{1/2u}$ is the bonding combination of U $6p_{1/2,1/2}$ and O $2s_{1/2}$, while the highest orbital is mostly U $6p_{3/2,1/2}$ and O $2s_{1/2}$. The middle level contains both U $6p_{3/2,1/2}$ and U $6p_{1/2,1/2}$ and not so much O 2s. The strong mixings that are found (Table 7) again show that there is a large interaction between U 6p and O 2s. In our calculation we have the U $6p_{3/2,1/2}$ character both above and below the U $6p_{3/2,3/2}$ in $2e_{1/2u}$ and $3e_{1/2u}$, both levels also containing substantial O character. It is thus not possible to assign the splitting of U $6p_{3/2}$ to the difference between $1e_{3/2u}$ and $3e_{1/2u}$ as Veal et al. [16] did, and also their assignment of individual atomic levels for the peaks is untenable.

Our results are in agreement with previous studies [9..11]. Walch and Ellis [9], using a relativistic Dirac Slater approach, find considerable (50%) admixture of O 2s in $3e_{1/2u}$ and 75% U 6p in $1e_{1/2u}$, which is close to our values. Thus a large interaction between U and O 2s takes place which makes a simple crystal field splitting of U $6p_{3/2}$ incorrect. Wood et al. [10] agree with these results: The U $6p_{3/2,1/2}$ and $6p_{3/2,3/2}$ are strongly mixed and what Veal et al. [16] assign as the U $6p_{3/2,1/2}$ goes at infinite separation to O

2s. Note that our $3e_{1/2u}$ also has a dominating O 2s composition. Yang et al. [11] conclude that 'because $2e_{1/2u}$ and $3e_{1/2u}$ both contain significant amounts of O 2s, the separation between $3e_{1/2u}$ and $1e_{3/2u}$ cannot strictly be classified as a U $6p_{3/2}$ ligand field splitting'. Their conclusion was drawn from calculations without inclusion of indirect relativistic effects. For the ionizations this is not much in error, because for O 2s and U 6p indirect relativistic effects are not large, but they completely miss the $3g$, $3u$ gap and the HOMO-LUMO gap, because the U 5f orbitals has a large indirect effect [12].

5. Conclusion

Concerning the excitation spectrum of $Cs_2UO_2Cl_4$, the assignment $u_u < u_u$, $u_u < u_u$ was proposed from calculations on $UO_2F_4^{2-}$ and it was shown to be in good agreement with experiment. Our assignment is based on an interplay of spin-orbit splitting and the ligand splitting for the f, f manifold and a large off-diagonal spin-orbit interaction between the $5/2$ and $5/2$ levels. Also CI effects are believed to play an important role.

Our ionization calculations on UO_2^{2+} were in good agreement with the experimental results and showed that it is not possible to assign the peaks in the X-ray spectrum to particular Atomic Orbitals and the electrostatic splitting of U $6p_{3/2}$ as Veal et al. [16] claimed, was not identified as such. It was shown that all these effects are related to the large interaction between U 6p and O 2s. A model was introduced where spin-orbit splitting is more important than Ligand Field splitting and acts first on the atomic U 6p.

The aspect that unites the above mentioned results is the importance of the sub-valence U 6p orbital. This orbital is very extended (larger than the valence U 5f) and the consequently large interaction with O leads to U 6p character in virtual orbitals: the 6p hole. This together with large mass-velocity elements from its core character explains the relativistic expansion of uranyl, as was demonstrated in Chapter 3 and in Ref. [12]. This expansion however is only present because the U-O distance is so short. Thus we arrive at the result of study described in Chapter 4a, i.e. our investigation i.e. our investigation of why the U-O distance is so short. The reason for it is the strong U 5f-O 2p interaction, which overcomes the large U 6p -O 2s u repulsion. The strong interaction of U 6p and O also has the consequence of the HOMO being of u symmetry and having much 5f character. This determines the excitation spectrum, which is therefore indirectly influenced by U 6p. Finally, also the U 6p and O 2s interaction is very large, and this leads to the impossibility of assigning individual Atomic Orbitals to the X-ray spectrum of uranyl compounds.

Therefore from the results of this and previous Chapters we conclude that the special character of the uranyl ion is caused by the U 6p orbital.

References.

- 1: Jørgensen and Reisfeld, *Chem. Phys. Lett.* **35** (1975) 441
- 2: C.K. Jørgensen and R. Reisfeld, *Structure and Bonding* **50** (1982) 121
- 3: C.K. Jørgensen, *Chem. Phys. Lett.* **89** (1982) 455
- 4: K. Tatsumi and R. Hoffmann, *Inorg. Chem.* **19** (1980) 2656
- 5: R.L. DeKock, E.J. Baerends, P.M. Boerrigter and J.G. Snijders, *Chem. Phys. Lett.* **105** (1984) 308
- 6: P.M. Boerrigter, Thesis, Vrije Universiteit Amsterdam, 1987
- 7: P. Pyykkö and L. Lohr, *Inorg. Chem.* **20** (1981) 1950
- 8: a) S. Larsson and P. Pyykkö, *Chem. Phys.* **101** (1986) 355
b) P. Pyykkö, L.J. Laaksonen and K. Tatsumi, *Inorg. Chem.* **28** (1989) 1801
- 9: P.F. Walch and D.E. Ellis, *J. Chem. Phys.* **65** (1976) 2387
- 10: J.H. Wood, M. Boring and S.B. Woodruff, *J. Chem. Phys.* **74** (1981) 5225
- 11: C.Y. Yang, K.H. Johnson and J.A. Horsley, *J. Chem. Phys.* **68** (1978) 1001
- 12: E.M. van Wezenbeek, E.J. Baerends and J.G. Snijders, *Theor. Chim. Acta* **81** (1991) 139
- 13: a) R.G. Denning, T.R. Snellgrove and D.R. Woodward, *Mol. Phys* **32** (1976) 419
b) R.G. Denning, T.R. Snellgrove and D.R. Woodward, *Mol. Phys* **37** (1979) 1089
- 14: T.J. Barker, R.G. Denning and J.R.G. Thorne, *Inorg. Chem.* **26** (1987) 1721
- 15: R.G. Denning and I.D. Morrison, *Chem. Phys. Lett.* **180** (1991) 101
- 16: a) B.W. Veal and D.J. Lam, *Phys. Rev. B* **10** (1974) 4902
b) B.W. Veal, D.J. Lam, W.T. Carnall and H.R. Hoekstra, *Phys. Rev. B* **12** (1975) 5651
- 17: a) E.J. Baerends, D.E. Ellis and P. Ros, *Chem. Phys.* **2** (1973) 42
b) E.J. Baerends and P. Ros, *Chem. Phys.* **2** (1973) 51
- 18: E.J. Baerends and P. Ros, *Int. J. Quant. Chem.* **S12** (1978) 169
- 19: P.M. Boerrigter, G. te Velde and E.J. Baerends, *Int. J. Quant. Chem.* **33** (1988) 87
- 20: a) J.G. Snijders and E.J. Baerends, *Mol. Phys.* **36** (1978) 1789
b) J.G. Snijders, E.J. Baerends and P. Ros, *Mol. Phys.* **38** (1979) 1909
- 21: J.C. Slater, *Phys. Rev.* **81** (1951) 385
- 22: S.H. Vosko, L. Wilk and M. Nusair, *Can. J. Phys* **58** (1980) 1200
- 23: H. Stoll, E. Golka and H. Preus, *Theor. Chim. Acta* **55** (1980) 29
- 24: T. Ziegler, V. Tschinke, E.J. Baerends, J.G. Snijders and W. Ravenek, *J. Phys. Chem* **93** (1989) 3050
- 25: T. Ziegler, J.G. Snijders and E.J. Baerends. *Chem. Phys.* **74** (1981) 1271
- 26: J.C. Slater, in 'Computational Methods in Band Theory', eds. P.M. Markus, Janak and Williams, Plenum Press. New York (1971)

Chapter 6

Organoactinide Chemistry: The ground electronic structure of UCp_3 and interaction with the ligands CO, NO and H

Abstract

The ground state of UCp_3 and its bonding to the ligands H, NO and CO were investigated. Scalar-Relativistic calculations on planar UCp_3 in a large number of possible electronic configurations showed that the ground state can best be described as $5f^3$. The bond between the fragments U^{3+} and Cp_3^{3-} , from which UCp_3 can be thought to be made of, has a ratio of ionic/covalent character of 2:1. For interaction with the ligands (L) H, NO and CO, pyramidal UCp_3 was prepared in the best suited start configuration. The bond energies of UCp_3 and the ligands were -3.26 , -3.83 and -1.93 eV for H, NO and CO respectively, with respect to the planar ground state. The interaction for NO and CO was split in donation from L to U in A_1 symmetry and back-donation to L in E symmetry. The main acceptor orbital is the U 6d with smaller contributions from U 5f and U 7s. The donation is stronger for CO than for NO, for which the higher energy and higher amplitude at C of the CO 5 are responsible. The back-donation in UCp_3CO is much stronger than in UCp_3NO , and is dominated by U 5f. The total bond energy is larger for NO due to the complete filling of the UCp_3 -2 bonding combination. In UCp_3H the bond between UCp_3 and H can be described by an electron pair bond, the dominating U contribution to which comes from U 6d.

Both U 6d and U 5f orbitals participate considerably in the bonding in the UCp_3 -L compounds, where in all cases U 6d is the most important acceptor orbital, and the back-donation is mainly provided by U 5f. An explanation for this behaviour is given. In the considered UCp_3L compounds a U 6p hole is found, again showing the large spatial extension of this orbital.

1. Introduction

In the last decades, organometallic chemistry of f block elements has become increasingly important. The first of this kind of compounds synthesized were the organolanthanides LnCp_3 ($\text{Cp} = \text{}^5\text{-C}_5\text{H}_5$: cyclopentadiene) by Birmingham and Wilkinson [1] and organoactinide complex UCp_3Cl by Reynolds and Wilkinson [2] in 1956, shortly after the discovery of ferrocene in 1952.

Since then, a large number of other organolanthanide and organoactinide compounds have been synthesized and studied, many containing the Cp or substituted Cp ligand. Recent reviews [3] give a good impression of the diversity of compounds in this part of organometallic chemistry. Although many heavy element organometallic compounds have been subject to investigation, the understanding of them is still not as complete as for organotransition metal (TM) chemistry. The reasons for this are diverse. At the experimental side, especially organoactinides are difficult to handle due to their radioactivity. And also from a computational point of view they are very demanding, because they have the f orbitals available for chemical bonding and the fact that they are heavy necessitates the inclusion of relativistic effects [4]. Since program packages that are able to deal with these large and heavy systems have become available, there has been a large increase in the level of understanding of especially organoactinide chemistry.

The presence of f electrons distinguishes lanthanides and actinides from the transition metal elements. Compounds can be made which do not have a TM analogue, the earliest example of which is the molecule $\text{U}(\text{COT})_2$ ($\text{COT} = \text{}^8\text{-C}_8\text{H}_8$: cyclooctatetraene), synthesized in 1968 by Streitwieser and Müller-Westerhoff [5]. The coordination of two planar C_8 rings is not known for TM compounds. This finding stimulated many experimental and later also theoretical studies on the actinocenes, and started the present discussion about the mode of bonding in these systems and organoactinide chemistry in general. A number of interesting questions concerning the bonding in this type of molecules can be asked. In the actinides, the 5f, 6d and 7s orbitals are available for chemical bonding. Therefore the questions are: how ionic or covalent are organoactinide compounds, or put differently, what is the importance of steric vs. electronic terms in the interaction? What is the relative importance of the 5f and 6d orbitals in chemical bonding and to what extent do they participate in the bonding? What are the effects of relativity, and does relativity change the above mentioned ionic/covalent or 5f/6d issues. And, connected to the previous, what do the frontier orbitals look like?

The lanthanides are bonded to ligands more or less in an ionic fashion [6,7]. There is little 4f contribution to the bonding compared to the actinide 5f ones, as the 4f orbitals are more contracted. Still some 5d, 6s and 6p interaction with ligands is found in lanthanides.

For the actinides the discussion concerning the above mentioned issues still is very much alive. In a 1980 review, Raymond and Eigenbrot concluded from X-ray structures of a large number of actinide compounds that the bonding was largely ionic [8]. Approximately from the same time on, quantum theoretical calculations on the bonding and structure in organoactinide chemistry have been done, which generally show covalent 5f contributions [4].

The Bursten group has found what they called a dichotomy in the role of the d and f orbitals, using Quasi-Relativistic X Scattered-Wave (QR-SW) calculations. They also called it FEUDAL: 'F Orbitals Essentially Unaffected, D orbitals Accomodate Ligands' [6]. The d electrons dominate the σ -bonding of ligands, while the metal electrons reside in f orbitals and are available for π interaction with ligands. This rule of thumb is based on a large number of calculations. For example, it was found that the donation into 6d was more important than into 5f in the systems UCp_4 , UCp_2Cl_2 and UCl_4 [9]. A study on UCp_3L (L = H, OH, NO and CO) showed that the 6d orbitals are involved in the σ -bonding of the ligands, but for CO and NO there is also π -backbonding from the U 5f orbital into the ligand π^* orbital [10]. Recently, an investigation on the bonding in the actinide compounds $AcCp_3$ showed that the 5f orbitals are less important than the 6d orbitals, even though they decrease in energy going to the right part of the actinides in the periodic system, while at the same time the 6d orbital rises in energy [7].

On the other hand there have been studies that contradict the Bursten picture, and show important 5f contributions to the bonding in actinide systems. Tatsumi and Nakamura [11] find about equal (but small) 6d and 5f contributions to the bond of UCp_3 and CH_3 using Relativistically parametrized Extended Hückel (EH) calculations. Also a study on the actinocenes $Ac(COT)_2$ by Boerrigter et al. [12] showed substantial 5f involvement. And recent calculations on the bonding in the uranyl ion UO_2^{2+} [13] showed a dominance of U 5f-O 2p bonding, which determines the extremely short U-O bond distance in this compound. An example of the completely different effects relativity has on the bonding and frontier orbitals of transition metals and actinides is provided by a recent investigation of van Wezenbeek et al. [14]. It was shown that the bond between the typical transition metal fragment $HfCl_3$ and H qualitatively has the same Hf 5d dominance in the non-relativistic and relativistic schemes. However, the bond between the actinide fragment $ThCl_3$ and H non-relativistically was dominated by the Th 5f orbital, while relativistically the 6d orbital was more involved. The reason for this reversal is the much larger indirect relativistic destabilization of the 5f orbital compared to the 6d. So for Th these results fit into the Bursten picture.

In the present work we will give the results of an investigation into the nature and strength of the bonding between UCp_3 and the ligands H, CO and NO. We studied the

relative importance of 5f vs. 6d contributions to the bond and also looked at the effects of U 6p in these compounds using Scalar-Relativistic calculations. From a study on uranyl UO_2^{2+} [13] we know that in this compound a 6p-hole exists, e.g. the 6p population is 1.5 instead of 2.0, partly explaining the relativistic bond lengthening for this compound. The occurrence of a 6p-hole can have a positive effect on the bonding. It is known that the antibonding combination of two interacting orbitals is destabilized more than the bonding one is stabilized [15]. So, if the 6p orbital is involved in destabilizing closed shell interactions, a not complete filling diminishes the antibonding effect. From our calculations on $\text{UCp}_3\text{-L}$ we will be able to say something about the effect of U 6p on the bond in these compounds. Although Bursten et al. [10] have studied the same $\text{UCp}_3\text{-L}$ compounds, our calculations are not just a duplication of theirs. We used the Density-Functional (DF)-LCAO method implemented in the Amsterdam DF program Package [16-18], which has proven to be highly accurate for heavy systems [19,20]. A brief description of this method will be given in Section 3. The bond energy can be obtained with respect to fragments chosen to optimally represent the important interactions when combining them. Moreover, the bond energy can conveniently be decomposed into a steric (electrostatic and occupied orbital /occupied orbital) interactions and electronic (occupied orbital/virtual orbital) contributions, the latter even with respect to the irreducible representations of the molecular point group, enabling e.g. a decomposition into σ -bonding and σ -backbonding energies. In the QR SW calculations of Bursten et al. [10] this energy analysis could not be made. Also bond energies have not been given in the previous calculations on the title systems, and would be questionable in view of the Muffin-tin approximation employed in the SW calculations. The present results may therefore lead to a more thorough understanding of the interactions between the typical organometallic fragment UCp_3 and ligands.

This chapter is organized as follows. In Section 2, we give a review of experimental and theoretical studies on UCp_3 and UCp_3L compounds. A description of the method we used in our calculations is given in Section 3, together with structural data for the molecules considered. In Section 4 the electronic ground state of UCp_3 is investigated, and Section 5 contains the results of our calculations on the bonding between UCp_3 and the ligands CO, NO and H. Our conclusions are summarized in Section 6.

2. UCp_3 and UCp_3L

After the synthesis of UCp_3Cl , a large number of other UCp_3L compounds have been made and studied. On the experimental side, Anderson and Crisler report from visible and IR spectra that the U-Cp bond in UCp_3Cl and UCp_3BH_4 is mainly ionic [21]. Also Amberger [22] studied the absorption spectrum of UCp_3Cl and concluded from Crystal

Field analysis that this is a f^2 system, not mentioning possible covalency. Fragala et al. [23] studied the U-X – bonds in UCp_3-X and $UCp_3'-X$ ($Cp' = C_5H_4CH_3$) compounds (with $X = Cl, Br, BH_4$) and in $(Indenyl)_3U-X$ ($X = Cl, Br, OCH_3, CH_3$) (Indenyl = C_9H_7) using PES. They found that ionization energies of the compounds containing the Cp' or Cp ligand are approximately equal, while the indenyl compounds showed smaller ionization energies. The differences in HeI and HeII spectra indicated largest 5f covalency in the metal-indenyl bonding. Also X-ray structures of UCp_3X ($X = F, Cl, Br, I$) have been reported [24].

On the theoretical side, approximately from the end of the 1970s, methods had been developed and the computational power had increased such that it became possible to include relativistic effects in quantum mechanical calculations, and therefore accurate calculations on organoactinides became possible. Although most of the considered compounds have substituted Cp ligands, in computations these are usually replaced by the Cp ligand. Although Bursten and Fang [9] only showed that this replacement is justified for Cp^* ($= C_5Me_5$), for other ligands it is usually done too. Replacement of Cp with the computationally much less demanding Cl is not correct [9]: Cp is a better electron donor than Cl , leading to larger splitting of valence orbitals. This leads to very different overall pictures for UCl_4 and UCp_4 .

As we are presently studying UCp_3L molecules, an interesting issue is the ground state configuration of UCp_3 itself. Up to now it has not been possible to synthesize UCp_3 [7], but UCp'_3 has recently been structurally characterized and shown to have a planar, pseudo- D_{3h} structure [25]. This means that $U-Cp(\text{centroid})_3$ has a D_{3h} geometry, the presence of the Cp -rings lowering the symmetry to C_{3v} . The ground state has not yet been determined experimentally [10], but there have been a number of theoretical investigations on planar UCp_3 . Tatsumi and Nakamura [11] found a f^3 ground state using Relativistically parametrized EH calculations, the 6d orbital was about 4.5 eV above the U 5f. Bursten found a ground state f^2d^1 [26], only 100 cm^{-1} below the f^3 state using QR SW-X calculations. Recently [4] a f^3 ground state was found when the spin-orbit interaction was taken into account. The similar Th compound, $ThCp''_3$ ($Cp'' = (Me_3Si)_2C_5H_3$) has been synthesized [27], and both experimentally by Kot [28] and theoretically (with the replacement of Cp'' by Cp) [26] exhibited a $6d^1$ ground state. In a recent QR-SW study on $AcCp_3$ complexes ($Ac = U$ to Cf), Bursten et al [7] found a dominating contribution of Ac 6d to the bonding in the beginning of the actinides, while at the end the 5f orbitals became more important. Although the 5f orbital decreased in energy going to the right of the actinide series, the extent of the 5f contribution to the bond did not vary, because the 5f orbital contracted at the same time. They used the destabilization of the antibonding U 5f- Cp combination with respect to the non-bonding f

orbital as a measure of the interaction. On the other hand, Quasi-Relativistic calculations including spin-orbit coupling on the actinocenes [12] with the Amsterdam DF program package as also used here showed a dominating d contribution at the left of the actinides (e.g. Th), but the 5f bonding increased to the right, contrary to what Bursten [7] found in the AcCp_3 series, where 5f bonding stayed the same.

In addition some calculations on UCp_3X have been done. In these systems too the question of the relative importance of the U 6d and U 5f was addressed. Vittadini et al. [29] found using non-relativistic DV-X α calculations that the U 6d orbital only had a small contribution to the bond between UCp_3 and F, Cl and I. Although their Transition State Ionization Energies agreed well with experimental results, the non-relativistic nature of the calculations can not be correct, as they noted too. Bursten and Fang [9] obtained a dominant donation from Cp or Cl into U 6d over U 5f in the systems UCp_4 , UCp_2Cl_2 and UCl_4 using the QR-SW method. Tatsumi and Nakamura [11] found using relativistically parametrized EH calculations, that the σ -bond between UCp_3 and CH_3 has equal contributions from 6d and 5f.

All above studies were on σ -only bonds between UCp_3 and ligands. The first suggestion that a π -bond could exist between UCp_3 and a ligand, viz. CO, was made by Tatsumi and Hoffmann [30], who mentioned the possible existence of UCp_3CO . They did not expect any significant π -backbonding to occur. Until then the only CO coordination to U had been found for $\text{U}(\text{CO})_6$ at very low temperatures by Slater and Sheline [31], using the matrix isolation method of DeKock [32]. They found no evidence for f participation to the bonding. Shortly after Tatsumi and Hoffmann 'predicted' its existence, Brennan et al. [33] reported the first room temperature stable actinide CO complex: UCp^*_3CO ($\text{Cp}^* = \text{Me}_3\text{SiC}_5\text{H}_4$). Its structure is given in Fig. 1 (with the substitution of Cp for Cp^*). The C-O stretching frequency ν_{CO} was 1976 cm^{-1} , which is considerably lower than that of free CO, convincing evidence of π -backbonding.

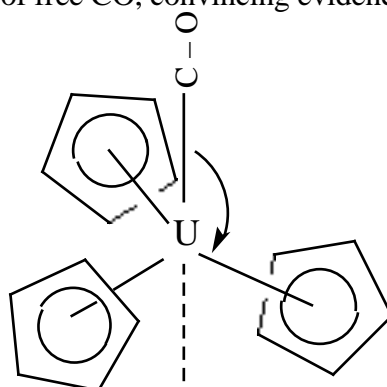


Figure 1. Geometry of UCp_3CO . The C-U-Cp(centroid) angles (θ) are equal (symmetry C_{3v}).

A large number of new molecules containing σ -bonds to uranium has been made and studied recently, a selection of which is provided by the work of the groups of Brennan and Cramer. They among others report uranium metallocenes [34a], UCp'_3 complexes with imide ligands [34b,34c,35], and complexes containing double bonds between U and P [34d], and CO (see also next paragraph) [33]. Cramer et al. characterized the exotic compound $\text{UCp}_3[(\text{NC}_6\text{H}_5)(\text{O})\text{CCHP}(\text{CH}_3)_2(\text{C}_6\text{H}_5)]$, which contains a four membered chelate ring U-O-C-N [36]. Brennan et al. [37] investigated the strength of U-L bonds by measuring the competition between thf (tetrahydrofuran) and phosphine, phosphites, pyridine, amines, ethers, thio-ethers and CO. The exchange reaction occurred in the order given above, where CO has the smallest affinity for U. A structural investigation gave similar results.

At the computational side, Bursten et al. [38] showed that there was extensive π -backbonding from the U 5f orbitals to CO 2 π . In a subsequent study [10] they also investigated the coordination of a σ -donor (OH), another π -acceptor (NO) and a σ -only (H) ligand to UCp_3 . Their results again fit the Bursten picture. The σ -bond is dominated by donation into 6d $_{z^2}$, with small contributions from 5f $_{z^2}$, 7s and 7p. The π -bond is dominated by 5f when it concerns backbonding into the 2 π of CO and NO, but the acceptance of electrons from the 1 π of OH is dominated by 6d. An interesting result of their calculations is the predicted stability of UCp_3NO , which should have a stronger σ -bond than the CO analogue. This corroborates a study on transition metals [39], where NO also was a stronger π -acid than CO. In agreement with this, Cramer [35] found stronger U-N multiple bonding than for U-O in the organoactinide imide compounds $\text{UCp}_3(\text{N or O})\text{P}(\text{C}_6\text{H}_5)_3$ using relativistically parametrized EH calculations.

The π -bonding is important in these systems. In the lanthanides the 4f orbital does not participate in bonding, it lies too deep. That CeCp'_3 does not react with CO under the reaction circumstances as UCp'_3 [37], indicates the importance of the 5f orbitals in UCp_3CO . Also $\text{U}(\text{N}(\text{SiMe}_3)_2)_3$ does not react with CO, contrary to the Cp'^* analogue [40]. It would be interesting to investigate whether steric effects are responsible for this feature, and/or other effects are the cause of it.

3. Method of Calculation and structural data

The structural information for the compounds studied in this work is given in Table 1. The data is taken from Bursten et al. [10,38], with the exception of the C-H distance in the Cp ring, which was set to 1.08Å, and the U-C and U-N distances for UCp_3CO and UCp_3NO were set at 2.33Å. For pyramidal UCp_3 the U-Cp(centroid)-z-axis angle is 100°, while for planar UCp_3 the angle is 90°.

Table 1. Structural data for UCp_3-L .

Compound	Parameter	Parameter value
UCp_3	U-Cp (centroid)	4.78 a.u. = 2.53 Å
	U-C (Cp)	5.27 a.u. = 2.79 Å
	C-C (Cp)	2.63 a.u. = 1.39 Å
	C-H (Cp)	2.04 a.u. = 1.08 Å
	(U-Cp (centroid)-z-axis)	90° (planar) 100° (pyramidal)
UCp_3L	(U-Cp (centroid)-L)	100°
UCp_3H	U-H	3.80 a.u. = 2.01 Å
UCp_3CO	U-C(CO)	4.40 a.u. = 2.33 Å
	C-O	2.17 a.u. = 1.155 Å
UCp_3NO	U-N	4.40 a.u. = 2.33 Å
	N-O	2.17 a.u. = 1.155 Å

All calculations have been carried out using the Amsterdam DF program package [16..18]. The LSD exchange potential was used, together with the Vosko-Wilk-Nusair [41] parametrization for correlation, with a correction of Stoll [42]. The calculations were done using the Scalar-Relativistic (SR) option, where the scalar relativistic mass-velocity, and Darwin operators are added to the non-relativistic operators. The SR method has proven to be better than FO perturbation theory [43], especially for elements heavier than third row transition metals [19,20]. The spin-orbit interaction can be determined self-consistently in a subsequent calculation using the SR orbitals as basis. In this study this was not done. The indirect effects, especially important for f electrons are automatically included. A more detailed discussion of the SR method has been given in Chapter 1.

The method for calculating bonding energies is an extension of the well known decomposition scheme of Morokuma [43] for closed shell systems, and has been described extensively before in Chapter 1. The bond energy E is calculated in two steps: First the steric repulsion E^0 is calculated, which is defined as the energy difference between the separate fragments and the overall system described by the anti-symmetrized product Ψ^0 of the overlapping fragment orbitals.

The steric energy may be divided in two contributions, a) $E_{el.stat}$, the electrostatic interaction between the unmodified fragments and b) E_{Pauli} , the Pauli, exchange, or overlap repulsion:

$$E^0 = E_{el.stat} + E_{Pauli} \quad (3)$$

The Pauli repulsion E_{Pauli} dominates over $E_{el.stat}$, making E^0 positive (repulsive).

In the second step, the wavefunction ψ^0 relaxes to the SCF solution ψ^{SCF} , which is accompanied by the orbital interaction energy E_{oi} . This term contains the charge transfer and polarization energies. The bond energy is thus given by:

$$E = E^0 + E_{\text{oi}} \quad (4)$$

If the orbital basis is symmetry adapted, the orbital interaction energy can be decomposed into contributions from the irreducible representations [44]. Denoting the irreducible representations by Γ , we can write:

$$E_{\text{oi}} = \sum_{\Gamma} E_{\text{oi}}^{\Gamma} \quad (5)$$

For the evaluation of the bond energy for the reaction of UCp_3 and H we used the open shell fragment method, described in Chapter 1 and in [45].

The $(1s-5s)$, $(2p-5p)$, $(3d-5d)$, and $4f$ orbitals on U and the $1s$ orbital on C, N, and O have been frozen. The valence basis was double- ζ for the U $6s$, $6p$ and $7s$, triple- ζ for $5f$ and $6d$ and double- ζ for C, N and O $2s$ and $2p$ and H $1s$. A single $7p$ on U, $3d$ on C (in CO), N and O, and $2p$ on H (as ligand in $\text{UCp}_3\text{-H}$) were added as polarization functions.

§4. The ground state of planar UCp_3

In this Section we describe the determination of the ground state of planar UCp_3 . As was mentioned in Section 2, the question is whether the ground state is $5f^26d^1$ or $5f^3$. We assume a pseudo D_{3h} planar structure for UCp_3 , corresponding to the experimental finding that UCp'_3 has such a structure. Due to the presence of the Cp rings the symmetry is only C_{3v} . The structure can be derived from that of UCp_3CO (Fig. 1), when θ is 90° and CO is left off. The most natural fragments to build UCp_3 from are U^{3+} and Cp_3^{3-} . We will show later that this is a good assumption. To get insight into the interactions in UCp_3 , it is important to look first at the orbitals of the fragment Cp^- . The highest occupied orbitals are $1a_2''$ and $1e_1''$ (in D_{5h} symmetry), which are denoted as ψ_1 and ψ_2 following Bursten et al. [10]. At the left of Fig. 2 the orbitals are given, including a pictorial presentation. Also the virtual $1e_2''$ orbitals (denoted by ψ_3) are involved in bonding to U and are included in the picture. All orbitals considered here are combinations of the carbon p_z orbitals. The ψ_1 orbital is the bonding combination, and is a σ -like orbital, isolobal with a ligand p orbital when viewed from a distance along the centroid of the Cp ring. The ψ_2 orbitals are p -like, perpendicular to the U-centroid axis, and the ψ_3 orbitals are π -like. Combining three Cp^- rings to the C_{3v} fragment Cp_3^{3-} , the ψ_1 orbitals transform as A_1+E , while the ψ_2 and ψ_3 orbitals transform as A_1+A_2+2E .

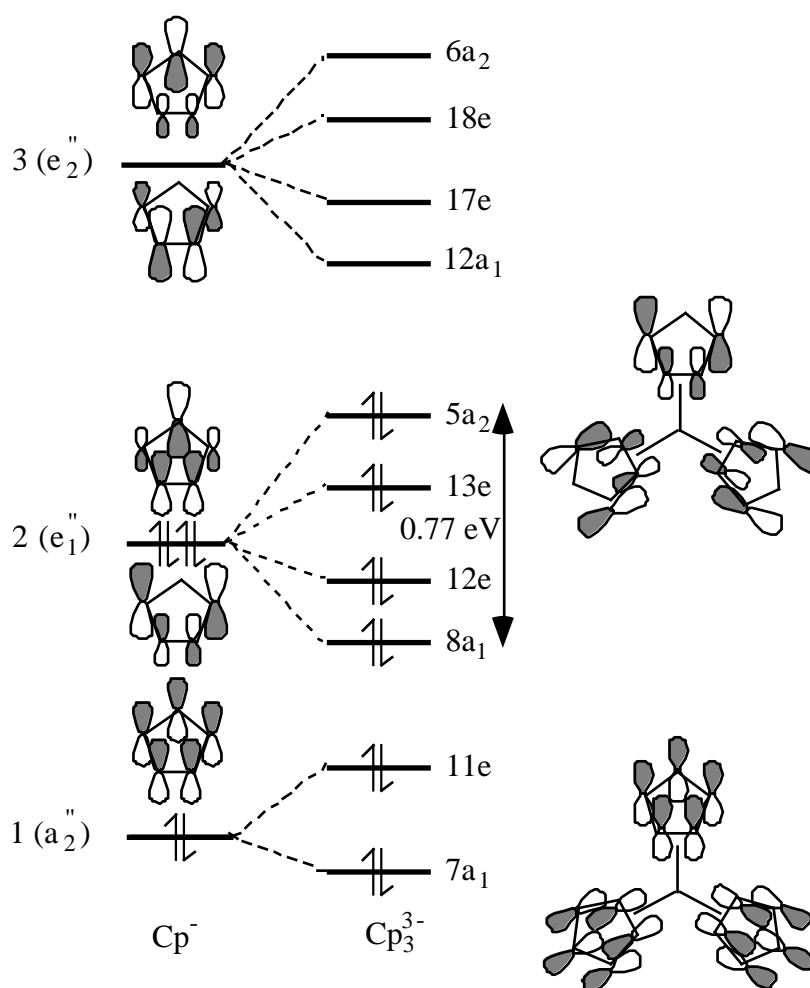


Figure 2. Interaction scheme for planar Cp_3^{3-} from 3 Cp^- .

At the right of Fig. 2 the resulting levels from the combination of the three Cp-rings are given. The orbitals are grouped into three sets, the lower of which results from the p-like 1 combinations, the middle one represents the combinations of the p-like 2 orbitals, and the highest set are the combinations of the -like 3 orbitals. In the calculations of Bursten et al. [10] the set of -like combinations was not mentioned, but we will show this set interacts with U orbitals in UCp_3 . The energy ordering is the result of the increasing nodes in the orbitals. Next to the $7a_1$ and $5a_2$ levels approximate plots of the orbitals are given, clearly showing that e.g. the $7a_1$ is entirely bonding between the Cp-rings, while for the highest orbital $5a_2$ of the 2 the antibonding character is maximal. At this point we note that the orbitals below the $7a_1$ are the combinations of the bonding Cp-ring orbitals, while a number of the combinations of virtual * ring orbitals are found in between the $5a_2$ and the $12a_1$ orbitals as the 9-11 a_1 and 14-16e orbitals.

The splitting of the e_2 orbitals is 0.77 eV in our calculations. For pyramidal Cp_3^{3-} we found a value of 0.84 eV, close to the value of 1 eV Bursten found using QR X-SW calculations [10]. As emphasized by Lauher and Hoffmann [46] an A_2 orbital can not be stabilized by interaction with a transition metal, since there are no metal orbitals of this symmetry available. For an actinide this is different. To show this, in Table 2 the symmetries present for the Cp_3^{3-} fragment and the U atomic orbital symmetries are given. We denote the orbitals on U by their linear symmetry labels. Note that the actinide metal U has orbitals for all Cp_3^{3-} symmetries, notably an orbital of A_2 symmetry, the $f_{y(3x^2-y^2)}$ ($f_{y(3x^2-y^2)}$), able to interact with the $5a_2$ orbital.

We now come to the determination of the groundstate of UCp_3 . We did SR calculations on a number of electronic configurations of UCp_3 . A level scheme for the interaction between U^{3+} and Cp_3^{3-} is given in Fig. 3, where also the atomic levels of U^{3+} are given. Note the level ordering $5f < 6d < 7s$. The configuration that was chosen here is $15e^2 11a_1$, the ground state configuration, as it will turn out. The main interactions are indicated with dotted lines in Fig. 3 and can also be read from the Mulliken Population analysis given in Table 3. The interaction is between U and the two groups of Cp_3 levels derived from the e_1 and e_2 orbitals and also the $12a_1$ and $17e$ orbitals of Cp_3 participate. Orbitals $7a_1$ and $10e$ are the Cp_3 $7a_1$ and $11e$ orbitals stabilized by bonding admixture of U $7s$ and U $6d$ respectively. This interaction represents donation from Cp to U, to $7s$ in $7a_1$ and to $6d$ in $10e$. Orbitals $13e$, $14e$, $10a_1$ and $5a_2$ are derived from the e_2 (p -like) set of Cp_3 ($8a_1$ - $5a_2$ in Fig. 2) and show approximately the same amount of donation to U as the e_1 (p -like) derived orbitals described above. Looking at Fig. 3, note that the Cp_3^{3-} $8a_1$ orbital is only slightly stabilized by U $5f$ and ends up above the $12, 13e$ derived pair as the $10a_1$. The E-pair interacts mostly with U $6d$ (d_{xz}, d_{yz}), with which the overlap (main quantum number) and interaction (see Table 3) is much larger: apparently the larger energy difference with U $6d$ is of minor importance.

Table 2. Splitting of orbitals in symmetry C_{3v} .

Representation	Cp_3^{3-} -combination	U
A_1	1	$s, p_z (p_z), d_{(z)^2} (d_{z^2})$
	2	$f_{z^3} (f_{z^3}), f_{x(x^2-3y^2)} (f_{x(x^2-3y^2)})$
	3	
A_2	2	$f_{y(3x^2-y^2)} (f_{y(3x^2-y^2)})$
	3	
E	1	$p_x, p_y (p_x, p_y)$
	2 (twice)	$d_{xz}, d_{yz} (d_{xz}, d_{yz}), d_{x^2-y^2}, d_{xy} (d_{x^2-y^2}, d_{xy})$
	3 (twice)	$f_{xz^2}, f_{yz^2} (f_{xz^2}, f_{yz^2}), f_{xyz}, f_z (f_{xyz}, f_z)$

The $8a_1$ does not interact with U $6d$ since the overlap is quite small due to the nodal structure of the Cp_3 $8a_1$ (p-like). This is not surprising, as these orbitals belong to different symmetries in D_{3h} .

Up to the $5a_2$ all orbitals are fully occupied, and are mainly Cp-like. The Cp_3^{3-} $5a_2$ orbital is stabilized considerably by the U $5f$, an interaction not possible for a transition metal as mentioned in the beginning of this section. The mixing of these orbitals is comparable to that between the 12,13e Cp_3^{3-} orbitals and U $6d$. Therefore from our results it is clear that the ability of the $5f$ orbitals to stabilize the $5a_2$ orbital of Cp_3^{3-} is important, but by no means it is the only important interaction.

The U^{3+} atom has 11 valence electrons, of which 8 are in the (6s,6p) shell, and the other three are $5f$ electrons. The three electrons that are available from the $5f$ orbital of U^{3+} have the 11 a_1 -13 a_1 and 15,16e orbitals available, the orbitals closest to $5a_2$. These orbitals are mainly $5f$ -orbitals, and occupying them results in a large number of configurations, of which $15e^2 11a_1$ is just one.

The orbitals 11-13 a_1 are essentially hybrids on U with dominant character according to the atomic level ordering, containing some mixing with the 12 a_1 combination of p-like Cp orbitals.

Table 3. Molecular Orbital compositions for the $15e^2 11a_1$ configuration of planar UCp_3 .

Orbital	Orbital character	Eigen-value (eV)	U		Composition (%)					Cp_3^{3-}	
			7s	6d	6d	6d	5f	5f	5f		5f
<i>unoccupied orbitals</i>											
17e	5f-6d to e a.b.	-0.02			46				14		12(13e), 25(17e)
6 a_2	5f - 5 a_2 a.b.	-1.58								86	14 5 a_2
13 a_1	5f	-2.15	1	6			83			2	3 8 a_1
16e	5f hybrid	-2.33			3			54	37		2 18e
12 a_1	5f-6d-7s hybrid	-2.35	23	34			1			42	1(11 a_1), 1(12 a_1)
<i>partially occupied orbitals</i>											
15e ^a	5f, -17e bond	-2.40			4			41	45		8 17e
11 a_1 ^b	5f -12 a_1 bond	-2.44	2	25			8			49	3(11 a_1), 10(12 a_1)
<i>occupied orbitals</i>											
5 a_2	5 a_2 - 5f bond	-5.27								15	83 5 a_2
10 a_1	8 a_1 (-5f bond)	-5.58					5				92 8 a_1
14e	13e - 6d bond	-6.00			13	1			3		6(12e), 74(13e)
13e	12e - 6d bond	-6.02			1	11					77(12e), 6(13e)
10e	11e- (6d bond)	-9.05				4					11(10e), 75(11e)
7 a_1	7 a_1 - 7s bond	-10.04	12							1	84 7 a_1
<i>gross populations</i>			0.26	0.25	0.70	0.44	0.19	0.85	1.04	0.83	
<i>Total charges</i>			U: 1.8 (12.2 electrons) and Cp: -0.6 (25.4 electrons)								

^a: occupied with 2.0 electrons ^b: occupied with 1.0 electron.

The f orbital (slightly antibonding with the $\text{Cp}_3^{3-} 8a_1$) ends up high as the $13a_1$, above the $U 5f$, $U 6d$ that are found in $11a_1$ and $12a_1$, where also some $U 7s$ character is present. The mixings in Table 3 show that the interaction between Cp_3^{3-} and U^{3+} is not very large, although the extensive mixings between U orbitals in $11a_1$ and $13a_1$ are a consequence of the Cp_3^{3-} ligand. These orbitals are found close together, and a strong interaction with a ligand may result in mixing among them. Concerning the e orbitals, the $15e$ is mainly a $5f$ hybrid, with some bonding interaction of both $U 5f$ and $U 5f$ with the $17e$ orbital of Cp_3 , a combination of the e -like Cp 3 orbitals (see Fig. 2). The $5f$ character is evenly distributed among $5f$ and $5f$.

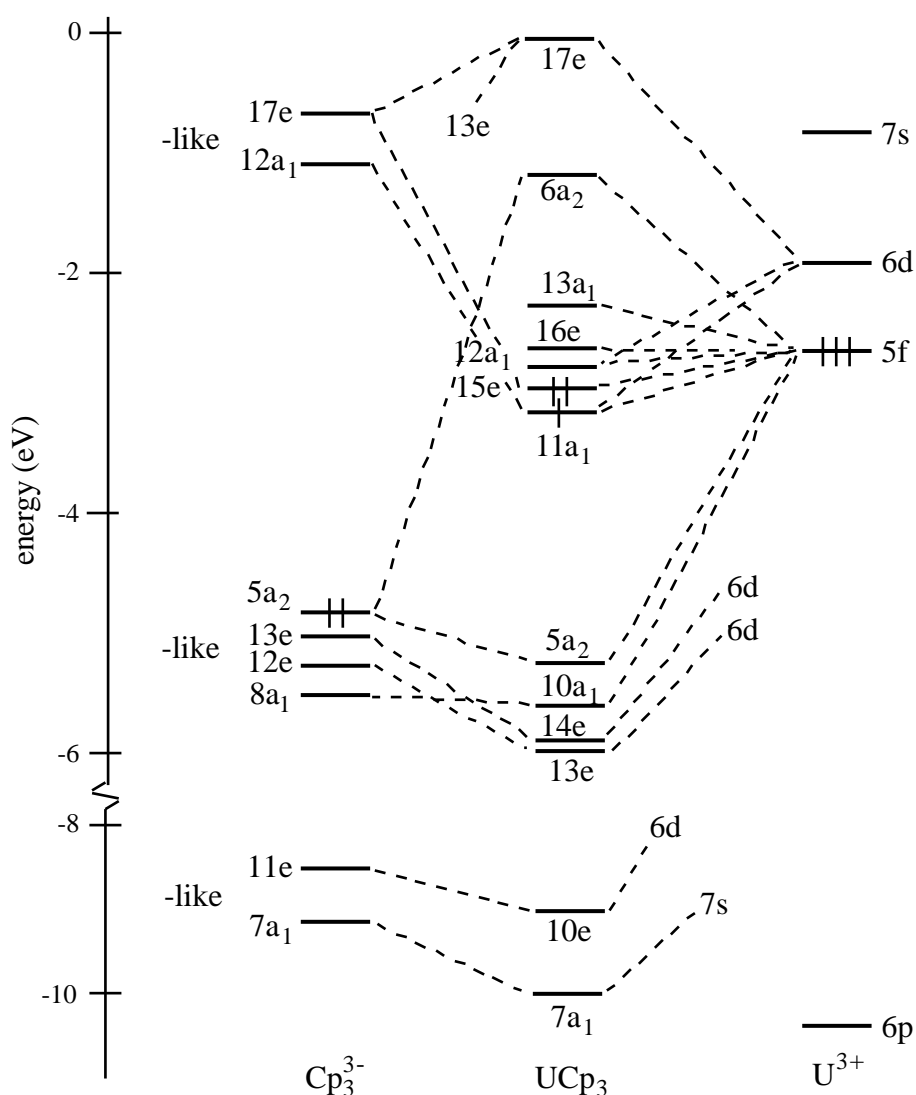


Figure 3. Level scheme for the configuration $15e^2 11a_1$ of planar UCp_3 . All levels below $11a_1$ are fully occupied.

The 16e orbital hardly has any bonding with Cp and is unoccupied in the $15e^2 11a_1$ configuration. The $11a_1$ orbital containing the odd electron, has a composition of 49% $5f$, 8% $5f$ and also contains 25% $6d$ character, all bonding with the (unoccupied) $12a_1$ of Cp_3 , an orbital that has a good overlap with U $5f$. The configuration for the three electrons is therefore closest to f^3 , viewing both $15e$ and $11a_1$ as pure $5f$ -orbitals, although there is quite some d character present also. The occupation for the three electrons can thus be approximated by $5f^1 5f^1 5f^1$. Because the $15e$ and $11a_1$ orbitals are nearly degenerate in the configuration $15e^2 11a_1$, placing one electron in the $11a_1$ and two electrons in the $15e$ would be favourable on account of exchange stabilization.

These results can not be compared with those of Bursten et al. [10], as there the *pyramidal* $E^2 A_1$ configuration of UCp_3 was studied, as a fragment for UCp_3L . We also did a calculation on this UCp_3 fragment, as basis for UCp_3H . The result for the highest orbitals is given in Table 5a. The result differs from Bursten et al. [10] in a number of aspects. We do not find a mainly $6d$ orbital below the f orbitals, although the $11a_1$ and $12a_1$ contain 24% and 26% $6d$ character respectively. Bursten finds a mainly $6d$ -like (66%) $10a_1$ orbital below the E and A_1 f -like orbitals. This orbital is kept unoccupied, as it is destabilized when a fourth ligand is attached to UCp_3 . Their $11a_1$ orbital is similar to ours and also occupied with 1.0 electron, but we find more d character (24% vs. 4%) and less $5f$ (58% vs. 93%). Moreover, Bursten mentions that the $5f$ content is a mixture of $5f$ and $5f$, while we find exclusively $5f$ character. Also the $12a_1$ orbitals are different, theirs is pure $5f$, while we have considerable $7s$ and $6d$ character besides $5f$. The E orbitals are similar, at least with respect to the total $5f$ content, as the populations were not axially split (i.e. for U $5f$ in f , f) in Ref. [10]. The differences between our calculations and those of Bursten might be due to the Muffin-tin procedure used in his work, and the approximate nature of his population analysis.

As to the interaction in A_2 symmetry, which would not have been possible for a transition metal, our 15% mixing of U $5f$ to the $Cp_3^{3-} 5a_2$ orbital is much less than the 29% Bursten et al. [10] find. For the planar geometry we also have 15% mixing (Table 3), which is much higher than the 8% found by Tatsumi and Nakamura [11] in relativistically parametrized EH calculations.

In the determination of the groundstate of planar UCp_3 , a large number of ways of dividing the three electrons among the $11-13a_1$ and $15,16e$ levels was tried. The configurations and bonding energy decomposition for the formation of the molecules from fragments U^{3+} and Cp_3^{3-} are given in Table 4. Only the total bond energy are given. Note that for these charged systems the electrostatic interaction is a major part of the total bond energy. As the fragments are the same for all electronic configurations, differences in bond energy are only due to the orbital interaction energy term E_{oi} (the difference between E and E^0).

Table 4. Bond energies (in eV) for electronic configurations of planar UCp_3 with respect to U^{3+} and Cp_3^{3-} .

Configuration	$E (= E^0 + E_{oi})$
$16e^3 = {}^3$	-55.03
$15e 16e^2$	-55.38
$15e^{3/2} 16e^{3/2}$	-55.50
$15e^2 16e$	-55.60
$16e^2 11a_1$	-55.74
$15e 16e 11a_1$	-55.79
$15e^2 11a_1$	-56.10
Steric terms:	
$E_{el.stat}$	-48.71 eV
E_{Pauli}	11.43 eV
E^0	-37.29 eV

Configurations that are not given in Table 4 would not converge (e.g. $16e^2 11a_1$). Also configurations with the $12a_1$ or $13a_1$ occupied could not be converged. The convergence is a real problem in these systems, as we have the U 5f and U 6d close together. Moreover different axial sublevels are present in the same symmetry, e.g. in E symmetry we have for example U 5f, U 5f, U 6d and U 6d. From Table 4 it is clear that the $15e^2 11a_1$ configuration is lowest in energy. In Table 3 it can be seen that for the 15e and $11a_1$ orbitals the mixing with the (π -like) Cp_3^{3-} orbitals is largest, and therefore these orbitals are preferably occupied. The configuration $15e^2 11a_1$ is not the only one with three electrons divided among 15e and $11a_1$, also $15e^3$ (same result as $16e^3 = {}^3$) was tried. However, from the much larger bond energy for the $15e^2 11a_1$ configuration it follows that moving one electron from a 15e orbital to the $11a_1$ orbital leads to more gain in A_1 interaction-energy than the loss from the E interaction energy. This points to a stronger interaction between the fragments in A_1 symmetry. This is also clear from the larger mixing in Table 3 between U and Cp in $11a_1$ than in 15e. The occupation of the $11a_1$ would also lead to the largest exchange stabilization for the three 5f electrons to be placed in the nearly degenerate 15e and $11a_1$, as was mentioned before. For the other configurations the orbitals did not change much and therefore are not given here, and the stronger mixing/interaction in the $11a_1$ orbital holds for all configurations. Only configurations with 1 electron in $11a_1$ could be converged, more than 1 electron led to too much 5f repulsion and a high energy.

In the present study we did not investigate the effect of spin-orbit splitting in the determination of the ground state. Preliminary results however showed that the effect of spin-orbit splitting does not alter the conclusion that the $15e^2 11a_1$ configuration is the ground configuration (in terms of non-spin orbit split levels).

The steric term in the bond energy (equal for all configurations) amounts to -37.29 eV, and is dominated by the ionic term $E_{\text{el.stat}}$. The formation of UCp_3 from U^{3+} and Cp_3^{3-} is therefore mainly an ionic process, approximately two-third of the total bond energy of -56 eV comes from the ionic term, while the covalent (orbital) interaction is about -19 eV, which is smaller than the ionic terms but still sizable. Viewing UCp_3 as being built up of U^{3+} and Cp_3^{3-} is justified when looking at the final charges on the fragments. The charge on the Cp-ring in UCp_3 is -0.6 , while the charge on U is 1.8 . The (6s,6p) shells contain the full 8 electrons. Charge has moved from the Cp-rings to U, which can be seen in the Mulliken analysis of Table 3. In UCp_3 the 5f electrons are more or less evenly divided among σ , π and δ , and due to donation from the Cp rings, the U 7s and 6d orbitals gained some charge.

In the calculations we do not find a large energy difference between pyramidal and planar configurations, the planar one that we find as ground state is some 0.05 eV lower in energy than its pyramidal analogue (see Section 5). This energy difference is of the order of the energy difference we found for planar and pyramidal Cp_3^{3-} from three Cp-fragments, which would indicate that the interaction between the Cp-rings is responsible for the planar structure of UCp_3 . The repulsion between the Cp-rings is lower in the planar structure. However, as the accuracy of our method is in the same order as this energy difference [50], we can only say that they are close in energy and rely on the experimental fact that UCp_3 is planar in determining the ground state.

5. Interaction of pyramidal UCp_3 with Ligands H, CO and NO

In this Section the interaction of UCp_3 with some typical ligands will be discussed. Following Bursten et al. [10], the choice of a σ -only ligand H and the π -acids CO and NO provides a good representation of possible ligands. Our study, although using the same fragments, is nevertheless very different from Bursten, as we use a detailed bond energy analysis to assess the mode and degree of bonding of the selected fragments to UCp_3 . The Mulliken populations in terms of UCp_3 and L, as well as in terms of U AOs are given in Tables 8,9. The Cp character of the orbitals is obtained by subtracting the U and L values from the total. Only in Table 8 we give the U 5f and U 6d populations, because they are needed in the discussion of UCp_3H . Occupation numbers for the highest orbitals are included in the tables.

5.1. Preparation of UCp_3 and Ligands

The UCp_3 state we used as a fragment for UCp_3L is different from the ground state configuration as described in Section 4. As in UCp_3L the structure of UCp_3 is pyramidal

(angle 100° in Fig. 1), we used the pyramidal UCp_3 as fragment for subsequent interaction with L. The electronic structure was chosen for optimal interaction with the ligand and was derived from the occupation found in UCp_3L . The preparation energy is defined as the energy difference of the prepared pyramidal UCp_3 configuration and the planar UCp_3 ground state which was described in Section 4. The energies of the prepared UCp_3 states relative to the planar ground state and their orbital population analyses are given in Tables 5a,5b.

For the interaction with H we took the $15e^211a_1$ state (Table 5a) and for interaction with CO and NO we took the UCp_3 fragment where the three f-electrons occupied the $16e$ (mainly f) orbital, and the configuration is denoted as $16e^3$ or 3 (Table 5b). In this way the fragment is prepared for back-bonding with the ligand 2 ($*$) orbitals. The configuration with the electrons in the $15e$ orbital is not suited for back-bonding interactions, as the f overlap with ligand 2 orbitals is zero. The two considered configurations are close in energy, the pyramidal $15e^211a_1$ is lowest, slightly above its planar analogue, the ground state. Comparing with the planar ground state configuration in Table 3, we see that there are some changes in the orbitals.

The $11e$ orbitals of the pyramidal configurations are similar to the $10e$ of the planar state (they are almost equal in energy), while for the $11e$ planar and $10e$ pyramidal (Cp-ring) orbitals the same holds. This difference is of no importance to us.

Table 5a. Molecular Orbital compositions for configuration $15e^211a_1$ ($\Delta E_{\text{prep}}=0.05$ eV) of pyramidal UCp_3 . In superscript occupation numbers for highest occupied and lowest virtual orbitals are given.

Orbital	Orbital character	Eigen-value (eV)	U Composition (%)								Cp_3^{3-}
Orbital	character	value (eV)	U 7s	U6d\	U6d\	U5f\	U5f\	U5f\	U5f\		
			s\do	s\do	s\do	s\do	s\do	s\do	s\do		
			3()	3()	3()	3()	3()	3()	3()		
17e	5f-6d to e a.b.	-0.17		46	5	1	14				12(13e), 19(17e)
6a ₂	5f - 5a ₂ a.b.	-1.51							86		14(5a ₂)
13a ₁	U (-8a ₁ a.b.)	-2.10	8	6		64			13		3 8a ₁
16e	5f, f	-2.24		9	1		43	42			1 17e
12a ₁ ^{0.0}	5f,6d -12a ₁ b., 7s a.b.	-2.32	21	26		30			22		1 12a ₁
11a ₁ ^{1.0}	5f,6d -12a ₁ b.	-2.37	2	24		1			57		10 12a ₁
15e ^{2.0}	5f - 17e b.	-2.38		1			50	40			8 17e
5a ₂ ^{2.0}	5a ₂ -5f b.	-5.21							15		84 5a ₂
10a ₁	8a ₁ (-6d, 5f b)	-5.71		3		3					90 8a ₁
14e	13e-6d bond	-5.80		7	3		1	2			15(12e), 68(13e)
13e	12e-6d bond	-6.17		7	9						67(12e), 14(13e)
11e	11e-6d bond	-9.02			4						11(9e), 80(11e)
7a ₁	7a ₁ - U7s b.	-10.04	11	1							83 7a ₁
<i>Gross Populations</i>			0.24	0.31	0.56	0.52	0.08	1.06	0.93	0.89	(0.60 in A ₁)

Table 5b. Molecular Orbital compositions for configuration $16e^3$ (π^3) ($\Delta E_{prep}=1.1$ eV) of pyramidal UCp_3 . In superscript occupation numbers for highest occupied and lowest virtual orbitals are given.

Orbital	Orbital character	Eigen-value (eV)	U							Cp_3^{3-}	
			U 7s	U6d\	U6d\	U6d\	U5f\	U5f\	U5f\	U5f\	
			s\do								
			3()	3()	3()	3()	3()	3()	3()	3()	
17e	5f-6d to e a.b.	0.10		39	7			23			19(13e), 19(17e)
13a ₁	5f -(8a ₁ a.b.)	-0.88	4	1			83				
16e ^{3.0}	5f	-1.14			5			81	6		1(17e)
6a ₂	5f - 5a ₂ a.b.	-1.50								86	14(5a ₂)
15e	5f - 17e b.	-1.81			7	1		7	68		15(17e)
12a ₁	6d -7s-5fhybr.	-1.89	32	47			6			8	5(12a ₁)
11a ₁ ^{0.0}	5f (12 a ₁ b.)	-2.34		6			1			84	7 12a ₁
5a ₂ ^{2.0}	5a ₂ -5f b.	-5.24								15	84 5a ₂
10a ₁	8a ₁ (-6d b.)	-5.62		3			1				92 8a ₁
14e	13e-U6d b.	-5.78			8	2		1	2		9(12e), 75(13e)
13e	12e-U6d b.	-6.17			5	10					73(12e), 8(13e)
11e	11e-U6d b.	-9.02				4					4(9e), 85(11e)
7a ₁	7a ₁ - U7s b.	-10.03	11	1							83 7a ₁
<i>Gross Populations</i>			0.21	0.06	0.67	0.51	0.04	2.49	0.30	0.32	(0.02 in A ₁)

Concerning the orbitals in A₁ symmetry, especially the orbitals 11-13a₁ differ considerably when the configuration is altered. They are much closer together in the 15e²11a₁ state and more heavily mixed than in ³, where we have a clear division between the mainly 5f orbital 11a₁, the 12a₁ is a U 6d ,7s hybrid and finally 13a₁ is mostly 5f . To understand the bonding between UCp₃ in the configuration 15e²11a₁ and H to be discussed in Section 5.2, we mention the main bonding characteristics for the 11-13a₁ orbitals. From Table 5a we note that in 11a₁ the interaction with Cp is (slightly) bonding f and d with 12a₁. In 12,13a₁ the f character is Cp-antibonding, and the d character is also Cp-bonding in 12a₁, and small in 13a₁. The f orbital is mainly found in 13a₁, while for U 7s we have antibonding character with Cp in 12,13a₁.

The effect on the orbitals in E symmetry is that for the ³ configuration the 15,16e are higher in energy than in 15e²11a₁, due to a larger repulsion. Also the relative contributions of U 5f and U 5f change. In the ³ configuration the 16e orbital is mainly U 5f , allowing maximal back-donation to the L 2 (* orbital) of CO and NO. In E symmetry we already noted for planar UCp₃ that the interaction with U 6d is large, and also for pyramidal UCp₃ this is the case. Both 13,14e (see Table 5b) contain U 6d character (bonding with Cp), while there is only a very small U 5f content.

In Table 6 we present overlaps between the H 1s, CO,NO 5 and U 5f ,6d and also the CO,NO 2 overlaps with U 5f ,6d . The larger donation into U 6d than into U 5f that will be found in Section 5.3 for CO and NO can immediately be understood from the

Table 6. Overlaps of U AOs with ligand orbitals.

Ligand	Orbital	U 6d	U 6d	U 5f	U 5f	U 7s	U 5f
H	1s	0.32		0.08		0.42	0.0
CO	5	0.30		0.08		0.35	0.0
	2		0.22		0.07		
NO	5	0.25		0.08		0.25	0.0
	2		0.16		0.06		

fact that the 5f orbital (mainly in the UCp_3 $13a_1$) is found higher in energy than the 6d in $12a_1$, and the much larger U 6d overlap with the L 5 orbitals. In E symmetry we already noted that the U 6d level is higher in energy than the U 5f one, caused by different interactions with Cp. In this case, the U 5f orbital is closer to L 2 and although the overlap of U 6d with L 2 is larger (Table 6), we find dominant U 5f interaction. For H the situation appears to be more complicated, there finally the dominance of U 6d in the pair bond is related to the larger overlap of U 6d with H 1s.

For clarity the highest energy levels of the ligands are given in Fig. 4 and their composition in Table 7a. Note the differences between NO and CO, which are important for the interaction with UCp_3 . Both the 5 and 2 orbitals are localized on the less electronegative atom, nitrogen and carbon respectively. The nature of the orbitals can be derived using perturbation theory starting from a homonuclear system [15]. Because carbon has a lower electronegativity than nitrogen, we find the CO orbitals higher in energy than the corresponding ones in NO, and there is a stronger localization at C. Note the CO 5 orbital, it is predominantly a carbon lone pair. Hence one expects a larger overlap of the CO 5 with UCp_3 orbitals than for NO. We find indeed larger overlaps for CO 5 in Table 6, and also the 2 overlaps are larger for CO.

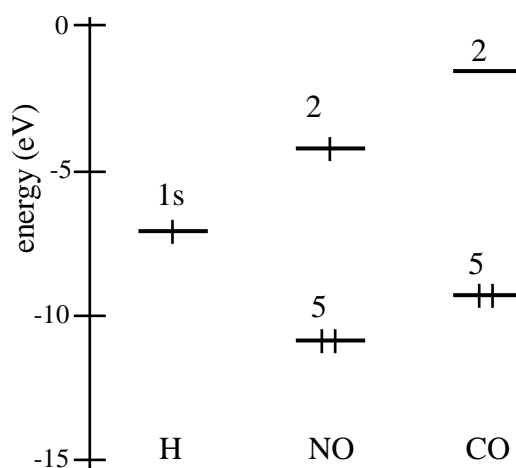
**Figure 4.** Highest molecular orbitals of ligands H, NO and CO.

Table 7a. Population analysis of ligand orbitals.

Ligand	Orbital	Eigenvalue (eV)	% Composition
H	1s	-6.77	H 1s
NO	2	-3.56	64% N 2p and 34 % O 2p
	5	-11.16	39% N 2s, 36% N 2p and 23% O 2p
CO	2	-1.96	75% C 2p and 24 % O 2p
	5	-8.75	61% C 2s, 31% C 2p and 8% O 2p

Table 7b. Bond energy decomposition for interaction of UCp_3 with different ligands.

Energy term (eV)	H	NO	CO
$E_{el. stat}$	-1.83	-1.53	-2.96
E_{Pauli}	2.28	3.19	3.79
E^0	0.46	1.66	0.83
E_{a1}	-3.78	-0.95	-1.44
E_e	0.05	-5.57	-2.34
E_{a2}	0.00	0.02	-0.02
E_{oi}	-3.76	-6.58	-3.86
E	-3.31	-4.93	-3.03
E_{prep}	0.05	1.10	1.10
E_{tot}	-3.26	-3.83	-1.93

In Table 7b the bond energy decomposition for the UCp_3 to L reactions are given. The steric repulsion E^0 is dominated by the Pauli repulsion, as expected. This results from the interaction of occupied fragment orbitals. The orbital interaction overcomes the steric repulsion, making the overall bonding attractive. The interaction terms will be discussed in the following subsections.

5.2. UCp_3 -H

The molecule UCp_3 -H was calculated with respect to the fragment UCp_3 in the configuration $15e^211a_1$ (Table 5a) and H. Using these fragments a bond between the $11a_1$ of UCp_3 and H 1s can be formed. We started from open shell fragments, using the procedure as described in Chapter 1. The Mulliken analysis for UCp_3 H is given in Table 8 and shows that the main bonding orbital of UCp_3 H is the $11a_1$, with a smaller contribution from the $10a_1$. The bond between UCp_3 and H appears not to be a simple

electron-pair bond between the UCp_3 $11a_1$ orbital and H $1s$. From Table 8 it is clear that admixing of the virtual $12,13a_1$ levels is equally important, not unexpected as these orbitals are close in energy in the fragment UCp_3 . In Fig. 5 an interaction scheme is given, with drawn and dashed lines indicating main and smaller interactions respectively. Both in the $11a_1$ and $10a_1$ orbitals the $11-13a_1$ UCp_3 orbitals have bonding character with H $1s$. The bonding with the UCp_3 $10a_1$ is of no importance (bonding in $10a_1$ and antibonding in $11a_1$) as this orbital is concentrated mainly on Cp_3^{3-} (Table 5, only 3% f, d character). This orbital therefore does not participate in bonding to H, its Mulliken population is 100% (sum of $10,11a_1$ in UCp_3H). The UCp_3 orbitals involved in the bonding are the $11-13a_1$. From the strong mixing with H, we conclude that the interaction is strong. If we compare the gross populations of UCp_3H and UCp_3 , we see the bonding to H leads to an increase in population of U $6d$, U $5f$ and U $7s$ of 0.25, 0.11 and 0.08e respectively. The ligand orbital H $1s$ also gained charge, 0.28e. The only orbital that lost charge is $5f$, which is not occupied at all in UCp_3H and lost 0.58e compared to its A_1 population in UCp_3 . The effects on the AO populations result from the rehybridization of the $11-13a_1$ orbitals of UCp_3 . These orbitals were close in energy and are heavily mixed by the bonding to H. From the gross populations we see that the rehybridization leads to a larger participation of AOs and U $5f$ loses charge, as it does not participate in bonding to H because the H $1s$ -U $5f$ overlap is zero.

The rehybridization may be looked upon as first order mixing of degenerate levels (cf. (quasi-) degenerate perturbation theory). The three UCp_3 orbitals $11-13a_1$ involved are mainly metal in character (see Section 4 and Table 5a). They mix under the influence of an external perturbation to form three new mainly metal orbitals as also indicated in Fig. 5, with lowest a d, f, 7s hybrid orbital, hybridized towards H, in the middle a mainly U

Table 8. Molecular Orbital composition for A_1 orbitals of UCp_3H .

Orbital		Eigen-	U Composition (%)					UCp_3	H
Orbital	character	value (eV)	7s	6p	6d	5f	5f		
<i>UCp₃H</i>									
$13a_1$	5f	-2.74	3		11	82		6($11a_1$), 51($12a_1$), 43 ($13a_1$)	
$12a_1^{0.0}$	5f	-3.28	2				92	62(a_1), 29, 8 ($11-13a_1$)	
$11a_1^{2.0}$	1s-6d, 7s, 5f b., p a.b.	-5.27	7	2	17	3		12($10a_1$), 14($11a_1$), 7($12a_1$), 20($13a_1$)	47 1s
$10a_1$	6d, 5f -H1s b	-5.93	1		11	6		88($10a_1$), 2($11a_1$), 1($12a_1$), 3($13a_1$)	6 1s
$7a_1$	7s-(H1s b.)	-10.25	9					97 $7a_1$	3 1s
$3a_1$	6p (- H1s b)	-22.28			32			96 $3a_1$	3 1s
$2a_1$	6p (- H1s b)	-22.89			59			97 $2a_1$	2 1s
<i>Gross Populations</i>			0.301	1.890	0.560	1.190	0.02		H1s: 1.28

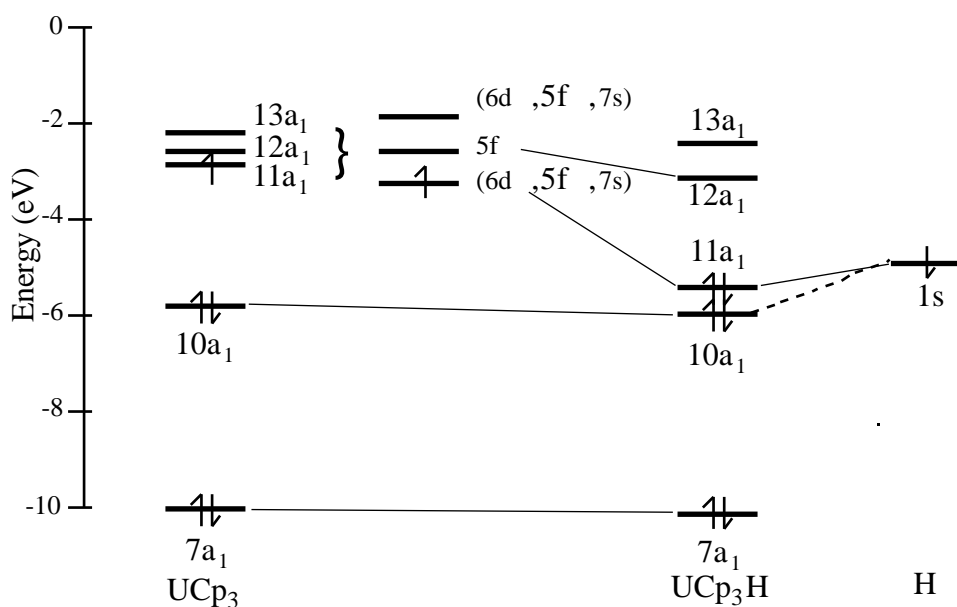


Figure 5. Interaction between UCp_3 and H in UCp_3H .

$5f$ orbital (ending up as the $12a_1$ in UCp_3H), and above in $13a_1$ a $d, f, 7s$ combination hybridized away from $H 1s$. We can understand the effects on the AOs by looking at the phases of the AOs in the UCp_3 MOs $12, 13a_1$ that admix to the $11a_1$.

We already mentioned the bonding characteristics of the $11-13a_1$ orbitals of UCp_3 in Section 5.1. The $11a_1$ is bonding f, d with the $Cp_3^{3-} 12a_1$. In the $12a_1$ the f character is Cp-antibonding, and for the d orbital it is Cp-bonding (as in $11a_1$) in $12a_1$ (the small percentage in $13a_1$ is not important). The $5f$ orbital is only found in $13a_1$, while the $U 7s$ is found mainly in $12a_1$ (antibonding with Cp, the bonding partner being the $7a_1$ orbital). From this we understand that admixing to the $11a_1$ of the virtual orbitals with the same $U 6d$ bonding character ($12a_1$), with $7s$ character in $12a_1$ and $5f$ in $13a_1$ could lead to an increasing population for these AOs. The decreasing $5f$ population is explained by the fact that in the $12a_1$ the $5f$ character is opposite (antibonding with respect to Cp_3^{3-}) compared to the $11a_1$. The $11a_1$ (1.0 electron in UCp_3) ends up with a population of some 0.32 e (16% Mulliken population in $10, 11a_1$). Therefore 0.68e ends up among the $12, 13a_1$ and $H 1s$. From the fact that 0.28e went from UCp_3 to $H 1s$, we conclude that the interaction with H can best be described by a covalent pair bond between $H 1s$ and a hybrid on UCp_3 .

We can also look at it in another way. Because the interaction between Cp_3^{3-} and U was small in $11-13a_1$, we can first view the interaction with H to take place, and subsequently the small perturbation by the Cp ligands. The relative importance of the U orbitals in the bonding with H then depends on the energy difference and overlap with H

1s. The U 6d orbital has the strongest participation in the bonding with H, which is mainly concentrated in the UCp₃H 11a₁, followed by the U 7s and U 5f. This can be understood by the fact that although U 7s has the largest overlap with H 1s (Table 6), this orbital has a larger energy separation than the U 6d, and the U 5f although being closest in energy to H 1s has at the same time a small overlap, making the participation small too. Finally the U 5f orbital has zero overlap with H and does not participate in the bond. In this way we understand the effect of the complicated rehybridization on UCp₃ in terms of a mainly atomic picture, and also the dominance of the U 6d orbital in the interaction with H 1s can be explained.

We look at the Mulliken populations of the orbitals that bond to H to assess the individual AO contributions. The main bonding orbital is the 11a₁, with the most important contribution from U 6d (17%), followed by U 7s (7%) and U 5f (3%). Note that there is some (antibonding) 10a₁ present, from which we know that it contains U 7s character. However, this is only a small amount (12%) of a mainly (92% see Table 5) Cp₃³⁻ orbital, and may therefore be neglected. The main U character thus comes from the 11-13a₁ orbitals of UCp₃. The quite strong mixing of U and H is an indication of a strong bond, -3.78 eV orbital interaction energy in A₁ symmetry from Table 7b. Because the steric repulsion is small (the H 1s and 11a₁ orbitals of UCp₃ have opposite spins), the overall bond energy is dominated by the orbital interaction energy, and amounts to -3.31 eV, and after correction for the preparation energy the bond energy with respect to the (planar) ground state is -3.26 eV.

The U 6d orbital is the most important orbital in the bond to H, in accordance with Bursten et al. [10]. They studied UCp₃H from the same fragments as we did and found a major bonding orbital with 56% H 1s character and 24% 6d, 8% 5f, 3% 7s and 3% 6p character. From their 56% H 1s character it seems that they also have a net donation to H 1s, although it was concluded in Ref. [10] that the donation was towards U. In our calculation the main bonding orbital is the 11a₁ orbital, with different AO participations. The differences in AO participation are ascribed to the approximate Muffin-tin potential representation in the SW calculations of Ref. [10].

Looking at Table 8 note the gross population of the U 6p orbital of 1.89e, there is a hole of 0.11e in this orbital. This means there is some antibonding U 6p-H 1s character in the virtual spectrum. We already mentioned in the introduction that in a destabilizing interaction a relief of repulsion can be obtained if the total population is less than maximal. The 6p population of 1.89 electrons could point to that mechanism. The fact that the U 6p orbital is involved in bonding to H is another manifestation of the large spatial extension of U 6p, which also was noted in a study on the relativistic expansion of uranyl [13]. Although deep in energy U 6p has a wide energy range for interaction with ligand orbitals due to its large spatial extension.

5.3 UCp₃-CO and UCp₃-NO

For interaction with CO and NO, UCp₃ was prepared in the $5f^3$ configuration (Table 5b). The population analysis for these molecules is given in Table 9. In A₁ symmetry the interaction is between the occupied ligand 5σ orbital and UCp₃ orbitals, while in E symmetry there is the possibility of back-bonding to the (empty in CO and filled with 1.0 electron in NO) ligand $2\pi^*$ orbital. In Figs 6,7 the schemes for the interaction in the UCp₃L compounds are given, where drawn and dashed lines indicate main and smaller interactions respectively. For clarity in these figures only the main interacting orbitals are given, the other orbitals can be seen from Table 9.

We first concentrate on the interaction in A₁ symmetry, which is indicated in Fig. 6. Note that the 5σ character in UCp₃NO is more spread out and present in lower orbitals 9-12a₁ than in UCp₃CO, where only 12a₁ contains considerable 5σ character. The explanation for this feature is that the NO 5σ level is lower in energy than the CO 5σ , as a result of the larger electronegativity of nitrogen, as explained at the beginning of this section. Connected to this, the CO 5σ is more localized on Carbon than the NO 5σ on Nitrogen, which results in a larger overlap with UCp₃ orbitals. The UCp₃ 12a₁ and 13a₁ orbitals are the ones into which donation to U can take place. These two levels both are higher than the CO 5σ . Therefore, not only from the higher energy of CO 5σ , being closer to the UCp₃ 12,13a₁, but also from a larger overlap with these UCp₃ orbitals, we expect stronger mixing in UCp₃CO. This is exactly what is found in the calculation, the admixing of the UCp₃ 12,13a₁ is larger in UCp₃CO and the gross populations of the Uranium orbitals to which donation takes place, U 6d, U 5f and U 7s, are larger.

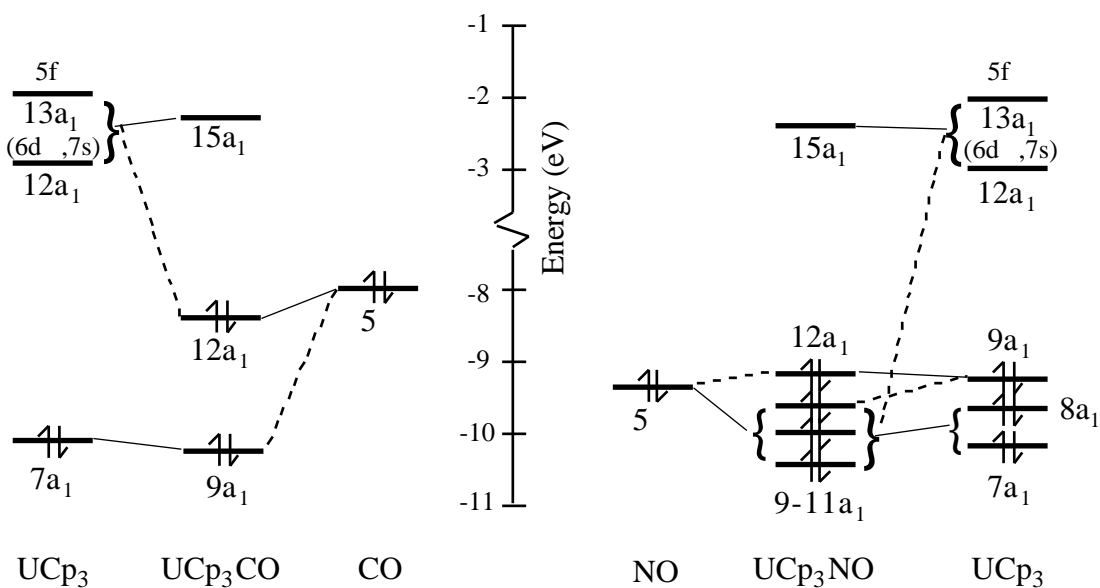


Figure 6. Interaction between UCp₃ and L in UCp₃CO and UCp₃NO in A₁ symmetry.

More in detail, in UCp_3NO the 7-9 a_1 and 12,13 a_1 orbitals of UCp_3 contribute to the bond with NO 5 π , of which the 8,9 a_1 are pure Cp-ring orbitals (not given in Table 5). The three orbitals 9-11 a_1 of UCp_3NO are all bonding with respect to the UCp_3 12,13 a_1 and NO 5 π orbitals, while there is no 12,13 a_1 character in 12 a_1 . In UCp_3CO the 7-9 a_1 UCp_3 orbitals are too low in energy for interaction with 5 π , and only interaction with the 12,13 a_1 orbitals is significant, mainly in the UCp_3CO 12 a_1 orbital. Both in CO and NO the donation into the UCp_3 12 a_1 (mostly U 6d) is larger than into 13 a_1 (5f). This is in line with the smaller energy difference with 12 a_1 and also with the fact that the 5 π overlap with U 6d is larger than with U 5f. From the gross Mulliken populations of Tables 5 and 9 the following picture results. There is donation from 5 π to U. In UCp_3NO there is donation of 0.17 electron to U 6d, 0.04 to U 5f and 0.03 to U 7s, while in UCp_3CO , the (larger) donation is 0.26 electron to U 6d, 0.06 to U 5f and 0.04 to U 7s.

The overall donation is 0.24 electron for UCp_3NO and 0.36 electron for UCp_3CO (1.5 times as much). The populations of the 5 π orbitals decreased by similar amounts and are 1.74 and 1.65 for UCp_3NO and UCp_3CO respectively, again showing the larger donation in UCp_3CO . Note that the 4 π orbital does not show up in Table 9. This orbital is localized mostly at O, and does not mix with any UCp_3 level. Even some 5 π character ends up lower, i.e. in the low A_1 orbitals. Our results are in line with those of Bursten et al. [10]. We can understand that U 6d is the most important acceptor orbital in the donation from L 5 π to U, by looking at the UCp_3 levels. The interaction between U^{3+} and Cp_3^{3-} leads to an 5f (13 a_1) orbital above U 6d (12 a_1). As the UCp_3 12,13 a_1 are energetically above the L 5 π orbital, both the energy ordering and the larger overlap of U 6d with L 5 π (Table 6) lead to the dominance of U 6d in the donation.

From Table 7b we see that the A_1 orbital interaction energies are -1.44 eV for UCp_3CO and -0.95 eV for UCp_3NO . Note that these values are lower than for UCp_3H . This is not so surprising, as there the interaction is between singly occupied orbitals.

Also in UCp_3CO and UCp_3NO there is a 6p hole, 0.07e and 0.04e for CO and NO respectively. In the low A_1 orbitals we have the bonding U 6p-5 π combinations, not given in Table 9. We also have some (antibonding) 6p character in the high A_1 orbitals. The larger hole for L=CO than for NO might be explained by the higher 5 π energy, leading to the antibonding CO 5 π -U 6p character being found more in the virtual spectrum. More detailed calculations are needed to show the origin of the difference in the extent of the holes, but for our purposes we need not go in more detail here. Again the U 6p orbital is involved in the bonding with ligands by virtue of its large spatial extent.

We now turn to E symmetry, where back-bonding to the 2 π orbitals of NO and CO is possible, as shown in other studies [10,11]. In Table 9 and Fig. 7 it can be seen that the interaction is concentrated entirely in orbital 16e, which mainly is the bonding combination

Table 9. Molecular Orbital compositions for UCp_3NO and UCp_3CO .

Orbital	U-L Orbital character	Eigen-value (eV)	U				Composition (%)				UCp ₃	Ligand
			7s	6d	6d	6d	5f	5f	5f	5f		
<i>UCp₃NO</i>												
<i>unoccupied orbitals</i>												
18e	2 -5f a. b.	-1.45			9		32	11			29(16e), 30(17e)	34 2
15a ₁	UCp ₃ 12,13a ₁	-2.38		13			77			1	38(12a ₁), 60(13a ₁)	
17e	5f	-2.82			5		4		80		96(15e), 2(17e)	1 2
14a ₁	5f	-3.33								94	96 11a ₁	
<i>occupied orbitals</i>												
16e	5f -2 b.	-2.86			3		54				2(15e), 59(16e)	37 2
5a ₂	UCp ₃ 5a ₂	-5.62								15	100 5a ₂	
13a ₁	UCp ₃ 10a ₁	-5.90		3			1				100 10a ₁	
15e	UCp ₃ 14e	-6.03			5	10					100 14e	
14e	UCp ₃ 13e	-6.41			8	2					100 13e	
12a ₁	Cp-5 a. b.	-9.24									3(8a ₁), 92 (9a ₁)	4 5
11e	UCp ₃	-9.34					4				9(10e), 91(11e)	
11a ₁	5 -6d b.	-9.68		5			1				5(7a ₁), 57(8a ₁), 7(9a ₁) 3(12a ₁), 2(13a ₁)	24 5
10a ₁	5 -6d b.	-9.97		6			1				21(7a ₁), 39(8a ₁), 3(12a ₁)	31 5
9a ₁	5 -7s b.	-10.46	14				1				73(7a ₁), 1(8a ₁), 1(12a ₁), 1(13a ₁)	22 5
<i>Gross Populations</i>			0.240	0.230	0.650	0.500	0.082	0.260	0.150	0.02	U6p :1.96 L:5 :1.74 2 :1.53	
<i>UCp₃CO</i>												
<i>unoccupied orbitals</i>												
18e	2 -U a. b.	-1.03			21	1	18	13			13(16e), 53(17e)	27 2
15a ₁	UCp ₃ 12,13a ₁	-2.32		12			80				36 (12a ₁), 61(13a ₁)	
17e	5f	-2.67			7			2	80		94(15e), 3(16e)	2 2
14a ₁	5f	-3.12								93	96 11a ₁	
<i>partially occupied orbitals</i>												
16e ^{3.0}	5f -2 b.	-2.72			4			69			4(15e), 73(16e)	21 2
<i>occupied orbitals</i>												
5a ₂	UCp ₃ 5a ₂	-5.53								15	100(5a ₂)	
13a ₁	UCp ₃ 10a ₁	-5.86		3			1				99 10a ₁	
15e	UCp ₃ 14e	-6.03			8	2				1	100 14e	
14e	UCp ₃ 13e	-6.41			5	10					100 13e	
12a ₁	5 -6d b.	-8.39	2	15			3				3(7a ₁) 3(8a ₁), 3 (9a ₁) 12(12a ₁), 6 (13a ₁)	64 5
11e	UCp ₃	-9.27					4				13(10e), 86 (11e)	
11a ₁	UCp ₃ 9a ₁	-9.27									97 9a ₁	2 5
10a ₁	UCp ₃ 8a ₁	-9.78									97 8a ₁	2 5
9a ₁	5 -7s b.	-10.32	14								94 7a ₁	4 5
<i>Gross Populations</i>			0.250	0.32	0.640	0.500	0.102	0.160	0.130	0.02	U6p :1.93 L:5 :1.65 2 :0.70	

Note: the gross population of U 5f only concerns A₁ symmetry.

of the UCp_3 16e and the ligand 2π . The analysis in terms of U AOs shows that 16e is the bonding combination of U 5f and L 2π , with also a small (bonding) contribution of U 6d -L 2π . For NO the U 5f and L 2π mixing is larger, 54%-37%, than for CO, where it is 69%-21%. This means that the NO 2π orbital was closer in energy to the UCp_3 16e orbital than the CO orbital, and both were higher than the 16e itself. This is unexpected from the CO and NO 2π orbital energies of Table 7a and the 16e orbital in Table 5b. We find approximately 1.5 times as much NO 2π character in the 16e as CO 2π character, while Bursten et al. [10] found 2.5 times as much NO 2π . Therefore we have qualitative agreement with those results, obtained with the X - SW method. The amount of 5f character we found in the main bonding orbital with the L 2π is also approximately the same, we have 69 and 54 % 5f character for CO and NO respectively, while the values from Ref. [10] are 81% and 59% 5f character (not axially split).

The orbital interaction energy for E symmetry is larger for NO, -5.57 eV, for CO the interaction energy is only -2.34 eV (Table 7b). To assess the amount of back-donation involved in the interaction we compare the gross populations of UCp_3 and UCp_3L , as only the 16e and L 2π orbitals are involved in the bonding. Interestingly, looking at the final 2π occupations, we see that formation of UCp_3L leads to donation from U to L of 0.53 electron for NO and 0.70 electron for CO. Therefore, although the mixing and orbital interaction energy in E symmetry are larger for NO, the amount of back-donation to 2π is larger for CO. The difference in the energy accompanying the back-donation and the back-donation itself is caused by the fact that the bonds between UCp_3 and L 2π are very different for NO and CO, because the NO 2π was occupied with 1.0 electron in NO. From Table 9 the bond between the UCp_3 16e and NO 2π can be viewed as a pair bond, while in UCp_3CO we have a pure donor-acceptor bond between the UCp_3 and CO 2π .

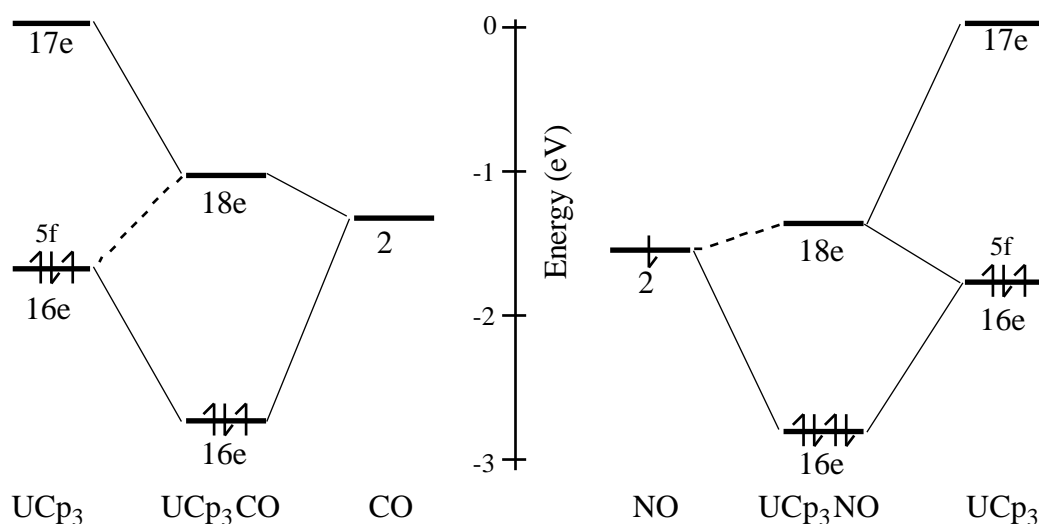


Figure 7. Interaction between UCp_3 and L in UCp_3CO and UCp_3NO in E symmetry.

The stronger mixing between the UCp_3 $16e$ and NO 2π then leads to a larger interaction energy, and at the same time to a smaller back-donation.

The final question is which U orbitals are responsible for the back-donation. From the main bonding orbital $16e$ it is clear that U $5f$ is the orbital that is mostly involved in the back-donation. This can be explained by the stronger U $6d$ -Cp mixing in UCp_3 (see Section 5.1) leading to mainly U $6d$ levels at higher energy. The U $5f$ is not much influenced by Cp, and although its overlap with L 2π is smaller, the interaction is larger. In Fig. 8 a plot is given for the bonding orbital $16e$ between the UCp_3 $16e$ and CO 2π . The plot clearly shows a dominating U $5f$ - CO 2π interaction. The total bond energy (Table 7b) for UCp_3NO is much larger than that of UCp_3CO , from the larger interaction energy accompanying the back-donation. Moreover, the steric term is smaller for NO, for which the electrostatic interaction is responsible. Comparing CO and NO, the larger steric repulsion for NO reduces the larger orbital interaction somewhat. The larger E^0 is caused by a smaller electrostatic term, partly compensated by a smaller Pauli repulsion.

The smaller $E_{el.stat}$ for NO might be the result of the extra electron in NO 2π , leading to a larger electron-electron repulsion. The stronger Pauli repulsion for CO is the result of the more extended 5π orbital. The bond energy is -4.93 eV for UCp_3NO and -3.03 for UCp_3CO , the difference being mainly caused by the interaction in E symmetry. The preparation energy is 1.10 eV, leading to total bond energies of -3.83 eV and -1.93 eV.

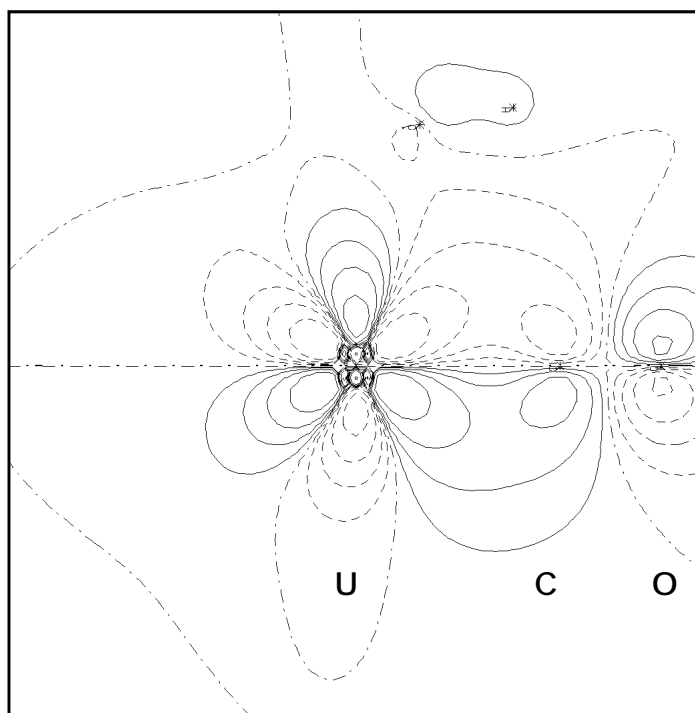


Figure 8. Back-donation from U $5f_{\pi}$ to CO 2π in orbital $16e$ of UCp_3CO . Orbital is plotted in xz -plane. Drawn lines: positive, dashed lines: negative, and dash-dotted lines: zero. Contour values: 0.5, 0.2, 0.1, 0.05, 0.02, 0.0, -0.02 , -0.05 , -0.10 , -0.20 , -0.50 .

The U 5f orbital is mostly responsible for the back-donation to the 2 orbital. This differs from transition metal carbonyl complexes, where it is the usually extended nd orbitals that participate in back-bonding. In actinides it is the much smaller (compared to the other valence orbitals) U 5f orbital that interacts with the 2 orbital.

The stronger π -acid character of NO is also found in transition metal complexes, as was mentioned in the introduction. Although up to now it has not been possible to synthesize UCp₃NO [10], it should exist, since our calculations as well as those of Bursten et al. [10] indicate a larger bond energy than for the already known UCp₃CO. Further experimental investigation on the existence of UCp₃NO is therefore justified.

6. Conclusion

Scalar-Relativistic calculations on planar UCp₃ showed that the ground state configuration was 15e²11a₁, which can be approximated by 5f¹5f¹5f¹. The 5f orbital was too high to be occupied. Putting one electron in orbital 11a₁ with its strong U-Cp interaction was favoured over a situation where all three (5f) electrons were put into E symmetry. As to the question of the importance of covalent/ionic terms in the formation of UCp₃, the covalent electronic interaction terms account for about one-third of the total bond energy.

For interaction with the ligands H, NO and CO, pyramidal UCp₃ was prepared in the optimal start configuration for bonding. The lowest pyramidal configuration was again the 15e²11a₁. The bond energies of UCp₃ and the ligands were after subtracting the preparation energy -3.26, -3.83 and -1.93 eV for H, NO and CO respectively. The interaction was split into contributions from A₁ and E symmetries (except for UCp₃H).

In A₁ symmetry the main effect was donation from the ligand orbitals to U, except for UCp₃H where we found donation to H. The largest interaction was found in UCp₃H, where H 1s formed a mainly covalent pair bond to UCp₃ with an orbital that could be viewed as the result of a rehybridization on UCp₃ between 11a₁ (occupied with 1.0 electron in UCp₃) and the virtual 12,13a₁. The main bonding orbital with H 1s showed a dominating U 6d contribution, and smaller 7s and 5f ones. The strong mixing between U levels and H is accompanied by 0.28e donation to H, and leads to the largest orbital interaction of all considered ligands in A₁ symmetry. For the other ligands, the main interaction consists of donation from L to the unoccupied UCp₃ orbitals 12,13a₁. In that case we can simply compare gross AO populations to assess the contributions to the donation, which gives the same picture as the Mulliken orbital analysis for the main bonding orbitals. The main acceptor orbital in A₁ symmetry is U 6d orbital with smaller contributions from U 5f and U 7s. The charge flow to U is accompanied by a loss of electrons of 0.26 from the NO 5 and even 0.35 from CO 5. For CO a stronger

interaction was found than for NO, for which the larger overlap (more localization at C) and higher energy of the CO π^* are responsible. Ultimately the differences between CO and NO are all caused by the larger electronegativity of N. We find a 6p hole in A_1 symmetry in all considered compounds, again showing the importance of the large radial extension of the 6p orbital.

In E symmetry there is back-donation from U to L in UCp_3CO and UCp_3NO , which is dominated by U 5f. The back-donation amounts to 0.70 electron to CO and 0.54 electron to NO. The energy gain accompanying the back-donation is larger in UCp_3NO because the U 5f and NO π^* mix more heavily (pair bond) than U 5f and CO π^* (donor-acceptor). Still the back-donation to NO π^* is smaller than to CO π^* by the fact that the NO π^* was occupied with 1.0 electron in the NO fragment. The overall bond energy for UCp_3NO is larger than for UCp_3CO mainly due to the larger E-interaction, and this justifies continued investigations into its existence.

Finally, we will make some remarks on the participation of U 5f and 6d to the bonding in the UCp_3L complexes. Our calculations have shown that the bond energies are large: a few eVs. Both U 6d and U 5f orbitals participate considerably in the bond. It was shown that U 6d is mostly involved as acceptor orbital in A_1 symmetry, while in E symmetry the U 5f orbital is mostly involved in back-donation into the ligand π^* orbitals. This result is in agreement with other studies [6,10]. We have given an explanation for this behaviour. The small interaction between U and Cp in A_1 symmetry leads to a mainly atomic level ordering in UCp_3 , and as U 6d has largest overlap with L, this orbital dominates the donation from L to U. In E symmetry, the larger U 6d interaction with Cp leads to a much higher U 6d orbital than U 5f. Although also in this case the overlap with U 6d is larger, the interaction with U 5f is more favourable due to a smaller energy difference.

References.

- 1: J.M. Birmingham and G. Wilkinson, *J. Am. Chem. Soc.* **78** (1956) 42
- 2: L.T. Reynolds and G. Wilkinson, *J. Inorg. Nucl. Chem.* **2** (1956) 246
- 3: a) T.J. Marks and R.D. Ernst, in 'Comprehensive Organometallic Chemistry', eds. G. Wilkinson, F.G.A. Stone and E.W. Abel, Pergamon Oxford 1982, ch. 21.
b) 'Organometallics of the f-Elements', eds. T.J. Marks and R.D. Fischer, Reidel Dordrecht 1979
c) 'Lanthanide and Actinide Chemistry and Spectroscopy', ed. N.M. Edelstein, A.C.S. Symposium series **131** 1980
d) 'Fundamental and technological aspects of Organo-f-Element Chemistry', Reidel Dordrecht 1985
- 4: a) B.E. Bursten and R.J. Strittmatter, *Angew. Chem.* **103** (1991) 1085

- b) B.E. Bursten and M. , Chem. Rev. **91** (1991) 719
- 5: A. Streitwieser Jr. and U. Müller-Westerhoff, J. Am. Chem. Soc. **90** (1968) 7364
- 6: C.J. Burns and B.E. Bursten, Comments Inorg. Chem. **9** (1989) 61
- 7: B.E. Bursten and R.J. Strittmatter, J. Am. Chem. Soc. **113** (1991) 552
- 8: K.N. Raymond and C.W. Eigenbrot, Jr., Acc. Chem. Res. **13** (1980) 276
- 9: B.E. Bursten and A. Fang, Inorg. Chim. Acta **110** (1985) 153
- 10: B.E. Bursten, L.F. Rhodes and R.J. Strittmatter, J. Am. Chem. Soc. **111** (1989) 2758
- 11: K. Tatsumi and A. Nakamura, J. organometal. Chem. **272** (1984) 141
- 12: P.M. Boerrigter, E.J. Baerends and J.G. Snijders, Chem. Phys. **122** (1988) 357
- 13: E.M. van Wezenbeek, E.J. Baerends and J.G. Snijders, Theor. Chim. Acta **81** (1991) 139
- 14: E.M. van Wezenbeek, T. Ziegler and E.J. Baerends, in preparation
- 15: T.A. Albright, J.K. Burdett and M.H. Whangbo, 'Orbitals Interactions in Chemistry', Wiley, New York, 1985
- 16: a) E.J. Baerends, D.E. Ellis and P. Ros, Chem. Phys. **2** (1973) 42
b) E.J. Baerends and P. Ros, Chem. Phys. **2** (1973) 51
c) E.J. Baerends and P. Ros, Int. J. Quant. Chem. **S12** (1978) 169
- 17: a) J.G. Snijders and E.J. Baerends, Mol. Phys. **36** (1978) 1789
b) J.G. Snijders, E.J. Baerends and P. Ros, Mol. Phys. **38** (1979) 1909
c) T. Ziegler, J.G. Snijders and E.J. Baerends. Chem. Phys. **74** (1981) 1271
- 18: P.M. Boerrigter, G. te Velde and E.J. Baerends, Int. J. Quant. Chem. **33** (1988) 87
- 19: T. Ziegler, V. Tschinke, E.J. Baerends, J.G. Snijders and W. Ravenek, J. Phys. Chem. **93** (1989) 3050
- 20: P.M. Boerrigter, Thesis, Vrije Universiteit Amsterdam, 1987
- 21: M.L. Anderson, L.R. Crisler, J. Organomet. Chem. **17** (1969) 345
- 22: H.-D. Amberger, J. Organomet. Chem. **116** (1976) 219
- 23: a) I. Fragalà, E. Ciliberto, R.D. Fischer, G.R. Sienel and P. Zanella, J. Organomet. Chem. **120** (1976) C9
b) I. Fragalà, J. Goffart, G. Granozzi and E. Ciliberto, Inorg. Chem. **22** (1983) 216
- 24: a) R.D. Fischer, R. v. Ammon and B. Kanellakopoulos, J. Organomet. Chem. **25** (1970) 123
b) R.R. Ryan, R.A. Penneman and B. Kanellakopoulos, J. Am. Chem. Soc. **97** (1975) 258
- 25: A. Zalkin, J.G. Brennan and R.A. Andersen, Acta Crystallogr. Sect. C **44** (1988) 2104
J.G. Brennan, Ph.D. Dissertation, University of California, Berkeley 1985

- 26: B.E. Bursten, L.F. Rhodes and R.J. Strittmatter, *J. Am. Chem. Soc.* **111** (1989) 2756
- 27: P.C. Blake, M.F. Lappert, J.C. Atwood and H. Zhang, *J. Chem. Soc., Chem. Commun.* **1986** 1148
- 28: W.K. Kot, G.V. Shalimoff and N.M. Edelstein, *J. Am. Chem. Soc.* **110** (1988) 986
- 29: A Vittadini, M. Casarin, D. Ajò, M. Bertocello, E. Ciliberto, A. Gulino and I. Fragalà, *Inorg. Chim. Acta* **121** (1986) L23
- 30: K. Tatsumi and R. Hoffmann, *Inorg. Chem.* **23** (1984) 1633
- 31: a) J.L. Slater, R.K. Sheline, K.C. Lin and W. Weltner, Jr., *J. Chem. Phys.* **55** (1971) 5129
b) J.L. Slater and R.K. Sheline, *Angew. Chem.* **87** (1975) 332
- 32: R.L. DeKock, *Inorg. Chem.* **10** (1971) 1205
- 33: J.G. Brennan, R.A. Andersen and J.L. Robbins, *J. Am. Chem. Soc.* **108** (1986) 335
- 34: a) J.G. Brennan, R.A. Andersen and A. Zalkin, *Inorg. Chem.* **25** (1986) 1761
b) J.G. Brennan and R.A. Andersen, *J. Am. Chem. Soc.* **107** (1985) 514
c) J.G. Brennan, J.C. Green and C.M. Redfern, *Inorg. Chim. Acta* **139** (1987) 331
d) J.G. Brennan, S.D. Stults, R.A. Andersen and A. Zalkin, *Organometallics* **7** (1988) 1329
- 35: R.E. Cramer, F. Edelman, A.L. Mori, S. Roth, J.W. Gilje, K. Tatsumi and A. Nakamura, *Organometallics* **7** (1988), 841
- 36: R.E. Cramer, J.H. Jeong and J.W. Gilje, *Organometallics* **6** (1987), 2010
- 37: J.G. Brennan, S.D. Stults, R.A. Andersen and A. Zalkin, *Inorg. Chim. Acta* **139** (1987) 210
- 38: B.E. Bursten and R.J. Strittmatter, *J. Am. Chem. Soc.* **109** (1986) 6606
- 39: B.E. Bursten and R.H. Cayton, *Organometallics* **6** (1987) 2004
- 40: J.L. Stewart, Ph.D. Thesis, Lawrence Berkeley Laboratory, University of California, Berkeley 1988
- 41: S.H. Vosko, L. Wilk and M. Nusair, *Can. J. Phys.* **58** (1980) 1200
- 42: H. Stoll, E. Golka and H. Preus, *Theor. Chim. Acta* **55** (1980) 29
- 43: a) K. Morokuma, *J. Chem. Phys.* **55** (1971) 1236
b) K. Kitaura and K. Morokuma, *Int. J. Quant. Chem.* **10** (1976) 325
- 44: T. Ziegler and A. Rauk, *Theor. Chim. Acta* **46** (1977) 1
- 45: F.M. Bickelhaupt, N.N. Nibbering, E.M. van Wezenbeek and E.J. Baerends, Submitted to *J. Phys. Chem.*
- 46: J.W. Lauher and R. Hoffmann, *J. Am. Chem. Soc.* **98** (1976) 1729

Samenvatting

Relativistische effecten zijn belangrijk in moleculen met zware atomen, omdat daar de electronen erg snel bewegen in de buurt van de kern. Het is essentieel te begrijpen wat de relativistische effecten op atomaire banen zijn, voordat relativiteit in moleculenonderzocht kan worden. Daarom begint dit proefschrift na een algemene inleiding in Hoofdstuk 1, waarin relativiteit en de gebruikte rekenmethode worden behandeld, met een hoofdstuk over relativistische effecten in atomen. Daarna komen moleculaire berekeningen aan de orde, waarbij o.a. gekeken wordt naar relativistische effecten op de binding en bindingslengte, en spectroscopie van moleculen die zware elementen bevatten. Ook worden in een relativistisch schema bindingen onderzocht in zware moleculen. Een aantal van de onderzochte systemen bestaat uit open schil fragmenten. De methode die ontwikkeld is om de bindingsenergie analyse ook voor deze gevallen te kunnen uitvoeren, wordt uitvoerig beschreven in Hoofdstuk 1. Het is hiermee mogelijk geworden de vorming van electron-paar bindingen te bestuderen, wat een belangrijk proces is in de Scheikunde. Hoofdstuk 4 bestaat uit toepassingen van de electron-paar binding methode.

Voor atomen zijn de relativistische effecten op de banen algemeen bekend: $s_{1/2}$ en $p_{1/2}$ banen worden gestabiliseerd en contraheren, d en f banen ondervinden destabilisatie en expanderen, en het effect op $p_{3/2}$ banen ligt tussen deze twee extremen in. Het onderzoek in Hoofdstuk 2 concentreert zich dan ook niet hierop, maar op de vraag wat de (ruimtelijke) oorsprong is van de relativistische effecten op atomaire banen. De aanleiding tot dit onderzoek vormde het gegeven dat de relativistische correcties op atomaire valentie baan eigenschappen van veel-electron atomen afhangen van de totale kernlading, en niet van de effectieve kernlading zoals men verwachtte. Het bleek mogelijk hiervoor een verklaring te geven, door in de uitdrukking voor de verwachtingswaarde van een baan eigenschap, de bol rond de kern waarover geïntegreerd wordt, op te delen in schillen. Deze schillen corresponderen met de gewone K,L,M etc. aanduiding van energieniveaus. Het blijkt dat de mass-velocity, Darwin en spin-baan correcties helemaal opgebouwd worden nabij van de kern, en derhalve afhangen van de totale kernlading. Het indirecte relativistische effect werd ook onderzocht. Vaak wordt dit geassocieerd met destabilisatie, vanwege contractie van naar binnen gelegen banen. Het onderzoek laat echter nieuwe gezichtspunten zien. Men moet bedenken dat terwijl relativistisch gecontraheerde s en p banen indirecte destabilisatie veroorzaken, expanderende d en f banen een indirecte stabilisatie tot gevolg kunnen hebben. Dit is vooral belangrijk als een gevulde d of f schil zich vlak onder een sterk penetrerende baan (s of p) bevindt. Hiermee worden nu de extreem grote relativistische effecten begrepen die optreden in de centrale kolommen van het periodieke systeem, met als bekendste voorbeeld Au en zijn verbindingen.

Het overige onderzoek betreft relativistische berekeningen aan moleculen, waarbij in een aantal gevallen gekeken werd naar de effecten van relativiteit op de bindingslengte, de bindingen en spectroscopie. Het uranyl molecuul UO_2^{2+} vormt een aanzienlijk deel van dit onderzoek. Dit molecuul blijkt speciale eigenschappen te bezitten, die uiteindelijk gerelateerd zijn aan het speciale karakter van de semi-core U 6p baan, die zowel core als valentie eigenschappen bezit. Deze baan is ruimtelijk zelfs uitgebreider dan de valentie U 5f baan, wat resulteert in grote overlaps in uranyl, waar de U-O afstand klein is (voor een verklaring zie Hoofdstuk 4a). Ook in UCp_3L (Hoofdstuk 6) speelt de U 6p baan een rol, maar minder dan in uranyl doordat de atomaire afstanden daar groter zijn.

Relativistische berekeningen laten een aanzienlijke bindingsverlenging zien in uranyl, in tegenstelling tot de bindingscontractie die voorheen bijna altijd gevonden werd voor moleculen. In Hoofdstuk 3 wordt aangetoond dat deze verlenging niet gerelateerd is aan de relativistische expansie van de voor de binding belangrijke U 5f baan. Het blijkt de U 6p baan te zijn, die zorgt voor de expansie. Het sterke valentiekarakter van deze baan leidt tot een grote overlap en interactie met O, mede ook door de korte U-O afstand. De sterke interactie met O 2p zorgt ervoor dat de antibindende U 6p-O 2p combinatie hoog in het virtuele spectrum terechtkomt, boven de U 5f. De interactie van U 5f met O 2p (in de antibindende U 6p-O 2p) leidt tot een HOMO met veel 5f karakter. De sterke deelname van U 6p aan de binding in uranyl leidt tot depopulatie van deze baan, er is nog ongeveer 1.5 electron over in U 6p: er is een "6p gat". Dit gat neemt toe bij kortere afstand, en het daaruit voortvloeiende aanzienlijke verlies van mass-velocity stabilisatie, groot voor de U 6p baan vanwege het core-karakter, heeft een bindingsverlengend effect. Het core-karakter zelf van U 6p draagt ook bij tot de expansie, door het niet-diagonale mass-velocity element met U 5p.

De laagste virtuele banen in uranyl zijn de nietbindende U 5f en 5f banen. Uit het voorgaande volgt dat het excitatie spectrum dan wordt bepaald door overgangen van de voornamelijk U 5f HOMO naar $f_{5/2}$, $f_{7/2}$. In Hoofdstuk 5 wordt een toekenning gegeven van het excitatie spectrum van $\text{Cs}_2\text{UO}_2\text{Cl}_4$, waarvoor $\text{UO}_2\text{F}_4^{2-}$ als model werd gebruikt. Ten gevolge van het F ligand veld ligt de $f_{5/2}$ baan boven de $f_{7/2}$. Met behulp van een model om de spin-baan interactie mee te nemen, wordt een toekenning van het spectrum gedaan: $u_{5/2} < u_{7/2}$, $u_{5/2} < u_{7/2}$. Dit is anders dan $u_{5/2}(2x) < u_{7/2}(2x)$ vermeld in de literatuur, echter alleen wat betreft de tweede en derde piek. Onze berekeningen laten zien dat de diagonaal spin-baan gesplitste $f_{5/2}$ en $f_{7/2}$ niveaus erg sterk mengen, en omdat juist deze tot de middelste pieken leiden is de toekenning als $u_{5/2}$ of $u_{7/2}$ moeilijk. In Hoofdstuk 5 worden ook de resultaten gepresenteerd van onderzoek naar het Xray fotoelectron spectrum van uranyl. Net als de grote interactie met O 2p, is de interactie van U 6p met O 2s ook sterk, de bindende en antibindende banen liggen 14 eV uit elkaar. In experimenten werden pieken toegekend aan individuele atomaire banen. De berekeningen

tonen echter aan dat dit niet correct is: door de sterke interactie van U 6p met O 2s zijn de banen waaruit geïoniseerd wordt sterk gemengd. Het resultaat van de interactie van U 6p en O 2s kan het best verklaard worden als eerst de spin-baan interactie werkt.

Het laatste onderzoek aan uranyl in Hoofdstuk 4a betreft de verklaring voor de korte U-O afstand, die veel kleiner is dan voor secundaire liganden. Voor dit onderzoek werd uranyl opgebouwd uit open schil fragmenten $U^{3+}(5f^3 5f^2)$ en $O_2^-(2s_u^2 2p_u 2p_g^4 2p_u^2)$. Om de energie-analyse te kunnen doen vanuit zulke open schil fragmenten, werd een methode ontwikkeld, die uitgebreid uiteengezet wordt in Hoofdstuk 1. Met behulp van deze methode kunnen paarbindingen bestudeerd worden. De eerste toepassing was de studie aan uranyl als hierboven vermeld, met paarbindingen tussen $5f -O 2p_u$ en $5f -O 2p_u$. De korte U-O afstand in uranyl is verrassend, omdat veel repulsie wordt verwacht ten gevolge van de ruimtelijk uitgebreide U 6p baan. Inderdaad is er een grote repulsieve bijdrage van de U 6p baan. De belangrijkste bijdrage aan de sterische interactie in uranyl komt van de gesloten schil U 6p -O 2s_u Pauli repulsie. Verrassend is het kleine U 6p -O 2p_u sterische effect, dat verklaard wordt door elkaar opheffende Pauli repulsieve en electrostatische interacties. Om dezelfde reden is ook de U 5f -O 2p_u sterische interactie klein. Dit resultaat laat zien dat kijken naar alleen de Pauli repulsie, zoals vaak gedaan wordt, niet genoeg is, electrostatische effecten spelen ook een rol. Het blijkt dat de U 5f-O 2p interactie verantwoordelijk is voor de korte U-O afstand. Zowel de U 5f -O 2p_u als de U 5f -O 2p_u interactie zijn belangrijk, de eerste omdat er geen sterische repulsie is tussen U 5f en O 2p_u en de tweede omdat het sterische effect van U 5f en O 2p_u klein is. De U 6d baan heeft een niet verwaarloosbare bijdrage aan de binding, maar het afstandsgedrag is vlak, en speelt derhalve geen rol bij het bepalen van de korte U-O afstand.

Twee andere toepassingen met open schil fragmenten worden beschreven in Hoofdstukken 4c en 4d. In Hoofdstuk 4b wordt het effect van relativiteit bekeken op de binding tussen H en enerzijds het overgangsmetaalfragment $HfCl_3$, en anderzijds het actinidefragment $ThCl_3$. Het blijkt dat de niet-relativistische en relativistische bindingen in $HfCl_3H$ niet veel verschillen, met een grotere 5d dan 6s bijdrage. In $ThCl_3H$ zijn de bindingen totaal verschillend, in het niet-relativistische schema zijn er gelijke bijdragen van 5f en 6d, terwijl relativistisch de bijdrage van 5f door zijn destabilisatie praktisch nihil wordt. Dit onderzoek toont aan dat voor overgangsmetalen de relativistische effecten niet zo groot zijn, en eerste orde stringtheorie voldoet, terwijl voor actinides quasi-relativistische berekeningen nodig zijn.

Hoofdstuk 4c betreft onderzoek naar de relatieve stabiliteit van de drie CN* isomeren NCCN (**1**), CNCN (**2**) en CNNC (**3**). Het is bekend dat de binding zwakker wordt in de reeks **1-3**, terwijl tegelijkertijd de centrale bindingsafstand afneemt. Een zeer uitgebreide bindingsenergie analyse, gebruik makend van de open schil methode die in Hoofdstuk 1

werd beschreven, laat zien dat niet alleen de paarbinding tussen de enkel bezette CN 5 banen een rol speelt, maar dat ook de dubbel bezette CN 4 banen (N lone pair) belangrijk zijn. De 5 baan is gelocaliseerd op C, en als alleen de paarbinding aanwezig was, verklaart dit direct de waargenomen stabiliteit. De situatie is echter veel gecompliceerder door de aanwezigheid van de 4 banen. Ten eerste is het zo dat de in-fase $4 +4'$ en $5 +5'$ combinaties een repulsieve interactie aangaan, die de paarbinding tegenwerkt. In NCCN is dit effect het grootst, omdat daar de $5 /5'$ overlap het grootst en de $4 /4'$ overlap het kleinst is en de in-fase combinaties dan dicht bij elkaar liggen. Ten tweede is er een donor/acceptor interactie tussen de uit-fase $4 -4'$ en $5 -5'$ combinaties, die tot een energie verlagende relaxatie leidt. Dit effect is ten gevolge van de overlaps juist het sterkst in CNNC, en is uiteindelijk verantwoordelijk voor de kortere centrale bindingsafstand gaande van **1** naar **3**. Ook wordt er in dit onderzoek een vergelijking gemaakt met de resultaten/interpretatie van andere onderzoekers. We tonen aan dat onze Orbital Correlatie Diagrammen (OCDs) een beter begrip geven van de complexe interacties in de CN dimeren. Een belangrijk aspect bij het tot stand komen van de OCDs is het feit dat men moet realiseren dat de CN 4 en 5 banen niet volledig gelocaliseerd zijn op N en C respectievelijk, maar dat beiden ook een aanzienlijke amplitude hebben op de andere kern.

Het afsluitende onderzoek in Hoofdstuk 6 van dit proefschrift betreft organoactinide chemie, sterk in opkomst sinds het begin van de jaren 80. Alle berekeningen in dit hoofdstuk zijn gedaan met de quasi-relativistische methode, nodig voor een goede beschrijving van actinides. In het eerste deel van dit onderzoek wordt aangetoond dat de grond electronen toestand van het "vlakke" UCp_3 het best beschreven kan worden als $5f^3 (f^1 f^1 f^1)$. De binding tussen de fragmenten Cp_3^{3-} en U^{3+} in UCp_3 heeft een ionisch/covalent karakter van 2:1. In het tweede deel wordt de interactie van pyramidaal UCp_3 met de liganden H, CO en NO onderzocht. De berekende UCp_3 -L bindingsterktes voor de reactie van UCp_3 met L zijn -4.37 , -1.93 en -3.83 eV voor $L = H, CO$ en NO t.o.v. de vlakke grondtoestandsconfiguratie. De interactie in UCp_3L bestaat uit donatie van L naar U in A_1 symmetrie, en back-donatie van U naar L in E symmetrie. In alle gevallen domineert U 6d de donatie, terwijl U 5f het belangrijkste is voor de back-donatie. De donatie vanuit CO is groter dan uit NO, vanwege de lagere electronegativiteit van C en diengevolge sterkere 5 localisatie en hogere CO 5 energie t.o.v. de NO 5. De back-donatie in de E symmetrie is groter in UCp_3CO dan in UCp_3NO , en bestaat uit de U 5f -L 2 interactie. Toch is de totale bindingsenergie in UCp_3NO groter omdat daar de bindende U 5f -L 2 combinatie volledig gevuld is. De grotere bindingsenergie voor UCp_3NO dan voor UCp_3CO rechtvaardigt verder onderzoek naar het bestaan van deze verbinding. Tenslotte, in de beschouwde systemen is er een klein "U 6p gat", wederom een manifestatie van de grote uitgebreidheid van deze baan.

Nawoord

Hierbij wil ik graag enkele mensen in the bijzonder bedanken voor hun bijdrage aan het tot stand komen van dit proefschrift.

Evert Jan Baerends, bedankt voor de vele stimulerende discussies in een prettige sfeer, en dat je ondanks drukke werkzaamheden als decaan toch steeds tijd vond om te helpen bij het oplossen van problemen.

Jaap Snijders, het herschrijven van het RHFS-programma zou veel moeilijker geweest zijn zonder de uitgebreide sessies die we hielden. Verder wil ik je bedanken voor het kritisch doorlezen van mijn proefschrift.

Prof. dr. Pekka Pyykkö, I am honoured to have you as a referent, and I am very grateful to you for carefully reading the manuscript.

Prof. dr. S. Balt, u heeft uw taak als derde lezer serieus opgevat, en daarvoor dank.

Tom Ziegler, I want to thank you for useful discussions on various subjects, and the warm hospitality and use of computer time during my stay at the University of Calgary. Furthermore I want to thank the other friends at the UofC, especially Elizabeth, Attila and Heiko for a great time in Calgary.

Pieter Vernooijs, jouw hulp bij het oplossen van technische problemen en het maken van het ingewikkelde schema om plaatjes zonder resolutieverlies vanaf de Cyber in de tekstverwerker te zetten, waardeer ik zeer. Zonder jou was dit boek veel dunner geweest.

Matthias Bickelhaupt, bedankt voor de prettige samenwerking bij het NCCN project.

Paul Nederkoorn, je had als student geen makkelijk onderwerp, maar je heb je er goed doorgeslagen. De veelbelovende resultaten van jouw onderzoek zullen gepubliceerd worden na enige aanvullende berekeningen.

Verder dank ik ook mijn collega's Bert, Eric, Gijsbert, Marcel en Robbert en de studenten voor de goede sfeer op onze afdeling.

Tenslotte bedank ik jou, Saskia, voor je geduld en liefdevolle ondersteuning, en ik wens je veel succes bij je eigen promotieonderzoek.

Curriculum Vitae

Egbelbertus Maria van Wezenbeek was born in 1963 on Oktober 18th at Emmeloord Noordoostpolder. He graduated from high school (Gymnasium) in 1982. In the same year he entered the Faculty of Chemistry of the Free University at Amsterdam. After studying Chemistry with Theoretical Chemistry as principal subject and Physics as subsidiary subject, he received his M.Sc. in Chemistry in 1987.

From July 1st 1987 he worked as a scientific research assistant at the Department of Theoretical Chemistry of the Free University at Amsterdam, where he carried out the work described in this thesis. The investigations described in Chapter 4b of this thesis were performed at the University of Calgary from August-September 1990.